

Modeling of bending-torsion couplings in active-bending structures. Application to the design of elastic gridshell.



Thèse n.xxxxx
présenté le 01 décembre 2017
à l'Ecole des Ponts ParisTech
laboratoire Navier
Université Paris-Est
pour l'obtention du grade de Docteur ès Sciences
par

Lionel du Peloux

acceptée sur proposition du jury:

Prof Name Surname, président du jury
Prof Name Surname, directeur de thèse
Prof Name Surname, rapporteur
Prof Name Surname, rapporteur
Prof Name Surname, rapporteur

Paris, Ecole des Ponts ParisTech, 2016

“Quia nominor leo.”

A Jacques & Christiane, mes grands-parents bien-aimés.

Acknowledgements

Lorem ipsum dolor sit amet, consectetuer adipiscing elit. Ut purus elit, vestibulum ut, placerat ac, adipiscing vitae, felis. Curabitur dictum gravida mauris. Nam arcu libero, nonummy eget, consectetuer id, vulputate a, magna. Donec vehicula augue eu neque. Pellentesque habitant morbi tristique senectus et netus et malesuada fames ac turpis egestas. Mauris ut leo. Cras viverra metus rhoncus sem. Nulla et lectus vestibulum urna fringilla ultrices. Phasellus eu tellus sit amet tortor gravida placerat. Integer sapien est, iaculis in, pretium quis, viverra ac, nunc. Praesent eget sem vel leo ultrices bibendum. Aenean faucibus. Morbi dolor nulla, malesuada eu, pulvinar at, mollis ac, nulla. Curabitur auctor semper nulla. Donec varius orci eget risus. Duis nibh mi, congue eu, accumsan eleifend, sagittis quis, diam. Duis eget orci sit amet orci dignissim rutrum.

Nam dui ligula, fringilla a, euismod sodales, sollicitudin vel, wisi. Morbi auctor lorem non justo. Nam lacus libero, pretium at, lobortis vitae, ultricies et, tellus. Donec aliquet, tortor sed accumsan bibendum, erat ligula aliquet magna, vitae ornare odio metus a mi. Morbi ac orci et nisl hendrerit mollis. Suspendisse ut massa. Cras nec ante. Pellentesque a nulla. Cum sociis natoque penatibus et magnis dis parturient montes, nascetur ridiculus mus. Aliquam tincidunt urna. Nulla ullamcorper vestibulum turpis. Pellentesque cursus luctus mauris.

Lausanne, 12 Mars 2011

D. K.

Preface

A preface is not mandatory. It would typically be written by some other person (eg your thesis director).

Lorem ipsum dolor sit amet, consectetuer adipiscing elit. Ut purus elit, vestibulum ut, placerat ac, adipiscing vitae, felis. Curabitur dictum gravida mauris. Nam arcu libero, nonummy eget, consectetuer id, vulputate a, magna. Donec vehicula augue eu neque. Pellentesque habitant morbi tristique senectus et netus et malesuada fames ac turpis egestas. Mauris ut leo. Cras viverra metus rhoncus sem. Nulla et lectus vestibulum urna fringilla ultrices. Phasellus eu tellus sit amet tortor gravida placerat. Integer sapien est, iaculis in, pretium quis, viverra ac, nunc. Praesent eget sem vel leo ultrices bibendum. Aenean faucibus. Morbi dolor nulla, malesuada eu, pulvinar at, mollis ac, nulla. Curabitur auctor semper nulla. Donec varius orci eget risus. Duis nibh mi, congue eu, accumsan eleifend, sagittis quis, diam. Duis eget orci sit amet orci dignissim rutrum.

Nam dui ligula, fringilla a, euismod sodales, sollicitudin vel, wisi. Morbi auctor lorem non justo. Nam lacus libero, pretium at, lobortis vitae, ultricies et, tellus. Donec aliquet, tortor sed accumsan bibendum, erat ligula aliquet magna, vitae ornare odio metus a mi. Morbi ac orci et nisl hendrerit mollis. Suspendisse ut massa. Cras nec ante. Pellentesque a nulla. Cum sociis natoque penatibus et magnis dis parturient montes, nascetur ridiculus mus. Aliquam tincidunt urna. Nulla ullamcorper vestibulum turpis. Pellentesque cursus luctus mauris.

Lausanne, 12 Mars 2011

T. D.

Abstract

Lorem ipsum dolor sit amet, consectetuer adipiscing elit. Ut purus elit, vestibulum ut, placerat ac, adipiscing vitae, felis. Curabitur dictum gravida mauris. Nam arcu libero, nonummy eget, consectetuer id, vulputate a, magna. Donec vehicula augue eu neque. Pellentesque habitant morbi tristique senectus et netus et malesuada fames ac turpis egestas. Mauris ut leo. Cras viverra metus rhoncus sem. Nulla et lectus vestibulum urna fringilla ultrices. Phasellus eu tellus sit amet tortor gravida placerat. Integer sapien est, iaculis in, pretium quis, viverra ac, nunc. Praesent eget sem vel leo ultrices bibendum. Aenean faucibus. Morbi dolor nulla, malesuada eu, pulvinar at, mollis ac, nulla. Curabitur auctor semper nulla. Donec varius orci eget risus. Duis nibh mi, congue eu, accumsan eleifend, sagittis quis, diam. Duis eget orci sit amet orci dignissim rutrum.

Nam dui ligula, fringilla a, euismod sodales, sollicitudin vel, wisi. Morbi auctor lorem non justo. Nam lacus libero, pretium at, lobortis vitae, ultricies et, tellus. Donec aliquet, tortor sed accumsan bibendum, erat ligula aliquet magna, vitae ornare odio metus a mi. Morbi ac orci et nisl hendrerit mollis. Suspendisse ut massa. Cras nec ante. Pellentesque a nulla. Cum sociis natoque penatibus et magnis dis parturient montes, nascetur ridiculus mus. Aliquam tincidunt urna. Nulla ullamcorper vestibulum turpis. Pellentesque cursus luctus mauris.

Key words:

Résumé

Lorem ipsum dolor sit amet, consectetuer adipiscing elit. Ut purus elit, vestibulum ut, placerat ac, adipiscing vitae, felis. Curabitur dictum gravida mauris. Nam arcu libero, nonummy eget, consectetuer id, vulputate a, magna. Donec vehicula augue eu neque. Pellentesque habitant morbi tristique senectus et netus et malesuada fames ac turpis egestas. Mauris ut leo. Cras viverra metus rhoncus sem. Nulla et lectus vestibulum urna fringilla ultrices. Phasellus eu tellus sit amet tortor gravida placerat. Integer sapien est, iaculis in, pretium quis, viverra ac, nunc. Praesent eget sem vel leo ultrices bibendum. Aenean faucibus. Morbi dolor nulla, malesuada eu, pulvinar at, mollis ac, nulla. Curabitur auctor semper nulla. Donec varius orci eget risus. Duis nibh mi, congue eu, accumsan eleifend, sagittis quis, diam. Duis eget orci sit amet orci dignissim rutrum.

Nam dui ligula, fringilla a, euismod sodales, sollicitudin vel, wisi. Morbi auctor lorem non justo. Nam lacus libero, pretium at, lobortis vitae, ultricies et, tellus. Donec aliquet, tortor sed accumsan bibendum, erat ligula aliquet magna, vitae ornare odio metus a mi. Morbi ac orci et nisl hendrerit mollis. Suspendisse ut massa. Cras nec ante. Pellentesque a nulla. Cum sociis natoque penatibus et magnis dis parturient montes, nascetur ridiculus mus. Aliquam tincidunt urna. Nulla ullamcorper vestibulum turpis. Pellentesque cursus luctus mauris.

Mots clefs :

Contents

Acknowledgements	v
Preface	vii
Abstract (English/Français/Deutsch)	ix
Contents	xiii
List of Figures	xix
List of Tables	xxiii
Index of notation	xxv
I Elastic gridshells	1
1 Elastic gridshells	3
1.1 Building free-forms	3
1.1.1 Non-standard forms	3
1.1.2 Importance of free-forms in modern architecture	3
1.1.3 Canonical approaches to build free-forms	3
1.1.4 Main challenges	3
1.1.5 Elastic gridshell : a definition	3
1.2 Elastic gridshells : a thorough project review	6
1.2.1 The beginnings : from the first prototype to the German Pavilion .	6
1.2.2 Mannheim Multihalle : the completion of a decade of research . .	10
1.2.3 The dry period : 25 years from Mannheim to Hannover	11
1.2.4 The signs of a renewal : Dorset and Doncaster	12
1.2.5 The renewal : Hannover, Downland and Savill	13
1.2.6 Gridshell in composite materials : a new perspective.	19
1.2.7 Flourishing timber gridshell pavilions	21
1.2.8 Recent experiments	22
1.3 Research works in the field of elastic gridshells : a review	24

Contents

1.3.1	Formfinding and structural analysis	24
1.3.2	Stability	24
1.3.3	Gridfinding	24
1.3.4	Morphology	24
1.3.5	New materials	24
1.3.6	Erection	24
1.3.7	Cladding	24
1.3.8	Rationalization	25
1.3.9	Robotisation	25
1.3.10	Structural optimisation	25
1.4	Gridshell structure : definition and classification	30
1.4.1	Historic overview	30
1.4.2	Rigid gridshell	30
1.5	Elastic gridshells : revisiting Mannheim	30
1.6	Elastic gridshells : the benefits of composite materials	30
1.6.1	Recent developments	31
1.6.2	Gridshell in composite material	31
1.7	References	35
2	Ephemeral cathedral : the first GFRP gridshell building	39
2.1	Introduction	39
2.1.1	Overview	39
2.1.2	Goals and contributions	40
2.1.3	Related work	40
2.2	Project overview	40
2.2.1	Context and challenges	40
2.2.2	Architectural considerations on the form	42
2.2.3	Placing of the building on the site	42
2.2.4	Entrance	43
2.2.5	Daylight	43
2.2.6	Technical description	43
2.3	Construction process	48
2.3.1	Assembly of the grid	48
2.3.2	Deformation of the grid	48
2.3.3	Bracing of the grid	48
2.3.4	Covering of the gridshell	50
2.4	Structural design	50
2.4.1	Overall design process	50
2.4.2	3D modelling of the intended shape	51
2.4.3	Meshing the surface	52
2.4.4	Formfinding and bending prestress	53
2.4.5	As-built geometry	57
2.4.6	Structural analysis	57
2.5	Designing with GFRP materials	59
2.5.1	Properties of the tubes	59

2.5.2	Codes for composite materials	59
2.5.3	Flexural strength of the tubes	61
2.5.4	Partial safety factors	61
2.6	Construction details	63
2.6.1	The swivel coupler	63
2.6.2	The sleeve system	69
2.6.3	Foundations	74
2.6.4	The membrane	74
2.7	Hygrothermal behavior	76
2.7.1	Temperature	76
2.7.2	Moisture	77
2.8	Cost analysis	80
2.8.1	Overall cost for the client	80
2.8.2	Cost details for the building	80
2.8.3	Strengths and weaknesses	81
2.9	Conclusions	90
2.10	Acknowledgements	90
2.11	References	91
II	Rich Kirchhoff beam model	93
3	Geometry of smooth and discrete space curves	95
3.1	Introduction	95
3.1.1	Goals and contributions	95
3.1.2	Related work	96
3.1.3	Overview	96
3.2	Parametric curves	96
3.2.1	Definition	96
3.2.2	Regularity	96
3.2.3	Reparametrization	97
3.2.4	Natural parametrization	97
3.2.5	Curve length	97
3.2.6	Arc length parametrization	97
3.3	Frenet trihedron	98
3.3.1	Tangent vector	98
3.3.2	Normal vector	99
3.3.3	Binormal vector	100
3.3.4	Osculating plane	100
3.4	Curves of double curvature	100
3.4.1	First invariant : the curvature	101
3.4.2	Second invariant : the torsion	103
3.4.3	Fundamental theorem of space curves	104
3.4.4	Serret-Frenet formulas	104
3.5	Curve framing	105

Contents

3.5.1	Moving frame	106
3.5.2	Adapted moving frame	108
3.5.3	Rotation-minimizing frame	109
3.5.4	Parallel transport	109
3.5.5	Frenet frame	110
3.5.6	Bishop frame	112
3.5.7	Comparison between Frenet and Bishop frames	114
3.6	Discrete curves	115
3.6.1	Definition	115
3.6.2	Regularity	117
3.6.3	Parametrization	117
3.7	Discrete curvature	118
3.7.1	Definition from osculating circles	118
3.7.2	Benchmarking : sensitivity to non uniform discretization	121
3.7.3	Benchmarking : accuracy in bending energy representation	123
3.8	Discrete tangent vector	126
3.8.1	Circumscribed case	127
3.8.2	Inscribed case	129
3.9	Discrete parallel transport	132
3.9.1	The rotation method	133
3.9.2	The double reflexion method	133
3.10	Conclusion	135
3.11	References	136
4	Elastic rod : variational approach	139
4.1	Introduction	139
4.1.1	Goals and contribution	139
4.1.2	Related work	139
4.1.3	Overview	139
4.2	Kirchhoff rod	140
4.2.1	Inextensibility	140
4.2.2	Euler-Bernouilli	140
4.2.3	Darboux vector	141
4.2.4	Curvatures and twist	141
4.2.5	Elastic energy	141
4.3	Curve-angle representation	142
4.3.1	Zero-twisting frame	142
4.4	Strains	143
4.4.1	Axial strain	143
4.4.2	Bending strain	143
4.4.3	Torsional strain	143
4.5	Elastic energy	144
4.6	Quasistatic assumption	144
4.7	Energy gradient with respect to θ : moment of torsion	145
4.7.1	Derivative of material directors with respect to θ	145

4.7.2	Derivative of the material curvatures vector with respect to θ	145
4.7.3	Computation of the moment of torsion	145
4.8	Energy gradient with respect to x : internal forces	147
4.8.1	Derivative of material directors with respect to x	147
4.8.2	Derivative of the material curvatures vector with respect to x	153
4.8.3	Computation of the forces acting on the centerline	153
4.9	Conclusion	156
4.10	References	158
5	Elastic rod : equilibrium approach	159
5.1	Introduction	159
5.1.1	Goals and contribution	159
5.1.2	Related work	159
5.1.3	Overview	160
5.2	Introduction to the special Cosserat theory of rods	162
5.2.1	Description of the motion	162
5.2.2	Time evolution	166
5.2.3	Strains	167
5.2.4	Parametrization of the centerline	167
5.2.5	To go further	168
5.3	Kirchhoff theory of rods	170
5.3.1	Description of the motion	172
5.3.2	Reparametrization	174
5.3.3	Strains	175
5.3.4	Balance of momentum	176
5.3.5	Equations of motion	182
5.3.6	Hookean elasticity	182
5.3.7	Deformation of cross-sections	183
5.3.8	Strain tensor	185
5.3.9	Stress tensor	185
5.3.10	Constitutive equations for internal forces and moments	185
5.3.11	Summary of the theory	187
5.3.12	Comments	189
5.4	Geometric interpretation of Kirchhoff's equations	191
5.5	Conclusion	198
5.6	References	199
6	Numerical Model	203
6.1	Introduction	203
6.1.1	Main hypothesis	203
6.1.2	Discret beam model	204
6.1.3	Modeling discontinuities	207
6.1.4	Matrix notation	207
6.1.5	Discret extension and axial force	208
6.1.6	Discret curvature and bending moment	209

Contents

6.1.7	Discret rate of twist and twisting moment	212
6.1.8	Discret shear force	213
6.1.9	Interpolation	214
6.2	Conclusion	214
6.3	References	216
III	Appendix	217
A	Calculus of variations	219
A.1	Introduction	219
A.2	Spaces	219
A.2.1	Normed space	219
A.2.2	Inner product space	219
A.2.3	Euclidean space	220
A.2.4	Banach space	220
A.2.5	Hilbert space	220
A.3	Derivative	221
A.3.1	Fréchet derivative	221
A.3.2	Gâteaux derivative	222
A.3.3	Useful properties	223
A.3.4	Partial derivative	223
A.4	Gradient vector	224
A.5	Jacobian matrix	224
A.6	Hessian	225
A.7	Functional	225
A.8	References	226
B	Parabolic interpolation	227
B.1	Introduction	227
B.2	Lagrange interpolating polynomial	227
B.3	Reparametrization	228
B.4	Characteristic values	228
B.5	Extremum value	229
Bibliography		231

List of Figures

1.1	Known elastic gridshells built by the past.	7
1.2	Steel gridshell built in 1962 in Berkeley, USA	8
1.3	Timber gridshell built in 1962 in Essen, Germany	9
1.4	Timber gridshell built in 1967 in Montreal, Canada	9
1.5	Timber gridshell built in 1962 in Essen, Germany	11
1.6	Roundwood gridshell built in 1995 in Dorset, England	13
1.7	Timber gridshells built in 1998 in Doncaster, England	13
1.8	Carboard gridshell built for Expo 2000 in Hannover, Germany	14
1.9	Timber gridshell built in 2003 in Downland, England	15
1.10	Timber gridshell built in 2002 in Pishwanton, England	16
1.11	Timber gridshell built in 2003 in Filmwell, England	17
1.12	Timber gridshell built in 2006 in Savill, England	18
1.13	Timber gridshell built in 2007 in Kent, England	19
1.14	GFRP gridshells built in 2007 and 2008 in Noisy-Champs, France	20
1.15	GFRP gridshell built in 2011 in Paris, France	20
1.16	GFRP gridshell built in 2013 in Cr��teil, France	21
1.17	Timber gridshells built by gridshell.it in Italy	21
1.18	Timber gridshells built in 2016 in France	22
1.19	Recent experiments built in 2016 in Champs-sur-Marne, France	23
1.20	Prototypes and projects of GFRP elastic gridshells.	30
1.21	Prototypes and projects of GFRP elastic gridshells.	33
1.22	Erection of the primary grid by two cranes	34
1.23	Erection plan and construction stages	34
2.1	Situation map	41
2.2	Architectural sketch	41
2.3	Exterior view	44
2.4	Interior view	44
2.5	Entrance	45
2.6	Key elements of the structural system	45
2.7	Transversal section of the building	47
2.8	Top view of the building	47

List of Figures

2.9	Construction process of the gridshell.	49
2.10	Benchmarking shapes regarding their curvature	51
2.11	How the compass method works	52
2.12	The compass method step by step	54
2.13	Each set of directrices leads to a different grid.	55
2.14	Meshing software as a plugin for <i>Grasshopper</i> .	56
2.15	Permanent bending stresses in the structure under self-weight	58
2.16	Reconstruction of the full 3D geometry	58
2.17	Flexural test of the GFRP tubes	62
2.18	Technical drawing of the swivel coupler	64
2.19	Influence of the interface layer on the sliding resistance	66
2.20	Influence of the tightening on the sliding resistance	67
2.21	Influence of the temperature on the sliding resistance	68
2.22	Technical drawing of the sleeve system.	69
2.23	Design and behavior of the the sleeve system	71
2.24	Typical failure modes when testing the sleeve system in traction	71
2.25	Tensile test of the pinned connection	72
2.26	Typical failure modes of a bolt in a pultruded element	73
2.27	Technical drawing of the footing.	75
2.28	Weather data at site location during opening hours	78
2.29	Temperature inside the building during opening hours	79
2.30	Cost allocation for the whole project	83
2.31	Cost allocation per square meter of covered area	83
2.32	Allocation of the man-hours spent by the volunteers	84
2.33	Cost allocation for masonry works	86
2.34	Cost allocation for the superstructure	88
3.1	Differential definition of Frenet's trihedron at given point P_0 .	99
3.2	Osculating circles for a spiral curve at different parameters.	101
3.3	Geometric torsion and rotation of the osculating plane. Note the existence of an inflexion point with a vanishing curvature and a discontinuity of both τ_f and the osculating plane.	105
3.4	Geometric interpretation of the angular velocity vector of a moving frame.	107
3.5	Adapted moving frame $F(s) = \{\mathbf{e}_3(s), \mathbf{e}_1(s), \mathbf{e}_2(s)\}$ where $\mathbf{e}_3(s) = \mathbf{t}(s)$.	108
3.7	Discrete curve representation and parametrization.	116
3.8	Several ways to define the osculating circle for discrete curves, leading to different notions of discrete curvature.	119
3.9	Review of several discrete curvature definitions mentioned in the literature.	119
3.10	Comparison of circumscribed (a-b) and inscribed (c-d) osculating circles for different values of the turning angle (φ).	122
3.11	Sensitivity of discrete curvatures to non uniform discretization ($\alpha \in [0.5, 2]$) over the whole domain of variation of the turning angle ($\varphi \in [0, \pi]$).	122
3.12	Discretization of a semicircle for discrete bending energies evaluation.	124

3.13	Relative error in the estimation of the smooth bending energy (\mathcal{E}) by the discrete bending energies (\mathcal{E}_1 and \mathcal{E}_3) regarding the sharpness of the discretization, for a semicircle.	124
3.14	Discretization (b) of a sequence of elastica curves (a) for discrete bending energies evaluation.	125
3.15	Relative error in the estimation of the smooth bending energy (\mathcal{E}) by the discrete bending energies (\mathcal{E}_1 and \mathcal{E}_3) regarding the sharpness of the discretization, for several elastica curves. The curves are chosen from fig. 3.14a (1,5,10,15,20,25,30).	125
3.16	Definition of the tangent vector (\mathbf{t}) and related curvature binormal vector ($\kappa\mathbf{b}$) at vertices (circumscribed definition).	128
3.17	Definition of the tangent vector (\mathbf{t}) and related curvature binormal vector ($\kappa\mathbf{b}$) at vertices (inscribed definition).	130
3.18	Parallel transport of vectors from $\{\mathbf{x}_i, \mathbf{t}_i\}$ to $\{\mathbf{x}_{i+1}, \mathbf{t}_{i+1}\}$	134
4.1	Repères de Frenet attachés à γ	148
4.2	F is obtained by rotating \tilde{F}_ϵ around \mathbf{t} of an angle Ψ_ϵ	149
4.3	\tilde{F}_ϵ is obtained by parallel transporting F_ϵ from \mathbf{t}_ϵ to \mathbf{t} . This operation could be seen as a rotation around $\mathbf{t}_\epsilon \times \mathbf{t}$ of an angle α_ϵ	149
5.1	Description of the motion for a Cosserat rod : longitudinal section	164
5.2	Description of the motion for a Cosserat rod : transverse section	165
5.3	Internal forces (\mathbf{F}) and moments (\mathbf{M}) acting on an infinitesimal beam slice of length ds . The beam is also subject to distributed external forces (\mathbf{f}) and moments (\mathbf{m}).	177
5.4	Typical deformation modes of cross-sections in Kirchhoff's theory	184
5.5	Flexion and torsion of an elementary slice of a Kirchhoff rod of length ds . Projections of the deformations are given in the material planes defined by $\mathbf{d}_1, \mathbf{d}_2, \mathbf{d}_3$	191
5.6	Influence of the curvature (κ) in the deflection of internal forces and moments along the centerline.	192
5.7	Influence of the first material curvature (κ_1) in the deflection of internal forces and moments along the centerline.	194
5.8	Influence of the second material curvature (κ_2) in the deflection of internal forces and moments along the centerline.	196
6.1	Biarc model for a discrete beam. The centerline is divided into curved segments (grey solid hatch). Each segment is defined as a three-noded element with uniform material and section properties. It has two end vertices (white) called <i>handle</i> as they are used to interact with the model, for instance to apply loads or restraints. It has one mid vertex (grey) called <i>ghost</i> as it is used only to enrich the segment kinematics and is not accessible to the end user.	205

List of Tables

1.1	Key numbers	27
1.2	Key numbers	28
1.3	Key numbers	29
2.1	Key numbers	46
2.2	Technical properties of the tube.	60
2.3	Technical properties of the membrane.	60
2.4	Flexural tests of the GFRP tubes	61
2.5	Short-term and long-term values for material resistance	63
2.6	Man-hours spent by the volunteers on the fabrication	85
2.7	Cost details for masonry works	87
2.8	Cost details for the superstructure	89
5.1	Summary of the notations	169

Index of notation

Geometry of curves

- t The unit tangent vector.
 n The unit normal vector.
 b The unit binormal vector.
 τ_f The torsion of Frenet.
 κb The curvature binormal vector.
 Ω The darboux vector.

Mechanics of rods

- $\gamma, \bar{\gamma}$ Centerline curve – reference configuration.
 γ The centerline curve – actual configuration.
 s The arc length of the centerline – reference configuration.
 s_t The arc length of the centerline – actual configuration.
 \bar{x} The centerline position vector – reference configuration.
 x The centerline position vector – actual configuration.
 $\bar{\nu}$ The force strain vector – reference configuration.
 ν The force strain vector – actual configuration.
 $\bar{\varkappa}$ The material curvature (or moment strain) vector – reference configuration.
 \varkappa The material curvature (or moment strain) vector – actual configuration.
 \mathcal{E}_s The streching energy.
 \mathcal{E}_b The bending energy.
 \mathcal{E}_t The twisting energy.

Elastic gridshells Part I

1 Elastic gridshells

1.1 Building free-forms

- 1.1.1 Non-standard forms
- 1.1.2 Importance of free-forms in modern architecture
- 1.1.3 Canonical approaches to build free-forms
- 1.1.4 Main challenges
- 1.1.5 Elastic gridshell : a definition

The invention of the gridshell concept is commonly attributed to Frei Otto, a German architect who devoted several years to gridshells. In 1975 he achieved the famous *Mannheim Multihalle* [HL75], a wooden shell of 7500 m², in collaboration with the engineer Edmund Happold (Arup). Literally, the word “gridshell” refers to grids behaving like shells : from a mechanical point of view that means stresses acting on the structure are mainly transmitted through compression and traction. These structures can cross large-span with very little material.

However, according to the historic evolution of the concept, characterizing a gridshell as the combination of a structural concept – a grid behaving like a shell – and a specific construction process – using the bending flexibility of the material – seems to be more accurate. The Mannheim project (in which a wooden regular and planar grid, lacking shear stiffness, is elastically deformed up to a targeted shape with the help of stays, and then braced and covered) is regarded as the starting point of this new concept.

The Mannheim project is regarded as the starting point of this new concept for which a wooden regular and planar grid, lacking shear stiffness, is elastically deformed up to a targeted shape with the help of stays, and then braced and covered. This type of gridshell,

known as elastic gridshell, offers a very elegant manner to materialize freeform shapes from an initially flat and regular grid, which obviously has many practical benefits: planar geometry, standard connection nodes, standard profiles and so on.

At present, the architectural significance of grid shells can hardly be fully envisioned. Too little experience has been gained as yet. However, the first signs of a grid shell architecture are already apparent. The projects planned and executed to date and the results of this research work indicate possibilities that open up a wide field of applications for grid shells. Two things stand out above all. The first is the nearly unlimited variety of forms that can be realized with grid shells, the second is the fact that there is no closed shell surface, but rather a simple, spatially curved grid composed of rods. Both features are of fundamental significance. They fully characterize the architectural essence of the grid shell support structure. [BHS74, p. 250]

“From the inverted form to the gridshell” [BHS74, p. 179]

1.2 Elastic gridshells : a thorough project review

No thorough historic review is available about executed projects of elastic gridshells although some partial reviews have been done time to time on the occasion of scientific works or construction projects. This review aims at filling this gap by giving an overview of the development of the concept from the very beginning to the very last experiments. Only known built projects have been identified and reported here. The only condition for a project to belong to this review is to comply with the definition of what an elastic gridshell is (see ??), independently to any other consideration (material, fabrication, size, cladding, ...).

The informations collected during this research work are given in table format in appendix (see ??). A synthetic presentation of these datas is proposed to the reader in fig. 1.1, where projects are ordered by date, span, covered area and material.

The books edited by the *Institut für leichte Flächentragwerke* are of great interest to understand the beginnings. *IL10 Grid Shells* [BHS74] has a precise inventory of the first experiments from 1962 to 1976, while *IL13 Multihalle Mannheim* [Bur+78] focuses on the construction of the Multihalle in Mannheim. *Timber Gridshells: Architecture, structure and craft* [CT17] is a significant effort but focuses exclusively on medium to large scale projects in timber. A small but general partial review is also available in [CC16]. An interesting review is also given by Quinn and Gengnagel [QG14] as part of his research work on new erection methods. A review of bracing and cladding systems is done in [Cuv+17]. A review of formfinding methods is done in [Kim16]. Finally, various valuable reviews are available in the thesis by Douthe [Dou07], Bouhana [Bou10], Tayeb [Tay15], and Lafuente Hernández [Laf15].

1.2.1 The beginnings : from the first prototype to the German Pavilion

Frei Otto started his studies in architecture in 1947 in Berlin, Germany, and completed his doctorate on tensile structures in 1953. This first work was published and translated later in the 60's. He then began to work in the field of lightweight structures using physical models such as soap films or hanging nets, and photographic measurements.^{1,2} These tools were essentials for his exploration of forms and structures as there were no computers at that time.

¹In the 19th and 20th centuries model testing was at the heart of structural innovation [Add13]. Analog models were employed successfully by well-known architects and engineers to go beyond the limits of existing knowledge (A. Gaudi, H. Isler, F. Candela, F. Otto, ...) and are still employed today where numeric models failed to represent accurately some physical phenomena (for instance in wind analysis for high rise towers and bridges).

²“Photography is the medium through which the form and content of a model are communicated. It is one of our most important tools in that it provides the basis for documentation and information, supplements our creative potential [...]” [BHS74, p. 56]

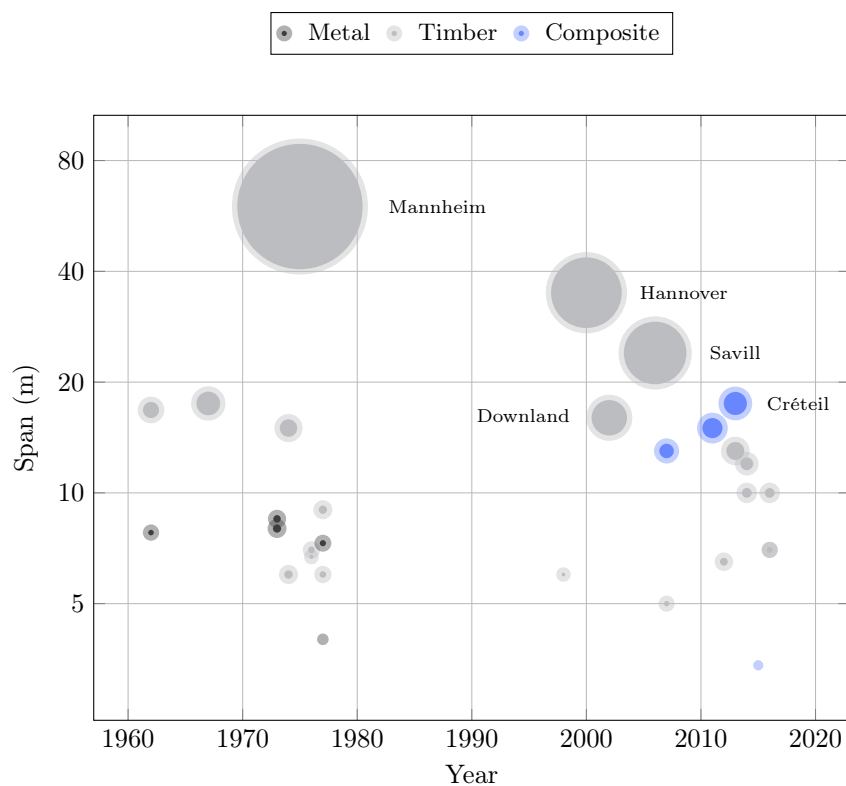
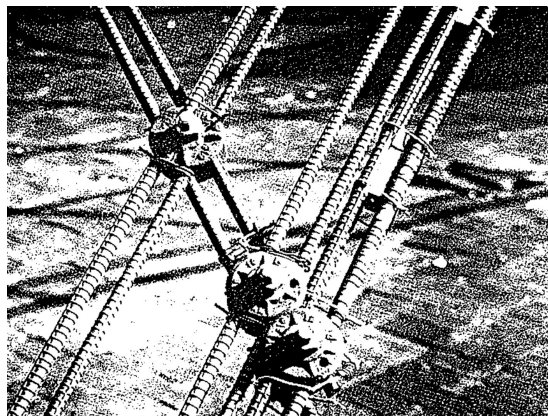


Figure 1.1 – Known elastic gridshells built by the past. The surface of the bubbles is proportional to the covered area. Color indicates the material employed for the rods.



(a) Knot detail



(b) Steel lattice

Figure 1.2 – Steel gridshell built in 1962 in Berkeley, USA.

Steel Gridshell, Berkeley, USA, 1962

Simultaneously, he became interested by the study of lightweight shells and the way they were form-found. One of his very first elastic gridshell was built in 1962 with students at Berkeley, USA [BHS74, p. 270]. It is funny to remark that this first gridshell was not a timber gridshell but a steel gridshell made out of twin steel rods linked in a grid fashion by bolts with clamping plates (see fig. 1.2a). This first experiment demonstrated at small scale the ability to bend a regular grid with no shear rigidity into a curved shape (see fig. 1.2b). The grid was loosely braced and shell effects were not investigated.

Essen Gridshell, Essen, Germany, 1962

The same year he designed and built a first timber gridshell at Essen, Germany [BHS74, p. 272]. The prototype – a single-layer gridshell spanning 17 m and covering an area of 198 m² – was made with 3-ply laminated timber profiles in hemlock pine (see fig. 1.3a). The cross-section of the profiles was rectangular (60 mm x 40 mm) and the elements were assembled in a grid fashion with simple steel bolts. Once erected, nothing was specifically done to improve the in-plane shear stiffness of the grid and activate a shell behavior. Finally, the structure was covered with a transparent plastic foil nailed directly on the grid's profiles (see fig. 1.3b).

German Pavilion Auditoria, Montreal, Canada, 1967

Fiver years later, on the occasion of the *1967 International and Universal Exposition* in Montreal, Canada, Frei Otto was appointed to design the German Pavilion : a large cable net tent prefiguring the realization of the olympic stadium of Munich, Germany, in

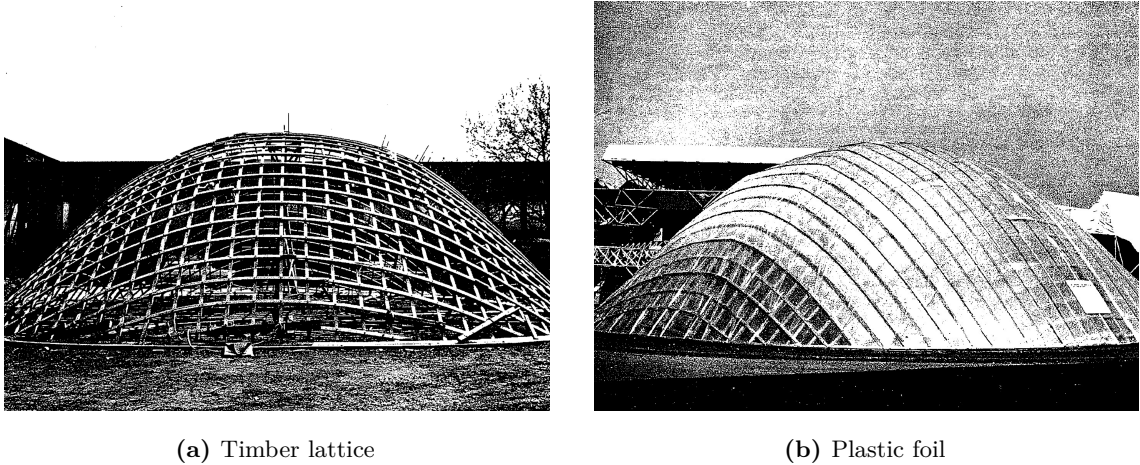


Figure 1.3 – Timber gridshell built in 1962 in Essen, Germany.

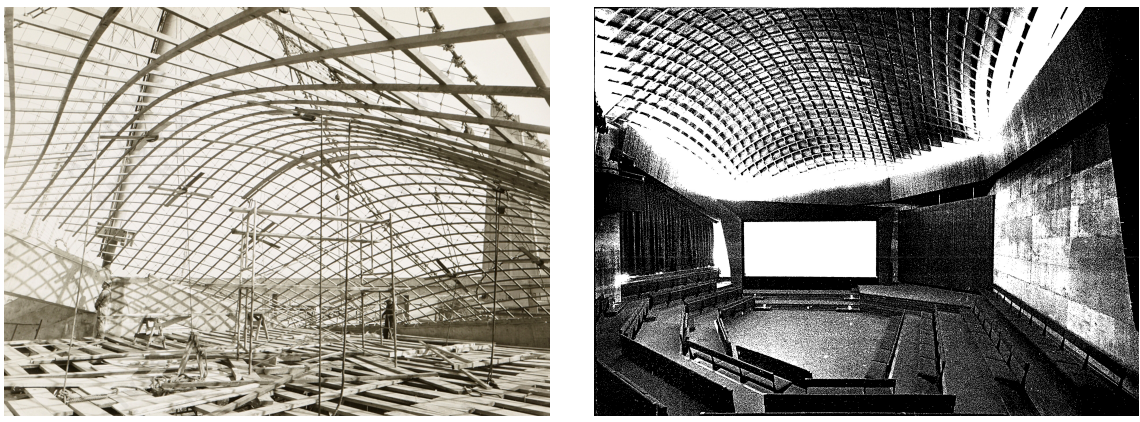


Figure 1.4 – Timber gridshell built in 1967 in Montreal, Canada.

1972.³ The pavilion required two auditoria and these were designed using the principle of elastic gridshell [BHS74, p. 274]. All together, the auditoria covered an area of 365 m² and spanned 17.5 m. The construction technique employed in Montreal was quite similar to the one developed in Essen, but this time the grid was fully braced with a layer of nailed plywood boards and offered a proper roofing made out of insulation panels covered with a PVC coated fabric (see figures 1.4a and 1.4b).

The two gridshells built in Montreal mark a significant step in the maturation process of the technique leading to the major realization of Mannheim in 1976 : a methodology has emerged to progress “from the inverted form to the gridshell” [BHS74, p. 179] ; main

³Actually, Frei Otto became the director of the newly founded *Institute for Lightweight Structures* (Institut für Leichte Flächentragwerke or IL) at the University of Stuttgart in 1964. It was the IL that was commissioned by the German government to conduct research in connection with the planning of the German pavilion for the exposition in Montreal.

construction details have been validated ; various erection methods have been tested ; mid-scale buildings have been built to host public. However, due to the over complexity of these structures, lots of unknowns remained unsolved at this stage and the behavior of the structures could not be fully predicted.⁴

It is worth to mention that several unexecuted large-scale projects were studied by Frei Otto between 1967 and 1973 at the *IL* or at the *Atelier Warmbronn*.⁵ These projects are basically documented in [BHS74, pp. 278 - 288] and reveal that he was training his capacity to master large-scale projects with the technique of elastic gridshells for more conventional building projects (wave pool, swimming hall, multi-purpose hall, auditorium, . . .).

1.2.2 Mannheim Multihalle : the completion of a decade of research

The project of the Multihalle started in 1970, when the decision was made that Mannheim, Germany, would hold the Bundesgartenschau in 1975.⁶ The architects of the project, *Carl Mutschler & Partners*, consulted Frei Otto at *Atelier Warmbronn* as he was starting to get known in the field of innovative lightweight structures. This is how the idea of the gridshell was introduced in the project [Lid15].

A thorough report on the project is available in [Bur+78]. A more condensed but still precise description of the engineering problematics related to this projects are available in the excellent papers from Happold and Liddell [HL75] and Liddell [Lid15].

Mannheim Multihalle, Mannheim, Germany, 1975

Mannheim is an unprecedented realization because it is more than twenty times larger than the previously built gridshells in Montreal and is meant to last many years and not only for the duration of a short-term exhibition. The timber lattice, still existing in 2017, covers an area of 7400 m² (see fig. 1.5b). It is composed of two interconnected domes, one for the multi-purpose hall (span : 60 m | height : 20 m) and one for the restaurant (span : 50 m | height : 18 m).

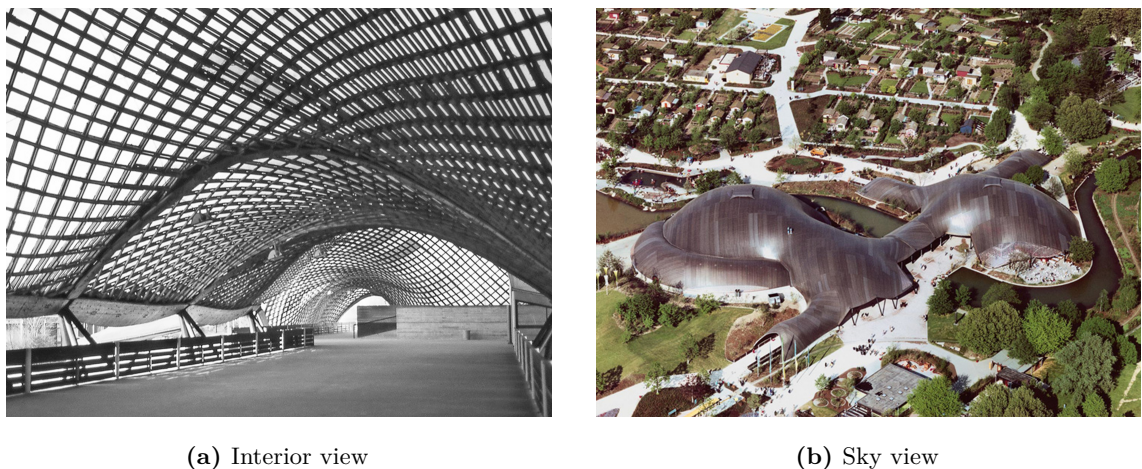
Although the constructif system deployed at Mannheim clearly inherited from the previous developments, the challenge was such that it had to be revisited. In particular the main additions were the introduction of the double-layer system and the proper bracing of the grid. A major advance was also the use of the very first numeric models to study the structure.

The double-layer system was introduced to tackle two issues : the grid needed some

⁴“Snow accumulations in the throat of the common edge beam probably caused one of the two grid shells of project Montreal to buckle in a relatively flat region. The diameter of the buckled area was about 3 meters. Neither grid rod was broken, i.e. the buckling progressed elastically. It might have been possible to press the buckled area back into shape.” [BHS74, p. 219]

⁵Atelier Warmbronn is the architectural studio founded by Frei Otto in 1969.

⁶The Bundesgartenschau is a national horticultural exhibition that takes place every two years in Germany.



(a) Interior view

(b) Sky view

Figure 1.5 – Timber gridshell built in 1975 in Mannheim, Germany.

flexibility to be bent into the desired shape, but once erected it should provide sufficient bending stiffness to resist disturbing loads and avoid a buckling collapse.⁷ One erected, the two grids, one sliding on top of the other one, were connected together to form a single grid with much higher ladder profiles (from 50 mm to 150 mm), increasing their bending stiffness by 26 (see fig. 1.5a).

Because the in-plane stiffness of the grid also plays a major role in the resistance to buckling, this question was considered with care. The bracing of the grid was first achieved by preventing the nodes to turn once the grid was erected. This was done by creating some friction in the nodes when tightening the bolts linking the laths, after the grid was erected. Additional bracing cables were put in the grid.

Finally, the project of Mannheim was a key project in the development of modern lightweight structures. Great engineers were born in touch with Frei Otto, following its footsteps or collaborating with him. This heritage has irrigated for several decades the engineering of lightweight structures in Europe and gave birth, directly or indirectly, to several studios among which we can cite *Buro Happold*, *Schlaich Bergermann & Partner* and *RFR*.

1.2.3 The dry period : 25 years from Mannheim to Hannover

Although the experience of Mannheim proved the feasibility and the potential of gridshell structures for large-scale projects, it also revealed that these projects were subject to an incredible complexity in terms of structural design, geometry, modeling, testing, team work, construction methods, ... At that time, very few people could pretend to master all the knowledge and techniques required to design and built timber gridshells and developed in the bosom of the *Institute for Lightweight Structures* in Stuttgart.

⁷Theoretically, self-weight loads would produce only compression in the members because the (funicular) form of the grid resulted from the inversion of a hanging chain model in pure tension.

This project was obviously well ahead of its time and the engineering cost to design such structures was probably prohibitive considering the tools available at that time. This certainly explains why no elastic gridshells were built during the 25 following years, despite the optimism of the pioneers of the Multihalle.⁸

Note that around 1975 small workshop and experiments lead to the construction of several but small elastic gridshells, as reported in [BHS74]. A non-exhaustive but quite extensive list of known executed gridshell projects is presented in fig. 1.1. The dry period is clearly visible.

1.2.4 The signs of a renewal : Dorset and Doncaster

It is only 20 years later that gridshells started to reappear, in the late 90's mainly in the United Kingdom, and for projects that had interest in environmental problematics.

Westminster Lodge, Dorset, England, 1995

In 1995, a small student residence named *Westminster Lodge* was built in Dorset, England. This dwelling was part of a larger project – Hooke Park – aiming at investigating how the local forest resources, in particular immature roundwood thinnings, could be better utilized. The project was lead by ABK, Frei Otto, Buro Happold and Cullinan Studio. Unlike Mannheim, the timber shell was bent and weaved rod by rod on a scaffold platform. But the structural system exhibited a double-layer gridshell pattern very similar to the one employed for the Multihalle (see fig. 1.6a). The rods were made out of splice-jointed roundwood to form long-length poles of diameter 200 mm. The development of this jointing technique, which could be produced directly in the forest, was part of the project's investigations [BDH98]. The grid was braced by a layer of diagonal boards nailed to the roundwoods. The structure was finally cladded with a planted turf roof (see fig. 1.6b).

Earth Center, Doncaster, England, 1998

At the same time, a project of a similar spirit arose for the *Earth Center* in Doncaster, England.⁹ The project planning started in 1994 and a series of small timber gridshells were designed by Buro Happold and then built in 1998. The landscape structures were single-layer timber gridshells made with oak laths. Once erected with a crane, the grids were braced with crossing diagonal stainless steel cables (see fig. 1.7a). Openings were possibly reinforced with curved timber frames (see fig. 1.7b).

These projects definitely trailed the technique in England and initiated the renewal period

⁸“For many years after its completion, Happold promoted the benefit of the timber gridshell as a construction technique and stated that he could not understand why it had not been adopted more widely. He perceived the benefits to be in the efficiency of the construction method to enable doubly curved (shell) structures to be constructed quickly and cost effectively.” [Har+03].

⁹“The Earth Centre Forest Garden was intended to demonstrate how managed woodland could supply the vast majority of all natural resources needed for human survival.”



(a) Interior view

(b) Exterior view

Figure 1.6 – Roundwood gridshell built in 1995 in Dorset, England.



(a) Interior view

(b) Exterior view

Figure 1.7 – Timber gridshells built in 1998 in Doncaster, England

(see §1.2.5). Although they remained small-scale projects for which modeling was achieved through physical models, they trained and restored partially the operational ability of Buro Happold to design timber gridshells as pointed by Harris et al. [Har+03].

1.2.5 The renewal : Hannover, Downland and Savill

What was missing for elastic gridshells to re-emerge after the major experiment of Mannheim was probably the development of modern numeric tools to ease and speed up the design process.¹⁰ Amongst those tools we should identify two main categories : geometry processing

¹⁰“The key to the modern use of timber gridshells is the development of computer methods in modelling complex three-dimensional shell structures. For the Mannheim structure, the primary method of form finding was the use of physical models. The Earth Centre structures were small and easily modelled using wire mesh, but when Buro Happold were commissioned to design the Japanese Pavilion for Expo 2000 in Hannover (Architect Shigeru Ban), it was apparent that much more sophisticated computer form finding



(a) Interior view



(b) Sky view

Figure 1.8 – Carboard gridshell built for Expo 2000 in Hannover, Germany.

softwares and structural analysis softwares. Recall that in the 70's, geometry processing was done through physical models and photographic measurements [BHS74, pp. 130-135] while structural analysis was conducted through a compound of physical model testing with scaling techniques [Bur+78, pp. 130-135], hand calculations and the very first numerical formfinding calculations [BHS74, pp. 184-193] and finite element calculations [BHS74, pp. 210-217].

In the late 90's, the rise in importance of computer methods offered new possibilities.

Japan Pavilion, Hannover, Germany, 2000

In 1997, architecte Shigeru Ban began to collaborate with Frei Otto and Buro Happold to design the *Japan Pavilion* for *Expo 2000* in Hannover, Germany [MOB06]. This pavilion was a large-scale corrugated gridshell made out of cardboard tubes, about 75 meters long and 25 meters wide. Corrugations bring curvature, and therefore enhance the strength of the shell. The tubes were tied together with a fabric tape, a very low-tech joint (see fig. 1.8a). The structure was covered with a paper membrane specially developed for the project to meet the requirements of the german fire regulations (see fig. 1.8b). For the occasion, a new erection method was set up in which the grid was laid out not at the ground level but at a higher level on a hydraulic scaffold platform. From there, the grid was pushed up into position using the platform's jacks. It was found late that the cardboard tubes were subject to a high level of creep. This required the introduction of new timber arches to reinforce the gridshell and to enlarge the existing timber rafters intended to brace the grid and support the paper membrane (see fig. 1.8a).

and analysis would be necessary." [Har+03]

Weald and Downland, Downland, England, 2002

The design of the *Downland* gridshell began right after the completion of the Westminster Lodge (see §1.2.4) where architects from E. Cullinan Studio became acquainted with the engineers from Buro Happold. At Downland, the project team truly revived the technique of large-scale timber gridshells while bringing lots of improvements to the system. The building opened to the public in 2002. Its corrugated shape recalls the one of the Japan Pavilion from which it was inspired (see fig. 1.9b).

The building is 50 meters long and 12.5 to 16 meters wide, covering an area of about 675 m^2 for a height varying from 7 to 9.5 meters [HK02]. The structure is a double-layer gridshell made of rectangular oak laths of cross-section 50 mm x 35 mm (see fig. 1.9a). To produce high grade timber elements, the continuous laths were re-formed from small carefully selected wood pieces, finger-jointed every 60 cm in 6.0 m length pieces. These pieces of lath were then scarf-jointed on site every 6 m to obtain the desired length, up to 50 m.

The grid pitch is 1.0 m except in weaker areas where it is 0.5 m. There, the grid is twice denser to achieve the required buckling resistance [Har+03]. Rib-lath bracing was preferred to steel cable bracing as ribs were deemed to offer a more convenient support for the cladding elements and to reduce the complexity of the connection. A new connection system was developed to avoid the cost of drilling thousands of slotted holes that would, in addition, reduce the cross-section area, while maintaining the required scissor behavior for the deformation of the timber lattice.¹¹



(a) Interior view



(b) Exterior view

Figure 1.9 – Timber gridshell built in 2003 in Downland, England.

The flat lattice was laid out on a scaffold platform. Unlike the Japan Pavilion, the lattice was progressively lowered down into position. This stage took 6 weeks. Once deformed, the shear blocks were introduced in the grid and bracing rib-laths were installed, giving its full

¹¹This detail was patented by the design team and the client.

strength to the shell. Finally the gridshell was cladded with a mix of polycarbonate plates (to let the light in) and timber boards on top of insulation panels and a rain screen.

It is worth to mentionne that for the first time the form was not found by inverting some sort of hanging chain model that would produce a pure funicular shape where only compression occurred. Instead, the shape was the result of a numerical computation that took into account the bending behavior of the laths.¹² Harris et al. [Har+03] argued that computer models enabled some interactivity in the formfinding process that would not be possible with physical models, leading to a better synergy between architectural and structural requirements. They also argued that physical models contributed invaluable to the development of a creative and efficient design throughout the project.

Lothian Gridshell, Pishwanton, Scotland, 2002

This project deserves somme attention because the developed approach was completely different from the projects exposed until now : “Previous projects have portrayed the method as a highly technical use of a low tech resource. This, however, need not be the case as we see with this project [...]” [Low02]. The structure was the result of : “[...] an unusual collaboration between sole practitioner Christopher Day, engineer David Tasker, a crowd of local volunteers and (more unusually) the philosophies of Rudolf Steiner and Johann Wolfgang Goethe” [Bdo02].¹³.



(a) Interior view



(b) Exterior view

Figure 1.10 – Timber gridshell built in 2002 in Pishwanton, England.

The single-layer gridshell was made out of local larch. Once erected by hands, the dome-like shape covered about 80 m^2 and spanned 10 meters. The grid was braced with timber boards (see fig. 1.10a) and covered with a planted turf roof (see fig. 1.10b). Some calculations were made but in the end, it had to carry load testing to prove its safety and gain its regulation

¹²This software was developed by Chris Williams of the University of Bath.

¹³From the online paper “The other gridshell” : <http://www.bdonline.co.uk/the-other-gridshell/1020435.article>

approval.¹⁴

Woodland Centre, Filmwell, England, 2003

The gridshell of the Woodland Center was built 7 years after the project had started.¹⁵ The building was designed by architect Feilden Clegg and engineers from Atelier One. It was part of a larger research and development project that aimed at developing chestnut – a low grade wood – as a construction material.¹⁶ The building, still existing, is composed of 5 barrel vaults spanning 12 meters and about 5 meters wide. Therefore, it covers about 300 m² [Low04]. Each vault module is a transportable unit composed of two curved arches. A single layer gridshell was then applied to this primary frame and braced with chestnut panels. The grid was made of laths with 75 mm x 25 mm rectangular cross-section, assembled with simple bolts. On top of that, insulation materials and a membrane as rainscreen [Fou03].



(a) Interior view



(b) Exterior view

Figure 1.11 – Timber gridshell built in 2003 in Filmwell, England.

Savill Garden, Savill, England, 2006

This project saw the light of day thanks to the reputation of the gridshell built in Downland. Again, Buro Happold did the structural design while Green Oak Carpentry realized it. But this time, the architect was Glenn Howells.

The *Savill* gridshell is 90 meters long and 25 meters wide. It covers an area of about 2000 m², and is therefore almost three times larger than the gridshell in Downland. Once again, the

¹⁴“There were a lot of calculations but no computer-generated models to show they all added up. In fact, the form was previously established with scale models. When it came to gaining Building Regulations approval, the team needed to prove that the building would be strong enough. So Tasker arranged for the unfinished structure to be loaded with about 18 tonnes of sand from a local quarry – equivalent to the maximum predicted snow load, plus a safety factor.” [Bdo02]

¹⁵More to be found at : [Growing and making Flimwell's chestnut gridshell](#).

¹⁶This project was conducted by the [Building Research Establishment](#).



(a) Interior view



(b) Exterior view

Figure 1.12 – Timber gridshell built in 2006 in Savill, England.

corrugated shape was defined by a parametric equation ($z = f(x, y)$) to enable interactivity between architects and engineers during the formfinding process (see fig. 1.12b). Chris Williams was responsible for this job.

In Savill, the forming strategy was quite different than those employed in Mannheim, Hannover or Downland [HHR08]. Firstly, a single layer gridshell – constituted by the bottom two laths jointed with simple bolts – was deformed into the target shape. Secondly, the shear blocks were screwed on these laths. Thirdly, the upper two laths were positioned and screwed on top of the shear blocks to re-form a double-layer gridshell. Finally, the grid was then braced with two alternate layers of plywood boards, 12 mm thick each. Bracing the grid with continuous panels instead of cables or diagonal elements was a major architectural choice (see fig. 1.12a). Moreover, it gave a well-defined surface for the cladding composed of 160 mm of insulation, covered by a waterproof aluminium layer made with standing-seam profiles supporting the oak boards [Tra06].

Another consequence of this forming process was the drastic simplification of the connexion. The system developed for Downland was of no utility in that case and only simple bolts and screws were required. In this project, the pitch of this grid is 1.0 m. The 20 kms of laths are made from larch and have a 80 mm x 50 mm rectangular cross-section. They are spaced from 100 mm to 150 mm by the shear blocks.

Of course, the steel perimeter is a major component of the project but is not in the scope of this thesis. For further details the reader is invited to refer to Harris et al. [HHR08] and Trada [Tra06].

Chiddingstone Castle Orangery, Kent, England, 2007

The gridshell covering the orangery of Chiddingstone Castle is a very small one. Built in 2007, it is 12 meters long, 5 meters wide and covers about 50 m² (see fig. 1.13b). The

structural system is derived from the one employed in Downland and is, once again, developed by Buro Happold and the Green Oak Caprentery. But this time the architecte is Peter Hulbert.



Figure 1.13 – Timber gridshell built in 2007 in Kent, England.

However this project embed some interesting innovations. Indeed, this time the gridshell is braced with a bidirectional cable network. Twin cables are employed to facilitate clamping on the node connection, which has been adapted from the previous version developed in Downland. Moreover, this connection is equipped with an additional threaded hole which can receive the clamping supports for the glazing (see [fig. 1.13a](#)). The timber shell is then glazed with triangular panels (note that the mesh quadrangles are not planar any more in the deformed configuration).

1.2.6 Gridshell in composite materials : a new perspective.

Starting from 2002, the laboratory [Navier](#) from the Ecole des Ponts ParisTech started a research program on elastic gridshells that is still ongoing. It focuses on both the use of new materials such as composite materials and the development of modern computer methods for the shape generation, the formfinding and the structural analysis.

Indeed, composite materials in glass fiber reinforced polymers (GFRP) are very suitable for this type of structures where both flexibility and strength of the profiles are required. On the level of mechanic behavior they surpass wood. And they are easy and cheap to produce in long length when they are manufactured by pultrusion, avoiding complex jointing issues.

GFRP Gridshell Prototypes, Champs-sur-Marne, France, 2007-2008

These developments have been validated by the construction of two prototypes (Figures [3.10da](#) and [3.10db](#)) covering were about 150 m^2 .



(a) First prototype (2007)



(b) Second prototype (2008)

Figure 1.14 – GFRP gridshells built in 2007 and 2008 in Noisy-Champs, France.

Solidays, Champs sur Marne, France, 2011

In 2011, the laboratory used its expert knowledge for a large-scale project [Bav+12], the forum of the Solidays festival (3.10d). This achievement, built by voluntary workers, has been the first composite material gridshell to house public.



(a) First prototype (2007)



(b) Second prototype (2008)

Figure 1.15 – GFRP gridshell built in 2011 in Paris, France.

Ephemeral Cathedral, Créteil, France, 2013

In 2012, the context is favorable for a new achievement named "*Temporary Cathedral of Créteil*". Although this gridshell has an area very similar to the Solidays one, the project raised new challenges, in particular the challenge of reliability. Indeed, its period of use is at least two years. Additionally, the skills coming from T/E/S/S company made possible important developments such as for doors, lacing edge beam, anchorages and sleeves.

1.2. Elastic gridshells : a thorough project review

Unlike the two first prototypes, the gridshells built for Solidays and at Créteil are based on a new approach regarding shape-structure relationship. Indeed, thanks to a numerical tool performing the compass method, the geometry of the object is no longer defined as the reversal of a hanging net – in this case, only the flat geometry could be mastered [Add13] – but now the flat geometry is straight deducted from the one proposed by the architect. This new approach opens up new architectural horizons, making possible the exploration of new shapes for gridshells.



(a) Interior view



(b) Exterior view

Figure 1.16 – GFRP gridshell built in 2013 in Créteil, France.

1.2.7 Flourishing timber gridshell pavilions

The impetus given by gridshell.it

Starting from Lecce, Italy, 2010 About 12 structures of small size.



(a) Lecce, 2010



(b) Toledo 2.0, 2014

Figure 1.17 – Timber gridshells built by gridshell.it in Italy.

Other similar timber pavilions

Uta, ZA,

The inputs from the laboratory Navier

Same constructive system but a reflexion on bracing (with cables and how to put tension in the cables. Also, generally they were made by a simple grid pattern (cross pattern or square with cutting corners.) Here the grids were exhibited from the compass method and the a formfinding tool developed by Navier. Computation were studied with GSA. Terrell. Wood testing were done by Navier with consultancy over detailing. Wood specification. Cross-section and specification of the system (grid pitch, number of layers, shear blocks, cross section of the laths, formfinding, timber specification).

Fist time that the same grid blocks are recombined in a new shape.



(a) Toulouse



(b) Montpellier

Figure 1.18 – Timber gridshells built in 2016 in France.

Toledo 1 : [DKZ14] Toledo 2 : [DAm+15a]

1.2.8 Recent experiments



(a) Robotic manufacturing



(b) Concrete bracing envelop

Figure 1.19 – Recent experiments built in 2016 in Champs-sur-Marne, France.

1.3 Research works in the field of elastic gridshells : a review

[Lab+16, FKB16]

1.3.1 Formfinding and structural analysis

Les méthodes numériques de Day, Barnes, Adriaenssen, Douthe, Lefevre, Tayeb 3/6/4 DOF, prise en compte de la torsion. Adriaenssens et al. [ABW99] and Adriaenssens and Barnes [AB01] [BAK13] [DKZ14] [DZK16] [Pou15] [Kim16]

[dPel+15] Malek [Mal12]

1.3.2 Stability

Flambement (Malek, Mesnil, Lefevre) **Mesnil2013** Mesnil et al. [MOD15] Mesnil et al. [Mes+17] Lefevre et al. [LDB15] Tayeb et al. [Tay+13]

1.3.3 Gridfinding

Le formfinding vs. grid finding (COmpas Lionel, Compas Baptise, GFFT, Compas Yannick singularité, Lina) Elisa Fuentes

[Pon+16] [dPel+11] [Laf15] [MM17]

1.3.4 Morphology

[Dou+16] [JBD13] Mesnil Description analytique de la forme (C. Williams)

1.3.5 New materials

Les matériaux composites

1.3.6 Erection

Les méthodes de montage. L'inflatable(Otto, Pugnale, Quinn) [BHS74] [QG14] [LP15] Liuti et al. [LPD16]

1.3.7 Cladding

Une reflexion sur l'enveloppe (booby ENPC). Lafuente Hernández and Gengnagel [LG14] Cuvilliers et al. [Cuv+17] [FN15]

1.3.8 Rationalization

La simplification (gridshell.it => ZA, UTSA, Cluj, quaternion + Navier, Navier)

1.3.9 Robotisation

La robotisation de la production (ENPC) [MKS16] ZA

1.3.10 Structural optimisation

Optimisation des sections [DAm+15b]

Des pistes ouvertes

N	Nickname	Year	City	Country	Type	Architecte	Engineer	Ref
1	Berkeley	1962	Berkeley	USA	Prototype	F. Otto	F. Otto	[BHS74]
2	Essen	1962	Essen	Germany	Pavilion	F. Otto	F. Otto	[BHS74]
3	German Pavilion	1967	Montreal	Canada	Pavilion	F. Otto	F. Otto	[BHS74]
4	Seibu	1973	hannover	Japan	Prototype	K. Matsushita	T. Shirayanagi	[Bur+78, p. 245]
5	Ahmedabad	1976	Ahmedabad	India	Building	G. Sarabhai	G. Ramaswamy	[Bur+78, p. 249]
6	Bamboo	1976	London	England	Workshop	J. Park	B. Oleiko	[Bur+78]
7	Mexico	1973	hannover	Japan	Prototype	J. Hennicke	J. Hennicke	[Bur+78]
8	Mexico	1973	hannover	Japan	Workshop	J. Hennicke	J. Hennicke	[Bur+78]
9	Mexico	1977	Zitacuaro	Mexico	House	F. Montero	F. Montero	[Bur+78]
10	Mannheim	1975	Mannheim	Germany	Building	C. Mutschler	Arup + F. Otto	[Bur+78]
11	Japan Pavilion	2000	Hannover	Germany	Pavilion	S. Ban + F. Otto	Buro Happold	[]
12	Downland	2002	Singleton	England	Building	E. Cullinan	Buro Happold	[Har+03]
13	Savill	2006	Englefield	England	Building	G. Howells	Buro Happold	[HHR08]
14	Chiddingstone	2007	Chiddingstone	England	Canopy	P. Hulbert	Buro Happold	[]

Table 1.1 – Key numbers.

N	Year	Nickname	Type	City	Country	Architecte	Engineer	Page	Citation
1	1962	Experimental structure	Workshop	Berkeley	USA	Students	F. Otto	p. 270	[BHS74]
2	1962	Exhibition pavilion	Pavilion	Essen	Germany	F. Otto	F. Otto	p. 272	[BHS74]
3	1967	German Pavilion	Pavilion	Montreal	Canada	F. Otto	Lehonardt	p. 274	[BHS74]
4	1973	Seibu	Experiment	hannover	Japan	IL	IL	p. 245	[Bur+78]
5	1974	Basket shell	Experiment	Amehabad	India	G. Sarabhai	IL	p. 304	[BHS74]
6	1974	Experimental structure	Experiment	London	England	Students	Arup + IL	p. 306	[BHS74]
7	1975	Mannheim Multihalle	Building	Mannheim	Germany	C. Mutshler	Arup + IL	p. 308	[BHS74]
8	1973	Ferrocement gridshell	Building	Ahmedabad	India	G. Sarabhai	G. Ramaswamy + IL	p. 248	[Bur+78]
9	1976	AA Bamboo Latice Shell	Workshop	London	England	Students	J. Park + B. Oleiko	p. 255	[Bur+78]
10	1976	Test structure of a gridshell	Experiment	Stuttgart	Germany	Students	J. Hennicke	p. 298	[BHS74]
11	1977	Small Pavilion	Workshop	Mexico City	Mexico	Students	J. Hennicke	p. 258	[Bur+78]
11	1977	Small Greenhouse	Workshop	Zitacuaro	Mexico	Students	F. Montero	p. 260	[Bur+78]
12	1977	Experimental structure	Workshop	Mexico City	Mexico	Students	F. Montero	p. 270	[Bur+78]
13	1977	Experimental structure	Workshop	Mexico City	Mexico	Students	F. Montero	p. 270	[Bur+78]
14	1995	Westminster Lodge	Building	Dorset	England	E. Cullinan	F. Otto + Happold	p. 90	[BDH98]
15	1998	Earth Center	Building	Doncaster	England	Grant	Happold		
16	2000	Japan Pavilion	Pavilion	Hannover	Germany	S. Ban + F. Otto	Happold		[MOB06]
17	2002	Downland	Building	Downland	England	E. Cullinan	Happold + C. William		[Har+03]
18	2003	Life Science Centre Trust	Building	Pishwanton	England				
19	2006	Savill	Building	Savill	England	G. Howells	Happold + C. William		[HHR08]
20	2007	Chiddingstone Orangery	Roofing	Kent	England	P. Hulbert	Happold		
21	2007	ENPC	Experiment	Noisy-Champs	France	Navier	Navier		[DBC06]
22	2011	Solidays	Pavilion	Paris	France	ENPC	Navier + T/E/S/S		[Bav+12]
23	2012	Toledo	Workshop	Naples	Italy	gridshell.it	B. D'Amico		[DKZ14]
24	2013	Créteil	Building	Créteil	France	T/E/S/S	T/E/S/S + Navier		[dPel+16]
25	2014	Toledo 2.0	Workshop	Naples	Italy	gridshell.it	B. D'Amico		[DAm+15a]
26	2016	JPO	Pavilion	Toulouse	France	Quaternion	Navier + Terrell		
27	2016	FAV	Pavilion	Montpellier	France	Quaternion	Navier + Terrell		
28	2016	CLC	Workshop	Noisy-Champs	France	ENPC	Navier		
27	2016	Trondheim	Workshop	Trondheim	Norway	Students	NTNU		[Had+16]

Table 1.2 – Key numbers.

Project				Structure		
Year	Nickname	Country	Duration	Material	Layer	Pitch
1975	Mannheim	Germany	LT	hemlock	double	0.5 m

Table 1.3 – Key numbers.

1.4 Gridshell structure : definition and classification

1.4.1 Historic overview

1.4.2 Rigid gridshell



(a) Forum Café, Solidays (2011).



(b) Prototype (2007).



(c) Prototype (2008).

Figure 1.20 – Prototypes and projects of GFRP elastic gridshells.

1.5 Elastic gridshells : revisiting Mannheim

1.6 Elastic gridshells : the benefits of composite materials

Glass fiber reinforced polymer (GFRP) tubes are at the heart of the presented technology. They can favorably replace wood where both resistance and bending ability of the material is sought [DCB10].

¹⁷German pavilion 1967 : <https://www.youtube.com/watch?v=Z0mtFMoseUk>

¹⁸German pavilion 1967 : <http://www.uncubemagazine.com/magazine-33-15508949.html/page1>

The tubes are made by pultrusion, “a continuous molding process whereby reinforcing fibers are saturated with a liquid polymer resin and then carefully formed and pulled through a heated die to form a part. Pultrusion results in straight constant cross section parts of virtually any shippable length”.¹⁹ This process is very economic and its standardization guarantees very stable material and mechanical properties. It frees designers from the problem of joining wood pieces with finger joints to obtain long and continuous members and of wood durability.

1.6.1 Recent developments

The Faraday Pavilion : [NLG13] The Pishwanton / lothian : [Pishwanton2003] The laboratory Navier tested various numerical methods to generate such grids [BBC09] Masson : [MM17].

1.6.2 Gridshell in composite material

The benefits of GFRP gridshells have been covered previously. We just recall the main aspects.

The gridshells built in composite material, being at the heart of this paper, are consistent with the framework defined previously, that is to say :

Glass fiber reinforced polymer (GFRP) tubes are at the heart of the presented technology. They can favorably replace wood where both resistance and bending ability of the material is sought [DCB10].

The tubes are made by pultrusion, “a continuous molding process whereby reinforcing fibers are saturated with a liquid polymer resin and then carefully formed and pulled through a heated die to form a part. Pultrusion results in straight constant cross section parts of virtually any shippable length”.²⁰ This process is very economic and its standardization guarantees very stable material and mechanical properties. It frees designers from the problem of joining wood pieces with finger joints to obtain long and continuous members and of wood durability.

Structural Typology

Their mechanical behaviour is very similar to the one of real shells even if the material is discrete and located in a grid more or less open. In spite of that, gridshells benefit from the same advantages as the ones showed by an eggshell : they can cross large span using a low amount of material. Their stiffness is mainly linked to their double-curved shape.

¹⁹Video explaining the pultrusion process : https://www.youtube.com/watch?v=4MoHNZB5b_Y

²⁰Video explaining the pultrusion process : https://www.youtube.com/watch?v=4MoHNZB5b_Y

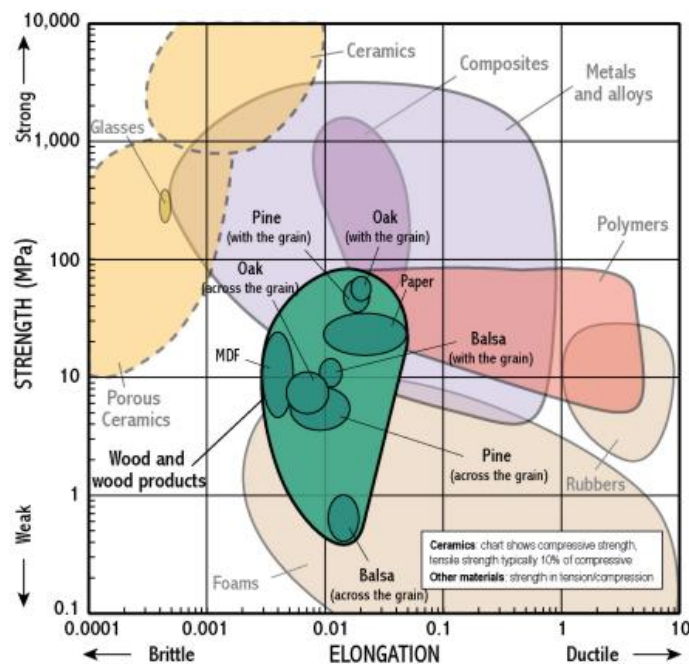
Material Flexibility for Structural Rigidity

In this field of application, composite materials like glass fibre reinforced polymer (GFRP) could favourably replace wood, where both resistance and bending ability of the material is sought [DCB10]. The stiffness of the structure does not derive from the intrinsic material rigidity but principally from its geometric curvature. Ideally, the composite profiles are produced by pultrusion, an economic continuous moulded process. The standardization of the process guarantees very stable material and mechanical properties. It frees designers from the painful problematic of wood joining and wood durability. The characterization of this material is presented further in the paper.

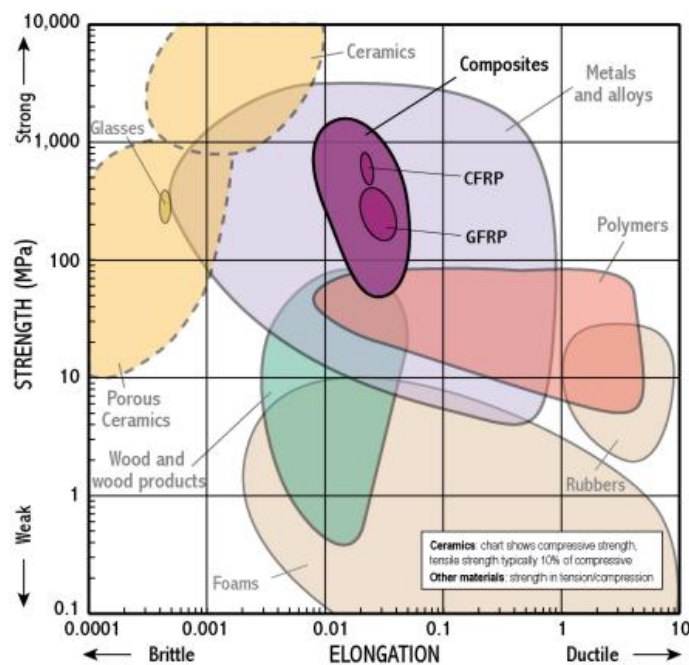
Erection Process

Usually, the grid morphology is not trivial and leads to design numerous costly and complex joints. To overcome this issue, an original and innovative erection process was developed that takes advantage of the flexibility inherent to slender elements. A regular planar grid made of long continuous linear members is built on the ground (Figure 1.23a). The elements are pinned together so the grid has no in-plane shear stiffness and can accommodate large-scale deformations during erection. Then, the grid is bent elastically to its final shape (Figure 1.22). Finally, the grid is frozen in the desired shape with a third layer of bracing members (Figure 1.23b) and the structure becomes a shell.

1.6. Elastic gridshells : the benefits of composite materials



(a) Forum Café, Solidays (2011).



(b) Prototype (2007).

Figure 1.21 – Prototypes and projects of GFRP elastic gridshells.



Figure 1.22 – Erection of the primary grid by two cranes

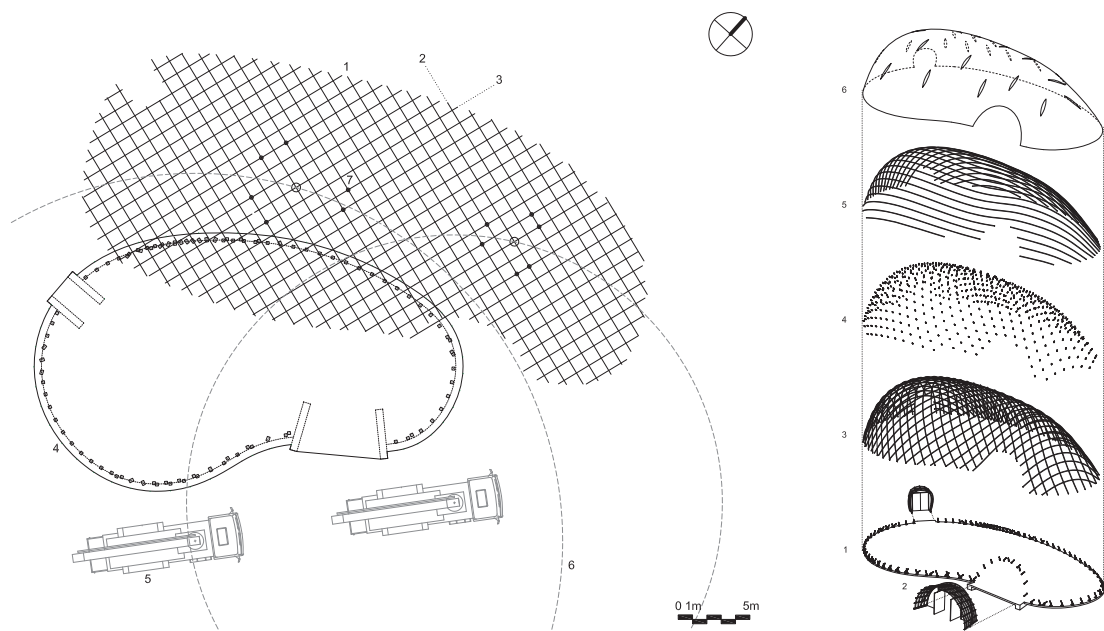


Figure 1.23 – Erection plan and construction stages

1.7 References

- [AB01] S. Adriaenssens and M. Barnes. “Tensegrity spline beam and grid shell structures”. In: *Engineering Structures* 23.1 (2001), pp. 29–36.
- [ABW99] S. Adriaenssens, M. Barnes, and C. Williams. “A new analytic and numerical basis for the form-finding and analysis of spline and gridshell structures”. In: *Computing Developments in Civil and Structural Engineering*. Ed. by B. Kumar and B. H. V. Topping. Edinburgh: Civil-Comp Press, 1999, pp. 83–91.
- [Add13] B. Addis. “‘Toys that save millions’ - A history of using physical models in structural design”. In: *The Structural Engineer* 91.4 (2013), pp. 12–27.
- [BAK13] M. Barnes, S. Adriaenssens, and M. Krupka. “A novel torsion/bending element for dynamic relaxation modeling”. In: *Computers & Structures* 119 (Apr. 2013), pp. 60–67.
- [Bav+12] O. Baverel, J.-F. Caron, F. Tayeb, and L. du Peloux. “Gridshells in composite materials : construction of a 300 m² forum for the solidays’ festival in Paris”. In: *Structural Engineering International* 22.3 (2012), pp. 408–414.
- [BBC09] L. Bouhana, O. Baverel, and J.-F. Caron. “Mapping two-way continuous elastic grid on an imposed surface : application to grid shells”. In: *IASS 2009*. Valencia, Spain, 2009, pp. 989–998.
- [BDH98] R. Burton, M. Dickson, and R. Harris. “The use of roundwood thinnings in buildings : a case study”. In: *Building Research & Information* 26.2 (1998), pp. 76–93.
- [Bdo02] Bdonline.co.uk. *The other gridshell*. 2002.
- [BHS74] B. Burkhardt, J. Hennicke, and E. Schauer, eds. *IL10 Grid Shells*. Institut für leichte Flächentragwerke (IL). Stuttgart, 1974.
- [Bou10] L. Bouhana. “Optimisation structurelle des gridshells”. PhD thesis. Université Paris-Est, 2010, p. 154.
- [Bur+78] B. Burkhardt, M. Chaitos, J. Langner, W. Langner, and G. Lubberger, eds. *IL13 Multihalle Mannheim*. Institut für leichte Flächentragwerke (IL). Stuttgart, 1978.
- [CC16] M. Collins and T. Cosgrove. “A Review of the State of the Art of Timber Gridshell Design and Construction”. In: *Civil Engineering Research in Ireland*. 2016.
- [CT17] J. Chilton and G. Tang. *Timber Gridshells: Architecture, structure and craft*. Routledge, 2017.
- [Cuv+17] P. Cuvilliers, C. Douthe, L. du Peloux, and R. Le Roy. “Hybrid structural skin : prototype of an elastic gridshell braced by a fibre-reinforced concrete envelope”. In: *Journal of The International Association for Shell and Spatial Structures* (2017), pp. 1–12.
- [DAm+15a] B. D’Amico, A. Kermani, H. Zhang, A. Pugnale, S. Colabella, and S. Pone. “Timber gridshells: Numerical simulation, design and construction of a full scale structure”. In: *Structures* 3.May 2016 (2015), pp. 227–235.

- [DAm+15b] B. D'Amico, A. Kermani, H. Zhang, P. Sheperd, and C. Williams. “Optimisation of cross-section of actively bent grid shells with strength and geometric compatibility constraints”. In: *Computers & Structures* 154 (2015), pp. 163–176.
- [DBC06] C. Douthe, O. Baverel, and J.-F. Caron. “Formfinding of a grid shell in composite materials”. In: *Journal of the IASS* 47 (2006), pp. 53–62.
- [DCB10] C. Douthe, J.-F. Caron, and O. Baverel. “Gridshell structures in glass fibre reinforced polymers”. In: *Construction and Building Materials* 24.9 (2010), pp. 1580–1589.
- [DKZ14] B. D'Amico, A. Kermani, and H. Zhang. “Form finding and structural analysis of actively bent timber grid shells”. In: *Engineering Structures* 81 (2014), pp. 195–207.
- [Dou+16] C. Douthe, R. Mesnil, H. Orts, and O. Baverel. “New shapes for elastic gridshells covered by planar facets”. In: *Proceedings of the IASS Annual Symposium*. Tokyo, Japan, 2016, pp. 1–9.
- [Dou07] C. Douthe. “Etude de structures élancées précontraintes en matériaux composites : application à la conception des gridshells”. PhD thesis. Université Paris Est, 2007, p. 274.
- [dPel+11] L. du Peloux, O. Baverel, J.-F. Caron, and F. Tayeb. “From shape to shell : a design tool to materialize freeform shapes using gridshell structures”. In: *Design Modelling Symposium*. Berlin, Deutschland, 2011.
- [dPel+15] L. du Peloux, F. Tayeb, B. Lefevre, O. Baverel, and J.-F. Caron. “Formulation of a 4-DoF torsion / bending element for the formfinding of elastic gridshells”. In: *Proceedings of the International Association for Shell and Spatial Structures*. August. Amsterdam, 2015, pp. 1–14.
- [dPel+16] L. du Peloux, F. Tayeb, O. Baverel, and J.-F. Caron. “Construction of a large composite gridshell structure: a lightweight structure made with pultruded glass fibre reinforced polymer tubes”. In: *Structural Engineering International* 26.2 (2016), pp. 160–167.
- [DZK16] B. D'Amico, H. Zhang, and A. Kermani. “A finite-difference formulation of elastic rod for the design of actively bent structures”. In: *Engineering Structures* 117 (2016), pp. 518–527.
- [FKB16] J. G. Fernandes, P. H. Kirkegaard, and J. M. Branco. “Tectonic Design of Elastic Timber Gridshells”. In: *World Conference on Timber Engineering*. Vienna, Austria, 2016.
- [FN15] G. Filz and D. Naicu. “2 Landscapes – interaction of 2 gridshells based on a modified Stewart - Gough - principle”. In: *Proceedings of the IASS Working Groups 12 + 18*. Tokyo, Japan, 2015.
- [Fou03] Fourthdoor.org. *Growing and making Flimwell's chestnut gridshell*. 2003.

- [Had+16] J. Haddal Mork, S. Dyvik Hillersøy, B. Manum, A. Rønnquist, and N. Labonne. “Introducing the Segment Lath - a Simplified Modular Timber Gridshell Built in Trondheim Norway”. In: *World Conference on Timber Engineering*. 3. Vienna, Austria, 2016.
- [Har+03] R. Harris, J. Romer, O. Kelly, and S. Johnson. “Design and construction of the Downland Gridshell”. eng. In: *Building research and information* 31.6 (2003), pp. 427–454.
- [HHR08] R. Harris, S. Haskins, and J. Roynon. “The Savill Garden gridshell : Design and construction”. In: *The Structural Engineer* 86.17 (2008), pp. 27–34.
- [HK02] R. Harris and O. Kelly. “The structural engineering of the Downland gridshell”. In: *Space Structures* 5 1.April 2002 (2002), pp. 161–172.
- [HL75] E. Happold and I. Liddell. “Timber lattice roof for the Mannheim Bundesgartenschau”. In: *The structural engineer* 53.3 (1975), pp. 99–135.
- [JBD13] T.-J. Jensen, O. Baverel, and C. Douthe. “Morphological and mechanical investigation of interconnected elastic gridshells”. In: *International Journal of Space Structures* 28.3-4 (2013), pp. 175–186.
- [Kim16] L. Kim-Lan Vaulot. “Form-Finding of Elastic Gridshells”. PhD thesis. Massachusetts Institute of Technology, 2016.
- [Lab+16] N. Labonne, J. H. Mork, S. H. Dyvik, A. Rønnquist, and B. Manum. “Experimental and Numerical Study of the Structural Performance of a Timber Gridshell”. In: *World Conference on Timber Engineering*. 2. Vienna, Austria, 2016, pp. 3–10.
- [Laf15] E. Lafuente Hernández. “Design and Optimisation of Elastic Gridshells”. PhD thesis. Universität der Künste Berlin, 2015.
- [LDB15] B. Lefevre, C. Douthe, and O. Baverel. “Buckling of elastic gridshells”. In: *Journal of the IAASS* September (2015).
- [LG14] E. Lafuente Hernández and C. Gengnagel. “A new hybrid: Elastic gridshells braced by membranes”. In: *WIT Transactions on the Built Environment* 136 (2014), pp. 157–170.
- [Lid15] I. Liddell. “Frei Otto and the development of gridshells”. In: *Case Studies in Structural Engineering* 4 (2015), pp. 39–49.
- [Low02] O. Lowenstein. “Lothian Gridshell”. In: *Building for a Future Winter* (2002), p. 29.
- [Low04] O. Lowenstein. “Gridshells in England. Ideas from the U.K. make stunning use of small timber”. In: *Wood Design & Building* (2004).
- [LP15] A. Liuti and A. Pugnale. “Erection of post-formed gridshells by means of inflatable membrane technology membrane technology”. In: *International Conference of the Architectural Science Association*. 2015, pp. 678–687.
- [LPD16] Liuti, A. Pugnale, and B. D’Amico. “Building timber gridshells with air : Numerical simulations and technique challenges”. In: *Structures and Architecture* (2016).

- [Mal12] S. R. Malek. “The effect of geometry and topology on the mechanics of grid shells”. PhD thesis. MIT, 2012.
- [Mes+17] R. Mesnil, C. Douthe, O. Baverel, and B. Léger. “Linear buckling of quadrangular and kagome gridshells: A comparative assessment”. In: *Engineering Structures* 132 (2017), pp. 337–348.
- [MKS16] A. Menges, O. D. Krieg, and T. Schwinn. *Advancing Wood Architecture. A computational approach*. Routledge, July 2016, p. 256.
- [MM17] Y. Masson and L. Monasse. “Existence of global Chebyshev nets on surfaces of absolute Gaussian curvature less than 2 pi”. In: *Journal of Geometry* 108.1 (2017), pp. 25–32.
- [MOB06] M. McQuaid, F. Otto, and S. Ban. “Building the Japan pavilion”. In: *Shigeru Ban*. Phaidon Press, 2006, pp. 8–11.
- [MOD15] R. Mesnil, J. Ochsendorf, and C. Douthe. “Stability of Elastic Grid Shells”. In: *International Journal of Space Structures* 30.1 (2015), pp. 27–36.
- [NLG13] P. Nicholas, E. Lafuente Hernández, and C. Gengnagel. “The Faraday Pavilion : activating bending in the design and analysis of an elastic gridshell”. In: *Proceedings of the Symposium on Simulation for Architecture & Urban Design*. April. San Diego, CA, USA, 2013, Article No. 21.
- [Pon+16] S. Pone, G. Mirra, E. Pignatelli, D. Lancia, and S. Colabella. “Specialised algorithms for different project stages in a post-formed timber gridshell design”. In: *Structures and Architecture* September (2016), pp. 259–266.
- [Pou15] E. Poulsen. “Structural design and analysis of elastically bent gridshells”. PhD thesis. Chalmers University of Technology, Gothenburgn Sweden, 2015.
- [QG14] G. Quinn and C. Gengnagel. “A review of elastic grid shells, their erection methods and the potential use of pneumatic formwork”. In: *WIT Transactions on the Built Environment* 136 (2014), pp. 129–144.
- [Tay+13] F. Tayeb, J.-F. Caron, O. Baverel, and L. du Peloux. “Stability and robustness of a 300m² composite gridshell structure”. In: *Construction & Building Materials* (2013).
- [Tay15] F. Tayeb. “Simulation numérique du comportement mécanique non linéaire de gridshells composés de poutres élancées en matériaux composites et de sections quelconques”. PhD thesis. 2015.
- [Tra06] Trada. “The Savill Building. A visitor centre with a timber gridshell roof Gridshell structures”. In: *TRADA* (2006), pp. 1–7.

2 Ephemeral cathedral : the first GFRP gridshell building

2.1 Introduction

The Ephemeral Cathedral of Créteil, France, is an elastic gridshell structure made of composite materials [dPel+16]. Built in 2013, this 350 m² religious edifice was initially a temporary church meant to gather the parishioners during the two years renovation (2013 - 2015) of their permanent cathedral (see fig. 2.1). At the time of writing, this building is still in activity and has been erected for almost five years. Although this structure is no more a church it has entered in a reconversion process to become a space for community activities and is now the property of the city of Créteil, France.

2.1.1 Overview

This large-scale prototype represents a first in the building industry which still shows excessive apprehension for the use of non-traditional materials such as composites, especially when it comes to structural applications. This is emphasized by the fact that only pre-norms or professional recommendations exist for composite materials, which is quite insufficient when one has to deal with insurers and legal technical controls. Although this structure is not the first elastic gridshell ever built in *Glass Fiber Reinforced Polymer* (GFRP) composite material, it should be regarded as the first true building using this technology. Indeed, this prototype – which can legally accommodate up to 500 people – complies with all the required performances : structural stiffness, fire safety, waterproofness, lightning, thermal comfort, etc. To our knowledge, this building is still the only one of this kind ever built.

It is worth to mentionne that this project arises thanks to a long-term collaboration between T/E/S/S atelier d'ingénierie¹ and the laboratory Navier² and marks the accomplishment

¹A structural design firm based in Paris, France : <http://tess.fr>

²Architected Materials and Structures (AMS) research team, specializes in the field of mechanics of

of a ten years research project in this field.³ More over, this challenge was both technical and human as the structure was built by the parishioners them selves.

2.1.2 Goals and contributions

This project was at the heart of the motivations for this thesis as it acted as a proof of feasibility and as a validation of the design tools and methods developed until then. The gained experience has highlighted further research directions that are presented in this manuscript.

In this chapter, we present the key aspects of the design and construction of this building. The main contribution of this work is to exhibit a method to design and build gridshells in a shape-driven design process. In such a process, architecture plays its full role as it is less dependent on purely structural considerations. Moreover, a building is much more than a shelter and has to satisfy serious requirements. To fill this gap, a meticulous attention was brought to the development of construction details. These technical developments lead to numerous testings. This chapter focus on this fundamental aspect as it is also a key contribution. Finally, we point out and analyze our experience, and we draw up some recommendations for further developments.

2.1.3 Related work

A thorough review is given in ??.

2.2 Project overview

2.2.1 Context and challenges

Créteil is a city of 90.000 inhabitants in the southeast suburb of Paris. Its urbanization began in the late 50's, impelled by the French architect Charles-Gustave Stoskopf. In 1976 he designed Notre Dame of Crétéil, a modest catholic church made of concrete, which became a cathedral 10 years later (see item 2 in fig. 2.1). Recently, the diocese of Crétéil has undertaken a major architectural redevelopment project of its cathedral, including a timber shell covering the religious area and the creation of a new cultural area. Once transformed, the edifice shall be more visible, more hospitable and livelier for citizens. Inevitably, such a molt takes time and a temporary place of worship was required to ensure liturgical services during the two-years work. In November 2011, T/E/S/S, the structural design office in charge of the cathedral renovation project, made an ambitious proposal to the diocese : based on a previous successful experience – the construction of a composite

materials and structures : <http://navier.enpc.fr/Materiaux-et-Structures?lang=en>

³Note that I developed this project in 2012 while I was a structural engineer at T/E/S/S, using the knowledge I had previously gained on the gridshell project for the Solidays music festival in 2011 while I was a research engineer at Navier. I started this thesis in octobre 2014, 18 months after the opening of the temporary cathedral to pursue my research on this topic started in may 2010.

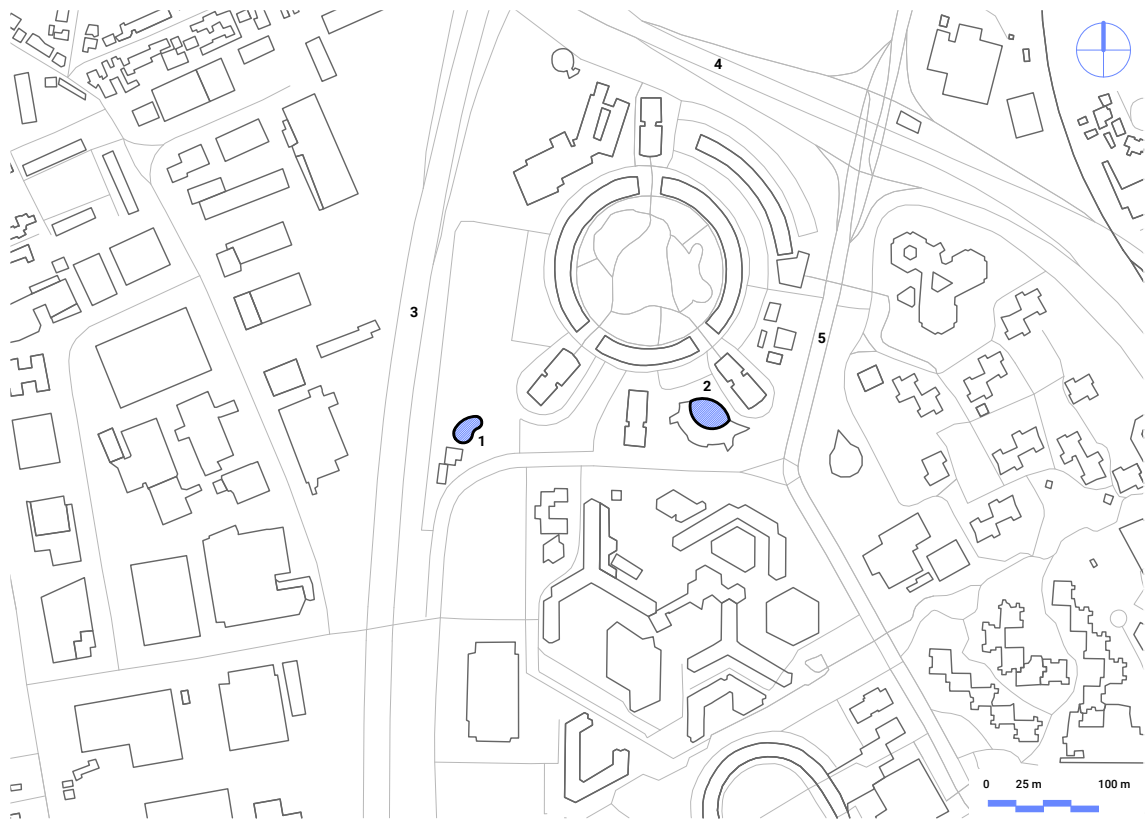


Figure 2.1 – Situation map. The temporary gridshell (1) was built very close to the permanent cathedral (2). Remark that the two buildings cover a quite similar projected area.

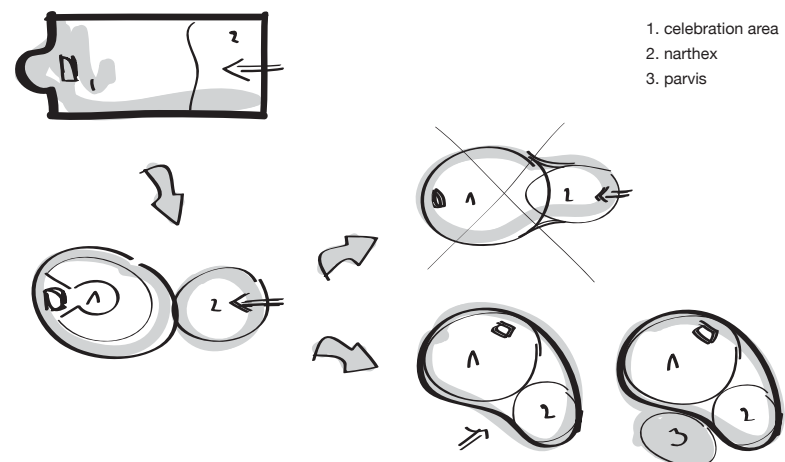


Figure 2.2 – Architectural sketch. Major and minor volumes are agglomerated into one volume. Here, the morphological register allowed by elastic gridshells appears to be relevant.

gridshell for the festival Solidays [Bav+12] – T/E/S/S suggested that rather installing a basic tent, the parishioners should construct themselves a temporary cathedral.^{4,5}

2.2.2 Architectural considerations on the form

The origin of this building form was driven by two objectives, that is, to provide a variety of appropriate internal spaces within which the community could assemble, and to provide an externally welcoming and visually interesting form. According to the architect Tom Gray, today, the internal organization of a roman catholic church is in large part driven by the post Vatican II vision of a religious celebration being a collective gathering of the community around the Eucharist, center of spiritual life. A circular seating arrangement is often considered the most convivial form to create a sense of belonging while minimizing a sense of hierarchy. However the community is not only using the building for religious celebration but also for encounters on a more informal manner, for example spontaneous gatherings after religious ceremonies. In the early Roman church, such gathering of the community was facilitated by the presence of an anti-space to the main space called a *narthex*, through which one passed on entering the church. It was therefore felt appropriate that the formal freedom which the gridshell system offered would be used to explore forms composed of an agglomeration of major and a minor volumes which contain the two functions : formal and informal gatherings (see item 1 and 2 in [fig. 2.2](#)).

Formal explorations were undertaken using modeling clay. The final form is based loosely on two adjacent semi spherical volumes of different size, which are merged into one complex form. Externally the fear of the design team was that the totally convex blob form could look intimidating. It was therefore decided that the two spherical virtual forms, which would be joined to make the final form, would be arranged not in a symmetrical axial manner, but in an asymmetrical curved composition. The resulting form seen in plan is convex on one side and concave on the other. The concave form in plan allows for double curvature to be introduced into what would be otherwise a simpler blob and gives sensuality and visual interest to the building.

2.2.3 Placing of the building on the site

The temporary cathedral is located on a land owned by the municipality, which is used for sporting and other communal gatherings. The curve in the building defines an external area where the church community could meet in the open air and this is where the entrance to the church is situated. The building was positioned on the site so that the entrance addresses a grass planted area forming a garden forecourt or “parvis” (see item 3 in [fig. 2.2](#)). A service building housing plant, toilets and vestry are housed in a port cabin positioned to the rear of the building (see [fig. 2.8](#)).

⁴See the video of the construction of Solidays’ gridshell here : <https://youtu.be/24LLfcVIZWw>.

⁵See the video of the construction of Creteil’s gridshell here : <https://youtu.be/jLq-UfOdnQQ>.

2.2.4 Entrance

It is formally quite difficult to integrate doors, which must be verticals, into a complex geometry. Either the gridshell could be deformed to accommodate the geometrical requirements of doors, or the doors could be integrated into an independent form. The latter approach was chosen. In looking for forms to house the doors, reference was made to the conical monumental doorways with rings of concentric decoration, which welcome the faithful to romanesque and gothic churches in France. The conical forms were found to be coherent to the overall geometry of the building. The entrance doors were therefore inserted into a conical hooded form made of rolled steel plates and stiffened by concentric steel tubes, which not only make reference to historic precedence but also refer to the gridshell to be discovered inside (see [fig. 2.5b](#)). The cone of the entrance doors was positioned in the concave side of the building giving access directly to the narthex part of the internal volume. To the rear of the church is situated a service door. The steel hood, which houses this door, is curved tightly around the door and takes up an ovoid form.

2.2.5 Daylight

The gridshell is covered in a PVC membrane, which is opaque. How to introduce daylight into the interior was a major subject of reflection. The simplest way found was to use transparent membrane placed occasionally on the membrane. A small amount of light was required in the interior to create a contemplative atmosphere. The lights would in consequence glow and would be seen as luminous insertions in the vault, like stars in the celestial vault or the apse of some Romanesque churches. The stars were patterned on the joints of the PVC membrane. The almond shape came from simplification of the cutting into the panels either side of the joints and to avoid stress concentrations around cuts in the membrane. This shape, known as Mandela, is frequently used in Marian religious imagery. The distribution of the transparent insertions is quite uniform but gets denser above the pinnacle.

2.2.6 Technical description

The gridshell structure is made of long glass fibre tubes ($\varnothing 42$ mm) fastened together with scaffold swivel couplers (see, [fig. 2.6a](#)). The structural members of the grid, all of different lengths, are built from one, two or three composite tubes connected with steel sleeves (see [fig. 2.6b](#)). The length of the tubes is limited to 12 m to enable transportation through standard trucks. The tubes are organized in three layers. During assembly, the first two layers are first placed perpendicular to one another on the ground. They form the *quadrangular primary grid*. The distance between the tubes of these two layers is constant, resulting in a regular grid. This primary grid is elastically deformed to obtain the final shape. The third layer of tubes acts as bracing. It gives the structure a shell-like behavior. The tubes are fixed to the primary grid once the shape has been obtained

The structure is anchored to a concrete strip footing with a special anchorage system, which ensures transfer of loads from the composite structure to the ground (see [fig. 2.6c](#)).

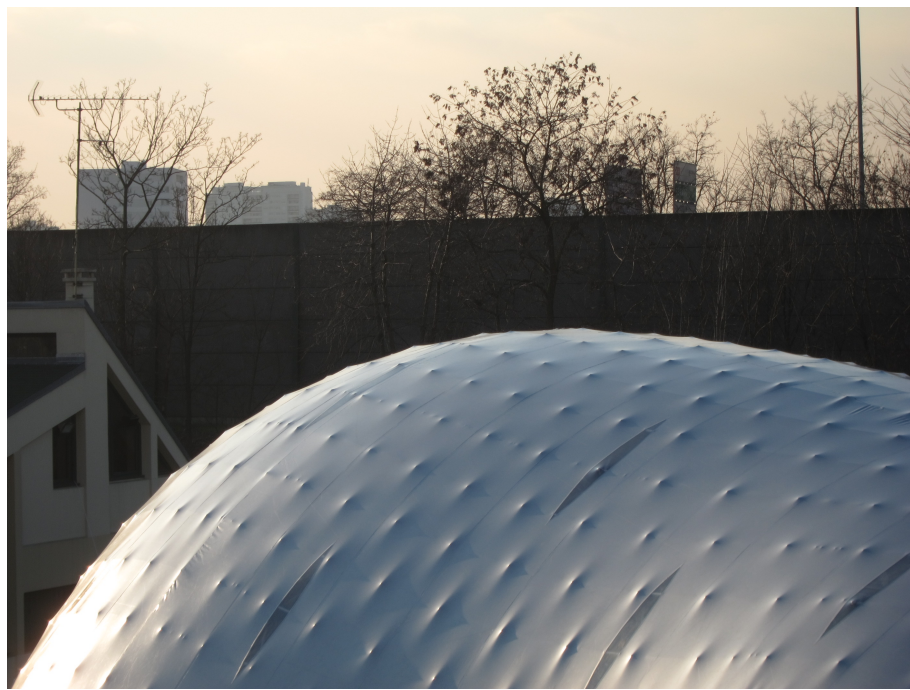


Figure 2.3 – Exterior view. The connections mark the fabric suggesting the interior grid structure. This texture enriches the perception of the building viewed from the outside and creates effects with the light reflections – © L. du Peloux for T/E/S/S.



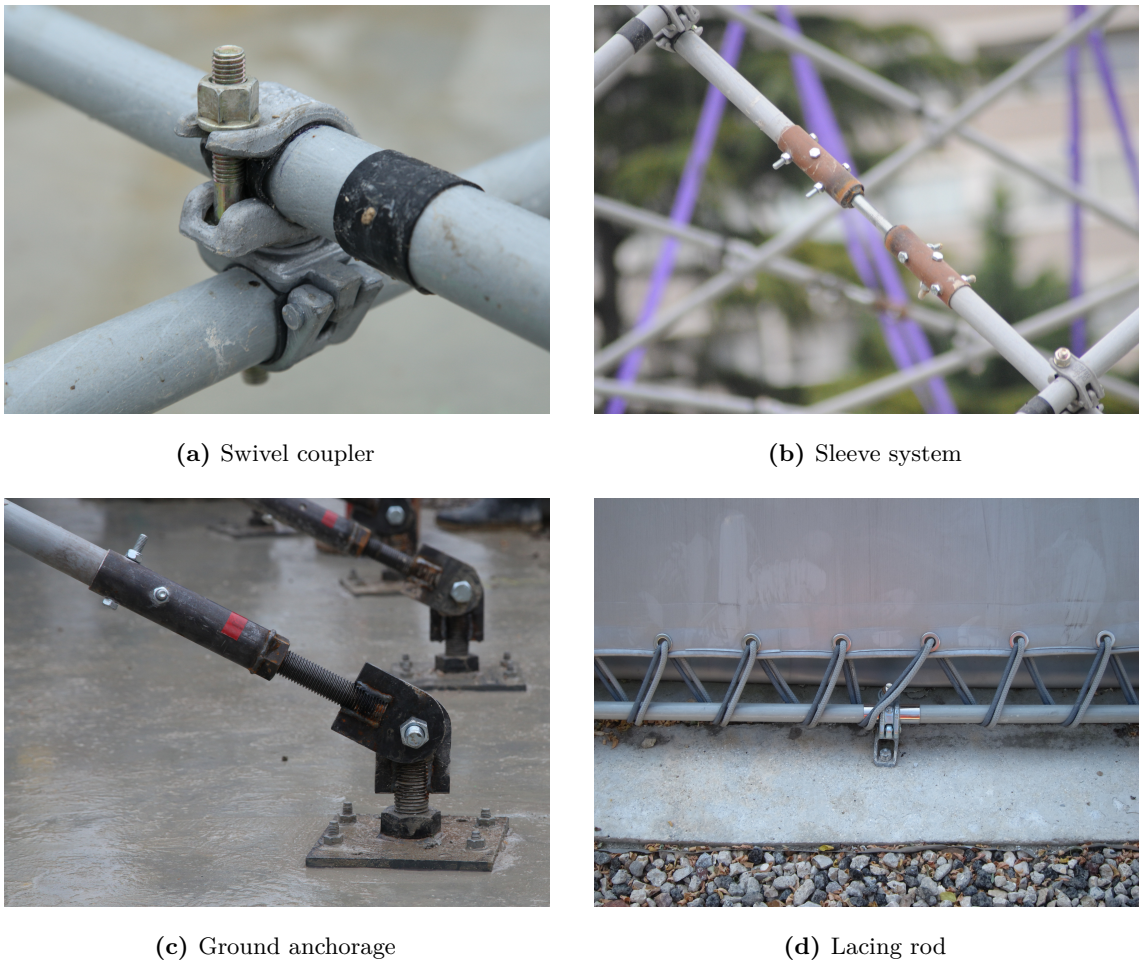
Figure 2.4 – Interior view. The grid pattern highlights the lightness of the structure and gives its tempo to the internal space. Lines converge to the altar, the heart of the liturgical area where the mass is offered on – © C. Moissinac for T/E/S/S.



(a) Exterior

(b) Interior

Figure 2.5 – Entrance. Two steel doors allow the entrance inside the building.



(c) Ground anchorage

(d) Lacing rod

Figure 2.6 – Key elements of the structural system.

A similar system enables fixation of the structure to the doors (see [fig. 2.5b](#)).

A PVC coated fabric (see [fig. 2.3](#)), tailor-made for the purpose, covers the structure. The transparent portion of the structure allows daylight inside the gridshell. The fabric is stretched on the peripheral edge of a dedicated beam with a double-lacing system (halyard and strap, see [fig. 2.6d](#)). At the ground level, the lacing edge of the beam is made of a bent, composite rod nailed to the concrete slab. At the grid–door junction, a steel arch is welded to the doorframe (see [fig. 2.5a](#)).

The PVC fabric is waterproof and, since it is a continuous membrane, has no joints except at the perimeter. At the perimeter, a continuous strip of membrane is prefixed to the internal surface of the membrane and fixed to the ground slab. At the doors, a flexible strip of the membrane is riveted to the doorframe.

Category	Item	Unit	Quantity
Public	seating	p	360
	standing	p	500
Dimensions	length	m	29
	width	m	17
	height	m	7
	contour	lm	75
	area	m^2	350
	volume	m^3	1600
Gridshell	tubes (x176)	lm	1775
	connections		1130
	sleeves		125
	anchorage		127
	<i>ground (single)</i>		77
	<i>ground (double)</i>		16
	<i>door (single)</i>		18
	weight	kg/m^2	5
Fabric	opaque	m^2	530
	transparent	m^2	12
	lacing rod	lm	67
	weight	kg/m^2	1

Table 2.1 – Key numbers.

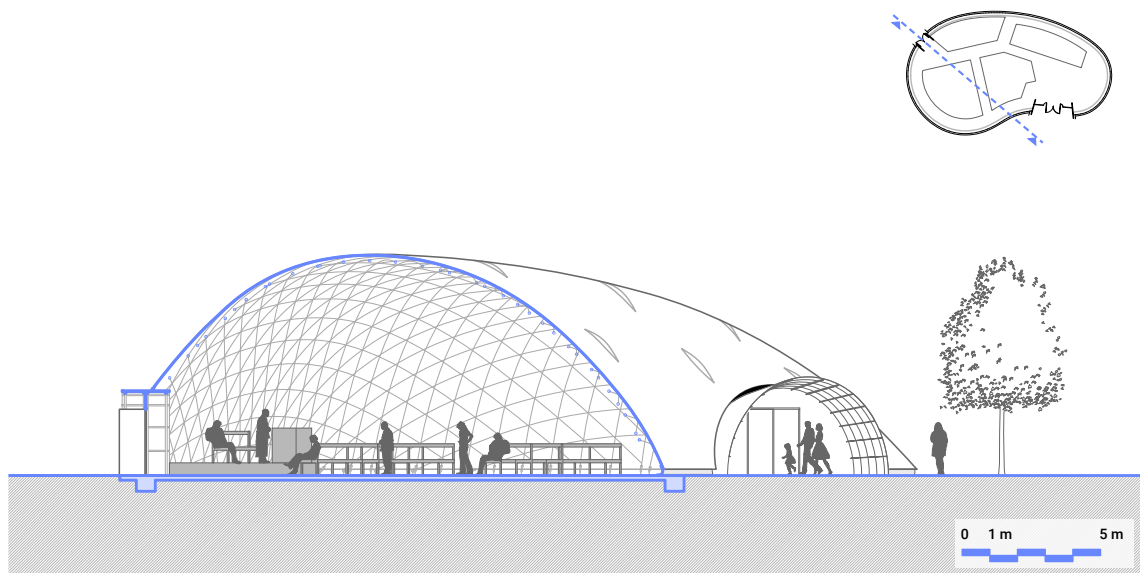


Figure 2.7 – Transversal section of the building. Observe how the grid gets denser at the choir. Two doors give access to the building. The height at the pinnacle is about 7 m.

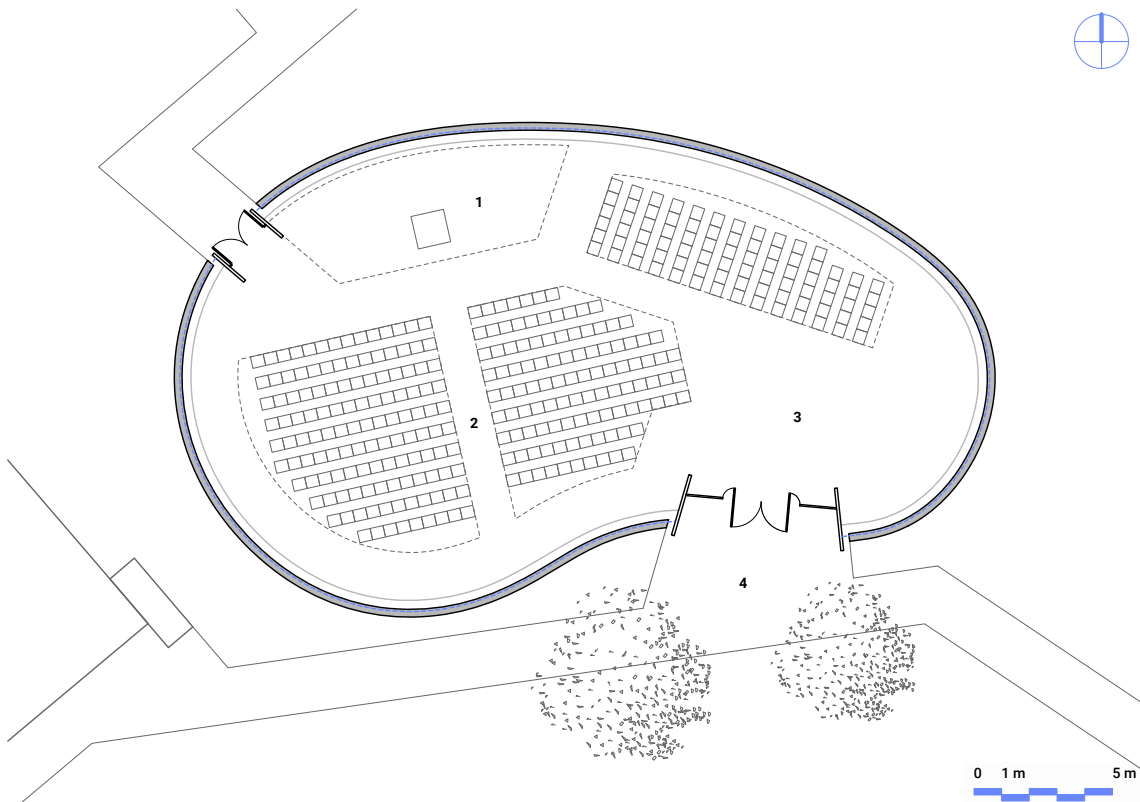


Figure 2.8 – Top view of the building. The interior space is composed of a choir (1), a place of assembly (2) and a narthex (3). The main entrance overlook the parvis (4). The shell spans about 29 m in the longitudinal direction and about 17 m in the transversal direction. The covered area is about 350 m². The space can accommodate 360 seating people or 500 standing people.

2.3 Construction process

2.3.1 Assembly of the grid

The first two directions of tubes were assembled perpendicularly on the ground with the swivel couplers (see [fig. 2.6a](#)) to form the *primary grid*. The resulting grid covered about 600 m² (see [fig. 2.9a](#)). At each intersection, the tubes were fastened together with a coupler, installed manually by the volunteers. They were asked not to tighten the bolts but just to engage the collars in order to prevent potential damages from the collar over the tube. Once the assembly of the primary grid was complete, the swivel couplers were tightened with a torque wrench to the optimal torque specified by the laboratory Navier. The whole stage took two full days. Note that because the anchorages stucked out from the slab, it was decided not to assemble the grid on the concrete slab to ensure that the grid would be able to slide freely on the ground and not get clung in the anchorages during the erection stage.

2.3.2 Deformation of the grid

The next stage consisted in lifting the grid simultaneously with two mobile cranes (35t). Once lifted up, the grid took nearly its final form (see [fig. 2.9b](#)). The structure was slowly moved above the slab until tube endings faced at best their respective anchor points. Then, tube after tube, the workers pinned the grid to the ground anchorages (see [fig. 2.9c](#)). This stage is tricky, especially at the beginning because only few tubes are connected to the ground. If the grid moves it can easily break these few tubes. The action of pinning a tube is done with a single bolt. The end of each composite tube is equipped with a rotating steel clevis. Similarly, each ground anchorage is composed of a steel plate fixed to the concrete slab and a rotating clevis. To pin a tube to an anchorage, their clevis are aligned one to each other and a pin is positioned in their central hole (see [fig. 2.6c](#)). When all the tubes were pinned to their anchorage, the grid was stable and secured and the cranes were removed (see [fig. 2.9d](#)). The stage lasted one full day.

2.3.3 Bracing of the grid

Once the primary grid was deformed into the final shape, it was braced by a third direction of tubes called the *triangulation*. The triangulation tubes split the quadrangular mesh of the primary grid into triangles (see [fig. 2.9e](#)). This work was tedious as it required working at height in aerial buckets. Tubes were hand-conveyed in the structure and attached to the tubes of the second layer with an additional swivel coupler. Each node of the structure would then be composed of two connections (see [fig. 2.18](#)). Once triangulated the structure behaves like a shell and its stiffness increases largely.

2.3. Construction process



(a) Flat grid



(b) Erection



(c) The grid is anchored



(d) Deformed grid



(e) Grid is braced



(f) Membrane

Figure 2.9 – Construction process of the gridshell.

2.3.4 Covering of the gridshell

Finally, the structure is covered with a PVC coated fabric. The membrane comes rolled up. The roll is positioned at one side. Then it is progressively unrolled toward the other side (see [fig. 2.9f](#)). This step requires professional rope workers. Once the membrane is in place, it is hand tensioned with a system of halyard and strap (see [fig. 2.6d](#)). All included, this stage lasted no more than a single day for a team of six workers.

This step appears as the moment of truth : if the membrane perfectly fits the gridshell, making no crease, that means the structural analysis were successfully conducted with the required accuracy (see ??).

2.4 Structural design

In this section, we exhibit a methodology to design a gridshell with a shape-centered approach. This is one of the key originality of this work and it was first implemented for the Solidays gridshell in 2011. The idea is to identify a grid and a set of supports that once the grid is bended and anchored to its foundations has a geometry as close as possible to the target shape designed by the architect.

Solving this inverse problem is quite a challenge. It requires a lot of back-and-forth between architects and engineers about the definition of the shape. To build a suitable solution the designers need agile tools to get deep insights quickly and adapt their design iteratively until convergence is reached. Unfortunately, existing structural analysis softwares are more validation tools than agile design tools. Although they are necessary to fully validate the feasibility of a given structure, they are quite limited to explore the space of solutions.

The presented methodology tackles this issue by providing appropriate design criteria to the designer. These criteria can be implemented in real-time softwares, thus approaching the agility of the physical models employed in the past [[Add13](#)].

2.4.1 Overall design process

The goal of the design process is to identify a gridshell structure that works and respects as faithfully as possible the architectural project with respect to the shape and program. The design of the gridshell represents “the path from shape to structure”. Its progress is iterative and revolves around three major stages :

- shape : modeling a shape from the architectural brief
- mesh : meshing the shape to obtain the geometry of the grid
- structure : analyze the structural efficiency of the grid

Developing this structural design was a complex process. Indeed, for each step, the method, the tool and the criteria that offer both a sufficient explorative richness in order to find

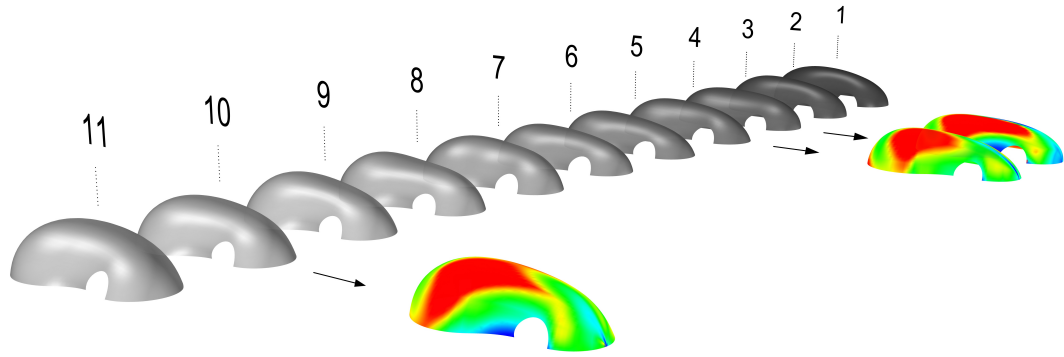


Figure 2.10 – Benchmarking shapes regarding their minimum principal curvature.

potential candidate solutions, and the means to evaluate and compare the suitability of those solutions, had to be found. In the next part of this section, the studied options and the selected evaluation criteria for each previously mentioned stage are presented.

2.4.2 3D modelling of the intended shape

The first step of the process consists in building a precise geometric model from the sketch of the architect and evaluating its mechanical potential (see [fig. 2.10](#)). At this stage, the goal is to estimate quickly the probability a given shape would lead to the generation of a structurally feasible gridshell.

Stresses in the grid are mainly due to the bending of the tubes. Therefore, they can be derived directly from the measurement of the geometric curvature of the tubes. Because the principal curvatures of the surface give a quantitative measurement of the local curvature of any curve drawn on a surface, they are relevant indicators to evaluate the stress rate of laying a grid on the said surface.⁶ Particularly, the following condition has to be satisfied everywhere :

$$E \cdot \frac{r}{R_{min}} < \frac{\sigma_{k,flex}}{\gamma_{lt}} \quad (2.1)$$

where, r is the tube's outer radius, R_{min} is the minimum principal radius of curvature of the surface, E is the flexural modulus, $\sigma_{k,flex}$ the characteristic flexural strength and γ_{lt} the long-term partial coefficient of material resistance (see [§2.5.4](#)).

Ideally, the shape is controlled by few key parameters. Thus, it is easier to adapt and optimize the shape through an iterative process towards the above criterion [eq. \(2.1\)](#).

⁶Indeed, any normal section of the surface will have its curvature bounded by the principal curvatures of the surface. Therefor, this seems reasonable to seek grids that fulfill this criterion as the structural elements would probably not resist too large variations of curvatures in the plane of the surface.

2.4.3 Meshing the surface

During the second step, the candidate surface is meshed and the mechanical potential of the resulting grid is evaluated. At this stage, the probability of a given mesh leading to the generation of a viable gridshell structure is estimated. Simultaneously, meshes are compared according to their architectural relevance.

In this step, the geometric curvature of the polylines drawn on the surface is an appropriate criterion to characterize the mechanical potential of the grid. Unlike the previous step, this criterion takes into account the curvature of the studied mesh and not the minimum principal curvature. In particular, it has to be ensured that the following condition is satisfied everywhere :

$$E \cdot \frac{r}{R_{\text{spline}}} < \frac{\sigma_{k,\text{flex}}}{\gamma_{lt}} \quad (2.2)$$

where R_{spline} is the spline's local curvature radius. The mesh is obtained by the compass method (see §2.4.3), which develops a regularly spaced grid on a surface from two secant curves lying on the surface and called *directrix*. This method, proposed by **Otto 1974**, was first implemented for the Solidays gridshell in 2011. The method guarantees that the grid is made of parallelograms when developed in a plane. This geometric property is exactly what we are looking for to ensure the necessary degree of freedom of the grid responsible for its deployment (see §2.6.1). For a given shape, there are an infinite number of possible meshes (see fig. 2.13). The aim is to identify at least one grid which satisfies both the architectural and the structural requirements.

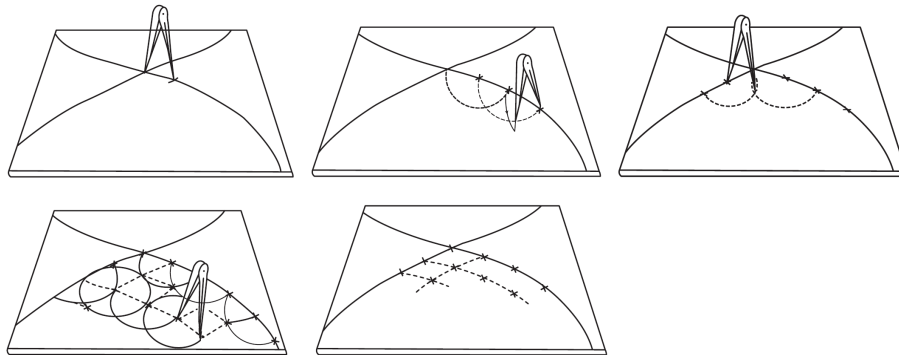


Figure 2.11 – How the compass method works.

Compass method

This process propagates a two way mesh of constant pitch on any NURBS surface (see fig. 2.11). Two secant directrices are drawn on the surface to mesh. These curves mark the boundary of four quarters. Each half directrix is then subdivided with a compass of constant distance (the pitch). Finally, from two consecutive half directrix quadrants are meshed with the same compass distance.

The compass method does not allow to spread the mesh everywhere on a given surface

because it stops when a directrix reaches the boundary of the surface. Only a portion of the surface can be meshed and the covered area varies according to the chosen set of directrices. To overcome this difficulty, we consider the gridshell surface (see [fig. 2.12a](#)) as a part of a larger domain surface (see [fig. 2.12c](#)). Trimmed by a plane, this domain surface should give back the intended shape to build (see [fig. 2.12b](#)). Therefor, it is possible to mesh the domain surface (see [fig. 2.12d](#)) and to retrieve a Chebyshev net that cover completely the initial surface (see [fig. 2.12f](#)).

The method is easily extended to meshes with variable pitch. This idea was explored to find optimal grids with genetic algorithm by Bouhaya et al. [[BBC14](#)]. It is worth to mention an attempt to extend this method for multilayer Chebyshev grids by Lefevre et al. [[LDB15](#)].

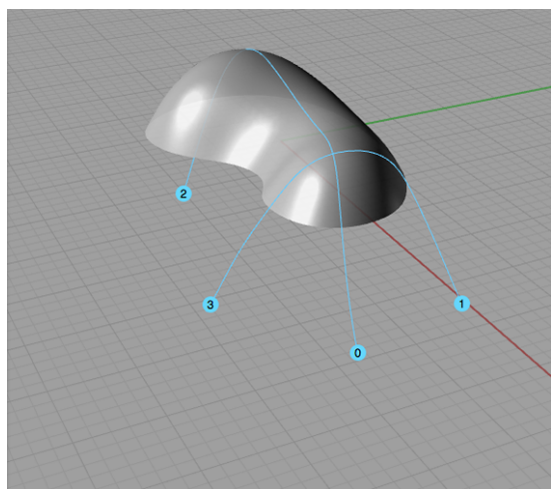
Numerical tool

Here, a specific software developed by du Peloux et al. [[dPel+11](#)] for *Rhinoceros* and *Grasshopper* allows generating this kind of mesh on any non-uniform rational B-spline surface (NURBS). It performs the following elementary operations : surface meshing with the compass method, trimming, control of the geometry's integrity and flattening of the grid (see [figures 2.12](#) and [2.13](#)). The tool also generates automatically a text file, which can be imported into a structural analysis software, containing all the required information to build programmatically the analysis model and then perform the formfinding of the structure (see [fig. 2.14](#)). In particular, an add-on feature facilitates loads application of various complexities (snow, wind, etc.), which is otherwise difficult in conventional analysis softwares for freeform structures. However, the tool does not provide any computation facilities itself and this is exactly the goal of the second part of this thesis.

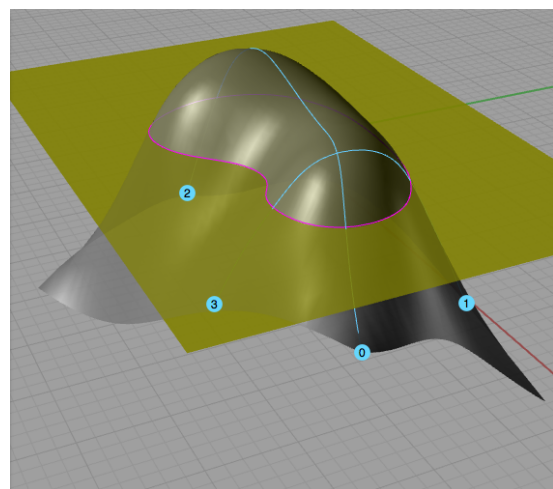
2.4.4 Formfinding and bending prestress

In the previous steps, the initial form was optimized and promising meshes for the materialization of the future gridshell were identified. However, the produced meshes do not take into account any of the mechanical reality, because only geometrical rules were used in their generation. The formfinding step consists precisely in finding the geometry of the grid at mechanical equilibrium, and the corresponding permanent bending stresses. The calculation is performed numerically thanks to a dynamic relaxation algorithm with kinetic damping and comprise the following steps :

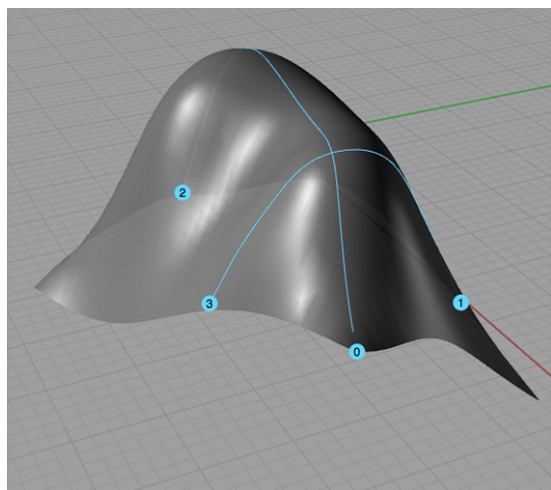
1. The grid is bent by a set of applied displacements from its resting position to the compass position.
2. The grid is then relaxed until it falls in its mechanical equilibrium.
3. Bending stresses of the triangulation are calculated relative to the geometry of the equilibrium.
4. Geometry and bending stresses of the triangulation are re-injected into the model in step 2.



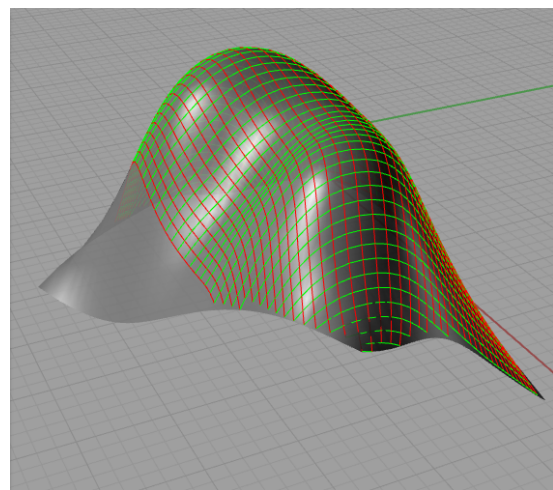
(a) Target shape



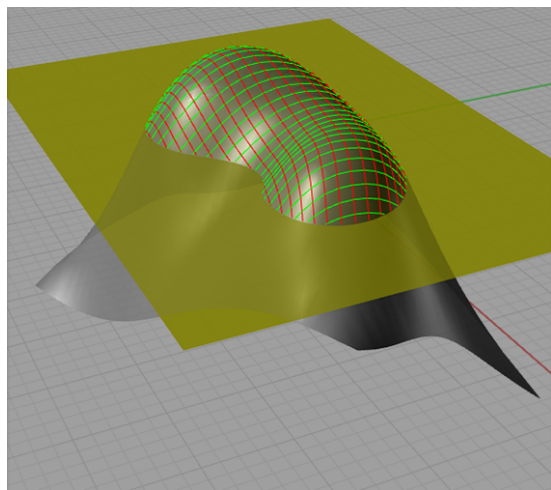
(b) Domain and trimming surfaces



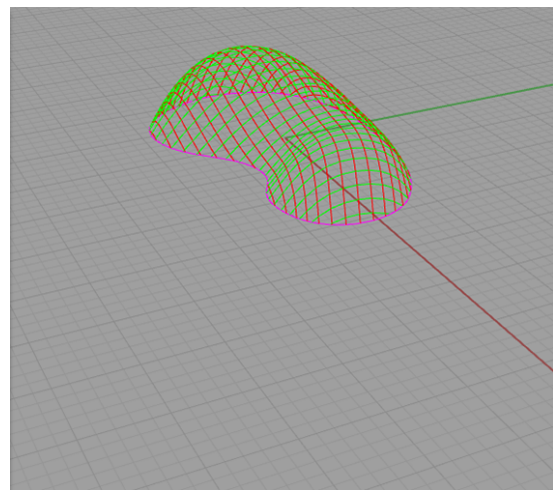
(c) Secant directrices



(d) Resulting mesh

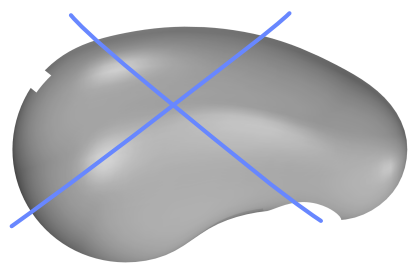


(e) Trimmed mesh

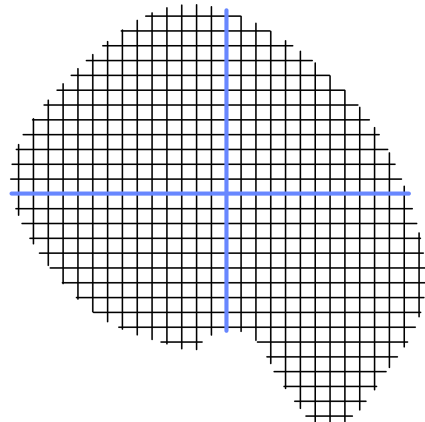


(f) Final grid

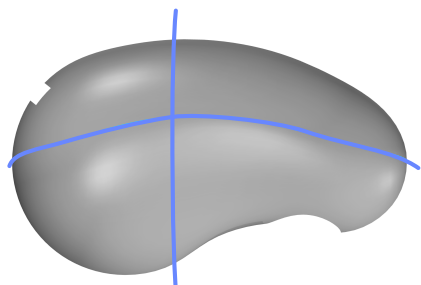
Figure 2.12 – The compass method step by step.



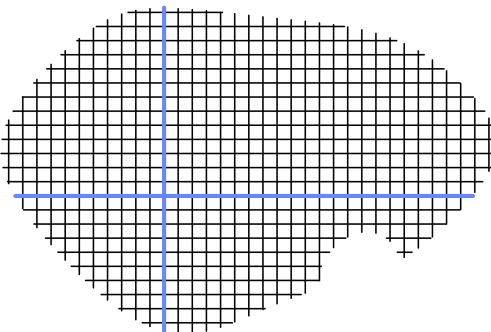
(a) First set of directrices



(b) First grid



(c) First set of directrices



(d) Second grid

Figure 2.13 – Each set of directrices leads to a different grid.

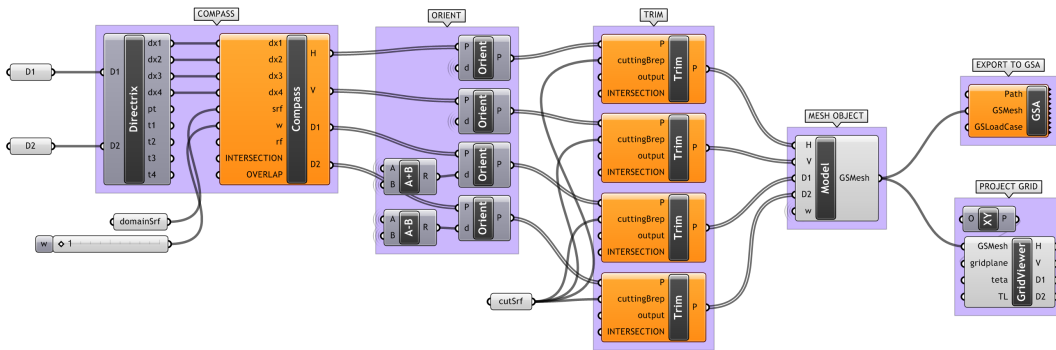


Figure 2.14 – Meshing software as a plugin for *Grasshopper*.

Two analysis models were built during this process to study the structure with and without bracing tubes.

The computations were realized with the formfinding module of the software Oasys GSA.⁷ It relies on a 6-DOF dynamic relaxation algorithm with either viscous or kinetic damping such as the one introduced in 2000 by Adriaenssens [Adr00]. In practice, making the computations to converge was a really difficult and time-consuming task, highlighting the necessity of a dedicated formfinding tool with a higher level of interactivity. This issue that the coupling between rotational and translational degrees of freedom could cause ill-conditioning problems was already noticed by Adriaenssens and Barnes [AB01]. In the same paper, they proposed a 3-DOF element valid for torsion-free cases. Simpler and faster, it is also a lot more stable. This element was reused and extended later for the formfinding of elastic gridshells in composite materials with complex connections by Douthe [Dou07].

To tackle numeric instabilities the model had to be simplified :

- Connections between elements were modeled as rotation-free joints, enforcing only position constraints without taking into account the eccentricity between the tubes. This becomes a problem when it comes to evaluating the stability of the gridshell as eccentricity can play a major role [LDB15]. This is also problematic when determining the production length of the tubes and the position of the anchorages (see §2.4.5).
- The triangulation could not be embedded from the start in the model and had to be treated separately and re-injected later on.

The formfinding process should not be regarded as a pure computational stage where only the equilibrium shape has to be found while all other design parameters are fixed. Indeed, as the goal is to find a suitable geometry with the most relaxed permanent bending stresses in the structure, this process could itself be employed to explore optimal geometries that will lead to more relaxed static equilibriums. In the present project the supports were allowed to move slightly around their target position by the mean of spring supports with

⁷<http://www.oasys-software.com/products/engineering/gsa-suite.html>

orthotropic stiffness. This allowed to decrease the overall level of permanent bending stress in the tubes while granting very minor changes in the geometry.

Finally the process converges when the shape and the pattern drawn by the mesh are suitable for the architect while the permanent bending stresses are acceptable for the tubes (see §2.5.4). The end results for this stage are presented in fig. 2.15. Note the smoothness of the mesh and the convergence of the tubes near the altar. Bending stresses are well distributed and inferior to the maximum design stress allowed (133 MPa in that case). Only few tubes are heavily loaded, in the areas where the curvature is the highest.

2.4.5 As-built geometry

Although, the eccentricity ($e = 136$ mm) remains small compared with the span of the shell ($l = 17$ m), it is not negligible compared with the mesh size ($w = 1.0$ m). Thus, the tube lengths and anchorage positions could not be determined with sufficient accuracy without taking into account the thickness of the structural grid due to this eccentricity. The employed method, purely geometrical, assesses that the neutral fibre of the shell is equidistant from the first two layers of pipes. The form-finding is performed only with those two layers. Connection axes has to be parallel to the local normal of the shell surface. This assumption was not exact, but, in this case, gave sufficient accuracy. The red pipe was offset by $-e/2$, the green by $+e/2$ and the blue by $+e/2$ along the surface normal.

2.4.6 Structural analysis

A full structural analysis is finally performed on the gridshell, using the two mechanical models created previously during the formfinding stage. The non-braced model is used to check the grid's behavior during the construction stages. In particular, it must be verified that the primary grid - the one with no triangulation tubes - has no risk of buckling, both for obvious safety reasons and to ensure the accuracy of the final geometry. Indeed, the more the form is likely to buckle, the more it can be triangulated in a buckled geometry different to the targeted geometry. The model with the triangulated grid is used to confirm the gridshell complies with all the structural requirements during its lifetime. Its behavior under standard loadings is evaluated.

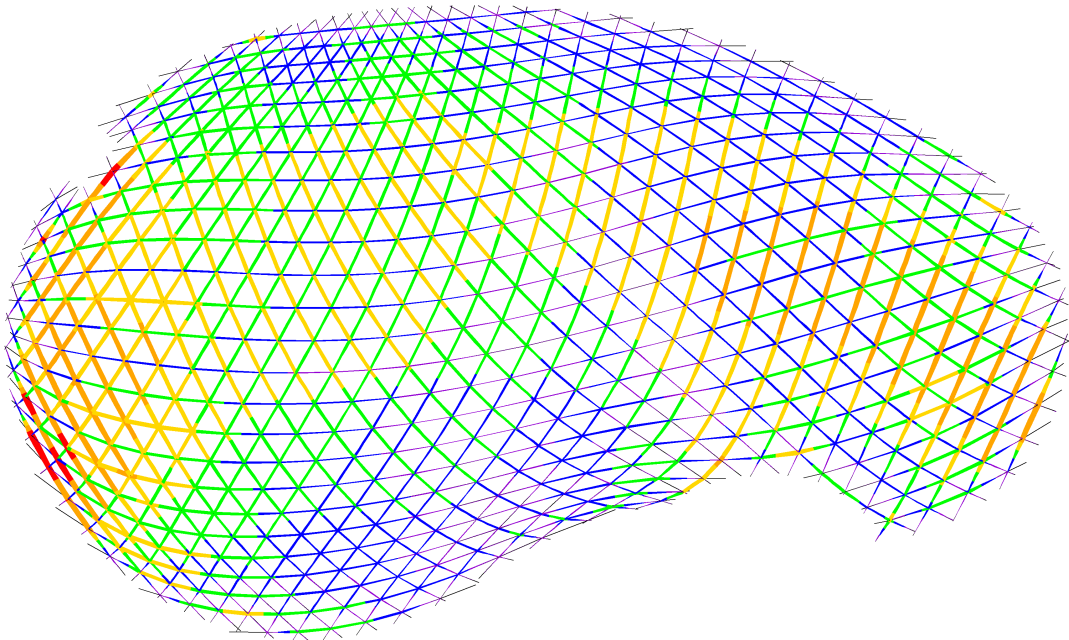


Figure 2.15 – Permanent bending stresses in the structure under self-weight (red tubes : 130 MPa).

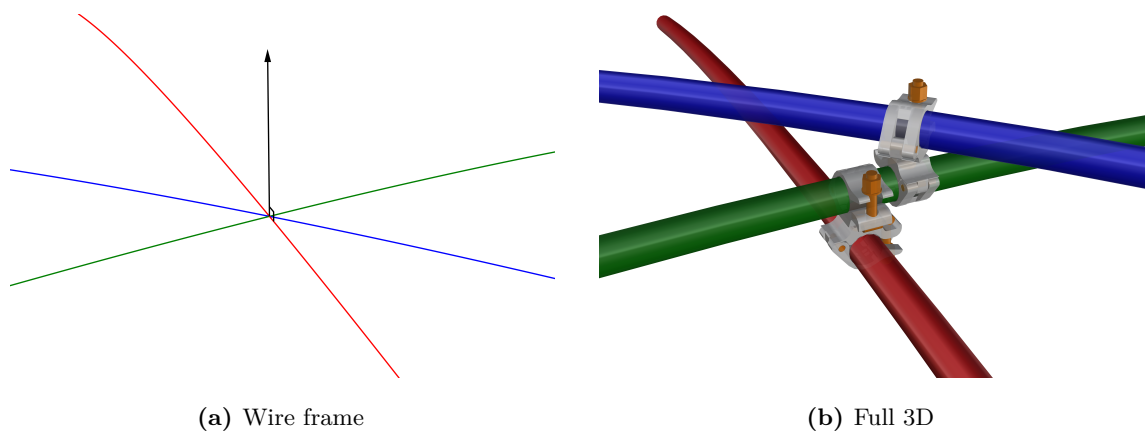


Figure 2.16 – Reconstruction of the full 3D geometry.

2.5 Designing with GFRP materials

This section focuses on the GFRP tubes employed for the structure. We present how we managed to deal with this composite material in the eyes of the existing regulatory framework although there is no applicable norms for composite materials (see §2.5.2). Beyond the administrative strategy, we present how their flexural strength was evaluated (see §2.5.3) and how the corresponding partial safety factors were determined (see §2.5.4).

2.5.1 Properties of the tubes

The technical properties of the tube employed for this project are given in tab. 2.2. Although these data were provided by the manufacturer at the time of the project, a test campaign was done to verify the flexural resistance of the tubes taking into account the influence of the swivel couplers clamped on the tubes (see §2.5.3).

2.5.2 Codes for composite materials

Beyond the technical difficulties related to both design and structural analysis of the shell, the regulatory framework was a vital issue for the success of the project. As it was the first time a structure of this kind was going to host a large number of people for over two years, the question of its reliability over time was a major issue. In order to be built, the gridshell had to comply with existing standards, which do not take into account such an innovative edifice, all in composite material. The strategy adopted to bypass this obstacle is presented herafter.

First level : administrative classification of the building

The first level, administrative, consisted of obtaining from the French authorities an appropriate classification for the building, taking into consideration the project's real-time requirement : a light-weight structure with a short lifespan. As expected, the structure was classified as a "building open to the public" (EPR in French) from the category "big tops and tents" (CTS in french) [Sit]. In this classification, construction procedures and regulations are adapted to the short lifespan of buildings.

Second level : compliance with existing standards

The second level, normative, consisted of ensuring that most of the existing regulatory framework justified the compliance of a structure that would not, at first sight, be considered by standards that do not include composite materials.

As far as possible, the design was made in compliance with the Eurocode, where the structural design is done according to the limit states under normalized loadings (self-weight, snow, wind, etc.). Although, the Eurocodes do not directly take into account composite materials, they propose some probabilistic methods to introduce new materials

Item	Standard	Polyester Mat-Roving-Mat
External diameter		41.7 mm
Internal diameter		34.7 mm
Wall thickness		3.5 mm
Section area		$4.20 \times 10^{-2} \text{ m}^2$
Section moment of inertia		$7.7259 \times 10^{-4} \text{ m}^4$
Torsion constant		$15.4518 \times 10^{-4} \text{ m}^4$
Shipping length		12.0 m
Glass content by weight	ISO 1172	60 %
Specic weight	ASTM D792	1.75 kg/m^3
Linear weight		0.735 kg/lm
Coefficient of thermal expansion	ASTM D696	$11 \times 10^{-6} \text{ K}^{-1}$
Tensile strength	ASTM D638	400 MPa
Tensile modulus	ASTM D638	26 GPa
Flexural strength	ASTM D790	400 MPa
Flexural modulus	full bending	25 GPa
Compressive strength	ASTM D695	220 MPa
Compressive modulus	ASTM D695	20 GPa

Table 2.2 – Technical properties of the tube.

Item	Standard	Précontraint 702 Opaque Alu
Yarn		1100 dtex PES HT
Weight	EN ISO 2286-2	830 g/m^2
Width		267 cm
Standard jumbo roll		50 lm or 300 lm
Finish		2-face acrylic varnish
Tensile strength (warp/weft)	EN ISO 1421	280/280 daN/5 cm
Tear strength (warp/weft)	DIN 53.363	30/28 daN
Elongation under load (warp/weft)	NF EN 15619	< 1 % / < 1 %
Adhesion	EN ISO 2411	10 daN/5 cm
Solar transmission	NFP 38511	13.5 %
Flame retardancy	NFP 92-507	M2
	DIN 4102-1	B1
Euroclass	EN 13501-1	B-s2, d0
Cold resistance	ISO 4675	-30 °C
Heat resistance	DIN 4102-1	70 °C

Table 2.3 – Technical properties of the membrane.

(EN1990, Annexe D). The mechanical properties of the GFRP pipe were determined as far as possible by tests in conformance with these methods. Alternatively, values were taken according from the Eurocomp [Cla03].⁸ In some cases, such as for the sleeve, the construction design also benefited from this approach.

2.5.3 Flexural strength of the tubes

The characteristic flexural strength ($\sigma_{k,flex}$) of the GFRP tube was used to verify if the structure complied with the Eurocode. This parameter had a critical impact on the structure's reliability because in this particular application stresses in the tubes are mainly due to the bending. Thus, it was important to confirm the manufacturer's permitted value through testing. Three-point flexural tests were carried out with and without connections (see fig. 2.17) to determine the characteristic strength according to the Eurocode protocol (Annex D) :

$$\sigma_{k,flex} = \bar{\sigma}(1 - k_n \sigma_x) \quad (2.3)$$

For five tests, the factor $k_{n,5\%}$ is 1.80 assuming a normal distribution. It has been proved in [Tay15] that the connections caused more scattering in the results. Finally, the manufacturer allowed value of 400 MPa was confirmed and retained for further calculations.

Connection	σ_1	σ_2	σ_3	σ_4	σ_5	σ_k
Without	456	441	445	460	477	430
With (20 Nm)	444	478	434	479	427	408

Table 2.4 – Flexural tests of the GFRP tubes (MPa).

2.5.4 Partial safety factors

The partial coefficients of material resistance (see tab. 2.5) used in the project were calculated according to the Eurocomp. The short-term coefficient proposed in Eurocomp ($\gamma_{st} = 1.3$) was increased to consider the critical stage of erection, where the deformations could not be controlled accurately. When dealing with long-term effects in permanently loaded, pultruded composite materials subjected to creeping and relaxation designers should be careful [Kot12, Ban06]. In this project, this was reflected in the high partial coefficient for long-term effects.

⁸The Eurocomp is a kind of pre-standard intended for the structural design of buildings and civil engineering works using GFRP composites, consistent with the Eurocode approach. It is considered as the reference design code for GFRP materials.

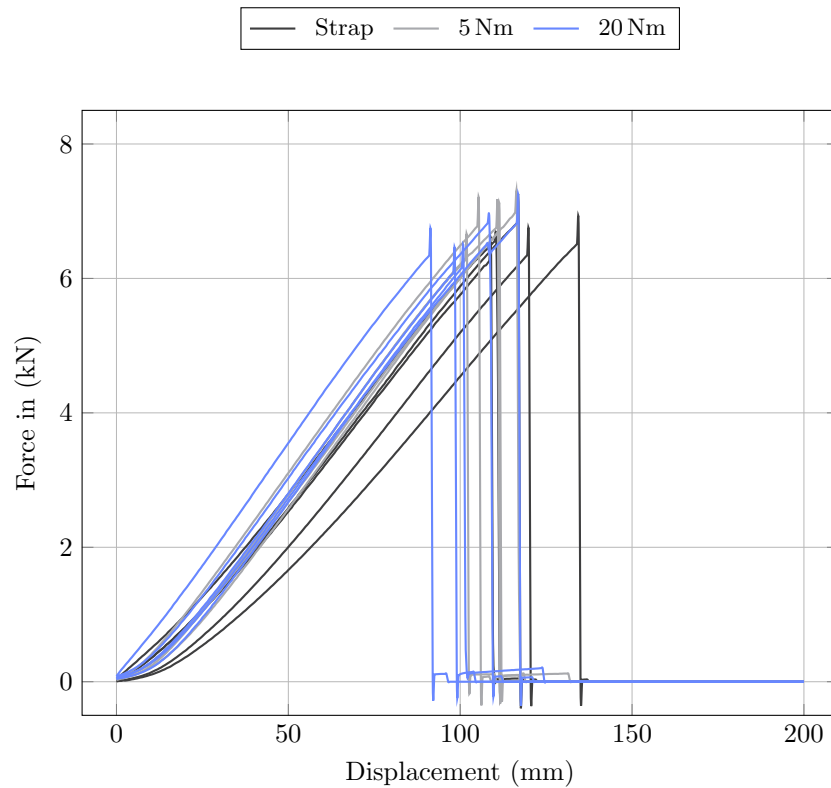


Figure 2.17 – Flexural test of the GFRP tubes. Results from [Tay15].

Time scale	γ	σ_d
Short-term	2.0	200
Long-term	3.0	133

Table 2.5 – Short-term and long-term values for material resistance. γ is the partial coefficient for safety factor. σ_d is the flexural design strength.

2.6 Construction details

In this project, one can identify 4 major structural details : the swivel coupler for connecting composite tubes to assemble the grid (see [fig. 2.6a](#)) ; the steel sleeve for connecting several composite tubes to obtain long members from initially short pieces of tubes (see [fig. 2.6b](#)) ; the ground anchorages for fixing the structure to the concrete slab (see [fig. 2.6c](#)) and the lacing edge beam of the fabric (see [2.6d](#)). The challenging issue of connecting the steel and composite parts was solved similarly sleeve and anchorage details.

2.6.1 The swivel coupler

Tubes are connected together with scaffold swivel couplers (see [fig. 2.6a](#)). Each connection is composed of two collars (\varnothing 42 mm and 38 mm wide) linked by a steel axis (see [fig. 2.18](#)). Thus the collars can freely rotate around the axis of the connection. This degree of freedom is responsible for the lack of in-plane shear stiffness of the primary grid and this is precisely this mechanism that allows the flat grid to deform into a free form surface. Each collar is itself composed of two hemicylindrical parts so that it can be opened to easily engage a tube. A M12 nut and a swivel T-bolt allow to lock the tube in the collar using friction. Collars are positioned over a 1.5 mm thick epdm ribbon wrapped around the tubes (see [fig. 2.18](#)). Once clamped in the connection, the tubes are spaced by a 68 mm distance from axis to axis. Although the mechanical consequences of this eccentricity could be neglected to a first-order approximation, this is not the case for the geometric consequences it induces as explained in §[2.4.5](#).

Interface layer

This coupler is made to assemble two scaffold steel tubes together. Workers should tight strongly the collars of the coupler to ensure that the steel tubes won't slide in their collar. Here, it is clearly impossible to do that. Indeed the GFRP tube is to thin (only 3.5 mm thick) and tightening the collars to the maximum would damage it or even make it collapse. However, preventing the connections to slide along the tubes is critical to maintain the in-plane shear degree of freedom of the grid. If connections would slide, the grid would probably not deploy in space as intended. The grid kinematic would be blocked at some points, developing high stresses that would lead to breakages. To maintain a sufficient level of sliding resistance while preserving the material integrity it was decided to introduce an interface layer to :

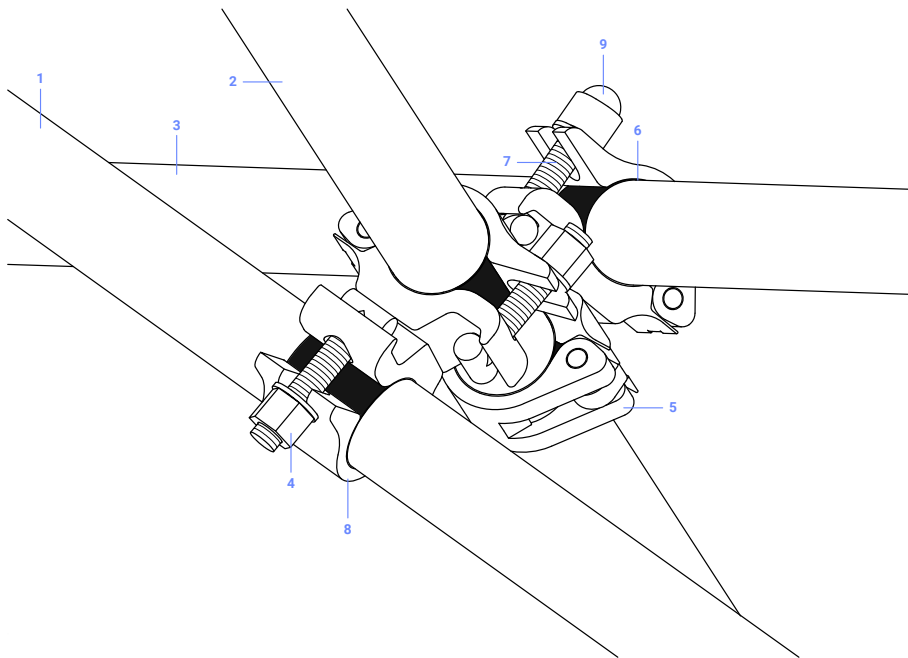


Figure 2.18 – Technical drawing of the swivel coupler. GFRP tubes (1, 2, 3). Swivel couplers (5, 8). EPDM layer (6). M12 swivel T-bolt (7). M12 nut (4) and plastic cap (9).

- increase the poor friction coefficient between the steel collar and the GFRP tube ;
- improve the distribution of stresses generated by the transverse compression of the collar over the tube, thus allowing a stronger clamping of the collar.

Several materials were tested in different thickness. Some of the results are presented in [fig. 2.19](#). A 1.5 mm thick EPDM ribbon was found to be suitable for the design requirements of the project. This layer improves significantly the sliding resistance from about 300 N to about 1200 N. Once the interface layer had been chosen, further tests were conducted to determine the appropriate clamping for the connections. The aim was to maximize the clamping to get the best sliding resistance (see [fig. 2.20](#)) while preserving the integrity of the tubes. It was found that a tightening torque between 15 Nm to 20 Nm was the optimal solution [[Tay15](#)].

Finally, the ribbons were ordered with a double sided tape (DST) face to facilitate their placement on the tubes. The influence of the temperature regarding the presence of the adhesive has been investigated. The results show that after 40 °C the scotch creeps and a loss of resistance occurs (see [fig. 2.21](#)). A recent thermal study of the structure has demonstrated that with no cooling system the temperature inside the building could rise up to 70 °C (see §[2.7.1](#) and [figures 2.29a and 2.29b](#)).

Benefits and drawbacks

This connection has the advantage to be available almost every where, to be really cheap and indestructible compare to the GFRP members. However, there are some drawbacks as

it is not tailor-made for this application :

- The weight of this part is 1.16 kg, which is very heavy compare to the lightness of the system. In this project, the weight of the swivel couplers represents one third of the overall weight of the structure. This could easily be reduced with a dedicated design.
- The actual design is not adapted to resist sliding. This is critical as explained previously. This problem occurred locally during the lifting of the grid and it was a pain to finish the deployment of the structure (see ??).
- Although the clamping of the collars enhance the resistance to sliding of the couplers, they also activate the ability to transfer some torsion to the tubes. Unfortunately, the tubes are very weak regarding this type of sollicitation (see tab. 2.2). A better design would propose a kinematics that allow the rotation of each collar around the axis of the connection and the axis of the tube.
- As the number of connections is quite huge, the clamping process should be at the heart of the design. The later has to guarantee that the workers will not damage unintentionally the structural members. If clamping would be found to be the way to go – which indeed might be an relevant option – the structural elements will have to be stronger to resist both clamping and torsion.

Furthermore, other design criterion should be taken into account such as the fact that the connection must not damage the membrane. This was resolved in the project thanks to plastic caps (see fig. 2.22). It is worth to mentionne that the problematic of the connection should be treated in symbiosis with the difficult question of the bracing and the covering as it interacts with all the key parts of the system : grid, bracing and membrane. Some propositions to this complex problem were designed and tested during this thesis and are presented in ?????. A noticeable design attempt was proposed in the roof of Chiddingstone's orangery ??.

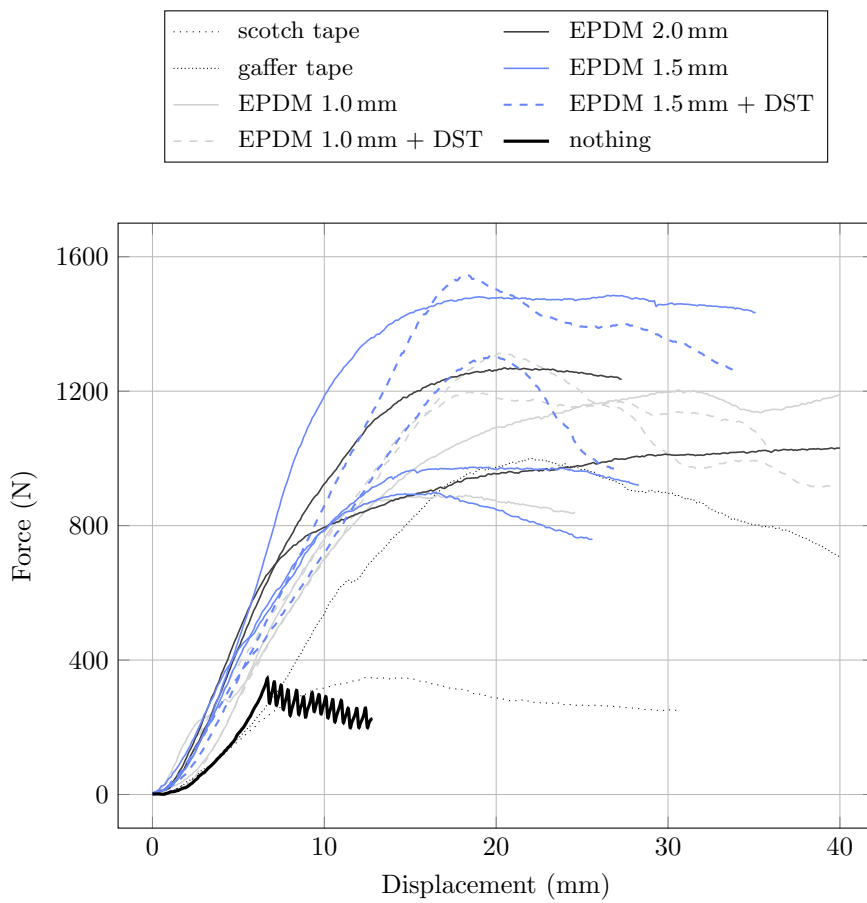


Figure 2.19 – Influence of the interface layer on the sliding resistance (5 Nm). Results from [Tay15].

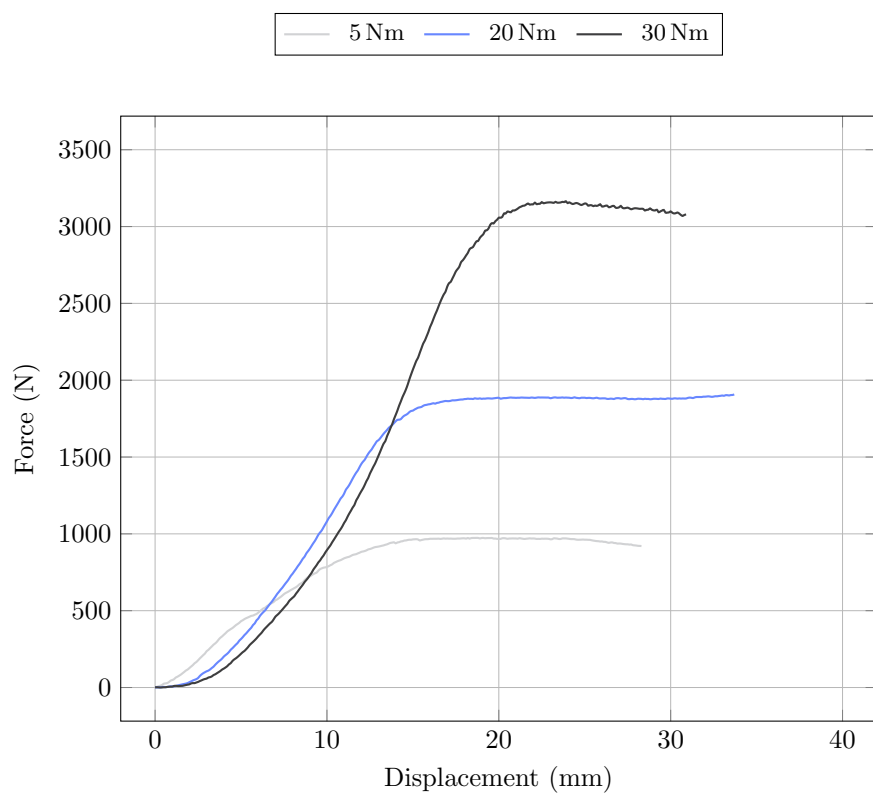


Figure 2.20 – Influence of the tightening on the sliding resistance for a 1.5 mm EPDM layer. Results from [Tay15].

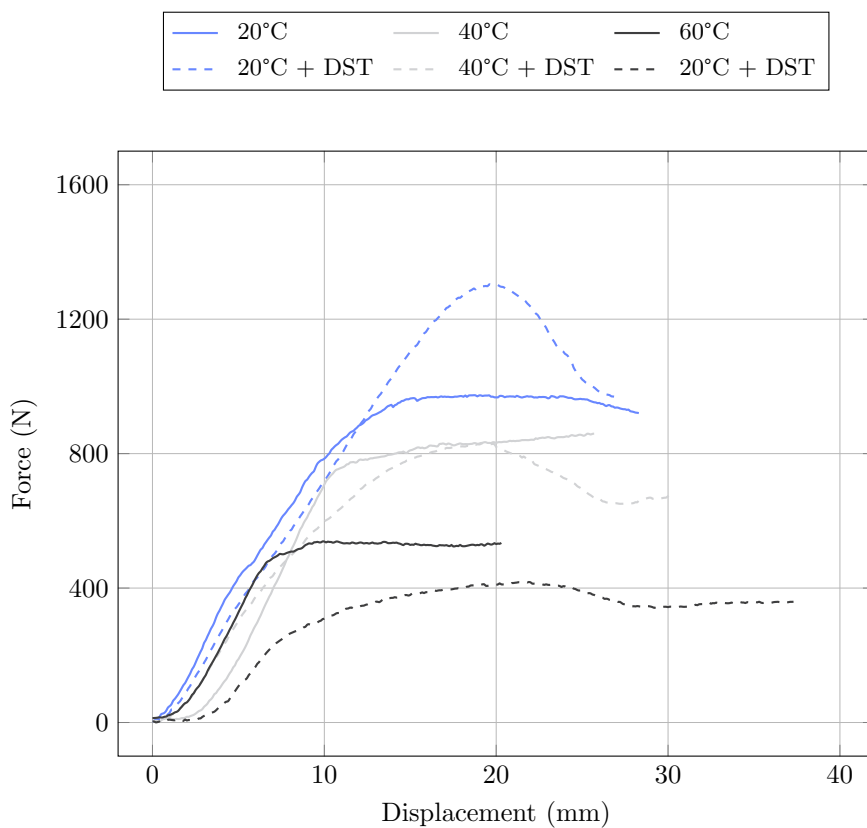


Figure 2.21 – Influence of the temperature on the sliding resistance for a 1.5 mm EPDM layer.
Results from [Tay15].

2.6.2 The sleeve system

Sleeves are major components in the structural system. The presented design is an important innovation compared with the composite gridshells built previously, where members were simply interrupted or overlapped (see [fig. 2.23a](#)). By establishing mechanical and architectural continuities between tubes, the new sleeve system brought the real behavior of the shell closer to its theoretical behavior (see [fig. 2.23b](#)).

The sleeve is a steel system that provides mechanical continuity between two adjacent composite tubes for both tension and bending. It is made of three parts : two connectors linked by a threaded rod (see [fig. 2.22](#)). Each connector is a 48.3 × 2.9 mm steel tube, slightly larger than the composite tubes it connects, with a welded M20 nut at one end. The connector is pinned to the composite tube with three 10 mm bolts. Some structural adhesive was also employed to fill the gaps and to guarantee good rigidity of the assembly. However, the sleeve is designed to ignore the contribution of the adhesive to the mechanical strength of the system. A M20 threaded rod links the two connectors. It allows tension forces and bending moments to pass from one tube to the other. It does not transfer any torsion.

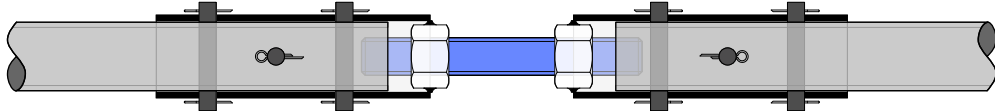


Figure 2.22 – Technical drawing of the sleeve system.

Mechanical behaviour

Tension forces are transferred from the composite tube to the connector through shear in the pins. Owing to a lower bearing resistance in the composite than in the steel, each of the three pins could be gradually loaded. When loading the system, initially, only one of the three pins is in contact with both the steel tube and the composite tube, because of inevitable minor manufacturing gaps. When the axial load is increased, this pin started to “eat” into the composite tube until the second pin also comes in contact. Thus, the axial load is transferred equally between the two pins. This scheme could work for more until another failure mode occurs. For this mode of composite failure, which prevailed in this case, the total bearing capacity of the assembly was thus three times the capacity of a single pin. This total bearing capacity can be calculated from the compressive strength, the composite thickness and the pin diameter :

$$F = 3 \times f_{u,c} \cdot d \cdot t = 3150 \text{ daN} \quad (2.4)$$

In the next section, tests carried out at the Navier laboratory to confirm the predicted value are presented. Bending moments were transferred through the threaded rod of the sleeve. This part was designed to reach the two following qualitative criterions simultaneously :

- Firstly, the bending stiffness of the rod should be roughly equivalent to the composite bending stiffness to preserve the curvature's continuity along the system (see [fig. 2.23c](#)). This continuity was of prime importance from an architectural point of view.

$$\frac{EI_{rod}}{EI_{gfrp}} \simeq 1 \quad (2.5)$$

- Secondly, the steel quality of the rod should be adjusted such that plastification begins when the composite tube tends to approach its maximum design stress (a third of the yield stress). Thus the rod acted as a “fuse” : if the curvature of the system reaches the maximum allowed curvature, the steel rod starts their plastification. The plastic hinge accumulates the rotation thus preventing the curvature to increase in the composite tubes (see [fig. 2.23d](#)).

$$\frac{M_{rod}^{elastic\ max}}{M_{gfrp}^{\sigma=133\ MPa}} \simeq 1 \quad (2.6)$$

In this project, the numerical values for the ratios in [eq. \(2.5\)](#) and [\(2.6\)](#) were 0.79 and 0.96 respectively.

Testing the load-bearing capacity of the pinned connection

[fig. 2.25](#) shows the tensile test of a three-pin connection between a connector and the corresponding composite tube. The graph reflects the elastic behavior of the composite tube up to 35 kN, with slight deviations corresponding to the rearrangement of the pins. The compressive stress applied by each pin to the composite tube exceeds its compressive strength. Progressively, the pins are pulled through the tube under a residual force that tends to stabilize at around 20 kN.

The theoretical failure modes of a bolt in a pultruded profile are given in [\[Fib03\]](#) and are illustrated in [fig. 2.26](#). For the present design of the sleeve system, the observed failure modes were tearing (see [fig. 2.24a](#)) and contact compression (see [fig. 2.24b](#)). Note that this last failure mode is necessary to cumulate the load bearing capacity of each pin.

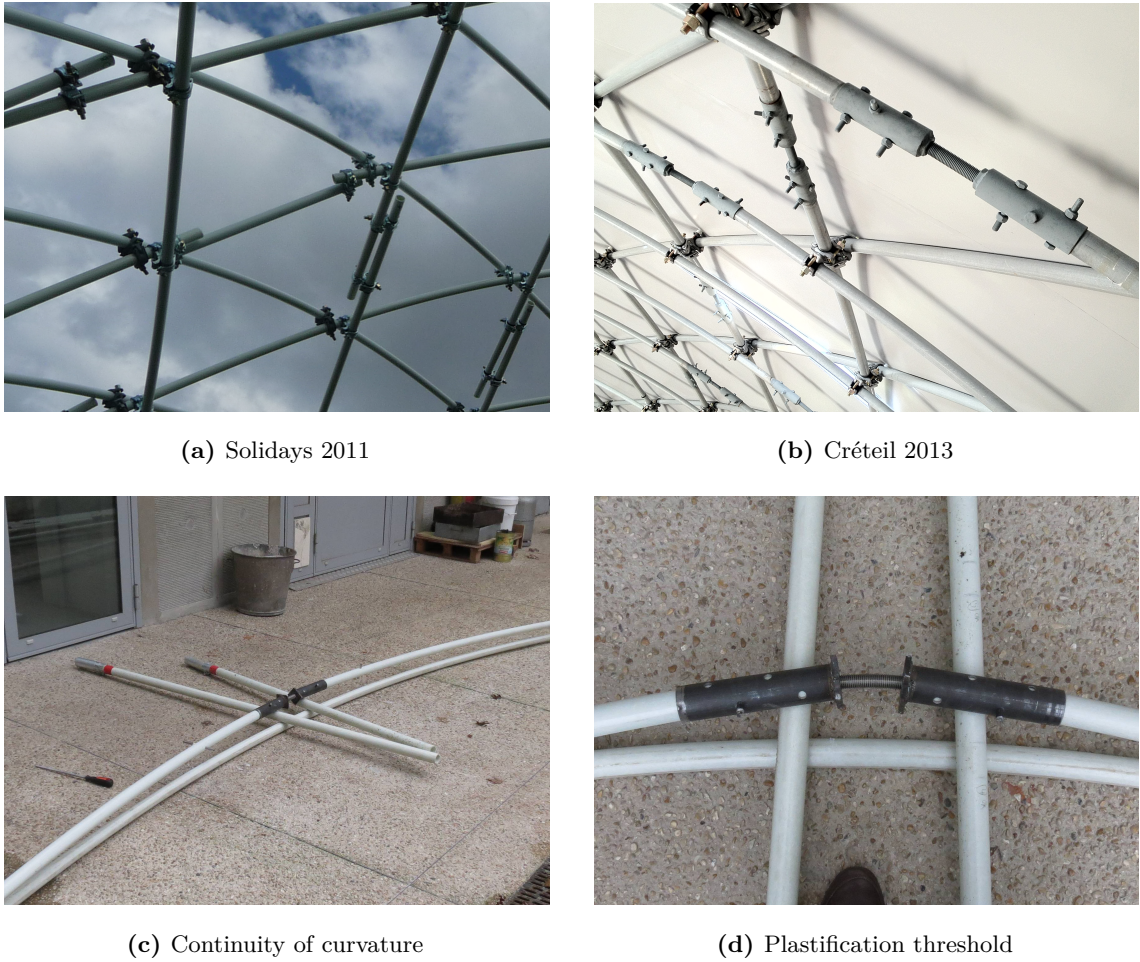


Figure 2.23 – Design and behavior of the the sleeve system.

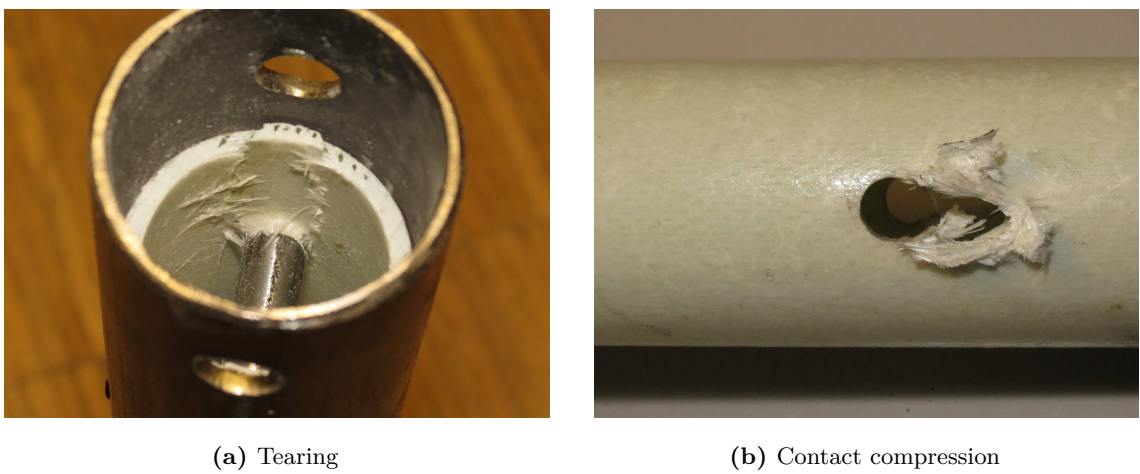


Figure 2.24 – Typical failure modes when testing the sleeve system in traction.

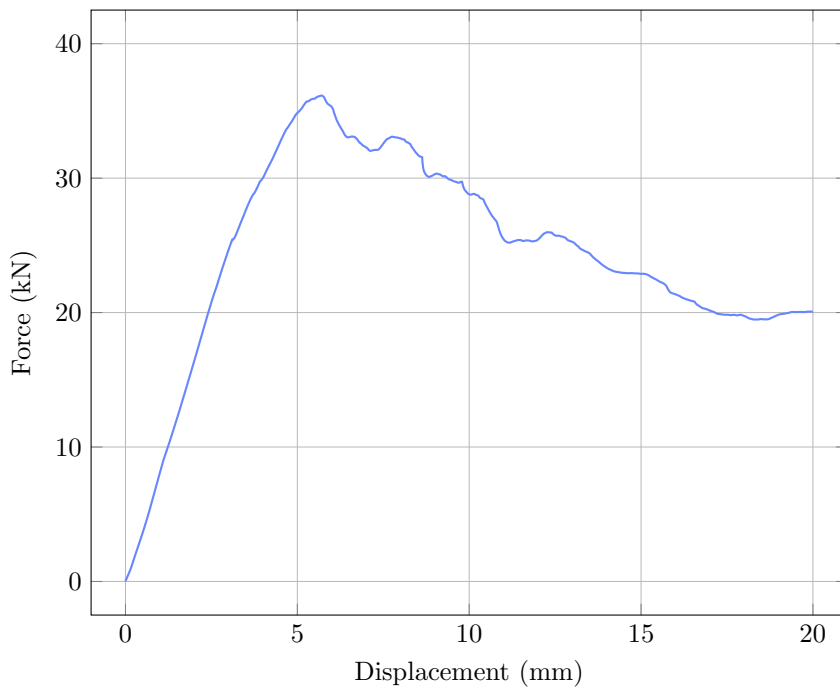


Figure 2.25 – Tensile test of the pinned connection. Results from [Tay15].

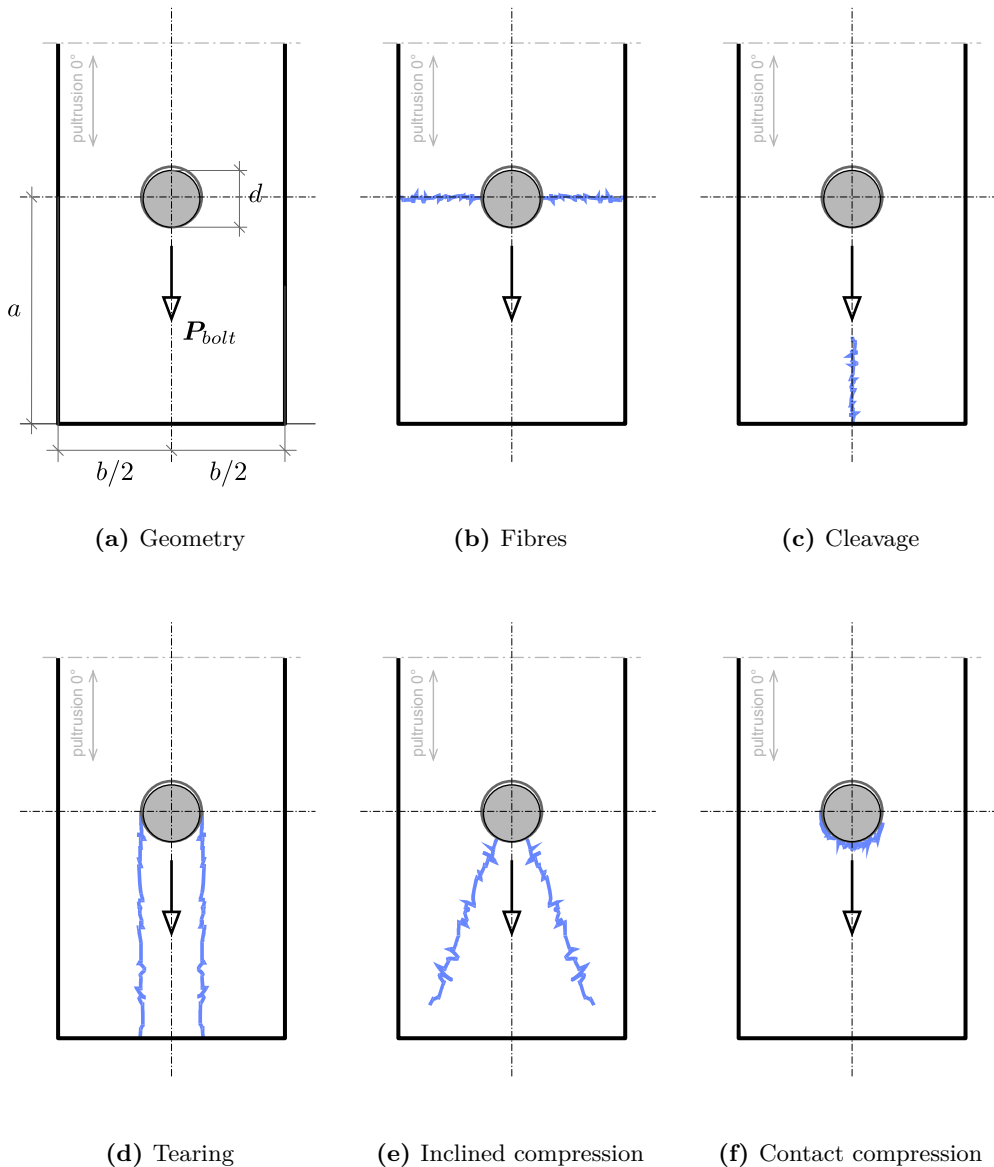


Figure 2.26 – Typical failure modes of a bolt in a pultruded element (0°).

2.6.3 Foundations

The detail of the footing was of major interest because it concentrated lots of technical difficulties and also had a strong visual impact (see [fig. 2.27](#)).

In the detail, the gridshell is fixed to the concrete strip thanks to the steel anchorages (6-15). Only the first tow layers of tubes are fixed to the ground or doors (4, 3). The anchorage is made of two parts : a steel connector (7) is pinned (6) to the composite tube (4) and equipped with a rotating steel clevis (9) ; a steel plate (15) is pinned to the concrete strip footing (26) and mounted with a vertical rotating steel clevis (11). The gridshell is connected to the ground by pinning the two parts of the anchorage. The three axis of rotations of the anchorage system – one for each clevis axis and one for the axis of the commun pin – allow to accommodate any orientations of the tube. More over, the rotation of the clevis is ensured by simple bolts (9,12) and nuts (8,13) that allow some adjustments in length. The system provides a quick and easy fixing of the gridshell capable of all the necessary adjustments required in real mounting conditions.

The membrane (1) is laced (17) to a composite rod (19). This rod is bent and clamped every 800 mm in a fixed scaffold collar (20) anchored in the concrete strip footing thanks to a steel part (21). This is a clever way to get a nice curved lacing rod at the bottom of the structure. The membrane strip (18) that ensures waterproofness is deported backward so the lacing remains visible. This has a strong and elegant visible impact. This detail runs all around the structure and is reproduced around the doors. This element is subject to heavy shear forces from the tension of the lacing (around 150 daN/lm) and this is why we chose a rod instead of a tube with a hollow section.

Thanks to the membrane strip and to a small step in the concrete slab (22) the water is evacuated into the drain, a simple trench full of gravels with two perforated flexible plastic pipes at the bottom.

2.6.4 The membrane

The membrane is nothing but a tailor-made one-piece clothing manufactured to dress up the structure. It was prefabricated based on the 3D model of the shape computed during the formfinding process (see ??) and not on some on-site geometric survey. The technical properties of the PVC coated fabric can be found in [tab. 2.3](#).

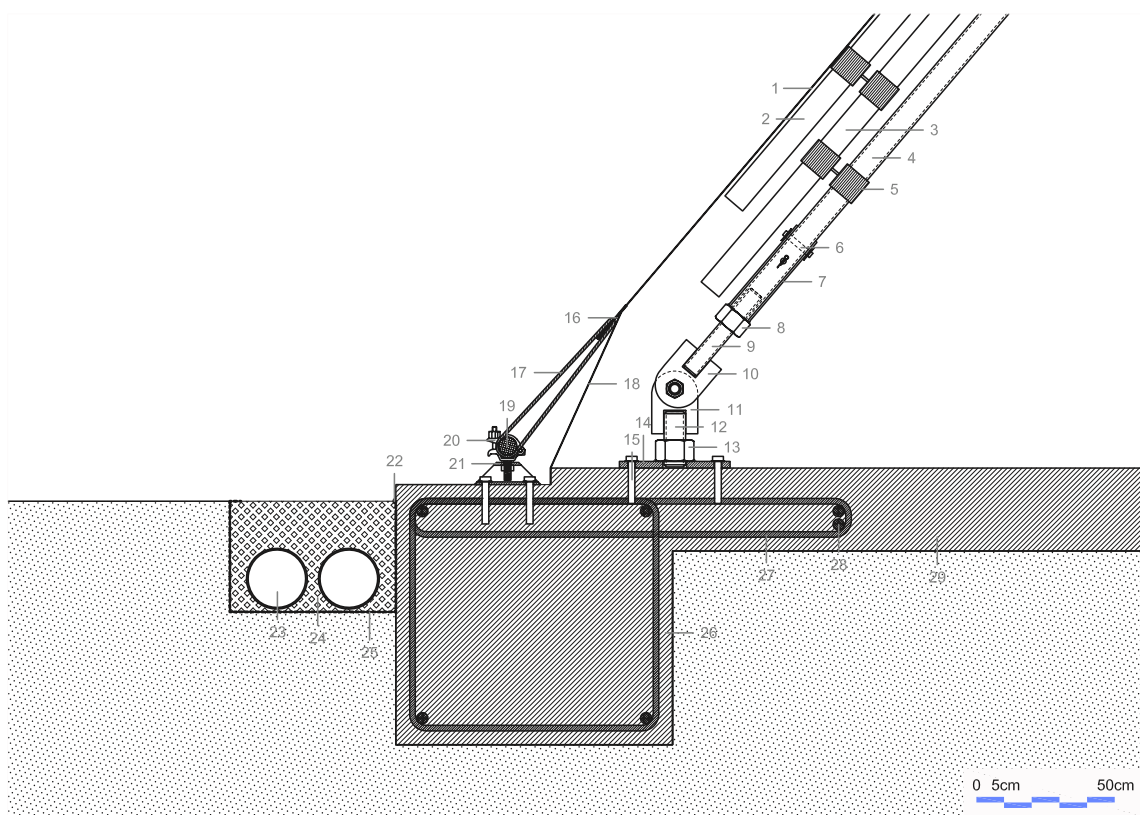


Figure 2.27 – Technical drawing of the footing.

2.7 Hygrothermal behavior

2.7.1 Temperature

During the first two years and a half of its service life, the building has shown that the thermal comfort was far from ideal as the membrane has very poor thermal properties (see [tab. 2.3](#)) :

- During winter, the comfort is ensured during mass by a forced-air heating system positioned on the equipments slab, few meters away from the main structure. This solution is adapted to infrequent occupations of the building. In that case, the energetic cost remains limited even if the solution is far from optimal because of the lack of insulation.
- During summer, the temperature raises very fast when the sun shines. The forced-air system is used to ventilate the interior volume. But the comfort level is rapidly insufficient as the interior temperature quickly exceeds 30 °C. The discomfort is amplified as the membrane gets very hot and radiates toward the inside, increasing the feeling of warm. Consequently, there was no choice but to scheduled the mass earlier at this period of the year. Cooling was not possible for economic reasons as the building was used only few hours a week.

At the time of writing, the building is being reconfigured and so its purpose is changing. A better thermal comfort is now required and solutions have to be found. Thus, a study on the thermal behavior of the structure has been done.⁹ The main results are gathered in this thesis. [fig. 2.28a](#) presents the monthly exterior temperatures observed at the site location from 8:00 AM to 7:00 PM, which corresponds to the new intended opening hours of the building. Note that the maximum value is given over one hour, that is the observed temperature exceeds this value during a one-hour-wide window in the day. The solar radiation is also given in [fig. 2.28b](#). Two scenarios are studied :

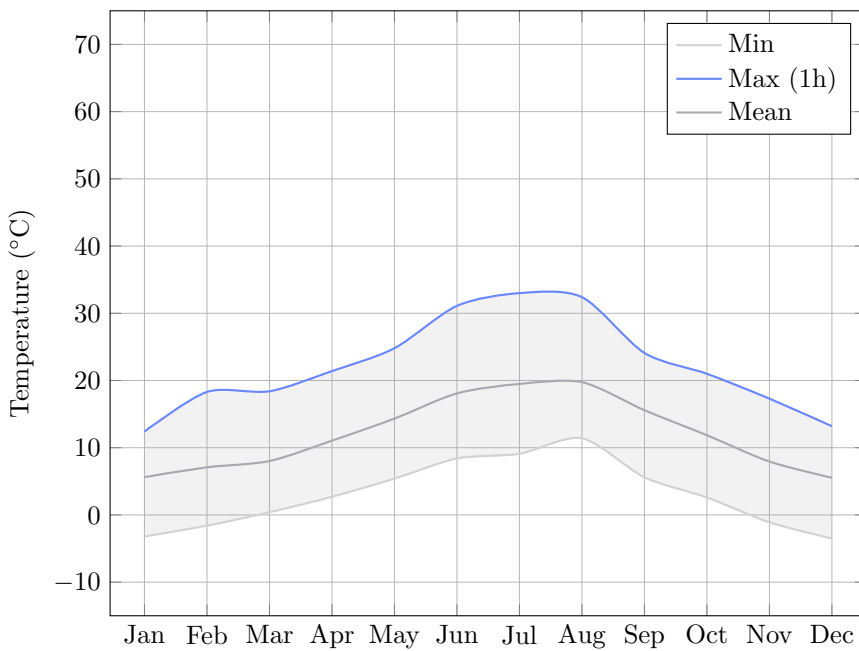
1. The structure is completely closed. No ventilation is put in place. The interior temperature can reach 70 °C (see [fig. 2.29a](#)).
2. The structure is ventilated but no cooling system is put in place. The maximum interior temperature is lowered significantly but it can still reach 50 °C (see [fig. 2.29b](#)).

This study confirms what the experience has shown : the temperature inside the building can be very high. Above 30 °C this is problematic for the comfort of the people. Above 50 °C and up to 70 °C it becomes problematic for the building itself. Indeed, this level of temperature is closed to the heat resistance of the membrane (see [tab. 2.3](#)) ; the interface layer faces a serious decrease of its capacity to resist to sliding ([fig. 2.21](#)) ; the creeping kinetics of GFRP tubes is speed up ([§2.5.1](#)).

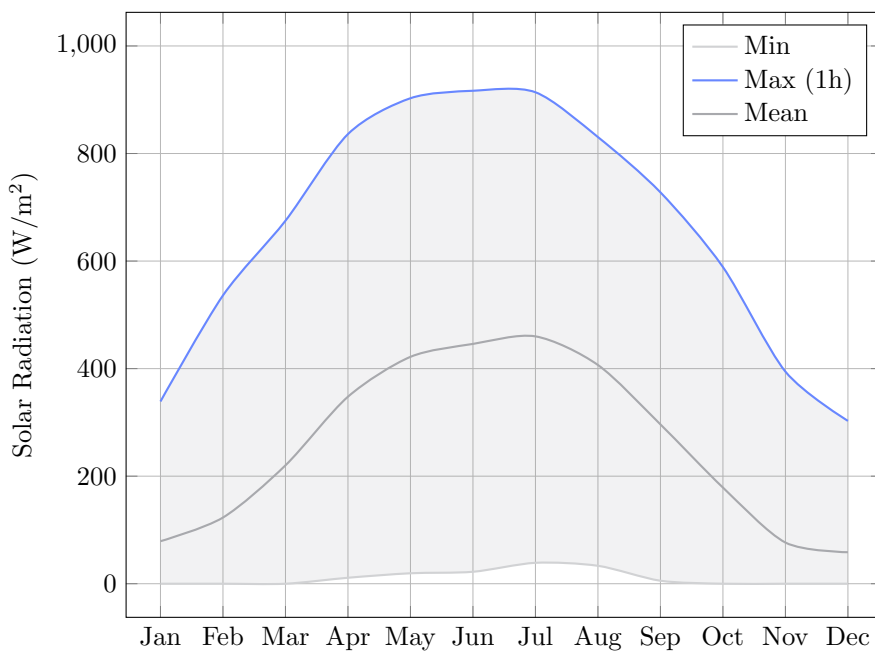
⁹This study was done in June 2017 by the design companies T/E/S/S and CHOULET for the reconfiguration project of the temporary cathedral.

2.7.2 Moisture

Condensation was also noticed in winter and shoulder season. Sometimes, droplets of water could fall abundantly and thus the wooden furnitures had to be protected. This phenomenon was particularly intense the first months because the concrete slab had not yet fully dry-out. To protect the structure and the furnitures, it was decided to maintain the inside temperature above 10 °C at all times.

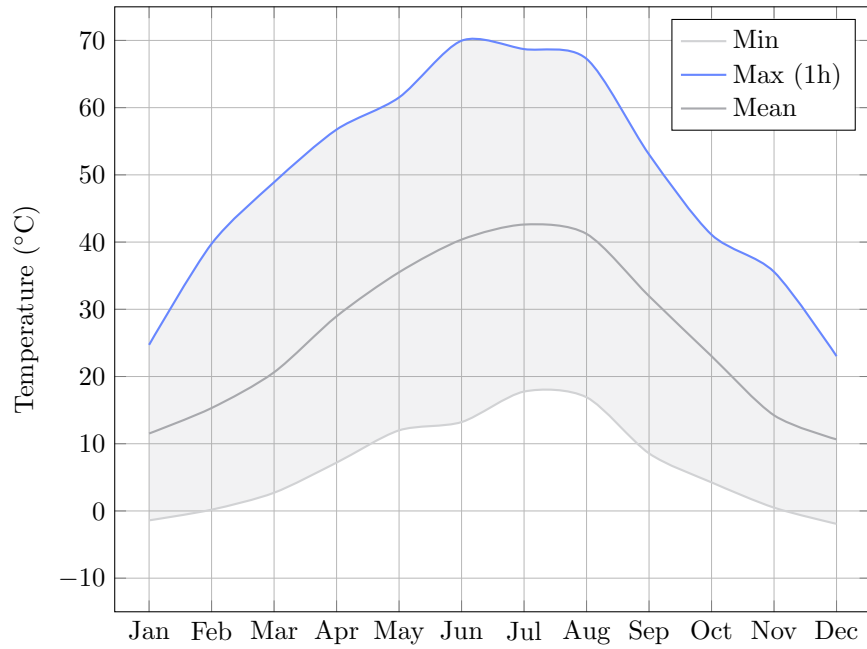


(a) Temperature.

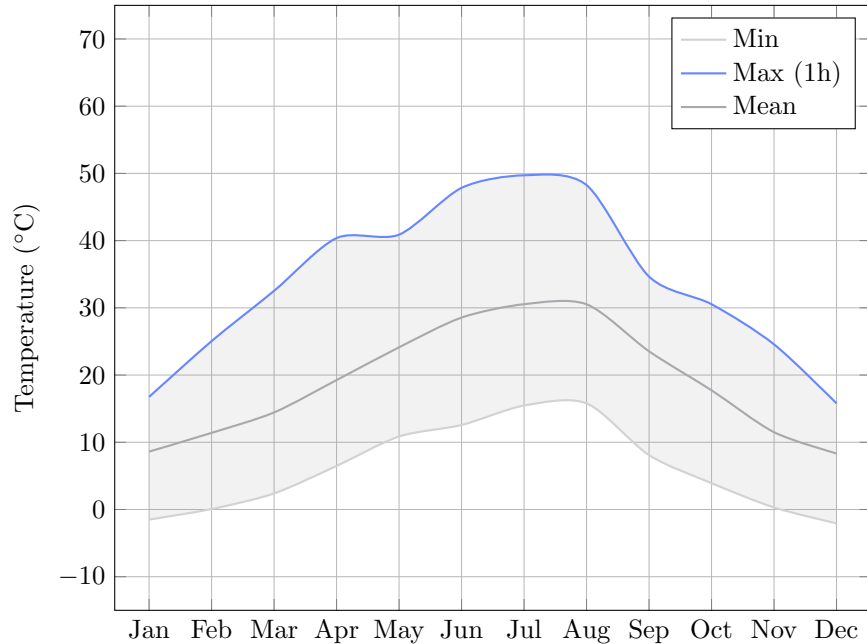


(b) Solar radiation.

Figure 2.28 – Weather data at site location during opening hours (8:00 AM to 7:00 PM).



(a) Without ventilation.



(b) With ventilation.

Figure 2.29 – Temperature inside the building during opening hours (8:00 AM to 7:00 PM).

2.8 Cost analysis

2.8.1 Overall cost for the client

The overall cost of the project – that is the amount of money paid by the client – was estimated to 324 000 € excluding taxes (see [fig. 2.30](#)). This price includes all the possible costs related to the construction of the project : the cost of the main building (masonry, doors, gridshell, envelop, fittings, heating, electricity, lightning, drainage, sewage, etc.), the cost of the service building, the cost of pedestrian pathways, the cost of the design studies, etc.

However, this cost does not take into account all the (free) man-hours spent by the volunteers to prefabricate, assemble, erect and brace the gridshell. The real cost of the gridshell system, when a cost is put on this labor, is estimated in [§2.8.2](#).

Moreover, this project required a lot of design studies and tests to verify the material properties and to validate the strength of key elements such as the swivel coupler with its EPDM layer, the sleeve system and the ground anchorage. The real cost of the studies was by far higher than what was really charged to the client and the difference must be regarded as an investment from the company T/E/S/S. In the same manner, people from the laboratory gave a consistent support during the construction stage as they were the only available experienced workers familiar with the construction of elastic gridshells in composite material [[DCB10](#), [Bav+12](#)] and this labor was not charged back to the client.

The project was favorably accepted by the client based on the estimation that the cost of the gridshell would not be more expensive by 30% than renting a simple tent. The rental of a 400 m² tent with its floor was evaluated to 110 000 € for a period of time of 18 months. Retrospectively this target was met, especially as the cathedral was finally used for almost two years and a half, far more than the 18 months expected initially, and with no additional cost because the diocese owned the building

2.8.2 Cost details for the building

Here we present the cost details for the main building, that is the cathedral itself. We try to understand what is the true cost of the gridshell system in this particular project and we thus eliminate side costs (for instance the cost of fittings, the cost of the pedestrian pathways, the cost of the service building, etc.). The cost allocation is presented per square meter of covered area in [fig. 2.31](#). The total price for the building, excluding studies, is 473 €/m². It is composed of :

- 100 €/m² : the cost of masonry works (levelling, footings, slab, drainage) detailed in [tab. 2.7](#). This construction works were made by a professional contractor named BATEM.
- 248 €/m² : the cost of the superstructure (anchorages, gridshell, membrane covering and doors) detailed in [tab. 2.8](#). This price includes the labor of the volunteers

(35 €/hour) and all the costs associated to construction of the structure, including the renting of all the necessary equipments (cranes, aerial buckets, etc.).

- 126 €/m² : the cost of the envelope (lacing rod, fabric, installation) detailed in [tab. 2.8](#). This construction works were made by a professional contractor named ESMERY CARON.

Here, the global amount of studies was charged around 83 300 €, that is 248 €/m² (see [fig. 2.30](#)). This heavy cost was compensated by the fact that volunteers provided a lot of free labor (see [fig. 2.32](#)). In a more standard commercial context, the design process would be optimized too and the price of studies would go down to 15% to 20% of the price of the building, that is 70 to 95 €/m². This would bring the final price of the building to 550 €/m². This price is clearly high if only its sheltering capability is required regarding other technologies.. However, if more than sheltering is mandatory, the quality and singularity of the space created here is probably worth the price ; then this technology becomes a lot more affordable than existing traditional systems that can materialized free-forms.

2.8.3 Strengths and weaknesses

In this project the prefabrication process represents almost half of the cost in man-hours (see [fig. 2.32](#)). The manufacturing of the grid (cutting pipes, marking nodes, preassembling swivel couplers, sleeves and anchorages, etc.) could easily be automated. Composite materials such as GFRP are easy to cut, mill and drill. Small robot arms can do the job quickly with a better accuracy. This idea has been tested in a workshop at the Ecole des Ponts ParisTech in september 2016.¹⁰ More over, a numerical production process would allow to answer quickly to a variety of forms with the same equipment and industrial process.

Lots of man-hours are spent in the installation of the sleeve system (88 h). That represents 35 % of the man-hours spent in the grid prefabrication. This part should be reimplemented to allow a simpler and faster installation. Similarly, the connection should be redesigned to avoid the application of the EPDM protection layer and to allow a faster positioning and fastening as it represents 23 % of the man-hours spent in the prefabrication of the grid. This would also be a preponderant factor of improvement in the bracing stage although this cost is not detailed in [tab. 2.6](#).

At first sight it seems that the time spending assembling the grid on the construction site – which represents 22 % of the man-hours, see [fig. 2.32](#) – can not easily be reduced. However, the grid system could be divided into transportable modules. These modules would be preassembled in the factory to increase the speed and quality of the production and to minimize on-site works. Thanks to the intrinsic grid kinematic, modules can be folded for transportation. Once on site, modules are unfolded and connected to each other to form the primary flat grid. This idea was tested successfully in two wooden gridshell projects

¹⁰See the video of the construction of a 50 m² wooden gridshell in the workshop “Building Free Froms” : <http://thinkshell.fr/freeform-wooden-gridshell-2016/>.

of 50 m² each, with students of the Ecole National d'Architecture de Toulouse and Ecole National d'Architecture de Grenoble in June 2016.¹¹

Bracing is yet another costly stage as it accounts for almost 30 % of the man-hours (see fig. 2.32). This work is not easily parallelizable as it requires working at height with proper lifting equipments such as cherry pickers. Thus almost a small and qualified team can do the job. For instance, on the gridshell of Créteil, the team was composed of 6 workers using two aerial lifts. This team spent three full days to complete this task, that is the same amount of days required to assemble the grid and lift it up. Several attempt have been made during this thesis to answer this problematic. The first attempt was to use a bidirectional cable network to brace the grid. The network is installed at the ground level before the grid is deformed. Thus, work at height is reduced to a minimum. The second attempt is a larger thought on the envelope of such structures and tries to tackle two issues with a thin fibre-reinforced concrete skin : the fact that bracing with a third direction of tubes is time consuming ; and the fact that membrane covering is not adapted for permanent buildings.

¹¹Construction of two wooden gridshell pavilions : <http://www.lemoniteur.fr/article/a-toulouse-les-architectes-se-rassemblent-sous-le-meme-pavillon-32398196>.

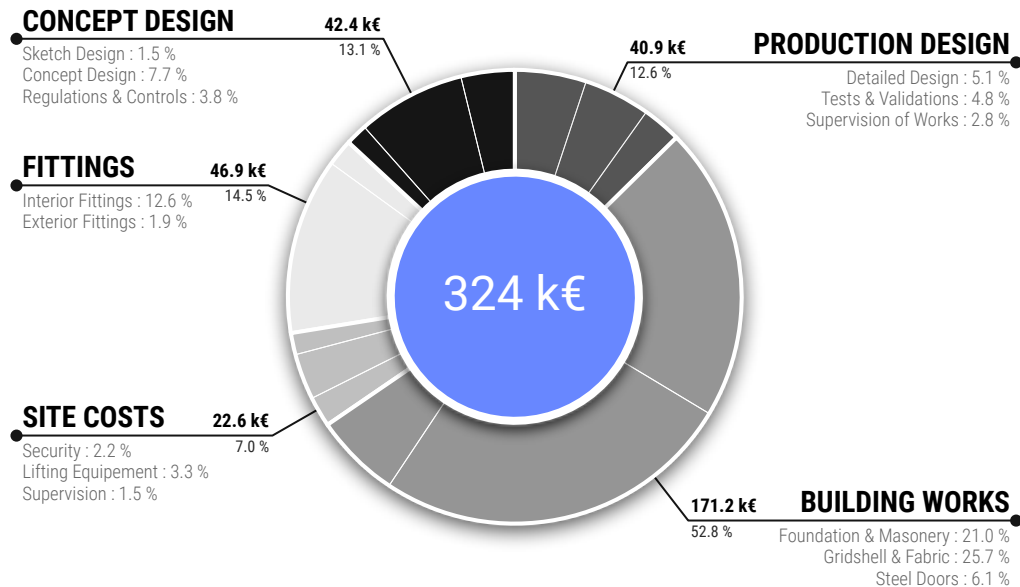


Figure 2.30 – Cost allocation for the whole project. This is the estimated overall final cost charged to the client. Prices are given excluding taxes (V.A.T).

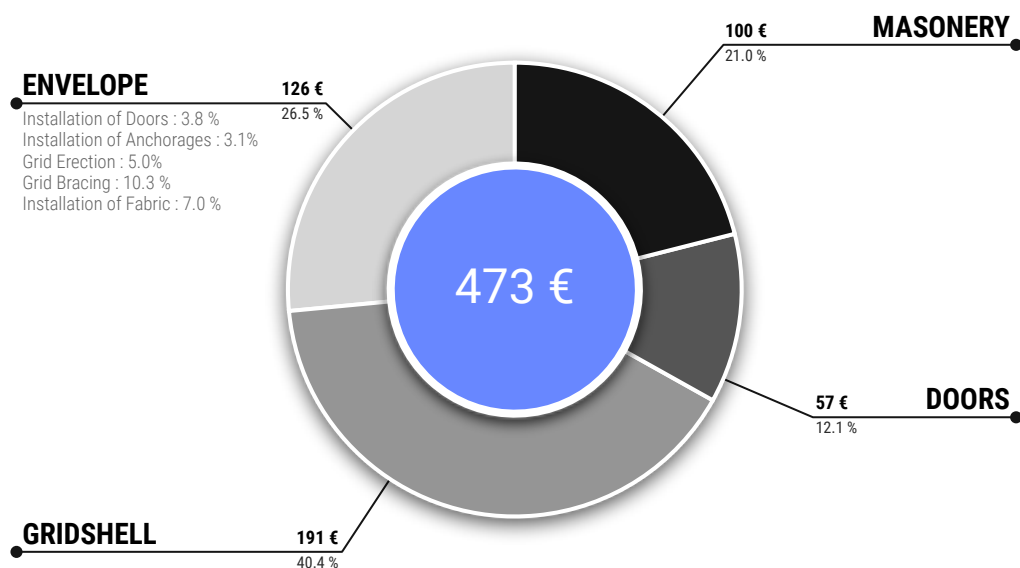


Figure 2.31 – Cost allocation per square meter of covered area. The cost of design is not included as it would not be representative. Prices are given excluding taxes (V.A.T).

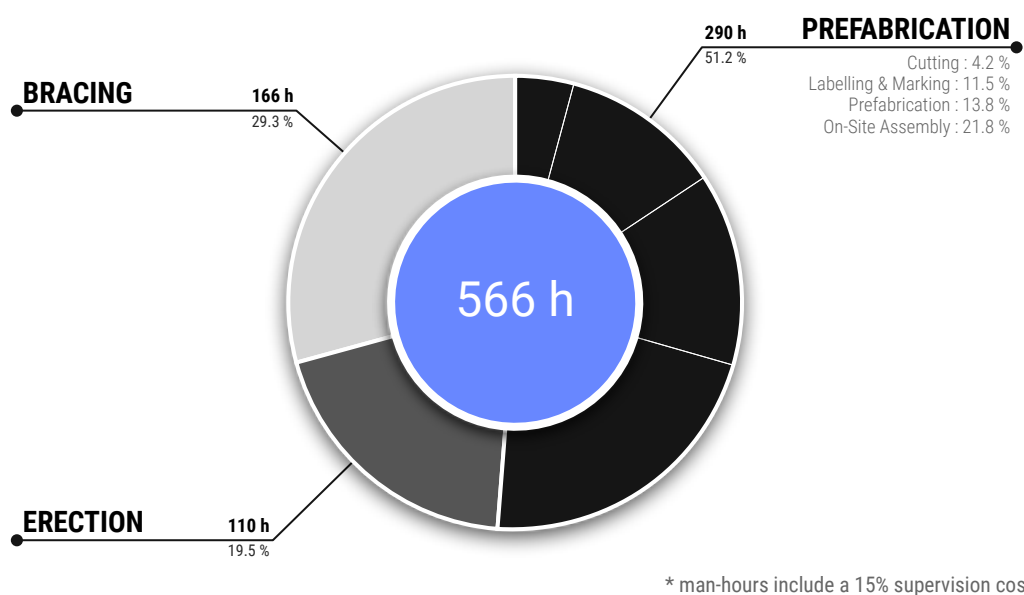


Figure 2.32 – Allocation of the man-hours spent by the volunteers on the fabrication of the gridshell. A 15% increase is considered to take into account coordination and supervision of the individual tasks. See [tab. 2.6](#) for detailed data.

Item	Unit Task		Man-Hours	
	Worker	Duration	Quantity	Hours
Workstation “Cutting”	4			20.53
Pick a raw tube from the stock	2	1' 00"	176	5.87
Mark it and cut it at right length	2	2' 00"	176	11.73
Put it into the labelling stock	2	0' 30"	176	2.93
Workstation “Labelling”	5			56.64
Pick a tube from the labelling stock	2	1' 00"	176	5.87
Label it at start and end	2	1' 00"	176	5.87
Mark the position of connection collars	1	0' 30"	2260	18.83
Mark the position of sleeves	1	0' 30"	250	2.08
Mark the position of anchorages	1	0' 30"	127	21.06
Put it into the prefabrication stock	2	0' 30"	176	2.93
Workstation “Prefabrication”	6			67.75
Pick a tube from the prefabrication stock	2	1' 00"	176	5.87
Put the EPDM ribbon	1	0' 30"	2260	18.83
Prefix the swivel collar on the tube	1	0' 30"	565	4.71
Glue the sleeves	3	2' 00"	250	25.00
Drill pin holes for the sleeves	1	1' 00"	250	4.16
Fix sleeve pins	1	1' 30"	250	6.25
Put it into the final stock	2	0' 30"	176	2.93
Workstation “Site Assembly”	12			107.34
Connect the sleeves with steel rods	5	5' 00"	125	52.08
Pick a tube and position it in the grid	2	3' 00"	176	17.60
Install swivel couplers (HV)	1	2' 00"	565	18.83
Controlled tightening of couplers (HV)	1	1' 00"	1130	18.83
Workstation “Grid Erection”	12	8:00' 00"	1	96.00
Workstation “Grid Bracing”	6	8:00' 00"	3	144.00
Grid prefabrication				252.00
Grid erection				96.00
Grid bracing				144.00
Cost of supervision (15%)				74.00
Total				566.00

Table 2.6 – Man-hours spent by the volunteers on the fabrication of the gridshell. A 15% increase is considered to take into account coordination and supervision of the individual tasks. See [fig. 2.32](#) for a graphical representation of these data.

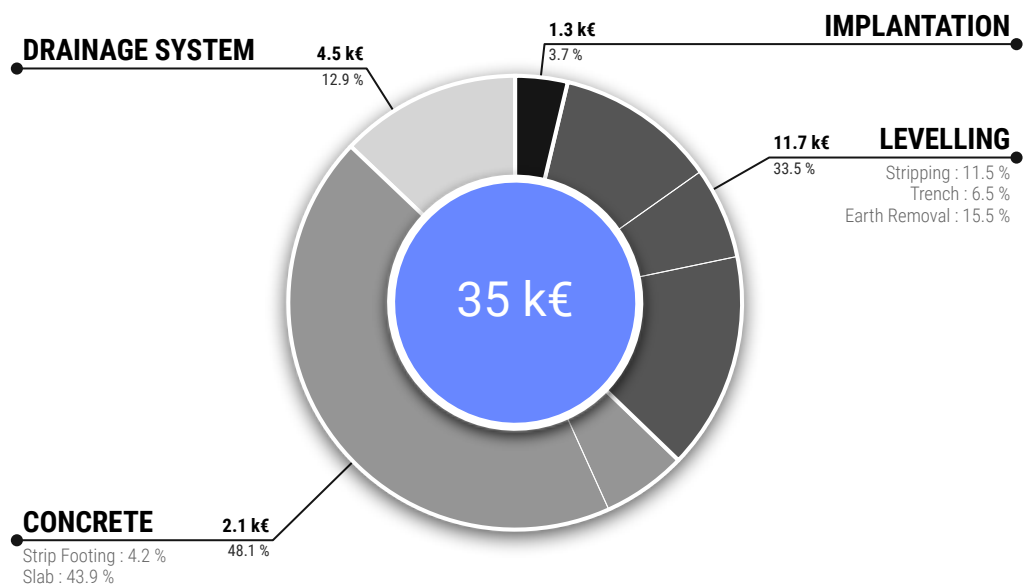


Figure 2.33 – Cost allocation for masonry works. Prices are given excluding taxes (V.A.T). Only costs associated to the structure are reported here ; for instance the works for the equipment slab and the pathways are omitted. See [tab. 2.7](#) for detailed data.

Item	Unit	Quantity	U.P. (€)	Price (€)
Building implantation		1	1 300.00	1 300.00
Leveling works				11 680.00
Top soil stripping	m ²	400	10.00	4 000.00
Trench for concrete strip footing	ml	76	30.00	2 280.00
Earth removal	m ³	180	30.00	5 400.00
Concrete				17 400.00
Concrete strip footing (200 kg/m ³ steel)	ml	70	30.00	2 100.00
Concrete slab (x2 welded wire mesh)	m ²	340	45.00	15 300.00
Drainage systems				4 500.00
French drain (x2 Ø100 mm pipes)	ml	70	30.00	2 100.00
Precast concrete inspection chamber		1	400.00	400.00
Drain line (PVC Ø125 mm pipe)	ml	30	30.00	900.00
Pre-assembled channel drain	ml	10	110.00	1 100.00
Masonry works	€/m ²	350	100	34 880.00

Table 2.7 – Cost details for masonry works. Prices are given excluding taxes (V.A.T). Only costs associated to the structure are reported here ; for instance the works for the equipment slab and the pathways are omitted. See [fig. 2.33](#) for a graphical representation of these data.

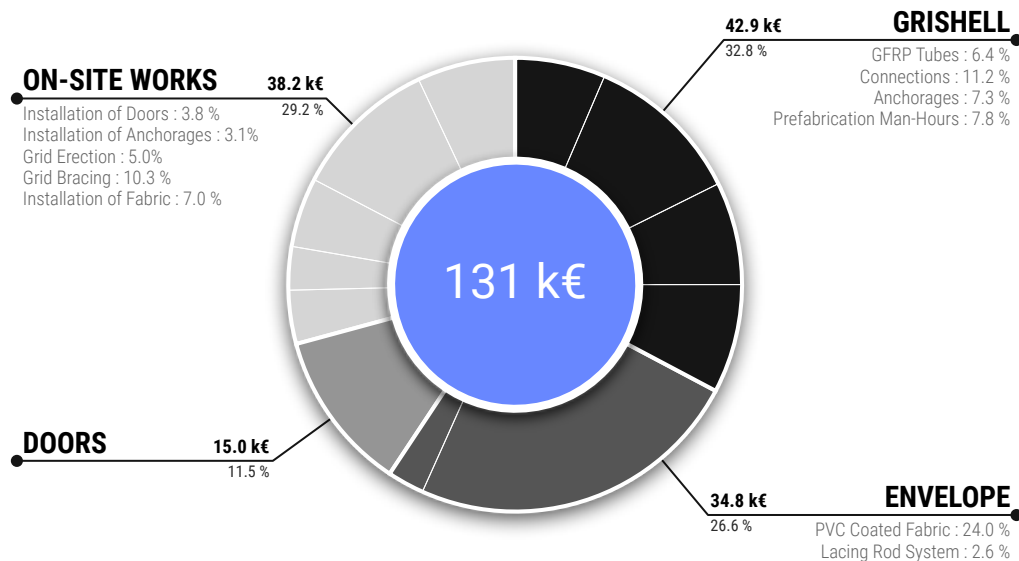


Figure 2.34 – Cost allocation for the superstructure. On-site works are isolated to identify pure manufacturing costs. To this end, the cost of the man-hours provided by the volunteers to prefabricate the grid has been assessed and allocated. See [tab. 2.8](#) for detailed data.

Item	Unit	Quantity	U.P. (€)	Price (€)
Manufacturing of the gridshell				42 853
GRFP tube (Ø42 mm)	ml	2304	3.66	8 433
Swivel connector (42x42 mm)		1295	3.95	5 115
Swivel connector (42x49 mm)		135	4.18	564
EPDM layer (1302x40x1.5 mm ribbon)		2775	0.36	1131
Welded steel sleeve system		150	50.00	7 500
ARALDIT 2047 glue (480 ml cartridge)		8	45.00	360
Ground anchorage (welded steel)		120	80.00	9 600
Man-hours (prefabrication)	h	290	35.00	10 150
Manufacturing of the envelope				34 769
GFRP lacing rod (Ø32 mm)	ml	96	14.00	1 134
Steel clip for the rod		125	15.00	1 875
Swivel collar (Ø34 mm)		120	3.50	420
PVC coated fabric	m ²	550	50.00	27 500
Option for transparent inclusion		12	320.00	3 840
Manufacturing of the steel doors				15 000
Main door		1	10 000.00	10 000
Small door		1	5 000.00	5 000
On-site works of installation				33 365
Installation of the doors		1	5 000.00	5 000
Installation of the anchorages and clips	h	90	45.00	4 050
Grid erection	h	110	35.00	3 850
cranes (x2 35T)	h	24	110.00	2 640
Grid bracing	h	167	45.00	7 515
aerial bucket (x2)		1	6 000.00	6 000
Installation of fabric		1	9 165.00	9 165
Total	€/m ²	374	363	130 842
Cost of structure			265	92 622
Cost of installation			109	38 220

Table 2.8 – Cost details for the superstructure. On-site works are isolated to identify pure manufacturing costs of the gridshell, the envelope and the doors. To this end, the cost of the man-hours provided by the volunteers to prefabricate the grid has been assessed and allocated. Prices are given excluding transport costs and excluding taxes (V.A.T.). Spare quantities are included. See fig. 2.34 for a graphical representation of these data.

2.9 Conclusions

This paper has presented the different steps for the design of a gridshell in composite material : a Temporary Cathedral at Crêteil, in Paris suburb, in 2013. The first step was the optimization of the shape in order to avoid local concentrations of curvature. The second step showed a tool to automatically mesh a surface using the compass method. With this tool, the orientation of the mesh is studied according to structural and architectural criterions. The last steps showed the structural analysis of the gridshell and how to get the as-built geometry from the analysis model. Architecturally, the structure offers a very interesting space where the textual richness of the tubes against the membrane accentuates the reading of the complex curved surfaces.

This project demonstrates that gridshells in composite material are suitable for constructing freeform buildings. However, the long-term behavior of these materials needs to be better characterized to extend their lifespan.

At the moment, further developments are conducted by the laboratory to take account for torsional effects and non axisymmetric sections in such structures, as it is studied in [BAK13].

2.10 Acknowledgements

First of all, the authors would like to thank the Catholic Church of Crêteil for their trust and their courage, which led to the initiation and successful completion of this ambitious project. Secondly, the authors would like to acknowledge the engineers from T/E/S/S, who had developed this challenging project over 18 months. They have carried out valuable work and permitted research to become a reality through this innovative edifice. Further thanks goes to Viry for the supervision of the construction works, including the delicate erection stage. Thirdly, the authors would like to thank warmly all the people involved in the construction process: the numerous parish volunteers, the technicians and researchers from the Navier laboratory and the engineers from T/E/S/S and Viry firms. Beyond the technical aspect, their enthusiasm made this project a powerful human experience. Fourth, the authors would like to thank the local firms for their work: BATEM (concrete), Eloi (steel), Esmery Caron (fabric), Solutions Composites (composite material), Axmann (connections) and ENSG.

2.11 References

- [AB01] S. Adriaenssens and M. Barnes. “Tensegrity spline beam and grid shell structures”. In: *Engineering Structures* 23.1 (2001), pp. 29–36.
- [Add13] B. Addis. “‘Toys that save millions’ - A history of using physical models in structural design”. In: *The Structural Engineer* 91.4 (2013), pp. 12–27.
- [Adr00] S. Adriaenssens. “Stressed spline structures”. PhD thesis. University of Bath, 2000.
- [BAK13] M. Barnes, S. Adriaenssens, and M. Krupka. “A novel torsion/bending element for dynamic relaxation modeling”. In: *Computers & Structures* 119 (Apr. 2013), pp. 60–67.
- [Ban06] L. C. Bank. *Composites for construction : structural design with FRP materials*. 2006, p. 560.
- [Bav+12] O. Baverel, J.-F. Caron, F. Tayeb, and L. du Peloux. “Gridshells in composite materials : construction of a 300 m² forum for the solidays’ festival in Paris”. In: *Structural Engineering International* 22.3 (2012), pp. 408–414.
- [BBC14] L. Bouhaya, O. Baverel, and J. F. Caron. “Optimization of gridshell bar orientation using a simplified genetic approach”. In: *Structural and Multidisciplinary Optimization* 50.5 (2014), pp. 839–848.
- [Cla03] J. L. Clarke. *Eurocomp design code and handbook : structural design of polymer composites*. 2003, p. 672.
- [DCB10] C. Douthe, J.-F. Caron, and O. Baverel. “Gridshell structures in glass fibre reinforced polymers”. In: *Construction and Building Materials* 24.9 (2010), pp. 1580–1589.
- [Dou07] C. Douthe. “Etude de structures élancées précontraintes en matériaux composites : application à la conception des gridshells”. PhD thesis. Université Paris Est, 2007, p. 274.
- [dPel+11] L. du Peloux, O. Baverel, J.-F. Caron, and F. Tayeb. “From shape to shell : a design tool to materialize freeform shapes using gridshell structures”. In: *Design Modelling Symposium*. Berlin, Deutschland, 2011.
- [dPel+16] L. du Peloux, F. Tayeb, O. Baverel, and J.-F. Caron. “Construction of a large composite gridshell structure: a lightweight structure made with pultruded glass fibre reinforced polymer tubes”. In: *Structural Engineering International* 26.2 (2016), pp. 160–167.
- [Fib03] Fiberline Composites A/S. *Fiberline design manual*. May. 2003, pp. 1–326.
- [Kot12] N. Kotelnikova-Weiler. “Optimisation mécanique et énergétique d’enveloppes en matériaux composites pour les bâtiments”. PhD thesis. Université Paris-Est, 2012, p. 310.
- [LDB15] B. Lefevre, C. Douthe, and O. Baverel. “Buckling of elastic gridshells”. In: *Journal of the IASS* September (2015).
- [Sit] Site Sécurité. *Règlement ERP type CTS (big tops & tents)*.

- [Tay15] F. Tayeb. “Simulation numérique du comportement mécanique non linéaire de gridshells composés de poutres élancées en matériaux composites et de sections quelconques”. PhD thesis. 2015.

Rich Kirchhoff beam model Part II

3 Geometry of smooth and discrete space curves

3.1 Introduction

idée : Rapprocher l'étude des courbes continues et des discrétisées avec le concept de modèle de la «courbe polygone» de Leibniz et de ses successeurs, une infinité de côtés infiniment petits. [Del11, p.235]

Voir aussi que la geometry des space curves semble intimement liée à celle des surface. [Coo13, Del11]

Car les courbes n'étant que des polygones d'une infinité de côtés, et ne diffèrent entre elles que par la différence des angles que ces côtés infiniment petits font entre eux; il n'appartient qu'à l'Analyse des infiniment petits de déterminer la position de ces cotés pour avoir la courbure qu'ils forment [...].

Attention à la terminologie smooth vs. continuous :

A smooth curve is a curve which is a smooth function, where the word "curve" is interpreted in the analytic geometry context. In particular, a smooth curve is a continuous map f from a one-dimensional space to an n -dimensional space which on its domain has continuous derivatives up to a desired order.¹

3.1.1 Goals and contributions

Dans ce chapitre, après un bref rappel sur le cadre mathématique d'étude des courbes paramétrique de l'espace, on présente les notions de courbures et de torsion géométrique

¹Definition of a smooth curve from mathworld : <http://mathworld.wolfram.com/SmoothCurve.html>

associées au repère de Frenet. On montre ensuite le cas plus général d'un repère mobile quelconque attaché à une courbe gamma. On définit enfin la particularité d'un repère mobile adapté à un courbe, et on présente, en sus du repère de Frenet, une approche différente pour accrocher des repères le long d'une courbe (Bishop / RMF / Zéro-twisting frame)

Contributions : présentation et comparaison de différentes façons d'estimer la courbure discrete

3.1.2 Related work

Bishop [Bis75] [Bis75] Bishop 1975

[Bis75] [Ber+08] [Hof08] [Bluth2014] [Fre52] [Del07] [Far+14] [Gug89] [Klo86]

3.1.3 Overview

3.2 Parametric curves

3.2.1 Definition

Let I be an interval of \mathbb{R} and $F: t \mapsto F(t)$ be a map of $\mathcal{C}(I, \mathbb{R}^3)$. Then $\gamma = (I, F)$ is called a *parametric curve* and :

- The 2-uplet (I, F) is called a *parametrization* of γ
- $\gamma = F(I) = \{F(t), t \in I\}$ is called the *graph* or *trace* of γ
- γ is said to be \mathcal{C}^k if $F \in \mathcal{C}^k(I, \mathbb{R}^3)$

Note that for a given graph in \mathbb{R}^3 they may be different possible parameterizations. Thereafter γ will simply refers to its graph $F(I)$.

3.2.2 Regularity

Let $\gamma = (I, F)$ be a parametric curve, and $t_0 \in I$ be a parameter.

- A point of parameter t_0 is called *regular* if $F'(t_0) \neq 0$.
The curve γ is called *regular* if γ is \mathcal{C}^1 and $F'(t) \neq 0, \forall t \in I$
- A point of parameter t_0 is called *biregular* if $F'(t_0)$ and $F''(t_0)$ are not collinear
The curve γ is called *biregular* if γ is \mathcal{C}^2 and $F'(t) \cdot F''(t) \neq 0, \forall t \in I$

3.2.3 Reparametrization

Let $\gamma = (I, F)$ be a parametric curve of class C^k , $J \in \mathbb{R}^3$ an interval, and $\varphi: I \mapsto J$ be a C^k diffeomorphism. Let's define $G = F \circ \varphi$. Then :

- $G \in C^k(J, \mathbb{R}^3)$
- $G(J) = F(I)$
- φ is said to be an admissible *change of parameter* for γ
- (J, G) is said to be another *admissible parametrization* for γ

3.2.4 Natural parametrization

Let γ be a space curve of class C^1 . A parametrization (I, F) of γ is called *natural* if $\|F'(t)\| = 1, \forall t \in I$. Thus :

- The curve is necessarily regular
- F is strictly monotonic

3.2.5 Curve length

Let $\gamma = (I, F)$ be a parametric curve of class C^1 . The length of γ is defined as :

$$L = \int_I \|F'(t)\| dt \quad (3.1)$$

Note that the length of γ is invariant under reparametrization.

3.2.6 Arc length parametrization

Let $\gamma = (I, F)$ be a regular parametric curve. Let $t_0 \in I$ be a given parameter. The following map is said to be the *arc length of origin* t_0 of γ :

$$s: t \mapsto \int_{t_0}^t \|F'(u)\| du , \quad s \in I \times \mathbb{R} \quad (3.2)$$

The arc length $s: I \mapsto s(I)$ is an admissible change of parameter for γ . Indeed, s is a C^1 diffeomorphism because it is bijective ($s' > 0$).

Let's define $G = F \circ s^{-1}$ and $J = s(I)$. Thus (J, G) is a natural reparametrization of γ and $\|G'(s)\| = 1, \forall s \in J$. This parametrization is preferred because the natural parameter s traverses the image of γ at unit speed ($\|G'\| = 1$).²

²Regular curves are also known as *unit speed* curves.

Thereafter, for a regular curve $\gamma : \gamma(t)$ will denote the point $F(t)$ of parameter $t \in I$; while $\gamma(s)$ will denote the point $G(s)$ of arc length $s \in J = [0, L]$.

3.3 Frenet trihedron

The Frenet trihedron is a fundamental mathematical tool from the field of differential geometry to study local characterization of planar and non-planar space curves. It is a direct orthonormal basis attached to any point P , of parameter $t \in I$, on a parametric curve γ . This basis is composed of three unit vectors $\{\mathbf{t}(t), \mathbf{n}(t), \mathbf{b}(t)\}$ called respectively the *tangent*, the *normal*, and the *binormal* unit vectors.³

Introduced by Frenet in 1847 in his thesis “Courbes à Double Courbure” [Fre52], it brings out intrinsic local properties of space curves : the curvature (κ) which evaluates the deviance of γ from being a straight line (see §3.4.1); and the torsion (τ_f) which evaluates the deviance of γ from being a planar curve (see §3.4.2).

These quantities, also known as “generalized curvatures” in modern differential geometry, are essential to understand the geometry of space curves. As stated by the *Fundamental Theorem of Space Curves*⁴, a curve is fully determined by its curvature and torsion up to a solid movement in space (see §3.4.3).

3.3.1 Tangent vector

The first component of the Frenet trihedron is called the *unit tangent vector*. Let $\gamma = (I, F)$ be a regular parametric curve. Let $t \in I$ be a parameter. The *unit tangent vector* is defined as :

$$\mathbf{t}(t) = \frac{\gamma'(t)}{\|\gamma'(t)\|} \quad , \quad \|\mathbf{t}(t)\| = 1 \quad (3.3)$$

For a curve parametrized by arc length, this expression simply becomes :

$$\mathbf{t}(s) = \gamma'(s) \quad , \quad s \in [0, L] \quad (3.4)$$

In differential geometry, the unit tangente to the curve γ at point P_0 is obtained as the limit of the (normalized) vector $\overrightarrow{P_0P}$, as P approaches P_0 on the path γ (fig. 3.1). For a regular curve, the left-sided and right-sided limits coincide as P^- and P^+ approach P_0 respectively from its left and right sides :

$$\mathbf{t}(P_0) = \lim_{P \rightarrow P_0} \frac{\overrightarrow{P_0P}}{\|\overrightarrow{P_0P}\|} = \lim_{P^- \rightarrow P_0} \frac{\overrightarrow{P_0P^-}}{\|\overrightarrow{P_0P^-}\|} = \lim_{P^+ \rightarrow P_0} \frac{\overrightarrow{P_0P^+}}{\|\overrightarrow{P_0P^+}\|} \quad (3.5)$$

³ Strictly speaking, the map $\mathbf{t} : t \mapsto \mathbf{t}(t)$ is a *vector field* while $\mathbf{t}(t)$ is a *vector* of \mathbb{R}^3 . For the sake of simplicity, and if there is no ambiguity, these two notions will not be explicitly distinguished hereinafter.

⁴The full demonstration of this theorem is attributed to Darboux in [Del07, p.11].

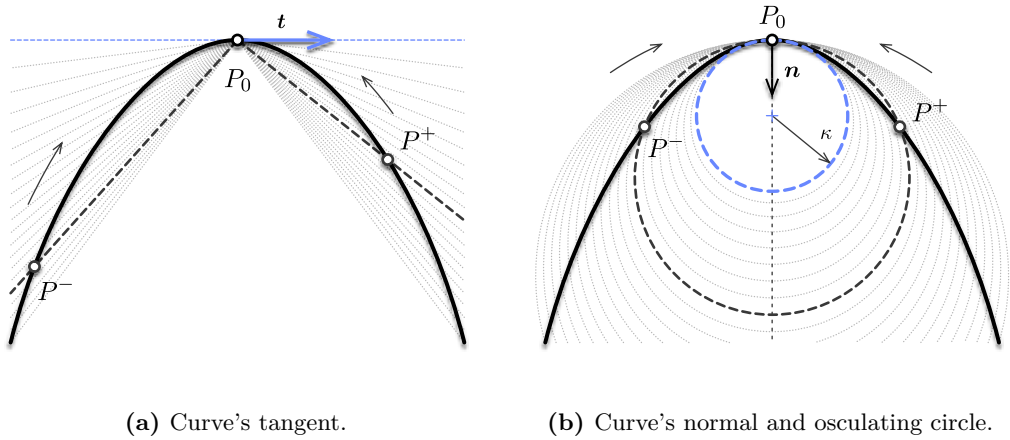


Figure 3.1 – Differential definition of Frenet’s trihedron at given point P_0 .

3.3.2 Normal vector

The second component of the Frenet trihedron is called the *unit normal vector*. It is constructed from \mathbf{t}' which is necessarily orthogonal to \mathbf{t} . Indeed :

$$\|\mathbf{t}\| = 1 \Rightarrow \mathbf{t}' \cdot \mathbf{t} = 0 \Leftrightarrow \mathbf{t}' \perp \mathbf{t} \quad (3.6)$$

Let $\gamma = (I, F)$ be a biregular parametric curve.⁵ Let $t \in I$ be a parameter. The *unit normal vector* is defined as :

$$\mathbf{n}(t) = \frac{\mathbf{t}'(t)}{\|\mathbf{t}'(t)\|} = \frac{\gamma'(t) \times (\gamma''(t) \times \gamma'(t))}{\|\gamma'(t)\|^3} , \quad \|\mathbf{n}(t)\| = 1 \quad (3.7)$$

For a curve parametrized by arc length, this expression simply becomes :

$$\mathbf{n}(s) = \frac{\mathbf{t}'(s)}{\|\mathbf{t}'(s)\|} = \gamma'(s) \times (\gamma''(s) \times \gamma'(s)) , \quad s \in [0, L] \quad (3.8)$$

In differential geometry, the unit normal to the curve γ at point P_0 is obtained as the limit of the (normalized) vector $\overrightarrow{P_0P^+} - \overrightarrow{P_0P^-}$, as P^- and P^+ approach P_0 respectively from its left and right sides (fig. 3.1) :

$$\mathbf{n}(P_0) = \lim \frac{\overrightarrow{P_0P^+} - \overrightarrow{P_0P^-}}{\|\overrightarrow{P_0P^+} - \overrightarrow{P_0P^-}\|} \quad (3.9)$$

Remark that the notion of *normal vector* is ambiguous for non-planar curves as there is an infinite number of possible normal vectors lying in the plane orthogonal to the curve’s tangent. In practice, the tangent derivative is a convenient choice as it allows to extend the notion of curvature from planar to non-planar space curves. However, we will see (§3.5.6) that other kind of trihedron can be constructed regarding this choice and that one of them

⁵Note that \mathbf{n} exists if and only if γ is biregular, that is \mathbf{t}' never vanishes or, equivalently, γ is never locally a straight line.

is especially suitable for the study of slender beams.

3.3.3 Binormal vector

The third vector of Frenet's trihedron is called the *unit binormal vector*. It is constructed from \mathbf{t} and \mathbf{n} to form an orthonormal direct basis of \mathbb{R}^3 . Let $\gamma = (I, F)$ be a biregular parametric curve. Let $t \in I$ be a parameter. The *unit binormal vector* is defined as :

$$\mathbf{b}(t) = \mathbf{t}(t) \times \mathbf{n}(t) = \frac{\gamma'(t) \times \gamma''(t)}{\|\gamma'(t) \times \gamma''(t)\|} , \quad \|\mathbf{b}(t)\| = 1 \quad (3.10)$$

For a curve parametrized by arc length, this expression simply becomes :

$$\mathbf{b}(s) = \mathbf{t}(s) \times \mathbf{n}(s) = \gamma'(s) \times \gamma''(s) , \quad s \in [0, L] \quad (3.11)$$

3.3.4 Osculating plane

The tangent and normal unit vectors $\{\mathbf{t}, \mathbf{n}\}$ form an orthonormal basis of the so-called *osculating plane*, whereas the binormal vector (\mathbf{b}) is orthogonal to it. This plane is of prime importance because it is the plane in which the curve takes its curvature (see §3.4.1).

As reported in [Del07, p.45], the osculating plane seems to have been first introduced by Bernoulli as the plane passing through three infinitely near points on a curve.⁶ Likewise, in modern differential geometry, the osculating plane is defined as the limit of the plane passing through the points P^- , P_0 and P^+ while P^- and P^+ approach P_0 respectively from its left and right side (fig. 3.1).

Note that the normal unit vector and the binormal unit vector $\{\mathbf{n}, \mathbf{b}\}$ define the so-called *normal plane*, while the normal tangent vector and the binormal unit vector $\{\mathbf{t}, \mathbf{b}\}$ define the so-called *rectifying plane*. These planes are secondary for the present study.

3.4 Curves of double curvature

The study of space curves belongs to the field of differential geometry. According to [Del07, p.28], the terminology *curve of double curvature* is attributed to Pitot around 1724.⁷ However, as stated in [Coo13, p.321] curvature and torsion were probably first thought by Monge around 1771.⁸ It is also interesting to note that, at that time, “curvature” was

⁶“Voco autem planum osculans, quod transit per tria curvae quae sitae puncta infinite sibi invicem propinqua” [Ber28, p.113].

⁷“Les Anciens ont nommé cette courbe Spirale ou Hélice ; parce que la formation sur le cylindre suit la même analogie que la formation d'une spirale ordinaire sur un plan; mais elle est bien différente de la spirale ordinaire, étant une des courbes à double courbure, ou une des lignes qu'on conçoit tracée sur la surface des Solides. Peut-être que ces sortes de courbes à double courbure, ou prises sur la surface des Solides, feront un jour l'objet des recherches des géomètres. Celle que nous venons d'examiner est, je crois, la plus simple de toutes.” [Pit26, p.28]

⁸“On appelle point d'inflexion, dans une courbe plane, le point où cette ligne, après avoir été concave dans un sens, cesse de l'être pour devenir concave dans l'autre sens. Il est évident que dans ce point, la

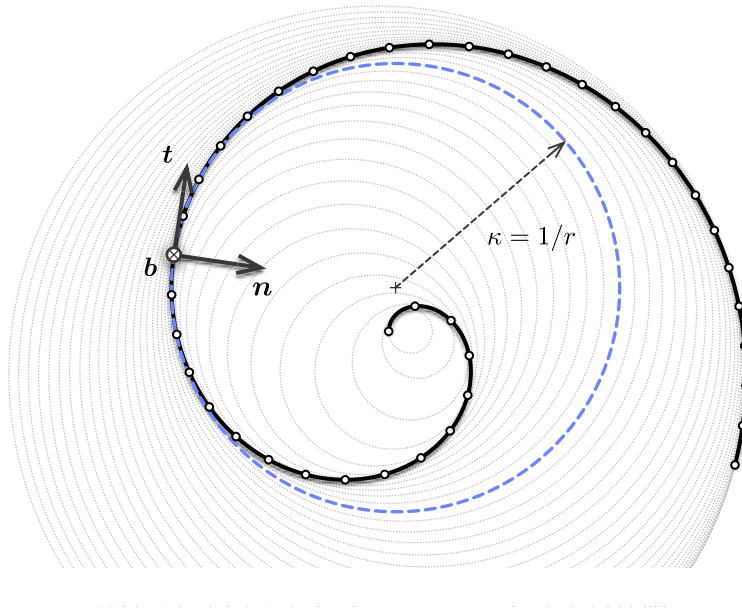


Figure 3.2 – Osculating circles for a spiral curve at different parameters.

also referred to as “flexure”, reflecting that the study of physical problems (e.g. *elastica*) and the study of curves of double curvature were intimately related to each other.

Space curves were historically understood as *curves of double curvature* by extension to the case of planar curves, where the curvature measures the deviance of a curve from being a straight line. The second curvature, nowadays known as the “torsion” or “second generalized curvature”, measures the deviance of a curve from being plane.

3.4.1 First invariant : the curvature

In differential geometry, the *osculating circle* is defined as the limit of the circle passing through the points P^- , P_0 and P^+ while P^- and P^+ approach P_0 (fig. 3.1). This circle lies on the osculating plane and its radius is nothing but the inverse of the local curvature of a curve.⁹ While the tangent gives the best local approximation of the curve as a straight line, the osculating circle gives the best local approximation of that curve as an arc.

The curvature is also known to be the *gradient of arc length* (see [Vou14, p.4]) and calculated as : $\nabla L = \kappa n$. Thus, the curvature gives the first-order variation in arc length

courbe perd sa courbure, et que les deux éléments consécutifs sont en ligne droite. Mais une courbe à double courbure peut perdre chacune de ses courbures en particulier, ou les perdre toutes deux dans le même point ; c'est-à-dire, qu'il peut arriver ou que trois éléments consécutifs d'une même courbe à double courbure se trouvent dans un même plan, ou que deux de ces éléments soient en ligne droite. Il suit de là que les courbes à double courbure peuvent avoir deux espèces d'inflexions; la première a lieu lorsque la courbe devient plane, et nous l'appellerons simple inflexion; la seconde, que nous appellerons double inflexion, a lieu lorsque la courbe devient droite dans un de ses points.” [Mon09, p.363].

⁹ As explained by Euler himself, at a given arc length parameter (s), the osculating plane is the plane in which a curve takes its curvature : “in quo bina filii elementa proxima in curvantur” [Eul75, p.364].

when deforming a curve γ in a closed enough curve $\gamma + \epsilon\delta\gamma$:

$$L(\gamma + \epsilon\delta\gamma) = L(\gamma) + \epsilon(\nabla L \cdot \delta\gamma) + o(\epsilon) \quad , \quad \nabla L \cdot \delta\gamma = \frac{d}{d\epsilon} L(\gamma + \epsilon\delta\gamma) \Big|_{\epsilon=0} \quad (3.12)$$

This is easily understood in the case of a circle of radius r extended to a circle of radius $r + dr$, where the total arc length variation is given by : $L(r + dr) - L(r) = \kappa dr L(r)$.

Note that due to the inner product with the normal vector, only the normal component of the deformation results in an effective extension of the curve. This point is worth to note as it will be related to the *inextensibility assumption* made later in our beam model.

Curvature

Let γ be a regular arc length parametrized curve. Let $s \in [0, L]$ be an arc length parameter. The *curvature* is a positive scalar quantity defined as :

$$\kappa(s) = \|\mathbf{t}'(s)\| \geq 0 \quad , \quad \mathbf{t}'(s) = \kappa(s)\mathbf{n}(s) \quad (3.13)$$

The curvature is *independent* regarding the choice of parametrization. This makes the curvature an *intrinsic property* of a given curve and that is why it is also referred to as a *geometric invariant*. Following [GAS06, pp.203-204] it can be computed for any parametrization (I, F) of γ as :

$$\kappa(t) = \frac{\|\gamma'(t) \times \gamma''(t)\|}{\|\gamma'(t)\|^3} \quad , \quad \mathbf{t}'(t) = \|\gamma'(t)\| \kappa(t) \mathbf{n}(t) \quad (3.14)$$

Note that in eq. (3.13) the prime denotes the derivative regarding the natural parameter (s) while it denotes the derivative regarding any parameter (t) in eq. (3.14). Consequently, the *speed* of the curve's parametrization appears in the latter equation :

$$v(t) = \frac{ds}{dt} = \|\gamma'(t)\| = s'(t) \quad (3.15)$$

The curvature measures how much a curve *bends instantaneously* in its osculating plane, that is how fast the tangent vector is rotating in the osculating plane around the binormal vector. In differential geometry this is expressed as :

$$\kappa(s) = \lim_{ds \rightarrow 0} \frac{\angle(\mathbf{t}(s), \mathbf{t}(s + ds))}{ds} = \lim_{ds \rightarrow 0} \frac{(\mathbf{t}(s + ds) - \mathbf{t}(s)) \cdot \mathbf{n}(s)}{ds} \quad (3.16)$$

This is equivalent as measuring how fast the osculating plane itself is rotating around the binormal vector. Consequently a curve is locally a *straight line* when its curvature vanishes ($\kappa(s) = 0$).

Radius of curvature

The *radius of curvature* is defined as the inverse of the curvature ($r = 1/\kappa$). From a geometric point of view, one can demonstrate that it is the radius of the osculating circle

(fig. 3.2). Remark that where the curvature vanishes the radius of curvature goes to infinity ; that is the osculating circle becomes a line, a circle of infinite radius.

Center of curvature

The *center of curvature* is defined as the center of the osculating circle (fig. 3.2). The locus of all the centers of curvature of a curve is called the *evolute*.

Curvature binormal vector

Finally, following [Ber+08] we define the *curvature binormal vector*. Let γ be a biregular arc length parametrized curve. Let $s \in [0, L]$ be an arc length parameter. The *curvature binormal vector* is defined as :

$$\kappa \mathbf{b}(s) = \mathbf{t}(s) \times \mathbf{t}'(s) = \kappa(s) \cdot \mathbf{b}(s) \quad , \quad \|\kappa \mathbf{b}(s)\| = \kappa(s) \quad (3.17)$$

This vector will be useful as it embed all the necessary information on the curve's curvature. We will see (§3.5.6) that this vector is associated to the angular velocity of a specific adapted moving frame attached to the curve and called the *Bishop frame*.

3.4.2 Second invariant : the torsion

Let γ be a biregular arc length parametrized curve. Let $s \in [0, L]$ be an arc length parameter. The *torsion* is a scalar quantity defined as :

$$\tau_f(s) = \mathbf{n}'(s) \cdot \mathbf{b}(s) = -\mathbf{b}'(s) \cdot \mathbf{n}(s) \quad (3.18)$$

The torsion is *independent* regarding the choice of parametrization. This makes the torsion an *intrinsic property* of a given curve and that is why it is also referred to as a *geometric invariant*. Following [GAS06, p.204] it can be computed for any parametrization (I, F) of γ as :

$$\tau_f(t) = \frac{(\gamma'(t) \times \gamma''(t)) \cdot \gamma'''(t)}{\|\gamma'(t) \times \gamma''(t)\|^2} \quad \text{when } \kappa(t) > 0 \quad (3.19)$$

The torsion measures how much a curve goes *instantaneously out of its plane*, that is to say how fast the normal or binormal vectors are rotating in the normal plane around the tangent vector. In differential geometry this is expressed as :

$$\tau_f(s) = \lim_{ds \rightarrow 0} \frac{\angle(\mathbf{n}(s), \mathbf{n}(s + ds))}{ds} = \lim_{ds \rightarrow 0} \frac{(\mathbf{n}(s + ds) - \mathbf{n}(s)) \cdot \mathbf{b}(s)}{ds} \quad (3.20)$$

This is equivalent as measuring how fast the osculating plane is rotating around the tangent vector. Consequently a curve is locally *plane* when its torsion vanishes ($\tau_f(s) = 0$).

Remark that the *torsion* is denoted “ τ_f ” and not simply “ τ ” as the latter will be reserved to denote any angular velocity of a moving adapted frame around its tangent vector. Thus, τ_f

refers to the particular angular velocity of the Frenet trihedron around its tangent vector. This torsion, which is a geometric property of the curve, will be indifferently referred to as the *Frenet torsion* or the *geometric torsion*.

3.4.3 Fundamental theorem of space curves

This two *generalized curvatures*, respectively the curvature (κ) and the torsion (τ_f), are *invariant* regarding the choice of parametrization and under *euclidean motions*. The *Fundamental theorem of space curves* states that a curve is fully described, up to a Euclidean motion of \mathbb{R}^3 , by its positive curvature ($\kappa > 0$) and torsion (τ) [GAS06, p.229].

3.4.4 Serret-Frenet formulas

The *Fundamental theorem of space curves* is somehow a consequence of the *Serret-Frenet formulas*, which is the first-order system of differential equations satisfied by the Frenet trihedron. Let γ be a biregular arc length parametrized curve. Let $s \in [0, L]$ be an arc length parameter. Then, the Frenet trihedron satisfies the following formulas :

$$\begin{cases} \mathbf{t}'(s) = \kappa(s)\mathbf{n}(s) \\ \mathbf{n}'(s) = -\kappa(s)\mathbf{t}(s) + \tau_f(s)\mathbf{b}(s) \\ \mathbf{b}'(s) = -\tau_f(s)\mathbf{n}(s) \end{cases} \quad (3.21)$$

This system can be seen as the *equations of motion* of the Frenet trihedron moving along the curve γ at unit speed ($\|\gamma'\| = 1$). Indeed, introducing its *angular velocity vector* also known as the *Darboux vector* (Ω_f), the previous system is expressed as :

$$\begin{bmatrix} \mathbf{t}'(s) \\ \mathbf{n}'(s) \\ \mathbf{b}'(s) \end{bmatrix} = \Omega_f(s) \times \begin{bmatrix} \mathbf{t}(s) \\ \mathbf{n}(s) \\ \mathbf{b}(s) \end{bmatrix} \quad \text{where} \quad \Omega_f(s) = \begin{bmatrix} \tau_f(s) \\ 0 \\ \kappa(s) \end{bmatrix} \quad (3.22)$$

Because the Frenet trihedron satisfies a first-order system of differential equations of parameters κ and τ_f it is possible, by integration, to reconstruct the trace of the moving frame and thus the curve, up to a constant of integration (a trihedron in this case).

Finally, those formulas can be generalized to any non unit-speed parametrization of a curve¹⁰. Let $\gamma = (I, F)$ be a biregular parametric curve. Let $t \in I$ be a parameter. Then the following *generalized Serret-Frenet formulas* hold :

$$\begin{cases} \mathbf{t}'(t) = v(t)\kappa(t)\mathbf{n}(t) \\ \mathbf{n}'(t) = -v(t)\kappa(t)\mathbf{t}(t) + v(t)\tau_f(t)\mathbf{b}(t) \\ \mathbf{b}'(t) = -v(t)\tau_f(t)\mathbf{n}(t) \end{cases} \quad (3.23)$$

Again, this system can be seen as the *equations of motion* of the Frenet trihedron moving

¹⁰See [GAS06, p.203] for a complete proof.

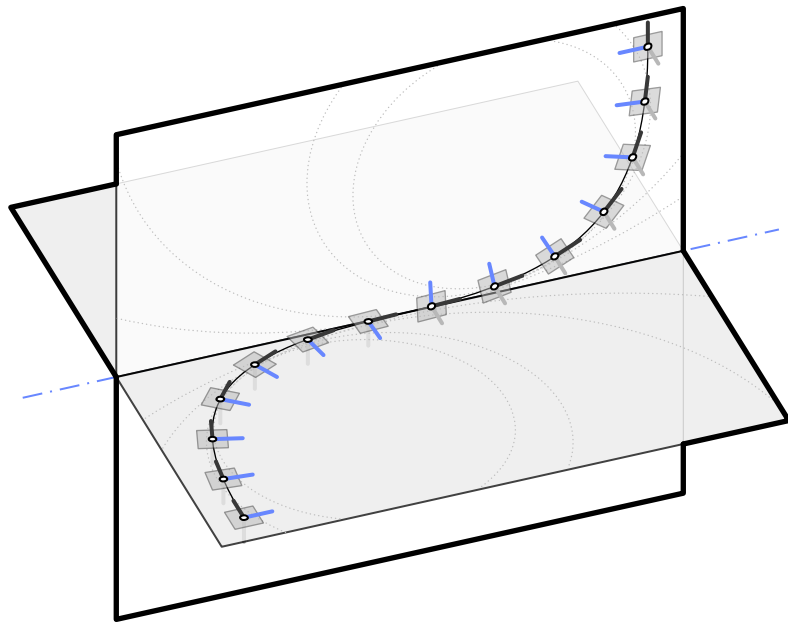


Figure 3.3 – Geometric torsion and rotation of the osculating plane. Note the existence of an inflexion point with a vanishing curvature and a discontinuity of both τ_f and the osculating plane.

along the curve γ at non unit-speed ($v(t) = \|\gamma'(t)\|$). This time the *angular velocity vector* (Ω) is distinct from the *Darboux vector* (Ω_f) and the previous system is expressed as :

$$\begin{bmatrix} \mathbf{t}'(t) \\ \mathbf{n}'(t) \\ \mathbf{b}'(t) \end{bmatrix} = \Omega(t) \times \begin{bmatrix} \mathbf{t}(t) \\ \mathbf{n}(t) \\ \mathbf{b}(t) \end{bmatrix} \quad \text{where} \quad \Omega(t) = v(t) \begin{bmatrix} \tau_f(t) \\ 0 \\ \kappa(t) \end{bmatrix} \quad (3.24)$$

3.5 Curve framing

While the Frenet trihedron “has long been the standard vehicle for analysing properties of the curve invariant¹¹ under euclidean motions” [Bis75, p.1], a curve can be potentially framed with any arbitrary *moving frame*, understood as an *orthonormal basis field*. Thus, the Frenet frame is not the only way to frame a curve and other frames may or may not exhibit some interesting properties.¹²

In his paper [Bis75] Bishop establishes the differential equation that a moving frame must satisfy and remarks that, because of the orthonormality condition, the first derivatives of the frame components can be expressed in terms of themselves through a skew-symmetric coefficient matrix. For such a frame, the understanding of its motion along the curve is thus reduced to the knowledge of only three scalar coefficient functions. He remarks that most of the interesting properties that the Frenet frame exhibits are due to the fact that

¹¹Namely the curvature (κ) and the Frenet torsion (τ_f).

¹²Recall the title of Bishop’s paper : “There is more than one way to frame a curve” [Bis75].

one of this coefficient function is vanishing everywhere on the curve (that is the frame is *rotation-minimizing* regarding one of its components) ; and that the Frenet frame is *adapted* to the curve (that is one of its components is nothing but the unit tangent vector).

In this section we introduce the *moving frame* notion and two properties of interest such a frame can exhibit in addition, that is : to be *adapted* to the curve ; and to be *rotation-minimizing* regarding a given direction. We then reconsider the case of the Frenet frame regarding this mathematical framework. Finally, we introduce the *zero-twisting* frame also known as the *bishop* frame.¹³ This tool will be fundamental for our futur study of slender beams.

3.5.1 Moving frame

Let γ be a curve parametrized by arc length. A map F which associates to each point of arc length parameter s a direct orthonormal trihedron is said to be a *moving frame* :

$$\begin{aligned} F : [0, L] &\longrightarrow \mathcal{SO}_3(\mathbb{R}) \\ s &\longmapsto F(s) = \{\mathbf{e}_3(s), \mathbf{e}_1(s), \mathbf{e}_2(s)\} \end{aligned} \quad (3.25)$$

Consequently, a moving frame F attached to γ satisfies for all $s \in [0, L]$:

$$\begin{cases} \|\mathbf{e}_i(s)\| = 1 \\ \mathbf{e}_i(s) \cdot \mathbf{e}_j(s) = 0 \quad , \quad i \neq j \end{cases} \quad (3.26)$$

The term “moving frame” will refer indifferently to the map itself (denoted $F = \{\mathbf{e}_3, \mathbf{e}_1, \mathbf{e}_2\}$), or to a specific evaluation of the map (denoted $F(s) = \{\mathbf{e}_3(s), \mathbf{e}_1(s), \mathbf{e}_2(s)\}$).

Governing equations

Computing the derivatives of the previous relationships leads to the following system of differential equations that the frame must satisfy for all $s \in [0, L]$:

$$\begin{cases} \mathbf{e}'_i(s) \cdot \mathbf{e}_i(s) = 0 \\ \mathbf{e}'_i(s) \cdot \mathbf{e}_j(s) = -\mathbf{e}_i(s) \cdot \mathbf{e}'_j(s) \quad , \quad i \neq j \end{cases} \quad (3.27)$$

Thus, there exists 3 scalar functions (τ, k_1, k_2) such that $\{\mathbf{e}'_3, \mathbf{e}'_1, \mathbf{e}'_2\}$ can be expressed in the basis $\{\mathbf{e}_3, \mathbf{e}_1, \mathbf{e}_2\}$:

$$\begin{cases} \mathbf{e}'_3(s) = k_2(s)\mathbf{e}_1(s) - k_1(s)\mathbf{e}_2(s) \\ \mathbf{e}'_1(s) = -k_2(s)\mathbf{e}_3(s) + \tau(s)\mathbf{e}_2(s) \\ \mathbf{e}'_2(s) = k_1(s)\mathbf{e}_3(s) - \tau(s)\mathbf{e}_1(s) \end{cases} \quad (3.28)$$

¹³Named after Bishop who introduced it.

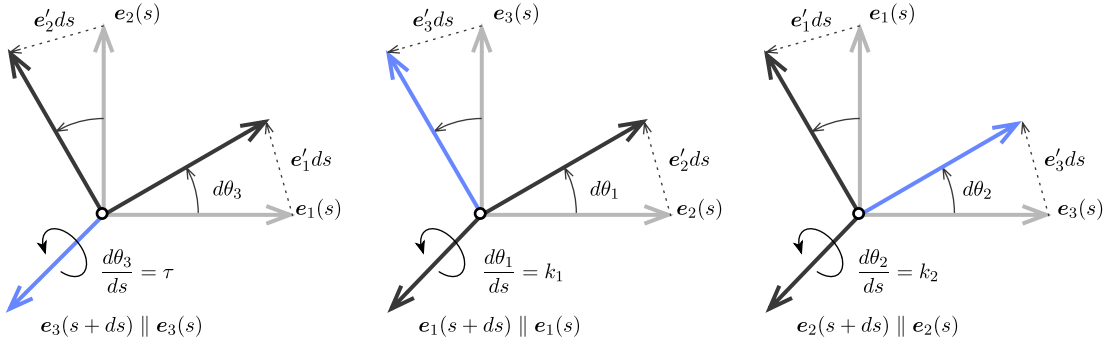


Figure 3.4 – Geometric interpretation of the angular velocity vector of a moving frame.

It is common to rewrite this first-order linear system of differential equations as a matrix equation : ^{14, 15}

$$\begin{bmatrix} \mathbf{e}'_3(s) \\ \mathbf{e}'_1(s) \\ \mathbf{e}'_2(s) \end{bmatrix} = \begin{bmatrix} 0 & k_2(s) & -k_1(s) \\ -k_2(s) & 0 & \tau(s) \\ k_1(s) & -\tau(s) & 0 \end{bmatrix} \begin{bmatrix} \mathbf{e}_3(s) \\ \mathbf{e}_1(s) \\ \mathbf{e}_2(s) \end{bmatrix} \quad (3.29)$$

Since the progression of any moving frame along γ is ruled by a first-order system of differential equations, a unique triplet $\{\tau, k_1, k_2\}$ leads to a set of moving frames equal to each other within a constant of integration.¹⁶ Basically, with a given triplet $\{\tau, k_1, k_2\}$, one can propagate a given initial direct orthonormal trihedron (at $s = 0$ for instance) through the whole curve by integrating the system of differential equations. In general, a moving frame will be fully determined by τ , k_1 and k_2 together with the initial condition $\{\mathbf{e}_3(s = 0), \mathbf{e}_1(s = 0), \mathbf{e}_2(s = 0)\}$.

Angular velocity

This system can be seen as the *equations of motion* of the frame moving along the curve γ at unit speed ($\|\gamma'\| = 1$). Indeed, introducing its *angular velocity vector* ($\boldsymbol{\Omega}$), the previous system is expressed as :

$$\mathbf{e}'_i(s) = \boldsymbol{\Omega}(s) \times \mathbf{e}_i(s) \quad \text{avec} \quad \boldsymbol{\Omega}(s) = \begin{bmatrix} \tau(s) \\ k_1(s) \\ k_2(s) \end{bmatrix} \quad (3.30)$$

This result is straightforward deduced from eq. (3.29). Note that the cross product reveals the skew-symmetric nature of the system, which could already be seen in eq. (3.29).

¹⁴In the case of a space curve, where \mathbf{e}_3 is chosen to be the curve tangent unit vector and \mathbf{e}_1 is chosen to be the curve normal unit vector, this set of equations is known as the *Serret-Frenet formulas*.

¹⁵In the case of a space curve drawn on a surface, where \mathbf{e}_3 is chosen to be the curve tangent unit vector and \mathbf{e}_1 is chosen to be the surface normal unit vector, this set of equations is known as the *Darboux-Ribaucour formulas*.

¹⁶This assumption reminds the *Fundamental theorem of space curves* (§3.4.3).

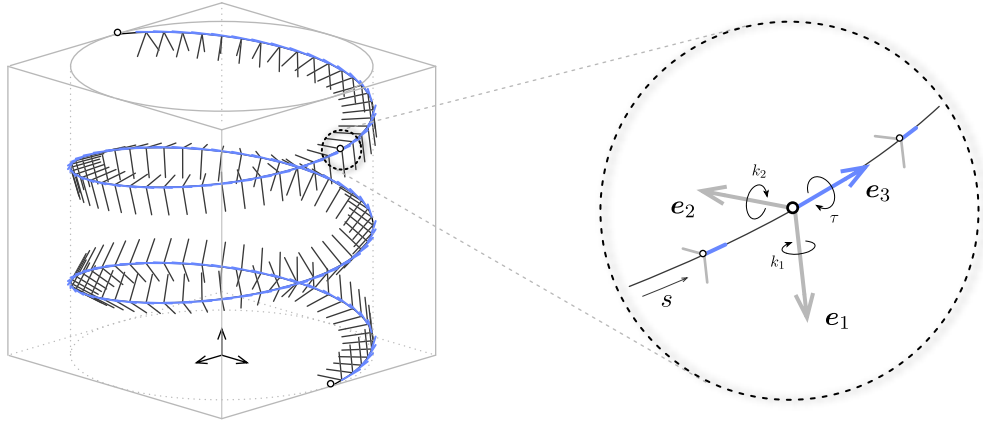


Figure 3.5 – Adapted moving frame $F(s) = \{e_3(s), e_1(s), e_2(s)\}$ where $e_3(s) = \mathbf{t}(s)$.

Geometrically, decomposing the infinitesimal rotation of the moving frame around its directors between arc length s and $s + ds$ (fig. 3.4) shows that the scalar functions τ , k_1 and k_2 effectively correspond to the angular speed of the frame moving along γ , respectively around e_3 , e_1 and e_2 :

$$\frac{d\theta_3}{ds}(s) = \tau(s) \quad , \quad \frac{d\theta_1}{ds}(s) = k_1(s) \quad , \quad \frac{d\theta_2}{ds}(s) = k_2(s) \quad (3.31)$$

3.5.2 Adapted moving frame

Let F be a moving frame as defined in the previous section. F is said to be *adapted* to γ if at each point $\gamma(s)$, $e_3(s)$ is the unit tangent vector of γ (fig. 3.5) :

$$e_3(s) = \mathbf{t}(s) = \frac{\gamma'(s)}{\|\gamma'(s)\|} \quad (3.32)$$

For an adapted frame, the components k_1 and k_2 of the angular velocity vector are related to the curvature of γ ¹⁷ :

$$\kappa(s) = \|e'_3(s)\| = \|k_2(s)e_1(s) + k_1(s)e_2(s)\| = \sqrt{k_1(s)^2 + k_2(s)^2} \quad (3.33)$$

Moreover, recalling the definition of the curvature binormal vector (κb) from eq. (3.17), it is easy to see that for an adapted moving frame the following relation holds :

$$\kappa b(s) = k_1(s)e_1(s) + k_2(s)e_2(s) \quad (3.34)$$

¹⁷Faire le lien avec l'énergie de flexion, qui ne dépend donc que de la géométrie de la courbe dans le cas d'une isotropic rod $\mathcal{E}_b = EI\kappa^2$.

Consequently, the angular velocity vector of an adapted moving frame can be written as :

$$\boldsymbol{\Omega}(s) = \kappa \mathbf{b}(s) + \tau(s) \mathbf{t}(s) \quad (3.35)$$

This last result is very interesting as it shows that any adapted moving frame will differ from each other only by their twisting speed as $\boldsymbol{\Omega}_\perp = \kappa \mathbf{b}$ only depends on the curve.

3.5.3 Rotation-minimizing frame

Following [Far+14, Wan+08] we introduce the *rotation-minimizing frame* notion. A frame $\{\mathbf{e}_3, \mathbf{e}_1, \mathbf{e}_2\}$ is said to be *rotation-minimizing* regarding a given direction \mathbf{d} if :

$$\boldsymbol{\Omega}(s) \cdot \mathbf{d}(s) = 0 \quad (3.36)$$

3.5.4 Parallel transport

The notion of *parallel transport* is somehow a generalization of the classical notion of collinearity in flat euclidean spaces (e.g. \mathbb{R}^2 or \mathbb{R}^3), to spaces that exhibit some non vanishing curvature (e.g. spheric or hyperbolic spaces).¹⁸

Relatively parallel fields

Following [Bis75], we define what is a (*relatively*) *parallel field*. Let γ be a regular curve parametrized by arc length. Let \mathbf{p} be a vector field along γ . The vector field \mathbf{p} is said to be *parallel* if its derivative is purely tangential, that is :

$$\mathbf{p}'(s) \times \mathbf{t}(s) = 0 \quad (3.37)$$

Consequently, for an adapted moving frame, the *normal fields* \mathbf{e}_1 and \mathbf{e}_2 are both *relatively parallel* if and only if the frame angular velocity is itself a normal field, that is :¹⁹

$$\boldsymbol{\Omega}(s) = \boldsymbol{\Omega}_\perp(s) = \kappa \mathbf{b}(s) \Leftrightarrow \boldsymbol{\Omega}(s) \cdot \mathbf{t}(s) = 0 \Leftrightarrow \tau(s) = 0 \quad (3.38)$$

In other words, a *relatively parallel normal field* : “turns, only whatever amount is necessary for it to remain normal, so it is as close to being parallel as possible without losing normality” [Bis75].

Parallel transport of vectors along a curve

Reciprocally, it is possible to define the *parallel transport* of a vector along a curve γ as its propagation along γ at angular speed $\kappa \mathbf{b}$. An initial vector $\mathbf{p}_0 = \mathbf{p}(s_0)$ is parallel transported at arc length parameter s into the vector $\mathbf{p}(s)$ by integrating the following

¹⁸<https://www.youtube.com/watch?v=p1tfZD2Bm0w>

¹⁹A vector field \mathbf{p} is said to be *normal* along a curve γ if : $\forall s \in [0, L], \mathbf{p} \cdot \mathbf{t} = 0$.

first-order differential equation along γ :

$$\mathbf{p}'(s) = \kappa \mathbf{b}(s) \times \mathbf{p}(s) \quad (3.39)$$

Consequently, the resulting vector field \mathbf{p} is a parallel field. Note that a parallel field is not necessarily a normal field.

From the point of view of differential geometry, this means that the next vector $\mathbf{p}(s + ds)$ is obtained by rotating the previous one $\mathbf{p}(s)$ around the curve binormal $\mathbf{b}(s)$ by an infinitesimal angle $d\theta(s) = \kappa(s)ds$. Note that $\mathbf{b}(s)$ has the same direction as $\mathbf{t}(s) \times \mathbf{t}(s + ds)$.

Parallel transport of frames along a curve

Identically, the *parallel transport* of an adapted frame is defined as the parallel transport of its components along γ .

3.5.5 Frenet frame

The Frenet frame is a well-known particular adapted moving frame. It is defined as the map that attach to any given point of γ the corresponding Frenet trihedron $\{\mathbf{t}(s), \mathbf{n}(s), \mathbf{b}(s)\}$ where :

$$\mathbf{t}(s) = \frac{\gamma'(s)}{\|\gamma'(s)\|} \quad , \quad \mathbf{n}(s) = \frac{\mathbf{t}'(s)}{\kappa(s)} \quad , \quad \mathbf{b}(s) = \mathbf{t}(s) \times \mathbf{n}(s) \quad (3.40)$$

Governing equations

The Frenet frame satisfies the *Frenet-Serret formulas* (see §3.4.4), which govern the evolution of the frame along the curve γ :

$$\begin{bmatrix} \mathbf{t}'(s) \\ \mathbf{n}'(s) \\ \mathbf{b}'(s) \end{bmatrix} = \begin{bmatrix} 0 & \kappa(s) & 0 \\ -\kappa(s) & 0 & \tau_f(s) \\ 0 & -\tau_f(s) & 0 \end{bmatrix} \begin{bmatrix} \mathbf{t}(s) \\ \mathbf{n}(s) \\ \mathbf{b}(s) \end{bmatrix} \quad (3.41)$$

Remember the generic system of differential equations of an adapted moving frame attached to a curve, established in eq. (3.29), where :

$$\mathbf{e}_3(s) = \mathbf{t}(s) \quad , \quad k_1(s) = 0 \quad , \quad k_2(s) = \kappa(s) \quad , \quad \tau(s) = \tau_f(s) \quad (3.42)$$

Angular velocity

Consequently, the angular velocity vector (Ω_f) of the Frenet frame, also known as the *Darboux vector* in this particular case, is given by :

$$\Omega_f(s) = \begin{bmatrix} \tau_f(s) \\ 0 \\ \kappa(s) \end{bmatrix} = \kappa \mathbf{b}(s) + \tau_f(s) \mathbf{t}(s) \quad (3.43)$$

Remark that the Frenet frame satisfies $\Omega_f(s) \cdot \mathbf{n}(s) = 0$ and is thus a *rotation-minimizing* frame regarding the normal vector (\mathbf{n}). The motion of this frame through the curve is known as “pitch-free”.

Note also that $\mathbf{t}'(s)$ and $\mathbf{b}'(s)$ are colinear to $\mathbf{n}(s)$. This means that the projection of $\mathbf{t}(s)$ and $\mathbf{b}(s)$ is conserved from one normal plane to another, that is \mathbf{t} and \mathbf{b} are parallel transported along the vector field \mathbf{n} .

Drawbacks and benefits

[20](#), [21](#), [22](#)

The Frenet frame is not continuously defined if γ is not C^2 . This is problematic for the study of slender beams as the centerline of a beam subject to punctual external forces and moments or to material discontinuities will not be C^2 but only piecewise C^2 . In that case, the centerline tangent will be continuously defined everywhere but the curvature will be subject to discontinuities, that is \mathbf{t}' will not be continuously defined.

Moreover, even if γ is C^2 , the Frenet frame is not defined where the curvature vanishes, which obviously is an admissible configuration for a beam centerline. This issue can be partially addressed by parallel transporting the normal vector along the straight regions of the curve. Thus, the extended frame will still satisfy the governing equations exposed in [eq. \(3.41\)](#). However, if the osculating planes are not parallel on both sides of a region of null curvature, torsion will be subject to a discontinuity and so the Frenet frame ([fig. 3.3](#)).²³ Again, if the region of null curvature is not a point, that is the region is not an inflection point but a locus where the curve is locally a straight line, the change in torsion on both sides of the region can be accommodated by a continuous rotation from one end to the other.

One benefit of the Frenet frame is that, when transported along a *closed curve*, the frame at the end of the curve will align back with the frame at the beginning of the curve, that is the frame will return to its initial value after a complete turn. During its trip, the frame

²⁰une perturbation de la courbe dans le sens de la courbure engendre une variation de longueur de la courbe proportionnelle à l'inverse de la courbure (au premier ordre) + schéma.

²¹une perturbation de la courbe dans le sens de la binormale (en tout point) préserve la longueur de la courbe au 1er ordre : c'est un déplacement qui conserve l'hypothèse d'inextensibilité au premier ordre.

²²Examiner la question de la fermeture sur une boucle fermée. Schéma.

²³This is also highlighted in [Blo90, Wan+08].

will make a total twist of $\int_0^L \tau_f(s)ds = 0[2\pi]$ around the tangent vector.

A second benefit is that any adapted frame can be obtained by a rotation of the Frenet frame around the unit tangent vector [Gug89, p.2].

3.5.6 Bishop frame

A *Bishop frame* denoted $\{\mathbf{t}, \mathbf{u}, \mathbf{v}\}$, also known as *zero-twisting* or *parallel-transported* frame, is an adapted moving frame that has no tangential angular velocity :²⁴

$$\boldsymbol{\Omega} \cdot \mathbf{t} = \tau = \mathbf{u}' \cdot \mathbf{v} = -\mathbf{u} \cdot \mathbf{v}' = 0 \quad (3.44)$$

Because a Bishop frame is an adapted frame, it can be defined relatively to the Frenet frame by a rotation around the unit tangent vector. A Bishop frame is a frame that cancels out the rotational movement of the Frenet frame around the tangent vector. At arc length parameter s , the Frenet frame has continuously rotated around its tangent vector of a cumulative angle : $\int_0^s \tau_f(t)dt$. Thus, any Bishop frame will be obtained, within a constant rotation angle θ_0 , through a rotation of the Frenet frame around the tangent vector by an angle :

$$\theta(s) = - \int_0^s \tau_f(t)dt + \theta_0(s) \quad (3.45)$$

Consequently, a Bishop frame can be expressed relatively to the Frenet frame as :

$$\begin{cases} \mathbf{u} = \cos \theta \mathbf{n} + \sin \theta \mathbf{b} \\ \mathbf{v} = -\sin \theta \mathbf{n} + \cos \theta \mathbf{b} \end{cases} \quad (3.46)$$

Governing equations

The Bishop frame satisfies the following system of differential equations, which govern the evolution of the frame along the curve γ :

$$\begin{bmatrix} \mathbf{t}'(s) \\ \mathbf{u}'(s) \\ \mathbf{v}'(s) \end{bmatrix} = \begin{bmatrix} 0 & \kappa(s) \sin \theta(s) & -\kappa(s) \cos \theta(s) \\ -\kappa(s) \sin \theta(s) & 0 & 0 \\ \kappa(s) \cos \theta(s) & 0 & 0 \end{bmatrix} \begin{bmatrix} \mathbf{t}(s) \\ \mathbf{u}(s) \\ \mathbf{v}(s) \end{bmatrix} \quad (3.47)$$

²⁴Bishop frames were introduced as *relatively parallel adapted frames* in [Bis75].

One can remember the generic differential equations of an adapted moving frame attached to a curve, where : ²⁵

$$k_1(s) = \kappa(s) \sin \theta(s) , \quad k_2(s) = \kappa(s) \cos \theta(s) , \quad \tau(s) = 0 \quad (3.48)$$

Angular velocity

Consequently, the angular velocity vector (Ω_b) of the Bishop frame is given by :

$$\Omega_b(s) = \begin{bmatrix} 0 \\ \kappa(s) \sin \theta(s) \\ \kappa(s) \cos \theta(s) \end{bmatrix} = \kappa b(s) \quad (3.49)$$

Remark that the Bishop frame satisfies $\Omega_b(s) \cdot t(s) = 0$ and is thus *rotation-minimizing* regarding the tangent vector. The motion of this frame through the curve is known as “roll-free”.

Because the motion of this frame is described by an angular velocity vector that is nothing but the curvature binormal vector ($\Omega_b = \kappa b$), it can be interpreted in terms of *parallel transport* as defined in §3.5.4. Thus, given an initial frame at arc length parameter $s = 0$, the Bishop frame at any arc length parameter (s) is obtained by parallel transporting the initial frame $\{t(0), u(0), v(0)\}$ along the curve from 0 to s .

Drawbacks and benefits

^{26,27}

One of the main benefits of the Bishop frame is that its generative method : “is immune to degeneracies in the curvature vector” [Blo90]. Although we first expressed the construction of the Bishop frame relatively to the Frenet frame (which exists wherever γ is biregular), the existence of the Bishop frame, understood in terms of parallel transport, is guaranteed wherever the curvature binormal ($\kappa b = t \times t'$) is defined. To be continuously defined over $[0, L]$, a Bishop frame only needs the curvature binormal vector to be piecewise continuously defined over $[0, L]$, which only requires that γ' is C^0 and that γ'' is piecewise C^0 . Obviously, those weaker existence conditions are profitables to bypass the drawbacks of the Frenet frame regarding the modeling of slender beams listed in §3.5.5.

Strictly speaking, a Bishop frame is not a reference frame as it is defined within an initial

²⁵

$$\begin{aligned} \tau &= u' \cdot v = (\Omega_f \times u + \theta' v) \cdot v = \tau_f - \tau_f = 0 \\ k_1 &= -t' \cdot v = -\kappa n \cdot v = \kappa \sin \theta \\ k_2 &= t' \cdot u = \kappa n \cdot u = \kappa \cos \theta \end{aligned}$$

²⁶[Gug89, Klo86, Blo90, Wan+08, PFL95, Men13]

²⁷“Regarder la méthode de la bi-reflexion pour le calcul du repère de bishop” [Wan+08, p.6]

condition. However, we will see later that strains in a beam are modeled as a rate of change in the Bishop frame, and consequently the initial condition will disappear in the equations.

Unlike the Frenet frame, when transported along a *closed curve*, the Bishop frame at the end of the curve will not necessarily align back with the frame at the beginning of the curve.²⁸ Even if the frame returns to its initial value after a complete turn, it may return in its position after several complete turns ($2k\pi$) around the curve tangent. During its trip, the frame will make a total twist of $\int_0^L \tau_f(s)ds = \alpha[2\pi]$ around the tangent vector. This difference of angle is related to the concept of *holonomy*.

Remark also that Frenet and Bishop frames coincide for planar curves ($\tau_f = 0$), within a constant rotation around the unit tangent vector.

3.5.7 Comparison between Frenet and Bishop frames

Application A : circular helix

Let γ be a *circular helix* of parameter a and k . In a cartesian coordinate system, it is defined as :

$$\mathbf{r}(t) = [a \cos t, a \sin t, kt] = a \cos t \mathbf{e}_x + a \sin t \mathbf{e}_y + kt \mathbf{e}_z \quad (3.50)$$

The speed of this parametrization, the curvature and the geometric torsion are uniform and given by :

$$v(t) = \sqrt{a^2 + k^2} \quad , \quad \kappa(t) = \frac{a}{a^2 + k^2} \quad , \quad \tau_f(t) = \frac{k}{a^2 + k^2} \quad (3.51)$$

The Frenet frame components are given by (with $\alpha = v\kappa$ and $\beta = v\tau_f$) :

$$\begin{aligned} \mathbf{t}(t) &= [-\alpha \cos t, \alpha \sin t, \beta t] \\ \mathbf{n}(t) &= [-\cos t, -\sin t, 0] \\ \mathbf{b}(t) &= [\beta \sin t, -\beta \cos t, \alpha] \end{aligned} \quad (3.52)$$

And the Bishop frame components are given by :

$$\begin{aligned} \mathbf{u}(t) &= [-\cos t \cos \beta t - \beta \sin t \sin \beta t, -\sin t \cos \beta t + \beta \cos t \sin \beta t, -\alpha \sin \beta t] \\ \mathbf{v}(t) &= [-\cos t \sin \beta t + \beta \sin t \cos \beta t, -\sin t \sin \beta t - \beta \cos t \cos \beta t, \alpha \cos \beta t] \end{aligned} \quad (3.53)$$

soit pour une spirale dont on connaît

²⁸“it is possible for closed curves to have parallel transport frames that do not match up after one full circuit of the curve” [HM95]

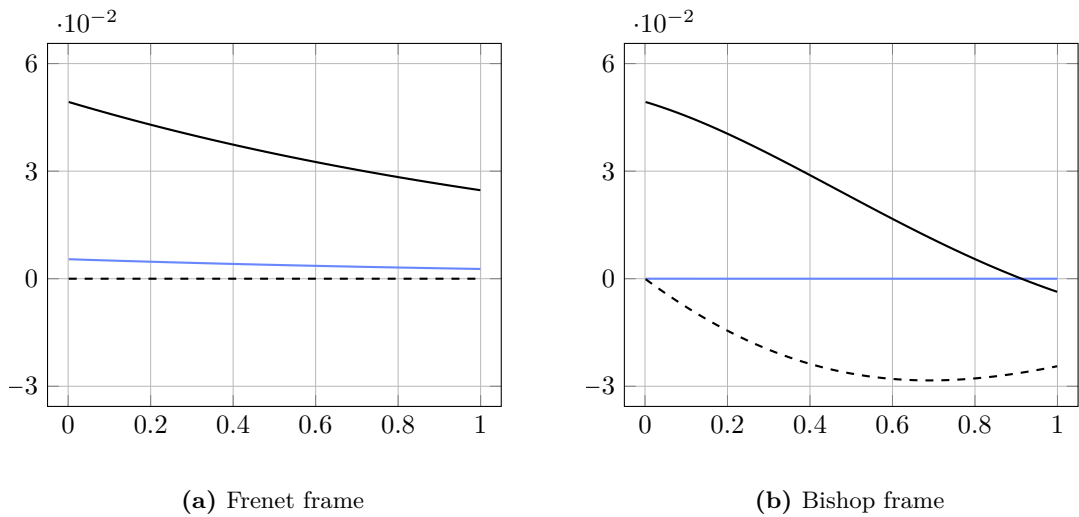


Figure 3.6 – Comparison between Frenet and Bishop frame velocity for a spirale curve.

3.6 Discrete curves

The previous section has introduced the fundamental analytical tools to develop a solid understanding of the geometry of smooth space curves. These tools will be essentials for the construction of the beam model presented later in ?? and ?. In this section, we look for equivalent notions in the case of discrete space curves, as the developed model will be implemented in a numerical program to solve real mechanical problems through a finite-difference method (see ??).

The study of those discrete equivalent notions belong to the recent field of *Discrete Differential Geometry* : “In some sense discrete differential geometry can be considered more fundamental than differential geometry since the later can be obtained from the former as a limit” [Hof08, p.7]. In particular, we will see that there are several ways to define the discrete equivalents of the curvature and the unit tangent vector. Though these various ways are equivalent and match their smooth counterpart by passing to the limit, they exhibit different capabilities at the discrete level.

“There is no general theory or methodology in the literature, despite the ubiquitous use of discrete curves in mathematics and science. There are conflicting definitions of even basic concepts such as discrete curvature κ , discrete torsion τ , or discrete Frenet frame.” [Car+14, p.1].

3.6.1 Definition

Let Γ be a discrete (or polygonal) space curve. Γ is defined as an ordered sequence $\Gamma = (\mathbf{x}_0, \mathbf{x}_1, \dots, \mathbf{x}_n) \in \mathbb{R}^{3(n+1)}$ of $n + 1$ pairwise disjoint vertices (see fig. 3.7). Consecutive pairs of vertices define n straight segments $(\mathbf{e}_0, \mathbf{e}_1, \dots, \mathbf{e}_{n-1})$ called edges, pointing from one vertex to the next one : $\mathbf{e}_i = \mathbf{x}_{i+1} - \mathbf{x}_i$. The midpoint of \mathbf{e}_i is a vertex denoted :

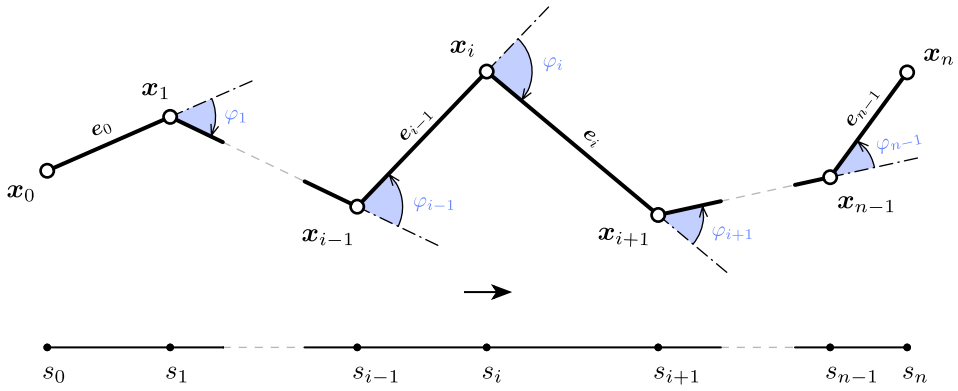


Figure 3.7 – Discrete curve representation and parametrization.

$\mathbf{x}_{i+1/2} = \mathbf{x}_i + \frac{1}{2}\mathbf{e}_i$. The length of \mathbf{e}_i is denoted $l_i = \|\mathbf{e}_i\|$. The total length of Γ is denoted $L = \sum_{i=0}^{n-1} \|\mathbf{e}_i\|$. Additionally, we define the vertex-based mean length at vertex \mathbf{x}_i :

$$\begin{cases} \bar{l}_0 = l_0 & i = 0 \\ \bar{l}_i = \frac{1}{2}(l_{i-1} + l_i) & i \in [1, n-1] \\ \bar{l}_n = l_{n-1} & i = n \end{cases} \quad (3.54)$$

Discrete unit tangent vector

Edge vectors lead to a natural definition of the *discrete unit tangent vector* along each edge : $\mathbf{u}_i = \mathbf{e}_i / l_i$. However, this definition makes no sense at vertices where all the curvature is *condensed* and measured by the turning angle (φ_i). This is explained in terms of the Gauß map as edges will map to points but vertices will map to curves on the unit sphere.

Discrete osculating plane

Consecutive pairs of edges lead to a natural definition of the *discrete osculating plane*, as the plane in which Γ locally lies on. This plane is well defined by its normal vector known as the *discrete unit binormal vector* ($\mathbf{b}_i = \frac{\mathbf{e}_{i-1} \times \mathbf{e}_i}{\|\mathbf{e}_{i-1} \times \mathbf{e}_i\|}$) only if \mathbf{e}_{i-1} and \mathbf{e}_i are non-collinear ; that is the curve is not locally a straight line, or equivalently the curvature does not vanish.

Discrete turning angle

The *turning angle* is defined as the oriented angle between two adjacent edges : $\varphi_i = \angle(\mathbf{e}_{i-1}, \mathbf{e}_i)$. It is defined only for all $i \in [1, n-1]$. It corresponds to the angle of rotation, in the osculating plane, around the binormal vector (\mathbf{b}_i), to align \mathbf{e}_{i-1} with \mathbf{e}_i . The sign of φ_i is taken in accordance to the right-hand rule regarding the orientation of \mathbf{b}_i . Thus, φ_i is necessarily bounded to $[0, \pi]$:

$$0 \leq \varphi_i \leq \pi \quad (3.55)$$

The next section will highlight the central role of the turning angle in the possible measurements of the discrete curvature.

Recall that for a planar curve, where φ denotes the angle between the tangent vector ($\mathbf{t} = \cos \varphi \mathbf{e}_x + \sin \varphi \mathbf{e}_y$) and the horizontal line of direction \mathbf{e}_x , the following relation holds : $\varphi(s_1) - \varphi(s_2) = \int_{s_1}^{s_2} \frac{d\varphi}{ds} ds = \int_{s_1}^{s_2} \kappa ds$.

3.6.2 Regularity

Let $\Gamma = (\mathbf{x}_0, \mathbf{x}_1, \dots, \mathbf{x}_n)$ be a discrete curve of edges $\mathbf{e}_0, \mathbf{e}_1, \dots, \mathbf{e}_{n-1}$. Γ is said to be :

- *regular* if it has no kinks : $\mathbf{e}_{i-1} + \mathbf{e}_i \neq 0 \Leftrightarrow \varphi_i \neq \pi \mid \forall i \in \llbracket 1, n-1 \rrbracket$
- *biregular* if no vertex is flat : $\mathbf{e}_{i-1} - \mathbf{e}_i \neq 0 \Leftrightarrow \varphi_i \neq 0 \mid \forall i \in \llbracket 1, n-1 \rrbracket$

3.6.3 Parametrization

In the literature, discrete curves are usually considered as maps defined on $I = \llbracket 0, n \rrbracket \in \mathbb{N}^{n+1}$. As a consequence, the discrete derivative of Γ is an edge-based quantity defined as :

$$\Gamma'_i = \frac{\Gamma(t_{i+1}) - \Gamma(t_i)}{t_{i+1} - t_i} = \mathbf{e}_i \quad , \quad \mathbf{x}_i = \Gamma(t_i) \quad , \quad t_i = i \quad (3.56)$$

Thus, as in the smooth case, a discrete curve is said to be parametrized by arc length if $\|\Gamma'\| = 1$, that is every edges are of unit length ($\|\mathbf{e}_i\| = 1$).²⁹ This constraint is sometimes relaxed to curves of constant edge length ($\|\mathbf{e}_i\| = c$) that are said to be parametrized *proportional* to arc length.

In the present work, to stick closer to the smooth case, we instead consider discrete curves as maps defined on $I = [t_0, t_1, \dots, t_n] \in \mathbb{R}^{n+1}$ where t denotes the discrete parametrization of Γ . As in the smooth case, the way to parametrize a curve is not unique.

Arc length parameter

By analogy with the smooth case, we define the curve arc length at vertices (see fig. 3.7) as :

$$\begin{cases} s_0 = 0 & i = 0 \\ s_i = \sum_{k=1}^i \|\mathbf{e}_{k-1}\| & i \in \llbracket 1, n-1 \rrbracket \\ s_n = L & i = n \end{cases} \quad (3.57)$$

²⁹This assumption leads to the assertion that “A discrete curve is parameterized by arc length or it is not” [Hof08, p.10].

This definition naturally extends to the whole domain by piecewise linear interpolation. This is not different as considering the discrete curve as a continuous polygonal curve. Indeed, for any $s \in [s_i, s_{i+1}]$ there exist a normalized parameter $t = \frac{s-s_i}{s_{i+1}-s_i} \in [0, 1]$ so that :

$$\begin{cases} s(t) = (1-t)s_i + ts_{i+1} = s_i + tl_i \\ \mathbf{x}(t) = (1-t)\mathbf{x}_i + t\mathbf{x}_{i+1} = \mathbf{x}_i + t\mathbf{e}_i \end{cases} \quad (3.58)$$

Note that this parametrization satisfies $\|\Gamma'\| = 1$ on $\cup_{i=1}^n [s_{i-1}, s_i]$ but Γ' remains undefined at vertices. This issue is the reason why defining the tangent vector at vertices can not be done unequivocally for discrete curves.

3.7 Discrete curvature

Several approaches. [Vou14] defines and compares three different definitions of the discrete curvature that does not suppose that $\|\mathbf{e}_i\| = cst$. By trying to mimic some properties of the curvature in the smooth case. [Bob15]. [Car+14] also defines and compares three different definitions of the discrete curvature from the osculating circle. One main drawback of all the said proposals is that the question of the curvature at start and end points is never treated. But this is of main importance when dealing with beams as the nature of the boundary condition can make the curvature to be null or not at its ends, depending if some moment has to be transferred or not. In this sense, the question of discrete curvature could not be treated separately with the question of the tangent vector.

[Rom13]

3.7.1 Definition from osculating circles

Curvature is defined from the osculating circle, which is the best approximation of a curve by a circle.

Vertex-based osculating circle (circumscribed)

Let Γ be a discrete curve parametrized by arc length. The *vertex-based* (or circumscribed) osculating circle at vertex \mathbf{x}_i is defined as the unique circle passing through the points \mathbf{x}_{i-1} , \mathbf{x}_i and \mathbf{x}_{i+1} (see fig. 3.8a). This circle leads to the following definition of the curvature : ³⁰

$$\kappa \mathbf{b}_i = \frac{2 \mathbf{e}_{i-1} \times \mathbf{e}_i}{\|\mathbf{e}_{i-1}\| \|\mathbf{e}_i\| \|\mathbf{e}_{i-1} + \mathbf{e}_i\|} , \quad \kappa_i = \|\kappa \mathbf{b}_i\| = \frac{2 \sin(\varphi_i)}{\|\mathbf{e}_{i-1} + \mathbf{e}_i\|} \quad (3.59)$$

This definition shows a good locality as the curvature is attached to the vertex \mathbf{x}_i , right in the place where it occurs on the discrete curve. In addition, this definition leads to a natural local spline interpolation by the circumscribed osculating circle itself. This interpolation

³⁰This curvature is also known as the *Menger curvature*.

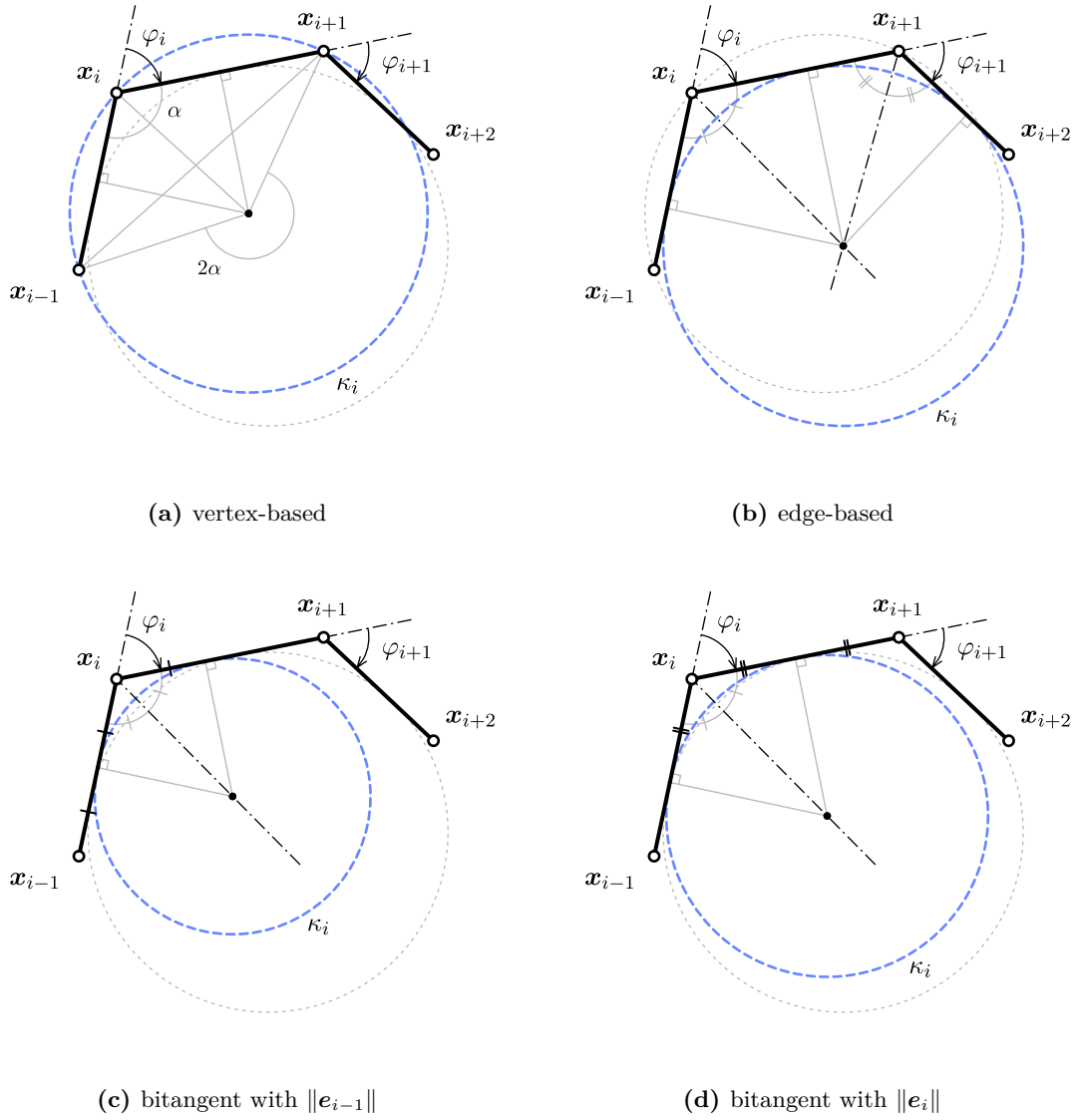


Figure 3.8 – Several ways to define the osculating circle for discrete curves, leading to different notions of discrete curvature.

Curvature (κ_i)	Locality	$\varphi \mapsto 0$	$\varphi \mapsto \pi$	Ends	Dim	Fitting
$\kappa_1 = \frac{2 \sin(\varphi_i)}{\ e_{i-1} + e_i\ }$	x_i	0	0, 2	yes	space	clothoid
$\kappa_2 = \frac{\tan(\varphi_i/2) + \tan(\varphi_{i+1}/2)}{l_i}$	e_i	0	∞	no	planar	circle
$\kappa_3 = \frac{2 \tan(\varphi_i/2)}{\bar{l}_i}$	x_i	0	∞	no	space	circles
$\kappa_4 = \frac{2 \sin(\varphi_i/2)}{\bar{l}_i}$	x_i	0	0, 2	no	space	clothoid
$\kappa_5 = \frac{\varphi_i}{\bar{l}_i}$	x_i	0	π/\bar{l}_i	no	space	elastica

Figure 3.9 – Review of several discrete curvature definitions mentioned in the literature.

has the advantage to pass exactly through three vertices, to lie on the osculating plane and to share the same curvature as Γ at \mathbf{x}_i . It also leads to a natural definition of the tangent vector at \mathbf{x}_i (see §3.8).

Moreover, while this definition is valid only on the current portion of Γ ($i \in [1, n - 1]$), it is straightforward extended to its endings ($i = 0, 1$), provided that a unit tangent vector \mathbf{t}_0 (respectively \mathbf{t}_n) is given at \mathbf{x}_0 (resp. \mathbf{x}_n), as the unique circle tangent to \mathbf{t}_0 (resp. \mathbf{t}_n) passing through \mathbf{x}_0 and \mathbf{x}_1 (resp. \mathbf{x}_{n-1} and \mathbf{x}_n) :

$$\kappa \mathbf{b}_0 = \frac{2 \mathbf{e}_0 \times \mathbf{t}_0}{\|\mathbf{e}_0\|^2} \quad , \quad \kappa \mathbf{b}_n = \frac{2 \mathbf{t}_n \times \mathbf{e}_{n-1}}{\|\mathbf{e}_{n-1}\|^2} \quad (3.60)$$

This property will be very profitable in the discrete beam model developed later in the manuscript. It is examined more in details in section §3.8 about the definition of the tangent vector.

However, there are some important drawbacks as the curvature is bounded to $[0, 2]$ (see fig. 3.11). When the curve tends to kinks ($\varphi \mapsto \pi$), one would expect the curvature to diverge toward infinity, but instead it tends to a finite value equals to 0 ($l_{i-1} \neq l_i$) or 2 ($l_{i-1} = l_i$). This issue can be bypassed if the discretization is refined “enough”. A criterion is given in the next section (??).

Edge-based osculating circle (inscribed)

Let Γ be a discrete curve parametrized by arc length. The *edge-based* osculating circle at edge \mathbf{e}_i is defined as the unique circle tangent to the edges \mathbf{e}_{i-1} , \mathbf{e}_i and \mathbf{e}_{i+1} (see fig. 3.8b).

$$\kappa_i = \frac{\tan(\varphi_i/2) + \tan(\varphi_{i+1}/2)}{\|\mathbf{e}_i\|} \quad (3.61)$$

This definition shows an appropriate behavior when the curve tends to kicks, as the radius of curvature tends to zero ($\tan \varphi/2 \mapsto \infty$), and when the curve tends to be a straight line, as the curvature tends to 0 ($\tan \varphi/2 \mapsto 0$).

However, it needs Γ to be planar which is by far too restrictive regarding our goal (the modeling of 3D slender beams). Finally, this way of defining the curvature is not as local as one would expect as it is defined relatively to the edge \mathbf{e}_i but not where the turning occurs, at vertices.

Bitangent osculating circle (inscribed)

Let Γ be a discrete curve parametrized by arc length. Following [Vou14] we define the curvature regarding the mean length \bar{l}_i attached to \mathbf{x}_i as : ³¹

$$\kappa \mathbf{b}_i = \frac{2}{\bar{l}_i} \left(\frac{\mathbf{e}_{i-1} \times \mathbf{e}_i}{\|\mathbf{e}_{i-1}\| \|\mathbf{e}_i\| + \mathbf{e}_{i-1} \cdot \mathbf{e}_i} \right) , \quad \kappa_i = \|\kappa \mathbf{b}_i\| = \frac{2}{\bar{l}_i} \tan(\varphi_i/2) \quad (3.62)$$

This other definition combines the good locality of the vertex-based approach (see eq. (3.59)) and the proper behavior at bounds of the edge-based approach (see eq. (3.61)). Given two adjacent edges \mathbf{e}_{i-1} and \mathbf{e}_i , there exist an infinite number of circles that are tangent to both edges (see fig. 3.8c and fig. 3.8d for two remarkable circles among them), which center points all lie on the $\varphi_i - \pi$ angle bisector line. The corresponding osculating circle, known as the *inscribed* circle, is constructed to touch both \mathbf{e}_{i-1} and \mathbf{e}_i at distance \bar{l}_i from \mathbf{x}_i . In the case of a constant edge length discrete curve, this definition of the osculating circle merges to the circles proposed in fig. 3.8c and fig. 3.8d.

However, this definition still exhibits some drawbacks as there is no natural way to extend it to the end vertices \mathbf{x}_0 and \mathbf{x}_{n-1} . The lack of a natural interpolation spline that passes through vertices and that is in correlation to the osculating circle is also detrimental in the context of our application.

Other definitions of osculating circles

In the literature, one can find other definitions for the discrete curvature that also correspond to the definition of an osculating circle. All these definitions are summarized in fig. 3.9. For further informations, the reader should refer to [Car+14, Vou14, Bob15, Rom13].

In particular, [Vou14] details which discrete curvature definitions parallel which property of the smooth curvature. It remarks that there is no “free-lunch” as none of the proposed definition satisfies every properties of the smooth curvature.

3.7.2 Benchmarking : sensitivity to non uniform discretization

In this section we compare the two main discrete curvature notions (circumscribed versus inscribed) regarding their sensibility to non uniform discretization.

This aspect is not treated in the actual literature, in which curves parametrized by arc length are usually treated as curves of constant edge length, though it is yet an important topic when it comes to the numerical modeling of true mechanical systems. Indeed, the presence of connexions between members will compromise the ability to enforce a constant discretization through all the elements of the structure. Additionally, vertices are obviously points of interest in a discrete model as they will be used to apply loads and enforce various constraints such as joints and support conditions. Finally, the accuracy of the discretized

³¹This definition is also presented in [Bob15, Car+14] but in the more restrictive case of constant edge length discrete curves ($l_i = cst$).

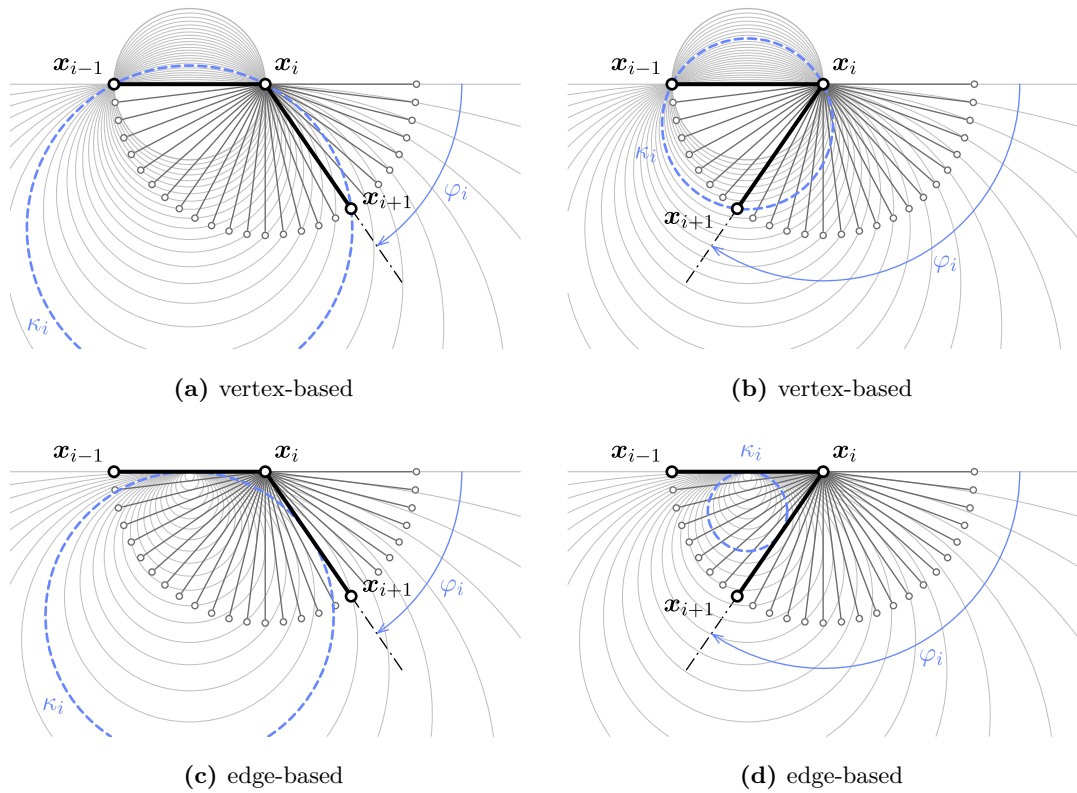


Figure 3.10 – Comparison of circumscribed (a-b) and inscribed (c-d) osculating circles for different values of the turning angle (φ).

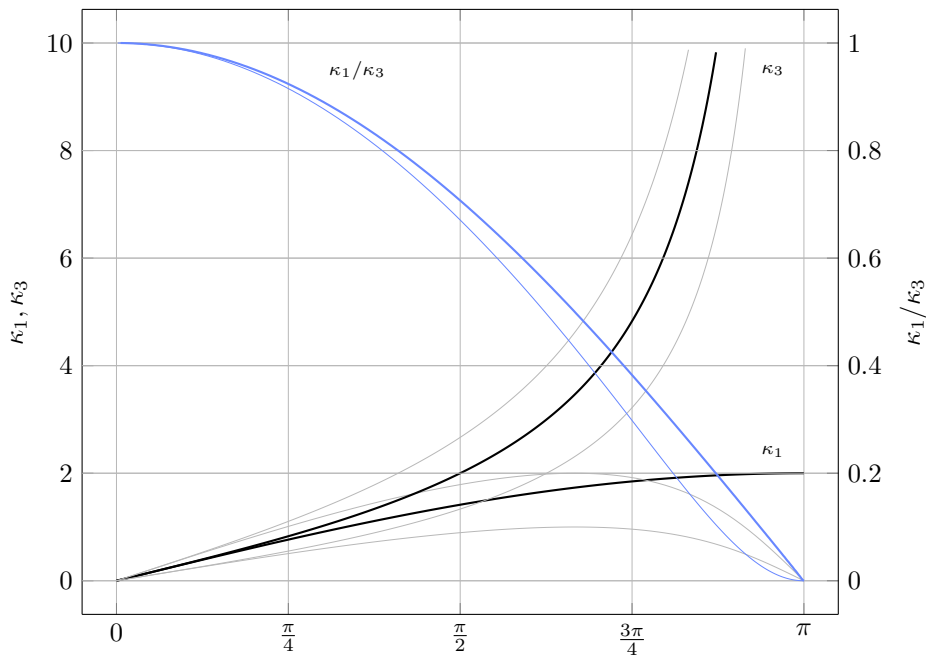


Figure 3.11 – Sensitivity of discrete curvatures to non uniform discretization ($\alpha \in [0.5, 2]$) over the whole domain of variation of the turning angle ($\varphi \in [0, \pi]$).

model is proportional to the sharpness of the discretization, whereas the computing time required to solve the model will grow as the sharpness increases. Consequently, one would distribute those points in the space as cleverly as possible and try to minimize their number as they increase the overall computation cost.

Introducing the coefficient $\alpha = \frac{\|e_{i-1}\|}{\|e_i\|}$, we rewrite the previous formulas for κ_1 and κ_3 as :

$$\begin{aligned}\kappa_1 &= \frac{2 \sin(\varphi)}{\|e_i\|(1 + \alpha^2 + 2\alpha \cos(\varphi))^{1/2}} \\ \kappa_3 &= \frac{4 \tan(\varphi/2)}{\|e_i\|(1 + \alpha)}\end{aligned}\tag{3.63}$$

These expressions lead to the following formula for the ratio κ_1/κ_3 , which relies only on α and the turning angle φ between the edges e_{i-1} and e_i :

$$\frac{\kappa_1}{\kappa_3}(\alpha) = \frac{\kappa_1}{\kappa_3}(1/\alpha) = \frac{(1 + \alpha) \cos^2(\varphi/2)}{((1 - \alpha)^2 + 4\alpha \cos^2(\varphi/2))^{1/2}}\tag{3.64}$$

Discrete curvatures are plotted in [fig. 3.11](#) for three values of α . The thickest line is for the case of uniform discretization ($\alpha = 1$), whereas the thin lines mark the boundary cases ($\alpha = 0.5, 2$). The ratio κ_1/κ_3 is plotted in blue and leads to only one thin line (remind [eq. \(3.64\)](#)). The graph shows that κ_1 and κ_3 have a very close behavior for small turning angles. The variability regarding α is small when φ remains small and gets negligible as φ gets smaller.

Passing $\pi/4$ and increasing φ , κ_3 exhibits a good behavior : as the discrete curves tends to kink κ_3 diverges towards the infinity as the smooth curvature would for

However, for a given curvature, the turning angle decreases as the sharpness of the discretization increases ($\lim_{\|e_i\| \rightarrow 0} \varphi_i = 0$). Thus, it is possible to adapted the discretization to make sure

3.7.3 Benchmarking : accuracy in bending energy representation

In this section we compare, for three remarkable types of curves (line, semicircle and elastica), the discrete bending energies \mathcal{E}_1 and \mathcal{E}_3 of the discrete curve, respectively based on definitions κ_1 and κ_3 (see [fig. 3.9](#)), to the bending energy \mathcal{E} of the smooth curve. We study the convergence of these energies as the sharpness of the discretization increases. The energies are defined as :

$$\begin{aligned}\mathcal{E} &= \int_0^L \kappa^2 ds \\ \mathcal{E}_i &= \sum_i \bar{l}_i \kappa_i^2\end{aligned}\tag{3.65}$$

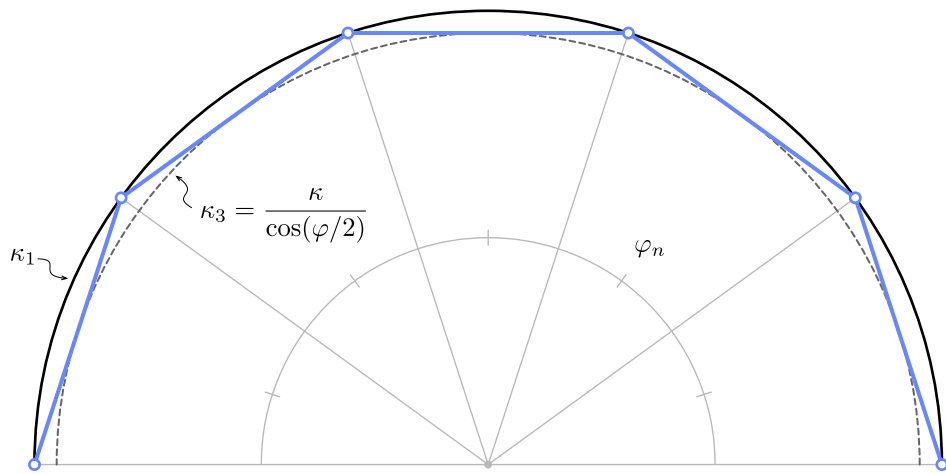


Figure 3.12 – Discretization of a semicircle for discrete bending energies evaluation.

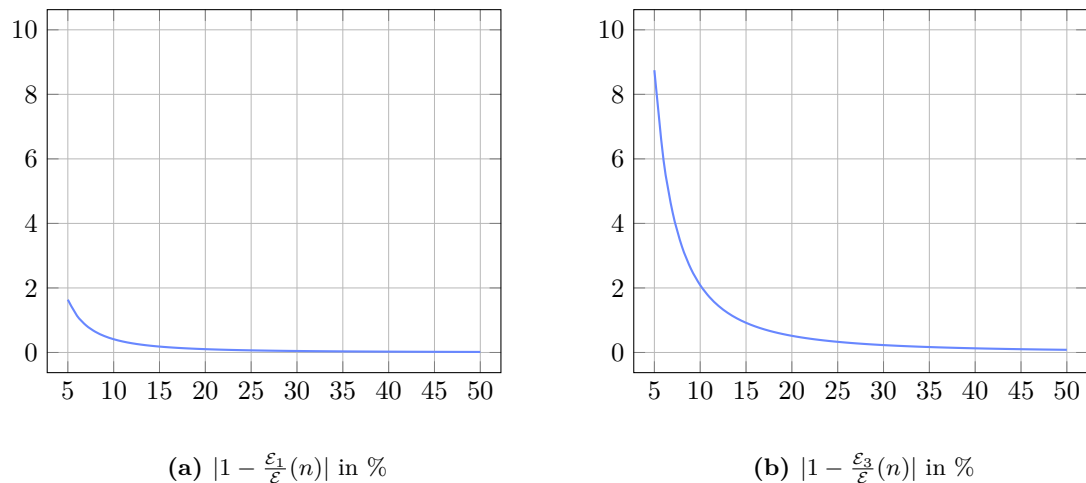


Figure 3.13 – Relative error in the estimation of the smooth bending energy (\mathcal{E}) by the discrete bending energies (\mathcal{E}_1 and \mathcal{E}_3) regarding the sharpness of the discretization, for a semicircle.

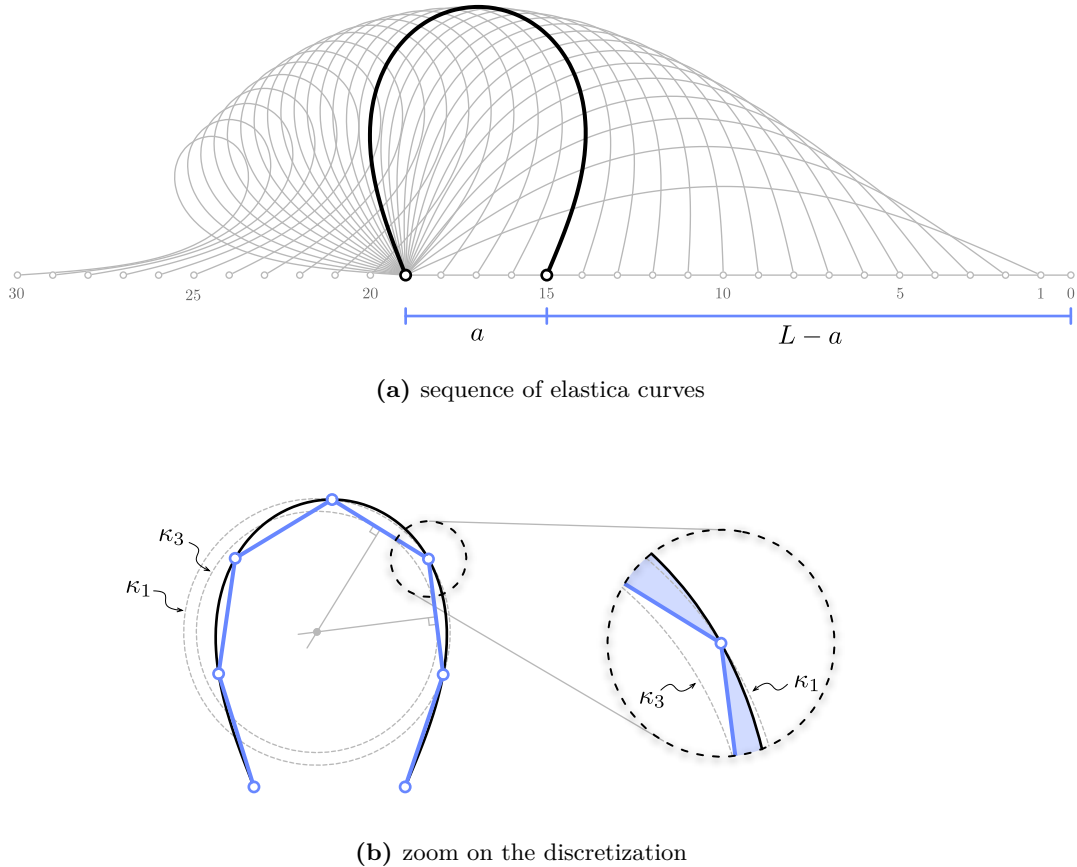


Figure 3.14 – Discretization (b) of a sequence of elastica curves (a) for discrete bending energies evaluation.

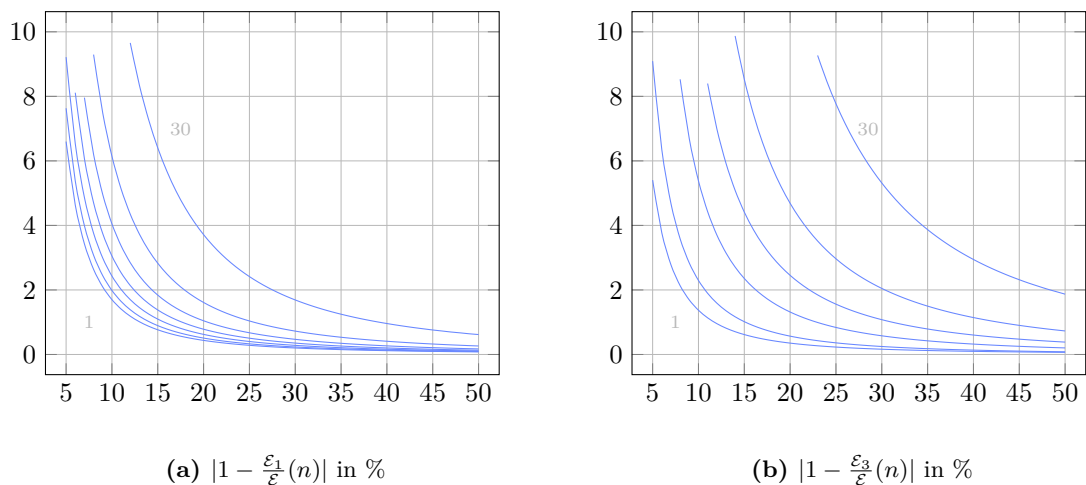


Figure 3.15 – Relative error in the estimation of the smooth bending energy (\mathcal{E}) by the discrete bending energies (\mathcal{E}_1 and \mathcal{E}_3) regarding the sharpness of the discretization, for several elastica curves. The curves are chosen from fig. 3.14a (1,5,10,15,20,25,30).

Straight line

We consider any straight line. Its smooth curvature is null. So are the discrete curvatures κ_1 and κ_3 (see fig. 3.9). In this case, the discrete bending energies perfectly match the bending energy of the smooth curve :

$$\mathcal{E} = \mathcal{E}_1 = \mathcal{E}_3 = 0 \quad (3.66)$$

Semicircle

We consider a semicircle of curvature $\kappa = 1/r$ and length $L = \pi r$. This curve is discretized into n edges of equal length $|\mathbf{e}_n| = 2r \sin(\varphi/2)$ where $\varphi = \frac{\pi}{n}$ (see fig. 3.12). The total length of the discrete curve is given by : $L_n = n|\mathbf{e}_n| = L \frac{\sin(\varphi/2)}{\varphi/2}$. In this simple case, the bending energies can be expressed analytically :

$$\mathcal{E} = L\kappa^2 \quad (3.67a)$$

$$\mathcal{E}_1 = L_n \kappa_1^2 = \frac{\sin(\varphi/2)}{\varphi/2} \cdot \mathcal{E} \quad (3.67b)$$

$$\mathcal{E}_3 = L_n \kappa_3^2 = \frac{\sin(\varphi/2)}{(\varphi/2) \cos^2(\varphi/2)} \cdot \mathcal{E} \quad (3.67c)$$

Note that κ_1 equals the curvature of the smooth curve. Consequently, the estimation error is only due to the estimation of the curve length ($L_n \neq L$). The ratios $\mathcal{E}_1/\mathcal{E}$ and $\mathcal{E}_3/\mathcal{E}$ are plotted in fig. 3.13. Graphs show that \mathcal{E}_1 converges to the smooth case faster than \mathcal{E}_3 .

Elastica

We consider a sequence of elastica curves of fixed length L and variable curvature κ (see fig. 3.14a). These curves correspond to a buckled shape of a straight pinned-pinned beam that would have been forced to retract its span. These curves are discretized into n edges of equal length (see fig. 3.14b). This time, there is no analytical expressions available for \mathcal{E} , \mathcal{E}_1 and \mathcal{E}_3 . Results are obtained by numerical integration and plotted in fig. 3.15. Again, graphs show that \mathcal{E}_1 converges to the smooth case faster than \mathcal{E}_3 for most of the curves excepted the ones with low overall curvature (1 to 5).

3.8 Discrete tangent vector

In this section we study how to define the discrete unit tangent vector relative to a discrete curve. While a natural definition exists along the edges (see §3.6.1), there is no obvious choice at vertices were the curve kinks.

The ability to define a unique tangent vector is very important to define the normal to cross section, control beam endings, and relate it to curvature. You will control the direction of the section (for a fixed/encastre support condition) or inversely, you would control the

moment and seek the corresponding tangent direction (for a pin boundary condition, you know there is no end moments so the curvature is null and your looking for the tangent).

Problème de définition. Facile de définir une tangente sur un edge. Mais une infinité de tangentes possibles à chaque vertex. So in case of an arc length parameterized curve the vertex tangent vector points in the same direction as the averaged edge tangent vectors [Hof08, p.12]. Nous verrons que le cercle 3 points, en plus de mieux représenter l'énergie d'une courbe discrete dans les cas typiques, offre un choix de tangente non ambigu.

3.8.1 Circumscribed case

We consider the case where the curvature is defined according to the circumscribed osculating circle (see fig. 3.16a).

Current portion

Let \mathbf{x}_i be a vertex in the current portion of Γ . The circumscribed osculating circle gives a smooth approximation of Γ in the vicinity of \mathbf{x}_i (see fig. 3.16a). It leads to a natural definition of a unit tangent vector for five remarkable vertices as the tangent to the osculating circle at those points (resp. \mathbf{x}_{i-1} , $\mathbf{x}_{i-1/2}$, \mathbf{x}_i , $\mathbf{x}_{i+1/2}$, \mathbf{x}_{i+1}) :

$$\mathbf{t}_i^- = 2(\mathbf{t}_i \cdot \mathbf{u}_{i-1})\mathbf{u}_{i-1} - \mathbf{t}_i \quad (3.68a)$$

$$\mathbf{t}_{i-1/2} = \mathbf{u}_{i-1} \quad (3.68b)$$

$$\mathbf{t}_i = \frac{\|\mathbf{e}_i\|}{\|\mathbf{e}_{i-1} + \mathbf{e}_i\|} \mathbf{u}_{i-1} + \frac{\|\mathbf{e}_{i-1}\|}{\|\mathbf{e}_{i-1} + \mathbf{e}_i\|} \mathbf{u}_i \quad (3.68c)$$

$$\mathbf{t}_{i+1/2} = \mathbf{u}_i \quad (3.68d)$$

$$\mathbf{t}_i^+ = 2(\mathbf{t}_i \cdot \mathbf{u}_i)\mathbf{u}_i - \mathbf{t}_i \quad (3.68e)$$

Note that \mathbf{t}_i^- (resp. \mathbf{t}_i^+) is obtained by a reflection of $-\mathbf{t}_i$ across the bisecting plane of \mathbf{e}_{i-1} (resp. \mathbf{e}_i). A very important property is that the curvature binormal vector at \mathbf{x}_i can be computed by three different ways :

$$\kappa \mathbf{b}_i = \frac{2 \mathbf{e}_{i-1} \times \mathbf{e}_i}{\|\mathbf{e}_{i-1}\| \|\mathbf{e}_i\| \|\mathbf{e}_{i-1} + \mathbf{e}_i\|} = \begin{cases} \frac{2 \mathbf{u}_{i-1} \times \mathbf{t}_i}{\|\mathbf{e}_{i-1}\|} \\ \frac{2 \mathbf{t}_i \times \mathbf{u}_i}{\|\mathbf{e}_i\|} \end{cases} \quad (3.69)$$

The first expression is interpreted as the unique circle passing through three points (\mathbf{x}_{i-1} , \mathbf{x}_i , \mathbf{x}_{i+1}) as explained in §3.7.1. Equivalently, there exist a unique circle defined by two points and a tangent vector. Precisely, the last two expressions in eq. (3.69) can be interpreted as the curvature binormal vector of the unique circle passing through \mathbf{x}_{i-1} , \mathbf{x}_i (resp. \mathbf{x}_i , \mathbf{x}_{i+1}) and tangent to \mathbf{t}_i at \mathbf{x}_i .

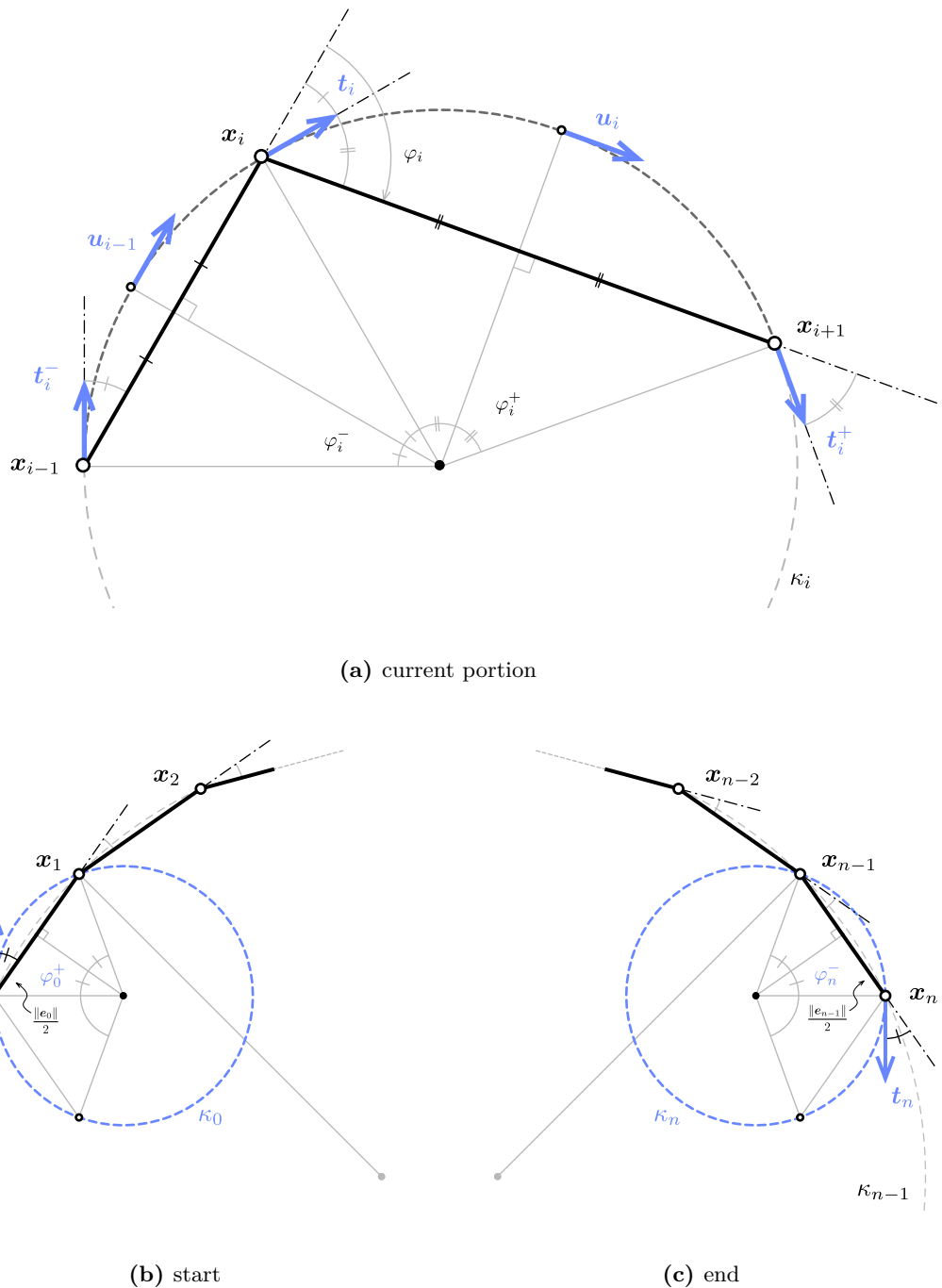


Figure 3.16 – Definition of the tangent vector (t) and related curvature binormal vector (κb) at vertices (circumscribed definition).

Discontinuity of curvature

Let \mathbf{t}_i^* be an arbitrary tangent vector at \mathbf{x}_i . Following eq. (3.69) we define the *left-sided* (resp. *right-sided*) discrete curvatures at \mathbf{x}_i in the circumscribed case as : as

$$\kappa b_i^-(\mathbf{t}_i^*) = \frac{2 \mathbf{u}_{i-1} \times \mathbf{t}_i^*}{\|\mathbf{e}_{i-1}\|} \quad (3.70a)$$

$$\kappa b_i^+(\mathbf{t}_i^*) = \frac{2 \mathbf{t}_i^* \times \mathbf{u}_i}{\|\mathbf{e}_i\|} \quad (3.70b)$$

The corresponding osculating circle will be called the *left-sided* (resp. *right-sided*) circumscribed osculating circle. When $\mathbf{t}_i^* = \mathbf{t}_i$, the limits agree one to each other ($\kappa b_i^- = \kappa b_i^+ = \kappa b_i$) and the osculating circles coincide. These definitions perfectly mimic the smooth case where, at a regular ($\|\gamma'\| \neq 0$) but not biregular ($\|\gamma''\| = 0$) point, the curvature is discontinuous while the tangent vector reminds smoothly defined.

In mechanics, this situation is likely to arise as discontinuities in material properties or punctual applied moments will necessarily lead to discontinuities in curvature (recall that $M = EI\kappa$).

Curve endings

The definition of the left and right sided curvatures given for a vertex in the current portion of Γ are still valid for the end vertices \mathbf{x}_0 and \mathbf{x}_n . Provided that a unit tangent vector \mathbf{t}_0^* (respectively \mathbf{t}_n^*) is given at \mathbf{x}_0 (resp. \mathbf{x}_n), the circumscribed osculating circle is defined as the unique circle passing through \mathbf{x}_0 and \mathbf{x}_1 (resp. \mathbf{x}_{n-1} and \mathbf{x}_n) tangent to \mathbf{t}_0^* (resp. \mathbf{t}_n^*) ; see fig. 3.16b and fig. 3.16c. It leads to the following curvature binormal vectors :

$$\kappa b_0 = \kappa b_0^+(\mathbf{t}_0^*) = \frac{2 \mathbf{t}_0^* \times \mathbf{e}_0}{\|\mathbf{e}_0\|^2} \quad (3.71a)$$

$$\kappa b_n = \kappa b_n^-(\mathbf{t}_n^*) = \frac{2 \mathbf{e}_{n-1} \times \mathbf{t}_n^*}{\|\mathbf{e}_{n-1}\|^2} \quad (3.71b)$$

Note that, contrary to the current portion, curvatures at endings are subjected to the definition of a unit tangent vector. This reflects the usual indetermination of boundary conditions. For a given beam whether the end is clamped, the tangent vector is known and one will seek the reacting moment due to the support ; whether the end is pinned, the reacting moment is null (so is the curvature) and one will seek the cross section orientation.

3.8.2 Inscribed case

We now consider the case where the curvature is defined according to the inscribed osculating circle (see fig. 3.17a). Remark that inscribed and circumscribed osculating circles are concentric when $l_{i-1} = l_i$.

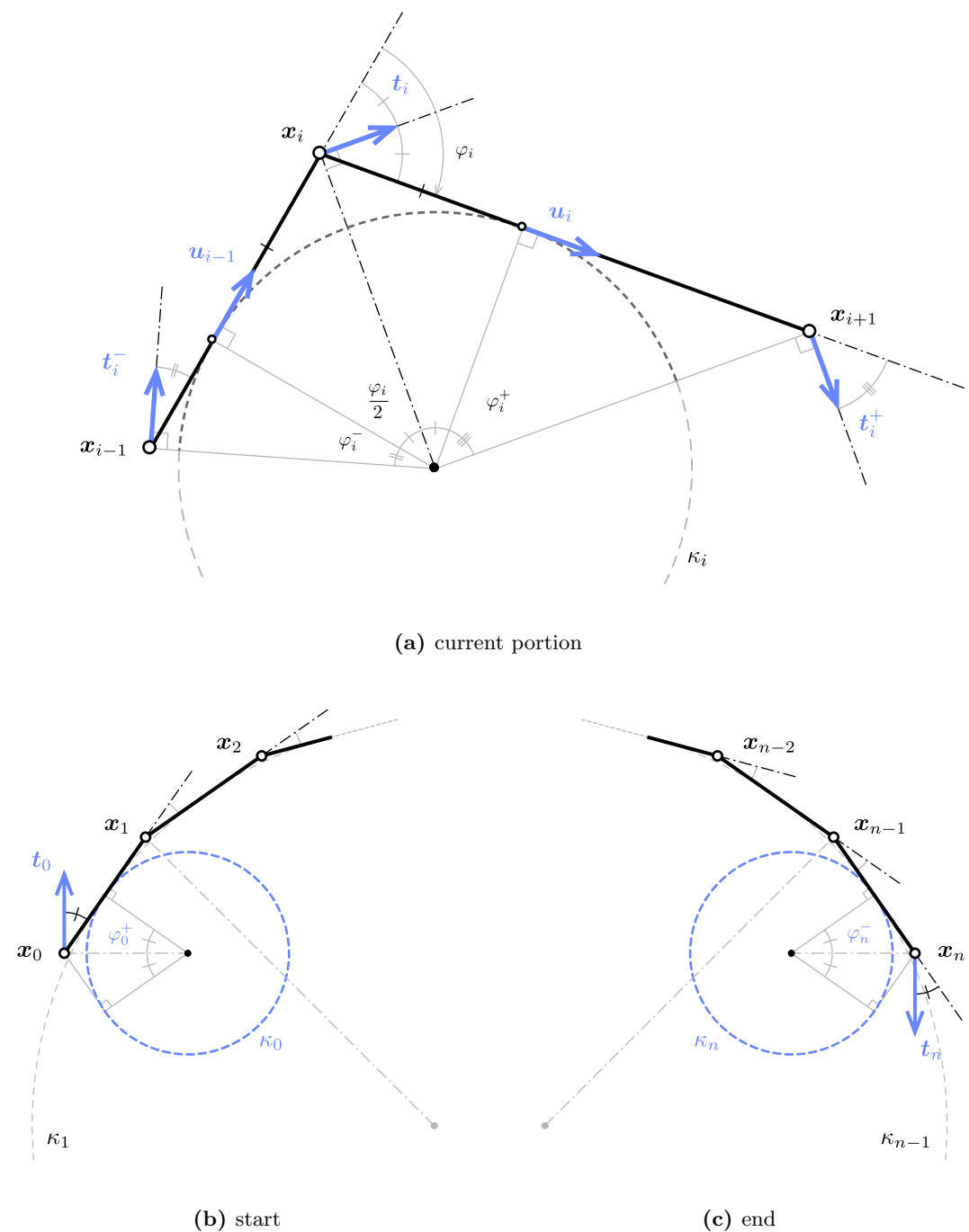


Figure 3.17 – Definition of the tangent vector (t) and related curvature binormal vector (κb) at vertices (inscribed definition).

Current portion

Let \mathbf{x}_i be a vertex in the current portion of Γ . The inscribed osculating circle gives a smooth approximation of Γ in the vicinity of \mathbf{x}_i (see fig. 3.17a) ; though this approximation does not pass through the vertices. It is again possible to construct some unit tangent vectors based on this circle, but the analytic expressions are less compact than in the circumscribed case (resp. at \mathbf{x}_{i-1} , \mathbf{x}_i , \mathbf{x}_{i+1}) :

$$\mathbf{t}_i^- = \cos\left(\frac{\varphi_i}{2} + \varphi_i^-\right) \frac{\mathbf{u}_{i-1} + \mathbf{u}_i}{\|\mathbf{u}_{i-1} + \mathbf{u}_i\|} + \sin\left(\frac{\varphi_i}{2} + \varphi_i^-\right) \frac{\mathbf{u}_{i-1} - \mathbf{u}_i}{\|\mathbf{u}_{i-1} - \mathbf{u}_i\|} \quad (3.72a)$$

$$\mathbf{t}_i^- = \frac{\mathbf{u}_{i-1} + \mathbf{u}_i}{\|\mathbf{u}_{i-1} + \mathbf{u}_i\|} \quad (3.72b)$$

$$\mathbf{t}_i^+ = \cos\left(\frac{\varphi_i}{2} + \varphi_i^+\right) \frac{\mathbf{u}_{i-1} + \mathbf{u}_i}{\|\mathbf{u}_{i-1} + \mathbf{u}_i\|} - \sin\left(\frac{\varphi_i}{2} + \varphi_i^+\right) \frac{\mathbf{u}_{i-1} - \mathbf{u}_i}{\|\mathbf{u}_{i-1} - \mathbf{u}_i\|} \quad (3.72c)$$

In this form, the expressions of \mathbf{t}_i^- and \mathbf{t}_i^+ exhibit lots of trigonometric computations. Consequently, they will be more costly to evaluate (numerically) than the ones given for the circumscribed case that exhibit only simple addition, product and division operations.

Though these points does not generally fall into mid-edge, the tangent vector can also be identified to \mathbf{u}_{i-1} (resp. \mathbf{u}_i) at point $\tilde{\mathbf{x}}_i^- = \mathbf{x}_i - \frac{1}{2}\bar{l}_i \mathbf{u}_{i-1}$ (resp. $\tilde{\mathbf{x}}_i^+ = \mathbf{x}_i + \frac{1}{2}\bar{l}_i \mathbf{u}_i$) :

$$\tilde{\mathbf{t}}_i^- = \mathbf{u}_{i-1} \quad (3.73a)$$

$$\tilde{\mathbf{t}}_i^+ = \mathbf{u}_i \quad (3.73b)$$

Similarly to the circumscribed case, one can remark that the curvature binormal vector at \mathbf{x}_i can be computed in three different manners :

$$\kappa \mathbf{b}_i = \frac{2}{\bar{l}_i} \left(\frac{\mathbf{e}_{i-1} \times \mathbf{e}_i}{\|\mathbf{e}_{i-1}\| \|\mathbf{e}_i\| + \mathbf{e}_{i-1} \cdot \mathbf{e}_i} \right) = \begin{cases} \frac{2}{\bar{l}_i} \left(\frac{\mathbf{e}_{i-1} \times \mathbf{t}_i}{\mathbf{e}_{i-1} \cdot \mathbf{t}_i} \right) \\ \frac{2}{\bar{l}_i} \left(\frac{\mathbf{t}_i \times \mathbf{e}_i}{\mathbf{t}_i \cdot \mathbf{e}_i} \right) \end{cases} \quad (3.74)$$

The first expression is interpreted as the unique circle bitangent to \mathbf{e}_{i-1} at $\tilde{\mathbf{x}}_i^-$ and \mathbf{e}_i at $\tilde{\mathbf{x}}_i^+$, as explained in §3.7.1. Equivalently, the last two expressions in eq. (3.74) can be interpreted as the curvature binormal vector of the unique circle which center is on the line normal to \mathbf{t}_i passing through \mathbf{x}_i , and that is tangent to \mathbf{e}_{i-1} (resp. \mathbf{e}_i) at $\tilde{\mathbf{x}}_i^-$ (resp. $\tilde{\mathbf{x}}_i^+$).

Discontinuity of curvature

Let \mathbf{t}_i^* be an arbitrary tangent vector at \mathbf{x}_i . Following eq. (3.74) we define the *left-sided* (resp. *right-sided*) discrete curvature at \mathbf{x}_i in the inscribed case as :

$$\kappa b_i^-(\mathbf{t}_i^*) = \frac{2}{\bar{l}_i} \left(\frac{\mathbf{e}_{i-1} \times \mathbf{t}_i^*}{\mathbf{e}_{i-1} \cdot \mathbf{t}_i^*} \right) \quad (3.75a)$$

$$\kappa b_i^+(\mathbf{t}_i^*) = \frac{2}{\bar{l}_i} \left(\frac{\mathbf{t}_i^* \times \mathbf{e}_i}{\mathbf{t}_i^* \cdot \mathbf{e}_i} \right) \quad (3.75b)$$

The corresponding osculating circle will be called the *left-sided* (resp. *right-sided*) inscribed osculating circle. When $\mathbf{t}_i^* = \mathbf{t}_i$, the limits agree one to each other ($\kappa b_i^- = \kappa b_i^+ = \kappa b_i$) and the osculating circles coincide. These definitions perfectly mimic the smooth case where, at a regular ($\|\gamma'\| \neq 0$) but not biregular ($\|\gamma''\| = 0$) point, the curvature is discontinuous while the tangent vector reminds smoothly defined.

Curve endings

The definition of the left and right sided curvatures given for a vertex in the current portion of Γ are still valid for the end vertices \mathbf{x}_0 and \mathbf{x}_n . Provided that a unit tangent vector \mathbf{t}_0^* (respectively \mathbf{t}_n^*) is given at \mathbf{x}_0 (resp. \mathbf{x}_n), the circumscribed osculating circle is defined as the unique circle passing through \mathbf{x}_0 and \mathbf{x}_1 (resp. \mathbf{x}_{n-1} and \mathbf{x}_n) tangent to \mathbf{t}_0^* (resp. \mathbf{t}_n^*) ; see fig. 3.17b and fig. 3.17c. It leads to the following curvature binormal vectors :

$$\kappa b_0 = \kappa b_0^+(\mathbf{t}_0^*) = \frac{2}{\|\mathbf{e}_0\|} \left(\frac{\mathbf{t}_0^* \times \mathbf{e}_0}{\mathbf{t}_0^* \cdot \mathbf{e}_0} \right) \quad (3.76a)$$

$$\kappa b_n = \kappa b_n^-(\mathbf{t}_n^*) = \frac{2}{\|\mathbf{e}_{n-1}\|} \left(\frac{\mathbf{e}_{n-1} \times \mathbf{t}_n^*}{\mathbf{e}_{n-1} \cdot \mathbf{t}_n^*} \right) \quad (3.76b)$$

Note that, contrary to the current portion, curvatures at endings are subjected to the definition of a unit tangent vector. This reflects the usual indetermination of boundary conditions. For a given beam whether the end is clamped, the tangent vector is known and one will seek the reacting moment due to the support ; whether the end is pinned, the reacting moment is null (so is the curvature) and one will seek the cross section orientation.

3.9 Discrete parallel transport

Discrete parallel transport can be computed by analogy to the smooth case as the rotation minimizing rotation around t : This method is unstable when t_1 and t_2 gets almost colinear.

Note that while these definitions of parallel transport are illustrated to transport vectors in space from one location $\{\mathbf{x}, \mathbf{t}\}(s)$ to another $\{\mathbf{x}, \mathbf{t}\}(s + ds)$, it is identically transposed to parallel transport in time from one location $\{\mathbf{x}, \mathbf{t}\}(t)$ to another $\{\mathbf{x}, \mathbf{t}\}(t + dt)$ as suggested in [Ber+10].

3.9.1 The rotation method

The rotation method is given in [Blo90]. First, the frame at \mathbf{x}_i is simply translated at vertex \mathbf{x}_{i+1} . Then, the translated frame is rotated so that \mathbf{t}_i aligns with \mathbf{t}_{i+1} . The rotation axis is chosen to be $\mathbf{b} = \mathbf{t}_i \times \mathbf{t}_{i+1}$ and the angle of rotation is denoted α (see fig. 3.18a). This is analogous as the smooth case.

3.9.2 The double reflexion method

The double reflection method is given by [Wan+08]. It is supposed to be of order $o(h^4)$ whereas the rotation method is only $o(h^2)$, where $h = \sup_{i \in [0,1]} \|\mathbf{e}_i\|$ is the sharpness of the discretization. Though their computation cost is quite similar, the double reflection method is not subjected to instability when \mathbf{t}_i and \mathbf{t}_{i+1} tend to be collinear, which is an obvious advantage.

We denote \mathcal{R}_x^n the reflection across the plane passing through the point \mathbf{x} and normal to the vector \mathbf{n} of unit length ($\|\mathbf{n}\| = 1$). Thus, \mathbf{v} is mapped through \mathcal{R} into $\mathbf{v}^* = \mathbf{v} - 2(\mathbf{v} \cdot \mathbf{n})\mathbf{n}$.

Let $\mathcal{R}_1 = \mathcal{R}_{x_{i+1/2}}^{n_1}$ be the reflection across the bisecting plane of \mathbf{e}_i ($\mathbf{n}_1 = \mathbf{u}_i$). Let $\mathbf{t}_i^* = \mathcal{R}_1(\mathbf{t}_i)$ be the image of \mathbf{t}_i by \mathcal{R}_1 . Let $\mathcal{R}_2 = \mathcal{R}_{x_{i+1}}^{n_2}$ be the reflection across the bisecting plane of the points $\mathbf{x}_{i+1} + \mathbf{t}_i^*$ and $\mathbf{x}_{i+1} + \mathbf{t}_{i+1}$. Thus, $\mathbf{n}_2 = \frac{\mathbf{t}_{i+1} - \mathbf{t}_i^*}{\|\mathbf{t}_{i+1} - \mathbf{t}_i^*\|}$ (see fig. 3.18b).

The parallel transport is defined as the *double reflection* through \mathcal{R}_1 and \mathcal{R}_2 :

$$\mathcal{P}_{\{\mathbf{x}_i, \mathbf{t}_i\}}^{\{\mathbf{x}_{i+1}, \mathbf{t}_{i+1}\}} = \mathcal{P}_i^{i+1} = \mathcal{R}_2 \circ \mathcal{R}_1 \quad (3.77)$$

Let $\mathcal{F}_i = \{\mathbf{t}_i, \mathbf{d}_1, \mathbf{d}_2\}$ be an orthonormal frame at \mathbf{x}_i . Let $\mathcal{F}_i^* = \mathcal{R}_1(\mathcal{F}_i) = \{\mathbf{t}_i^*, \mathbf{d}_1^*, \mathbf{d}_2^*\}$ be the image of \mathcal{F}_i by \mathcal{R}_1 . Then :

$$\mathbf{t}_i^* = \mathbf{t}_i - 2(\mathbf{t}_i \cdot \mathbf{n}_1)\mathbf{n}_1 \quad (3.78a)$$

$$\mathbf{d}_1^* = \mathbf{d}_1 - 2(\mathbf{d}_1 \cdot \mathbf{n}_1)\mathbf{n}_1 \quad (3.78b)$$

$$\mathbf{d}_2^* = \mathbf{d}_1^* \times \mathbf{t}_i^* \quad (3.78c)$$

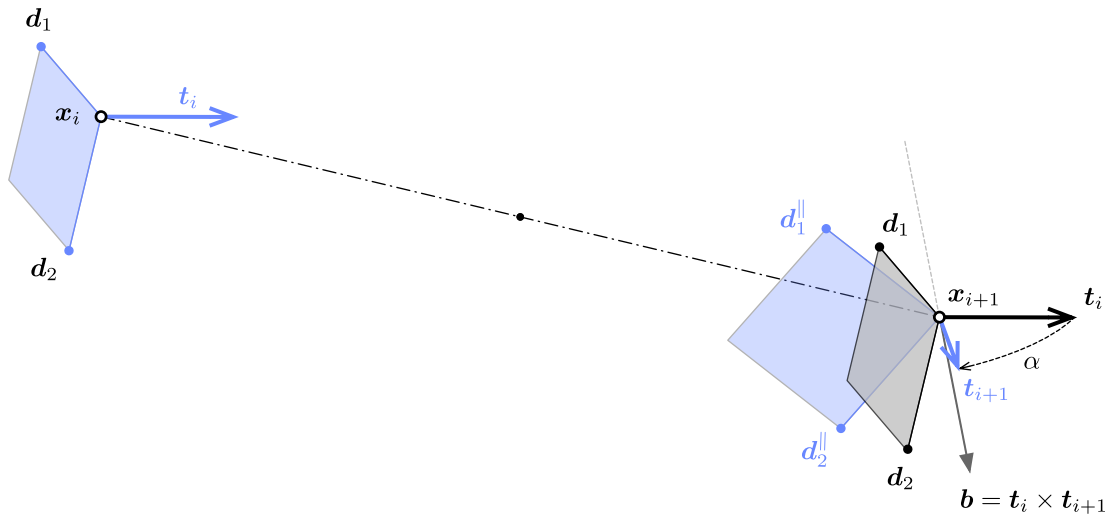
Let $\mathcal{F}_i^\parallel = \mathcal{R}_2(\mathcal{F}_i^*) = \{\mathbf{t}_{i+1}, \mathbf{d}_1^\parallel, \mathbf{d}_2^\parallel\}$ be the image of \mathcal{F}_i^* by \mathcal{R}_2 . Then the parallel transported vectors are given by :

$$\mathbf{d}_1^\parallel = \mathbf{d}_1^* - 2(\mathbf{d}_1^* \cdot \mathbf{n}_2)\mathbf{n}_2 \quad (3.79a)$$

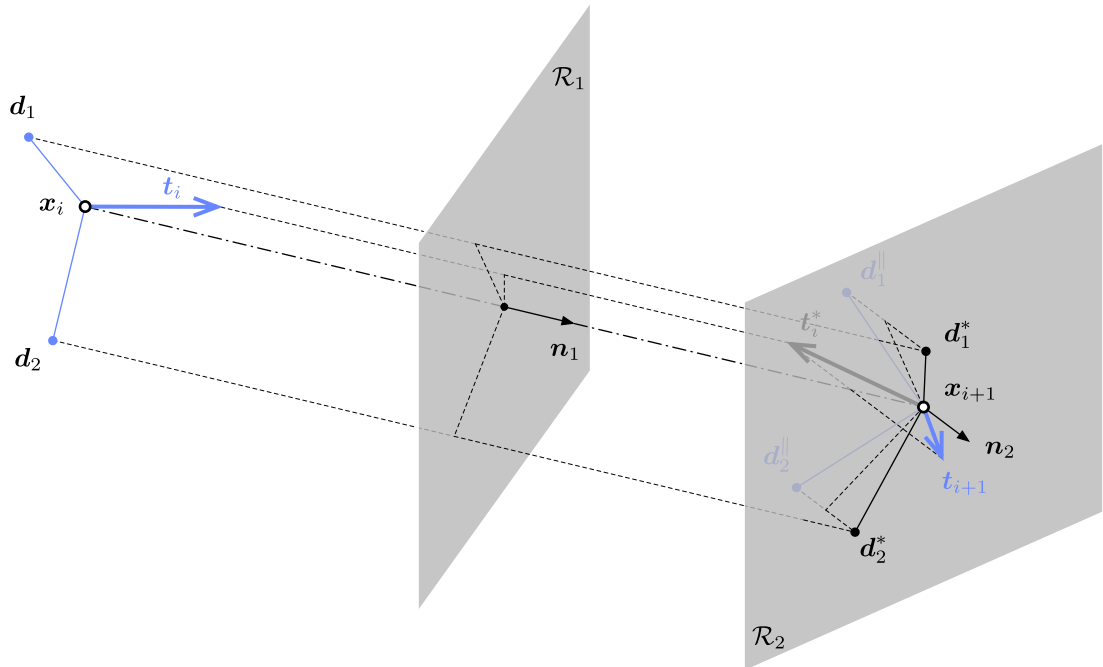
$$\mathbf{d}_2^\parallel = \mathbf{t}_{i+1} \times \mathbf{d}_1^\parallel \quad (3.79b)$$

The double reflection is equivalent to a rotation around the line \mathcal{D} defined as the intersection of the two reflection planes, of direction $\mathbf{b} = \mathbf{n}_1 \times \mathbf{n}_2$, by an angle $\alpha = 2\angle(\mathbf{n}_1, \mathbf{n}_2) = 2\arcsin(\|\mathbf{b}\|)$.

Ici il faudrait calculer les coordonnées du centre de rotation. Idem pour la méthode par rotation (translation + rotation = rotation ??) => trouver l'axe de rotation, l'angle et le centre la rotation équivalente. Comparer les méthodes.



(a) rotation method



(b) double reflection method

 Figure 3.18 – Parallel transport of vectors from $\{x_i, t_i\}$ to $\{x_{i+1}, t_{i+1}\}$.

Remark that for both the circumscribed (see fig. 3.16a) and inscribed (see fig. 3.17a) osculating circles :

$$\mathbf{t}_i = \mathcal{R}_{\mathbf{x}_{i-1/2}}^{u_{i-1}} \circ \mathcal{R}_{\mathbf{x}_i}^{t_i}(\mathbf{t}_i^-) \quad (3.80a)$$

$$\mathbf{t}_i = \mathcal{R}_{\mathbf{x}_i}^{t_i} \circ \mathcal{R}_{\mathbf{x}_{i+1/2}}^{u_i}(\mathbf{t}_i^+) \quad (3.80b)$$

3.10 Conclusion

Après un rappel sur les courbes continues de l'espace, nous avons introduit, pour le cas continu, les notions de courbure, torsion géométrique, interinsèque à la courbe. Puis nous avons introduit les repères mobiles : adapté, de Frenet, de Bishop.

Nous avons fait le passage en discret et ça augmente en complexité. EN particulier, nous avons vu que la définition de la courbure n'est pas univoque. Nous avons identifié 2 approches, que nous avons comparé. Bien que la seconde est le comportement désiré pour pénaliser les courbures importantes, l'autre présente bcp d'avantages. Localité parfaite, interpolation par un arc, compatibilité des courbures droite/gauche et 3 points. Extension de la définition aux extrémitées. Meilleur représentativité" de l'énergie pour une discréttization régulière sur des cas classiques.

Nous avons ensuite regardé la question de la définition du vecteur tangent pour ces 2 définitions. Et sa corrélation avec la courbure.

Enfin, nous avons exposé 2 méthodes pour le calcul du transport parallel sur une courbe discrète : la rotation et la double réflexion, qui ne présente pas d'instabilité lorsque la courbure tend à s'annuler. (donc $\mathbf{t}_i \mathbf{t}_{i+1}$ colinéaires).

[HM95, Wan+08]

3.11 References

- [Ber+08] M. Bergou, M. Wardetzky, S. Robinson, B. Audoly, and E. Grinspun. “Discrete elastic rods”. In: *ACM SIGGRAPH* (2008), pp. 1–12.
- [Ber+10] M. Bergou, B. Audoly, E. Vouga, M. Wardetzky, and E. Grinspun. “Discrete viscous threads”. In: *ACM Transactions on ...* (2010), pp. 1–10.
- [Ber28] J. Bernoulli. *Johannis Bernoulli... Opera omnia, tam antea sparsim edita, quam hactenus inedita*. IV. sumptibus Marci-Michaelis Bousquet, 1728, p. 584.
- [Bis75] R. Bishop. “There is more than one way to frame a curve”. In: *Mathematical Association of America* (1975).
- [Blo90] J. Bloomenthal. “Calculation of reference frames along a space curve”. In: *Graphics Gems*. Ed. by A. S. Glassner. Vol. 1. San Diego, CA, USA: Academic Press Professional, Inc., 1990, pp. 567–571.
- [Bob15] A. Bobenko. *Discrete differential geometry*. Second. 2015, p. 144.
- [Car+14] D. Carroll, E. Hankins, E. Kose, and I. Sterling. “A survey of the differential geometry of discrete curves”. In: *The Mathematical Intelligencer* 36.4 (2014), pp. 28–35. arXiv: [arXiv:1311.5862v1](https://arxiv.org/abs/1311.5862v1).
- [Coo13] J. L. Coolidge. *A history of geometrical methods*. Ed. by C. Corporation. Dover Books on Mathematics. Dover Publications, 2013, p. 480.
- [Del07] J. Delcourt. “Analyse et géométrie : les courbes gauches de Clairaut à Serret”. PhD thesis. Université de Paris VI, 2007, p. 302.
- [Del11] J. Delcourt. “Analyse et géométrie, histoire des courbes gauches de Clairaut à Darboux”. In: *Archive for History of Exact Sciences* 65.3 (2011), pp. 229–293.
- [Eul75] L. Euler. “Continens analysin, pro incuruacione fili in fingulis punctis inueniendia”. In: *Novi Commentarii academiae scientiarum Petropolitanae* 19 (1775), pp. 340–370.
- [Far+14] R. T. Farouki, C. Giannelli, M. L. Sampoli, and A. Sestini. “Rotation-minimizing osculating frames”. In: *Computer Aided Geometric Design* 31.1 (2014), pp. 27–42.
- [Fre52] F. Frenet. “Sur les courbes à double courbure”. In: *Journal de Mathématiques Pures et Appliquées* 17 (1852), pp. 437–447.
- [GAS06] A. Gray, E. Abbena, and S. Salamon. *Modern differential geometry of curves and surfaces with Mathematica*. Ed. by E. A. Salamon and Simon. Third. CRC Press, 2006, p. 1016.
- [Gug89] H. Guggenheimer. “Computing frames along a trajectory”. In: *Computer Aided Geometric Design* 6.1 (1989), pp. 77–78.
- [HM95] A. J. Hanson and H. Ma. *Parallel Transport Approach to Curve Framing*. Tech. rep. 1995.
- [Hof08] T. Hoffmann. “Discrete Differential Geometry of Curves and Surfaces”. In: 18 (2008).

-
- [Klo86] F. Klok. “Two moving coordinate frames for sweeping along a 3D trajectory”. In: *Computer Aided Geometric Design* 3.3 (1986), pp. 217–229.
- [Men13] T. Menninger. *Frenet curves and successor curves : generic parametrizations of the helix and slant helix*. Tech. rep. 2013, pp. 1–15. arXiv: [1302.3175](https://arxiv.org/abs/1302.3175).
- [Mon09] G. Monge. *Application de l'analyse à la géométrie*. 1809, p. 475.
- [PFL95] T. Poston, S. Fang, and W. Lawton. “Computing and approximating sweeping surfaces based on rotation minimizing frames”. In: *Proceedings of the 4th International Conference on CAD/CG*. 1995, pp. 1–8.
- [Pit26] H. Pitot. “Quadrature de la moitié d'une courbe des arcs appelée la compagne de la cycloïde”. In: *Mémoires de l'Académie Royale des Sciences (1724)* (1726), pp. 107–113.
- [Rom13] P. Romon. *Introduction à la géométrie différentielle discrète*. Références sciences. Ellipses, 2013, p. 216.
- [Vou14] E. Vouga. “Plane Curves”. In: *Lectures in discrete differential geometry*. 2014. Chap. 1, pp. 1–11.
- [Wan+08] W. Wang, B. Jüttler, D. Zheng, and Y. Liu. “Computation of rotation minimizing frames”. In: *ACM Transactions on Graphics* 27.1 (2008), pp. 1–18.

4 Elastic rod : variational approach

4.1 Introduction

4.1.1 Goals and contribution

In this section a novel element with 4 degrees of freedom accounting for torsion and bending behaviours is presented. The beam is considered in Kirchhoff's theory framework, so that it is supposed to be inextensible and its sections are supposed to remain orthogonal to the centreline during deformation. The reduction from the classic 6-DoF model to this 4-DoF model is achieved by an appropriate curve-angle representation based on a relevant curve framing. Energies are then formulated and leads to internal forces and moments acting on the beam. The static equilibrium is deduced from a damped fictitious dynamic with an adapted dynamic relaxation algorithm.

4.1.2 Related work

Basile [Ber+10] Basile [Ber+08] Basile [AAP10] Sina [Nab14] [Ful78], [dVri05], [Vau00], [Ber09]

Pou intro : [Jun+10]

Dynamic relaxation : [Lew03] En particulier, voir pour un comparatif avec une méthode implicite.

4.1.3 Overview

1. quaternion pour piloter les input / output ?
2. calcul de la hessienne au moins pour les θ comme Audoly. Ne serait-ce pas possible pour les x ? Avec ma technique du transport parallèle il me semble pourvoir avoir accès au DL à l'ordre 2 ...

3. Formulation pour les efforts ponctuels / moments extérieurs en vue d'une résolution par minimisation. Voir F. Bertails
4. prise en compte des contraintes => méméthide des multiplicateurs de lagrange

4.2 Kirchhoff rod

The geometric configuration of the rod is described by its centerline $\boldsymbol{x}(s)$ and its cross sections. The centerline is parameterized by its arc-length. Cross sections orientations are followed along the centerline by their material frame $\{\boldsymbol{d}_3(s), \boldsymbol{d}_1(s), \boldsymbol{d}_2(s)\}$ which is an adapted orthonormal moving frame aligned to section's principal axes of inertia. Here, "adapted" means $\boldsymbol{d}_3(s) = \boldsymbol{x}'(s) = \boldsymbol{t}(s)$ is aligned to the centerline's tangent. In the literature, this description is also known as a *Cosserat Curve* [ST07].

4.2.1 Inextensibility

Note the previous description is only valid for inextensible rods in order to follow material points by their arc-length indifferently in their rest or deformed configuration. As explained in [AAP10], this hypothesis is usually relevant for slender beams. Indeed, in practice, if a slender member faces substantial axial strain the bending behaviour would become negligible due to the important difference between axial and bending stiffness. The length of the rod will be denoted L and the arc-length s will vary (with no loss of generality) in $[0, L]$.

4.2.2 Euler-Bernouilli

Strains are supposed to remain small so that material frame remains orthogonal to the centerline in the deformed configuration. Thus, differentiating the conditions of orthonormality leads to the following differential equations governing the evolution of $\{\boldsymbol{d}_3(s), \boldsymbol{d}_1(s), \boldsymbol{d}_2(s)\}$ along the centerline :

$$\begin{bmatrix} \boldsymbol{d}'_3(s) \\ \boldsymbol{d}'_1(s) \\ \boldsymbol{d}'_2(s) \end{bmatrix} = \begin{bmatrix} 0 & \kappa_2(s) & -\kappa_1(s) \\ -\kappa_2(s) & 0 & \tau(s) \\ \kappa_1(s) & -\tau(s) & 0 \end{bmatrix} \begin{bmatrix} \boldsymbol{d}_3(s) \\ \boldsymbol{d}_1(s) \\ \boldsymbol{d}_2(s) \end{bmatrix} \quad (4.1)$$

La théorie des poutres est une application de la théorie de l'élasticité isotrope. Pour mener les calculs de résistance des matériaux, on considère les hypothèses suivantes :

- (1) hypothèse de Bernoulli : au cours de la déformation, les sections droites restent perpendiculaires à la courbe moyenne ;
- (2) les sections droites restent planes selon Navier-Bernoulli (pas de gauchissement).

L'hypothèse de Bernoulli permet de négliger le cisaillement dans le cas de la flexion : le

risque de rupture est alors due à l'extension des fibres situées à l'extérieur de la flexion, et la flèche est due au moment fléchissant. Cette hypothèse n'est pas valable pour les poutres courtes car ces dernières sont hors des limites de validité du modèle de poutre, à savoir que la dimension des sections doit être petite devant la longueur de la courbe moyenne. Le cisaillement est pris en compte dans le modèle de Timoshenko et Mindlin.

4.2.3 Darboux vector

Those equations can be formulated with the *Darboux vector* of the chosen material frame, which represents the rotational velocity of the frame along $\mathbf{x}(s)$:

$$\mathbf{d}'_i(s) = \boldsymbol{\Omega}_m(s) \times \mathbf{d}_i(s) \quad , \quad \boldsymbol{\Omega}_m(s) = \begin{bmatrix} \tau(s) \\ \kappa_1(s) \\ \kappa_2(s) \end{bmatrix} \quad (4.2)$$

Where $\kappa_1(s)$, $\kappa_2(s)$ and $\tau(s)$ represent respectively the rate of rotation of the material frame around the axis $\mathbf{d}_1(s)$, $\mathbf{d}_2(s)$ and $\mathbf{d}_3(s)$.

4.2.4 Curvatures and twist

The material curvatures are denoted $\kappa_1(s)$ and $\kappa_2(s)$ and represent the rod's flexion in the principal planes respectively normal to $\mathbf{d}_1(s)$ and $\mathbf{d}_2(s)$. The material twist is denoted $\tau(s)$ and represents the section's rate of rotation around $\mathbf{d}_3(s)$. Those scalar functions measure directly the strain as defined in Kirchhoff's theory (Figure 4). Recall that the Frenet frame $\{\mathbf{t}(s), \mathbf{n}(s), \mathbf{b}(s)\}$ defines the osculating plane and the total curvature (κ) of a spatial curve :

$$\mathbf{t}'(s) = \kappa(s) \mathbf{n}(s) \quad , \quad \kappa(s) = \|\mathbf{t}'(s)\| \quad , \quad \mathbf{b}(s) = \mathbf{t}(s) \times \mathbf{n}(s) = \frac{\mathbf{t}(s) \times \mathbf{t}'(s)}{\kappa(s)} \quad (4.3)$$

To describe the osculating plane in which lies the bending part of the deformation, let's introduce the *curvature binormal* $\kappa \mathbf{b}(s) = \mathbf{t}(s) \times \mathbf{t}'(s)$, the vector of direction $\mathbf{b}(s)$ and norm $\kappa(s)$. At each point of arc-length s the osculating plane is normal to $\kappa \mathbf{b}(s)$.

4.2.5 Elastic energy

Kirchhoff's theory assigns an elastic energy to beams according to their strain [AAP10]. In this theory, a beam is supposed to be inextensible. Thus the elastic energy (\mathcal{E}_p) only accounts for torsion and bending behaviors and is given by :

$$\mathcal{E}_p = \frac{1}{2} \int_0^L EI_1(\kappa_1 - \bar{\kappa}_1)^2 + EI_2(\kappa_2 - \bar{\kappa}_2)^2 ds + \frac{1}{2} \int_0^L \beta(\tau - \bar{\tau})^2 ds \quad (4.4)$$

Here, $\bar{\kappa}_1$, $\bar{\kappa}_2$ and $\bar{\tau}$ denote the natural curvature and twist of the rod in the rest position (no stress).

4.3 Curve-angle representation

The previous paragraph has shown how the elastic potential energy of a rod can be computed following both its centerline and its cross sections orientations, which represents a model with 6-DoF : 3 for centerline positions and 3 for cross section orientations.

Following [Ber+08], let's introduce a reduced coordinate formulation of the rod that account for only 4-DoF. This reduction of DoF relies on the concept of zero-twisting frame which gives a reference frame with zero twist along a given centerline. Thus, cross section orientations $\{\mathbf{d}_3(s), \mathbf{d}_1(s), \mathbf{d}_2(s)\}$ can be tracked only by the measure of an angle θ from this reference frame denoted $\{\mathbf{d}_3(s), \mathbf{u}(s), \mathbf{v}(s)\}$ (Figure 5).

Note that an alternative solution could be to parameterize the global rotations of local material frame and to compute the rotation needed to align two successive frames along the curve's tangent.

Ici, expliquer la succession des dépendances : les vecteurs matériaux dépendent du repère de bishop par la seule variable theta. Le repère de bishop quand à lui est entièrement déterminé (au choix d'une constante de départ près) par la donnée de la centerline x.

Faire un schéma explicatif.

quid du transport parallèle en temps et non en espace ?

4.3.1 Zero-twisting frame

Zero-twisting frame, also known as Bishop frame, was introduced by Bishop in 1964. Bishop remarked that there was more than one way to frame a curve [Bis75]. Indeed, for a given curve, any orthonormal moving frame would satisfy the following differential equations, where $k_1(s)$, $k_2(s)$ and $\tau(s)$ are scalar functions that define completely the moving frame :

$$\begin{bmatrix} \mathbf{e}'_3(s) \\ \mathbf{e}'_1(s) \\ \mathbf{e}'_2(s) \end{bmatrix} = \begin{bmatrix} 0 & k_2(s) & -k_1(s) \\ -k_2(s) & 0 & \tau(s) \\ k_1(s) & -\tau(s) & 0 \end{bmatrix} \begin{bmatrix} \mathbf{e}_3(s) \\ \mathbf{e}_1(s) \\ \mathbf{e}_2(s) \end{bmatrix} \quad (4.5)$$

For instance, a Frenet frame $\{\mathbf{t}(s), \mathbf{n}(s), \mathbf{b}(s)\}$ is a frame which satisfies $k_1(s) = 0$. Note that this frame suffers from major disadvantages : it is undefined where the curvature vanishes and it flips at inflexion points. A Bishop frame $\{\mathbf{t}(s), \mathbf{u}(s), \mathbf{v}(s)\}$ is a frame which satisfies $\tau(s) = 0$. By construction, this frame has no angular velocity (i.e. no twist) around the curve's tangent ($\mathbf{u} \cdot \mathbf{v}' = \mathbf{u}' \cdot \mathbf{v} = 0$). Its evolution along the curve is described by the corresponding Darboux vector : $\boldsymbol{\Omega}_b(s) = \kappa \mathbf{b} = \mathbf{t} \times \mathbf{t}'$. Remark that $\boldsymbol{\Omega}_b(s)$ only depends on the centerline and is well defined even when the curvature vanishes.

Thus, by the help of $\boldsymbol{\Omega}_b(s)$, it's possible to transport a given vector \mathbf{e} along the centerline with no twist : $\mathbf{e}' = \kappa \mathbf{b} \times \mathbf{e}$. This is called *parallel transport*.

4.4 Strains

4.4.1 Axial strain

There is no axial strain to be considered as far as the rod is supposed to be unstretchable.

Remark that the inextensibility hypothesis implies that any admissible perturbation ($\lambda \mathbf{h}_x$) of the rod's centerline (\mathbf{x}) is locally orthogonal to the centerline itself. Indeed, at each arc-length s an inextensible rod must satisfies :

$$\|\mathbf{x}'\| = \|(\mathbf{x} + \lambda \mathbf{h}_x)'\| = 1 \Rightarrow \mathbf{d}_3 \cdot \mathbf{h}'_x = -\frac{\lambda^2}{2} \|\mathbf{h}'_x\|^2 = o(\lambda) \simeq 0 \quad (4.6)$$

In other words, this means that the same arc-length parametrization can be used to locate beam sections along the centerline along the deformation path. This would not be the case if the centerline would shorten or stretch out during its deformation. It is worth to mention here that this property ($\mathbf{d}_3 \cdot \mathbf{h}'_x = 0$) will be used several times in the following sections.

4.4.2 Bending strain

Let's compute the bending strains κ_1 and κ_2 regarding the geometric configuration of the rod. Remark that :

$$\kappa \mathbf{b} \cdot \mathbf{d}_1 = (\mathbf{d}_3 \times \mathbf{d}'_3) \cdot \mathbf{d}_1 = (\mathbf{d}_1 \times \mathbf{d}_3) \cdot \mathbf{d}'_3 = -\mathbf{d}_2 \cdot \mathbf{d}'_3 = \kappa_1 \quad (4.7a)$$

$$\kappa \mathbf{b} \cdot \mathbf{d}_2 = (\mathbf{d}_3 \times \mathbf{d}'_3) \cdot \mathbf{d}_2 = (\mathbf{d}_2 \times \mathbf{d}_3) \cdot \mathbf{d}'_3 = \mathbf{d}_1 \cdot \mathbf{d}'_3 = \kappa_2 \quad (4.7b)$$

That is to say $\kappa \mathbf{b}$ is orthogonal to \mathbf{d}_3 :

$$\kappa \mathbf{b} = \kappa_1 \mathbf{d}_1 + \kappa_2 \mathbf{d}_2 \quad (4.8)$$

Thus, the vector of material curvatures ($\boldsymbol{\omega}$) expressed on material frame axes $\{\mathbf{d}_1(s), \mathbf{d}_2(s)\}$ is defined as :

$$\boldsymbol{\omega} = \begin{bmatrix} \kappa_1 \\ \kappa_2 \end{bmatrix} = \begin{bmatrix} \kappa \mathbf{b} \cdot \mathbf{d}_1 \\ \kappa \mathbf{b} \cdot \mathbf{d}_2 \end{bmatrix} = \begin{bmatrix} -\mathbf{x}'' \cdot \mathbf{d}_2 \\ \mathbf{x}'' \cdot \mathbf{d}_1 \end{bmatrix} \quad (4.9)$$

4.4.3 Torsional strain

Let's compute the twist or torsional strain τ regarding the geometric configuration of the rod. Decomposing the material frame on the bishop frame gives :

$$\begin{bmatrix} \mathbf{d}_1 \\ \mathbf{d}_2 \end{bmatrix} = \begin{bmatrix} \cos \theta & \sin \theta \\ -\sin \theta & \cos \theta \end{bmatrix} \begin{bmatrix} \mathbf{u} \\ \mathbf{v} \end{bmatrix} \quad (4.10)$$

Thus, the twist can be identified directly as the variation of θ along the curve :

$$\tau = \mathbf{d}'_1 \cdot \mathbf{d}_2 = (\theta' \mathbf{d}_2 + \kappa \mathbf{b} \times \mathbf{d}_1) \cdot \mathbf{d}_2 = \theta' + \mathbf{d}_3 \cdot \kappa \mathbf{b} = \theta' \quad (4.11)$$

Note that the Frenet frame does not lead to a correct evaluation of the twist.

4.5 Elastic energy

Introducing ω and θ , the elastic energy can be rewritten as follow :

$$\mathcal{E}_p = \mathcal{E}_b + \mathcal{E}_t = \frac{1}{2} \int_0^L (\omega - \bar{\omega})^T B (\omega - \bar{\omega}) ds + \frac{1}{2} \int_0^L \beta (\theta' - \bar{\theta}')^2 ds \quad (4.12)$$

Where B is the bending stiffness matrix along the principal axes of inertia and β is the torsional stiffness :

$$B = \begin{bmatrix} EI_1 & 0 \\ 0 & EI_2 \end{bmatrix}, \quad \beta = GJ \quad (4.13)$$

Recall that the rod is supposed to be inextensible in Kirchhoff's theory. Thus, there is no stretching energy associated with an axial strain. However, this constraint may be enforced via a penalty energy, which in practice is somehow very similar as considering an axial stiffness into the beam's

Remark that the twisting energy (\mathcal{E}_t) only depends on θ and is independent regarding x while the bending energy (\mathcal{E}_b) depends on both θ and x variables (remind that κ_1 and κ_2 are the projections of κb over d_1 over d_2). Thus, a coupling between bending and twisting appears as the minimum of the whole elastic energy is not necessarily reached for concomitant minimums of bending and twisting energies.

From this energy formulation, an interesting and well-known result on elastic rods could be highlighted : "torsion is uniform in an isotropic rod that is straight in its rest configuration" [ABW99].

Indeed, let's take an isotropic rod ($EI_1 = EI_2 = EI$) that is straight in its rest configuration ($\bar{\kappa}_1 = \bar{\kappa}_2 = 0$). Then, the bending energy becomes : $\mathcal{E}_b = EI_1\kappa_1^2 + EI_2\kappa_2^2 = EI\kappa^2$, and consequently doesn't depend on θ anymore. The curvature of the rod only depends on the geometry of its centerline ($\kappa = \|\kappa b\| = \|x' \times x''\|$). Thus, there is no more coupling between bending and twisting and the global minimum of elastic energy is reached while minimizing separately bending and twisting energies. That is to say the geometry of the rod (x) is the one that minimized \mathcal{E}_b . The minimum of \mathcal{E}_t is zero and is achieved for a uniform twist along the centerline, only prescribed by the boundary conditions.

4.6 Quasistatic assumption

Following [Ber+08], it is relevant to assume that the propagation of twist waves is instantaneous compared to the one of bending waves. Thus, internal forces f^{int} and moment of torsion m^{int} acts on two different timescales in the rod dynamic. Thus on the timescale of action of the force f^{int} on the center line, driving the bending waves, the twist waves

propagate instantaneously, so that $\forall s \in [0, L]$, $\delta \mathcal{E}_p / \delta \theta = 0$ for the computation of \mathbf{f}^{int} . This assumption may not be enforced, as in [Nabei2014], but leads to simpler and faster computations.

4.7 Energy gradient with respect to θ : moment of torsion

Internal moment of torsion and forces acting on the rod are classically obtained by differentiating the potential energy of the system with respect to θ and \mathbf{x} . Here, the calculus is a bit tricky as far as the differentiation takes place in function spaces. After a brief reminder on functional derivative, the main results of the calculations of the energy derivatives are given.

4.7.1 Derivative of material directors with respect to θ

Recalling that θ and \mathbf{x} are independant variables and that Bishop frame $\{\mathbf{u}, \mathbf{v}\}$ only depends on \mathbf{x} , the decomposition of material frame directors $\{\mathbf{d}_1, \mathbf{d}_2\}$ on Bishop frame leads directly to the following expression for the derivative of the material directors :

$$\mathbf{D}_\theta \mathbf{d}_1(s) \cdot h_\theta = \frac{d}{d\lambda} \mathbf{d}_1[\theta + \lambda h_\theta] \Big|_{\lambda=0} = (-\sin \theta \mathbf{u} + \cos \theta \mathbf{v}) \cdot h_\theta = \mathbf{d}_2 \cdot h_\theta \quad (4.14a)$$

$$\mathbf{D}_\theta \mathbf{d}_2(s) \cdot h_\theta = \frac{d}{d\lambda} \mathbf{d}_2[\theta + \lambda h_\theta] \Big|_{\lambda=0} = (-\cos \theta \mathbf{u} - \sin \theta \mathbf{v}) \cdot h_\theta = -\mathbf{d}_1 \cdot h_\theta \quad (4.14b)$$

4.7.2 Derivative of the material curvatures vector with respect to θ

Regarding the definition of the material curvatures vector and the derivative of material directors with respect to θ , it follows immediately that :

$$\mathbf{D}_\theta \boldsymbol{\omega}(s) \cdot h_\theta = \frac{d}{d\lambda} \boldsymbol{\omega}[\theta + \lambda h_\theta] \Big|_{\lambda=0} = \begin{bmatrix} \kappa \mathbf{b} \cdot \mathbf{d}_2 \\ -\kappa \mathbf{b} \cdot \mathbf{d}_1 \end{bmatrix} \cdot h_\theta = -\mathbf{J} \boldsymbol{\omega} \cdot h_\theta \quad (4.15)$$

Where \mathbf{J} is the matrix that acts on two dimensional vectors by counter-clockwise rotation of angle $\frac{\pi}{2}$:

$$\mathbf{J} = \begin{bmatrix} 0 & -1 \\ 1 & 0 \end{bmatrix} \quad (4.16)$$

4.7.3 Computation of the moment of torsion

The moment of torsion is given by the functional derivative of the potential elastic energy with respect to θ which can be decomposed according to the chaine rule :

$$\begin{aligned} \langle -m(s), h_\theta \rangle &= \mathbf{D}_\theta \mathcal{E}_p(s) \cdot h_\theta = \mathbf{D}_\theta \mathcal{E}_b(s) \cdot h_\theta + \mathbf{D}_\theta \mathcal{E}_t(s) \cdot h_\theta \\ &= \mathbf{D}_\theta \mathcal{E}_b[\boldsymbol{\omega}[\theta]](s) \cdot h_\theta + \mathbf{D}_\theta \mathcal{E}_t[\theta](s) \cdot h_\theta \end{aligned} \quad (4.17)$$

Derivative of the torsion energy with respect to θ

Decomposing the previous calculus gives:

$$\begin{aligned}
 \mathbf{D}_\theta \mathcal{E}_t[\theta](s) \cdot h_\theta &= \frac{d}{d\lambda} \mathcal{E}_t[\theta + \lambda h_\theta] \Big|_{\lambda=0} \\
 &= \frac{d}{d\lambda} \left(\frac{1}{2} \int_0^L \beta ((\theta + \lambda h_\theta)' - \bar{\theta}')^2 dt \right) \Big|_{\lambda=0} \\
 &= \int_0^L \beta (\theta' - \bar{\theta}') \cdot h'_\theta dt \\
 &= [\beta(\theta' - \bar{\theta}') \cdot h_\theta]_0^L - \int_0^L (\beta(\theta' - \bar{\theta}'))' \cdot h_\theta dt \\
 &= \int_0^L (\beta(\theta' - \bar{\theta}')) (\delta_L - \delta_0) - (\beta(\theta' - \bar{\theta}'))' \cdot h_\theta dt
 \end{aligned} \tag{4.18}$$

Derivative of the bending energy with respect to θ

The derivative of \mathcal{E}_b is obtained with the chaine rule :

$$\begin{aligned}
 \mathbf{D}_\omega \mathcal{E}_b[\omega](s) \cdot \mathbf{h}_\omega &= \frac{d}{d\lambda} \mathcal{E}_b[\omega + \lambda \mathbf{h}_\omega] \Big|_{\lambda=0} \\
 &= \frac{d}{d\lambda} \left(\frac{1}{2} \int_0^L ((\omega + \lambda \mathbf{h}_\omega) - \bar{\omega})^T \mathbf{B} ((\omega + \lambda \mathbf{h}_\omega) - \bar{\omega}) dt \right) \Big|_{\lambda=0} \\
 &= \int_0^L (\omega - \bar{\omega})^T \mathbf{B} \cdot \mathbf{h}_\omega dt
 \end{aligned} \tag{4.19}$$

Finally, reminding eq 4.14 :

$$\begin{aligned}
 \mathbf{D}_\theta \mathcal{E}_b[\omega[\theta]](s) \cdot h_\theta &= \mathbf{D}_\omega \mathcal{E}_b[\omega](s) \cdot (\mathbf{D}_\theta \omega[\theta](s) \cdot h_\theta) \\
 &= - \int_0^L (\omega - \bar{\omega})^T \mathbf{B} \mathbf{J} \omega \cdot h_\theta dt
 \end{aligned} \tag{4.20}$$

Moment of torsion

Thus, the

$$\begin{aligned}
 \langle -m(s), h_\theta \rangle &= \mathbf{D}_\theta \mathcal{E}_b[\omega[\theta]](s) \cdot h_\theta + \mathbf{D}_\theta \mathcal{E}_t[\theta](s) \cdot h_\theta \\
 &= \int_0^L \left((\beta(\theta' - \bar{\theta}')) (\delta_L - \delta_0) - (\beta(\theta' - \bar{\theta}'))' \right) - (\omega - \bar{\omega})^T \mathbf{B} \mathbf{J} \omega \cdot h_\theta dt
 \end{aligned} \tag{4.21}$$

Finally, we can conclude on the expression of the internal moment of torsion :

$$m(s) = - (\beta(\theta' - \bar{\theta}')) (\delta_L - \delta_0) - (\beta(\theta' - \bar{\theta}'))' + (\omega - \bar{\omega})^T \mathbf{B} \mathbf{J} \omega \tag{4.22}$$

Quasistatic hypothesis

$$(\beta(\theta' - \bar{\theta}'))' + (\omega - \bar{\omega})^T \mathbf{B} \mathbf{J} \omega = 0 \quad (4.23)$$

4.8 Energy gradient with respect to x : internal forces

Internal torsional moments and forces acting on the rod are classically obtained by differentiating the potential energy of the system with respect to θ and \mathbf{x} . Here, the calculus is a bit tricky as far as the differentiation takes place in function spaces. After a brief reminder on functional derivative, the main results of the calculations of the energy derivatives are given.

paragraphe entièrement à revoir. Expliquer le cheminement. \mathbf{x} fixe bishop et theta fixe d1,d2 par rapport à bishop. \mathbf{x} est indépendant de theta. Seul des CL peuvent créer des couplages entre \mathbf{x} et theta

Donc les vrais degrés de liberté du problème sont en fait les vecteurs matériels et les positions \mathbf{x} . Se reporter à une modélisation du pb dans SO3 comme Spillmann par exemple.

Le calcul des gradients se résume donc à calculer les gradients des vecteurs matériels par rapport à des perturbations infinitésimales en \mathbf{x} et theta. Pour theta, c'est facile. Pour \mathbf{k}_b , c'est facile. Reste la variation par rapport à \mathbf{x} , qui est en fait la variation de bishop qu'on explique avec le writhe (défaut de fermeture de bishop sur une boucle fermée) et le transport parallèle. Le calcul se fait aisément en écrivant la double rotation et en effectuant le DL au premier ordre.

Le reste est quasiment immédiat. Reste la question des CL et des termes aux bords.

Il faut aussi se positionner par rapport à l'article de Basile. Regarder la question applied displacement vs settlement pour imposer une CL.

4.8.1 Derivative of material directors with respect to x

ici expliquer le fonctionnement de la figure

A variation of the centerline \mathbf{x} by $\epsilon = \lambda \mathbf{h}_x$ would cause a variation in the Bishop frame because parallel transport depends on the centerline itself. As far as \mathbf{x} and θ are independent variables, this leads necessarily to a variation of the material frame. Let us denote :

- $F = \{\mathbf{t}, \mathbf{u}, \mathbf{v}\}$: the Bishop frame in the reference configuration ;
- $F_\epsilon = \{\mathbf{t}_\epsilon, \mathbf{u}_\epsilon, \mathbf{v}_\epsilon\}$: the Bishop frame in the deformed configuration ;
- $\tilde{F}_\epsilon = \{\mathbf{t}, \tilde{\mathbf{u}}_\epsilon, \tilde{\mathbf{v}}_\epsilon\}$: the frame obtained by parallel transporting F_ϵ back on F .

What we want to achieve is to write at arc-length s the Bishop frame in the deformed

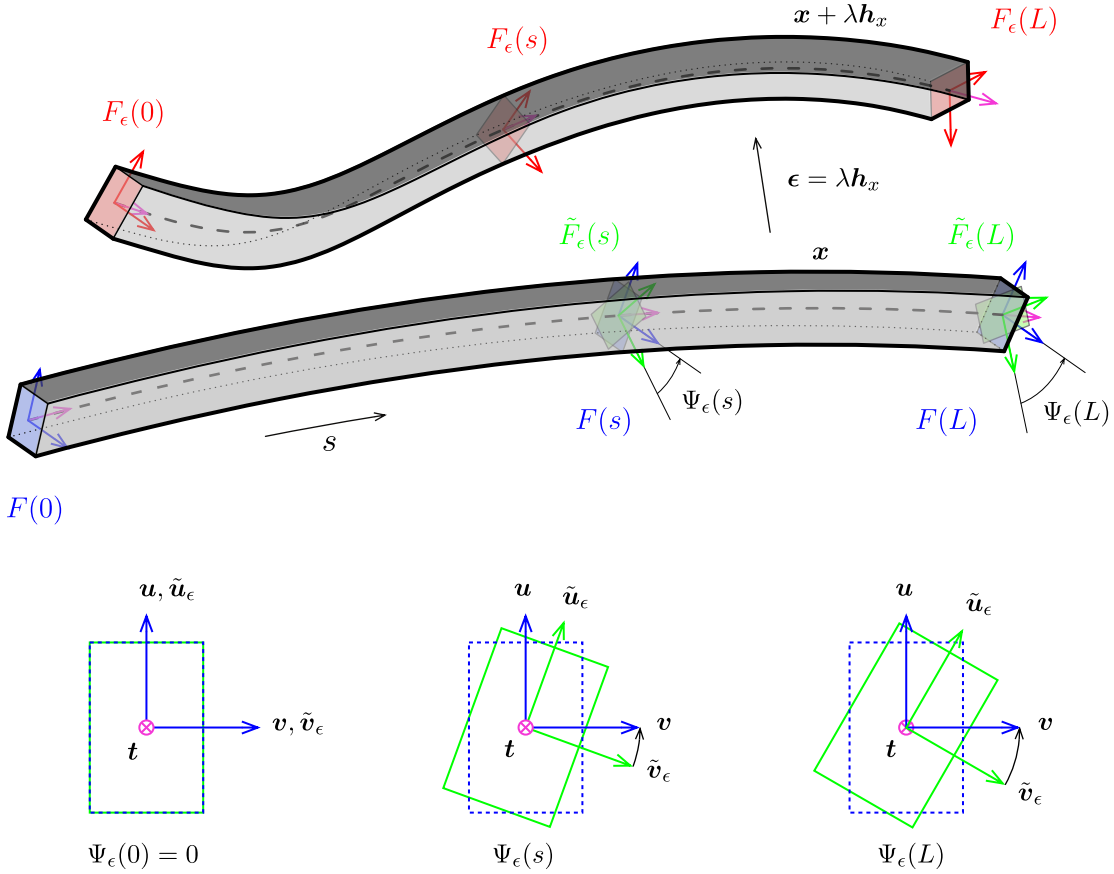


Figure 4.1 – Repères de Frenet attachés à γ .

configuration $\{\mathbf{t}_\epsilon, \mathbf{u}_\epsilon, \mathbf{v}_\epsilon\}$ on the Bishop frame in the reference configuration $\{\mathbf{t}, \mathbf{u}, \mathbf{v}\}$ for a small perturbation ϵ of the centerline. This transformation can be decomposed in two rotations :

- $F_\epsilon \rightarrow \tilde{F}_\epsilon$: parallel transporting F_ϵ from \mathbf{t}_ϵ to \mathbf{t} . This is equivalent to a rotation around $\mathbf{t}_\epsilon \times \mathbf{t}$ by an angle α_ϵ .
- $\tilde{F}_\epsilon \rightarrow F$: aligning \tilde{F}_ϵ over F . This is equivalent to a rotation around \mathbf{t} of an angle Ψ_ϵ .

Firstly, let's decompose $\{\mathbf{t}_\epsilon, \mathbf{u}_\epsilon, \mathbf{v}_\epsilon\}$ on the basis $\{\mathbf{t}, \tilde{\mathbf{u}}_\epsilon, \tilde{\mathbf{v}}_\epsilon\}$. Note that \tilde{F}_ϵ is expressed by rotating \tilde{F}_ϵ by an angle $\Psi_\epsilon[\mathbf{x}](s)$ around \mathbf{t} because \tilde{F}_ϵ is obtained by parallel transporting F_ϵ from \mathbf{t}_ϵ to \mathbf{t} .

Calculation of Ψ_ϵ

This variation is closely related to the writhe of closed curves. As explained in [Ful78] when parallel transporting an adapted frame around a closed curve it might not realigned with

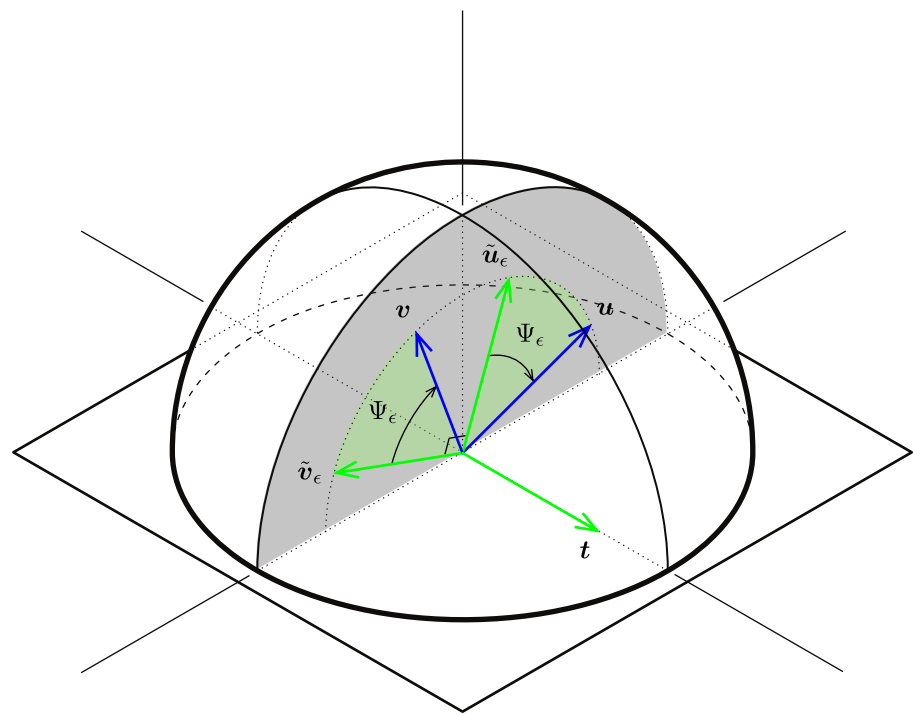


Figure 4.2 – F is obtained by rotating \tilde{F}_ϵ around t of an angle Ψ_ϵ .

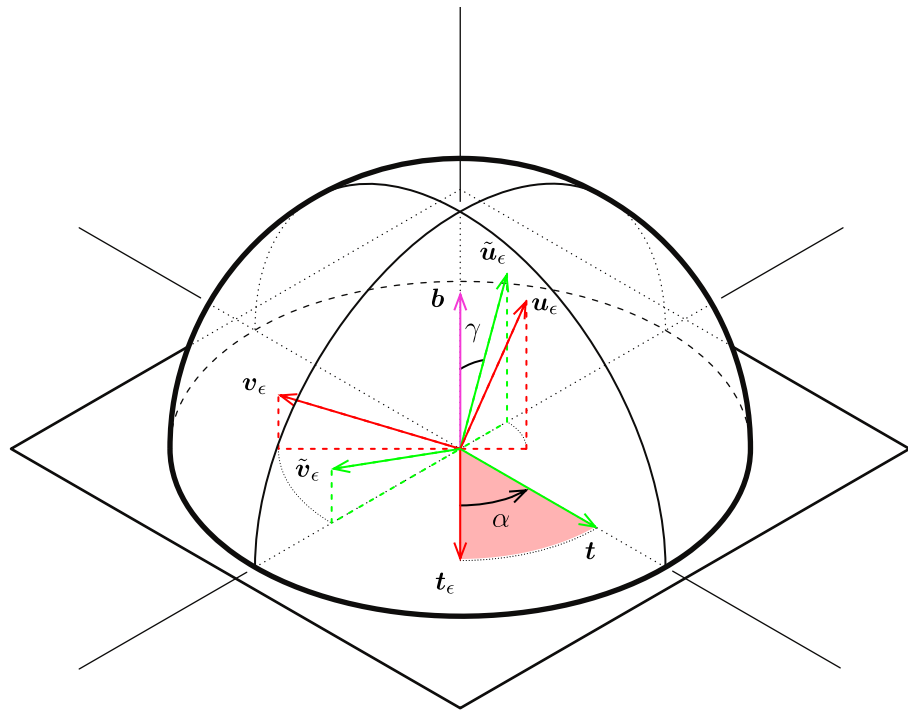


Figure 4.3 – \tilde{F}_ϵ is obtained by parallel transporting F_ϵ from t_ϵ to t . This operation could be seen as a rotation around $t_\epsilon \times t$ of an angle α_ϵ .

itself after one complete loop. This “lack of alignment” is directly measured by the change of writhe which can be computed with Fuller’s Formula [Ful78].

Note that the derivative of θ with respect to \mathbf{x} can be evaluated by the change of writhe in the curve as suggested in [dVri05]. This approach is completely equivalent.

One can also see this lack of alignment in terms of rotation. Parallel transport being a propagation of frame from $s = 0$, the cumulated rotation of Bishop frame from the deformed configuration around the initial configuration at arc-length s is the cumulated angle of rotation of $\mathbf{u}[\mathbf{x} + \lambda \mathbf{h}_x]$ around $\mathbf{d}_3[\mathbf{x}]$. Recalling the rotation rate of $\mathbf{u}[\mathbf{x} + \lambda \mathbf{h}_x]$ is $\kappa \mathbf{b}[\mathbf{x} + \lambda \mathbf{h}_x]$ by definition of zero-twisting frame, one can write :

$$\Psi_\epsilon[\mathbf{x}](s) = - \int_0^s \kappa \mathbf{b}[\mathbf{x} + \lambda \mathbf{h}_x] \cdot \mathbf{d}_3[\mathbf{x}] dt \quad (4.24)$$

The calculation of $\kappa \mathbf{b}[\mathbf{x} + \lambda \mathbf{h}_x]$ is straight forward from the curvature binormal definition :

$$\begin{aligned} \kappa \mathbf{b}[\mathbf{x} + \lambda \mathbf{h}_x] &= (\mathbf{x} + \lambda \mathbf{h}_x)' \times (\mathbf{x} + \lambda \mathbf{h}_x)'' \\ &= \kappa \mathbf{b}[\mathbf{x}] + \lambda(\mathbf{x}' \times \mathbf{h}_x'' + \mathbf{h}_x' \times \mathbf{x}'') + \lambda^2(\mathbf{h}_x' \times \mathbf{h}_x'') \\ &= \kappa \mathbf{b}[\mathbf{x}] + \lambda(\mathbf{x}' \times \mathbf{h}_x'' + \mathbf{h}_x' \times \mathbf{x}'') + o(\lambda) \end{aligned} \quad (4.25)$$

Thus, reminding that $\mathbf{d}_3[\mathbf{x}] = \mathbf{x}'$ and $\kappa \mathbf{b}[\mathbf{x}] \cdot \mathbf{d}_3[\mathbf{x}] = 0$, and using the invariance of circular product by cyclic permutation, one can express :

$$\begin{aligned} \Psi_\epsilon[\mathbf{x}](s) &= - \int_0^s \kappa \mathbf{b}[\mathbf{x} + \lambda \mathbf{h}_x] \cdot \mathbf{d}_3[\mathbf{x}] dt \\ &= -\lambda \int_0^s (\mathbf{x}' \times \mathbf{h}_x'' + \mathbf{h}_x' \times \mathbf{x}'') \cdot \mathbf{x}' dt + o(\lambda) \\ &= -\lambda \int_0^s \kappa \mathbf{b}[\mathbf{x}] \cdot \mathbf{h}_x' dt + o(\lambda) \end{aligned} \quad (4.26)$$

By integration by parts, dropping the implicit reference to \mathbf{x} in the notation, and denoting by δ_s and H_s the Dirac function and the Heaviside step function centered at s , $\Psi_\epsilon(s)$ could be rewritten as :

$$\begin{aligned} \Psi_\epsilon(s) &= -\lambda \int_0^s \kappa \mathbf{b} \cdot \mathbf{h}_x' dt + o(\lambda) \\ &= -\lambda \left(\left[\kappa \mathbf{b} \cdot \mathbf{h}_x \right]_0^s - \int_0^s \kappa \mathbf{b}' \cdot \mathbf{h}_x dt \right) + o(\lambda) \\ &= -\lambda \left(\int_0^s ((\delta_s - \delta_0) \kappa \mathbf{b} - \kappa \mathbf{b}') \cdot \mathbf{h}_x dt \right) + o(\lambda) \\ &= -\lambda \left(\int_0^L ((\delta_s - \delta_0) \kappa \mathbf{b} - (1 - H_s) \kappa \mathbf{b}') \cdot \mathbf{h}_x dt \right) + o(\lambda) \end{aligned} \quad (4.27)$$

Note that, as expected, $\Psi_\epsilon(s)$ is in first order of λ and thus gets negligible when λ tends to zero, that is to say when the perturbation of \mathbf{x} is infinitesimal :

$$\lim_{\lambda \rightarrow 0} \Psi_\epsilon(s) = 0 \quad (4.28)$$

$H_s : t \mapsto \begin{cases} 0, & t < s \\ 1, & t \geq s \end{cases}$ est la fonction de Heaviside.

$\delta_s : t \mapsto \delta(t - s)$ est la distribution de dirac centrée en s .

Calculation of α_ϵ

Recall that \tilde{F}_ϵ is obtained by parallel transporting F_ϵ from \mathbf{t}_ϵ to \mathbf{t} . \tilde{F}_ϵ results from the rotation of F_ϵ around $\mathbf{b} = \mathbf{t}_\epsilon \times \mathbf{t}$ by an angle α_ϵ .

Recall from (4.6) that because the rod is supposed to be unstretchable, \mathbf{t}_ϵ stays collinear to \mathbf{t} for an infinitesimal perturbation of the centerline :

$$\|\mathbf{t}\| = \|\mathbf{t}_\epsilon\| = 1 \Rightarrow (\mathbf{x} + \boldsymbol{\epsilon})' \cdot (\mathbf{x} + \boldsymbol{\epsilon})' = 1 \Leftrightarrow \mathbf{x}' \cdot \boldsymbol{\epsilon}' = -\frac{\lambda^2}{2} \|\mathbf{h}'_x\|^2 \quad (4.29)$$

Which leads to :

$$\cos \alpha_\epsilon(s) = \mathbf{t} \cdot \mathbf{t}_\epsilon = \mathbf{x}' \cdot (\mathbf{x} + \boldsymbol{\epsilon})' = 1 + \mathbf{x}' \cdot \boldsymbol{\epsilon}' = 1 - \frac{\lambda^2}{2} \|\mathbf{h}'_x\|^2 \quad (4.30)$$

Thus, at second order in λ :

$$\cos \alpha_\epsilon = 1 - \frac{\lambda^2}{2} \|\mathbf{h}'_x\|^2 \quad (4.31a)$$

$$\sin \alpha_\epsilon = \sqrt{1 - \cos^2 \alpha_\epsilon} = \lambda \|\mathbf{h}'_x\| + o(\lambda^2) \quad (4.31b)$$

$$\sin^2 \alpha_\epsilon / 2 = \frac{\lambda^2}{4} \|\mathbf{h}'_x\|^2 \quad (4.31c)$$

Finally, it's possible to conclude that $\alpha_\epsilon(s)$ is in first order of λ and thus gets negligible when λ tends to zero :

$$\lim_{\lambda \rightarrow 0} \alpha_\epsilon(s) = 0 \quad (4.32)$$

Aligning \tilde{F}_ϵ towards F_ϵ

Recall that aligning \tilde{F}_ϵ over F is nothing but a rotation around \mathbf{t} by an angle Ψ_ϵ . This leads to :

$$\tilde{\mathbf{u}}_\epsilon = \cos \Psi_\epsilon \mathbf{u} + \sin \Psi_\epsilon \mathbf{v} \quad (4.33a)$$

$$\tilde{\mathbf{v}}_\epsilon = -\sin \Psi_\epsilon \mathbf{u} + \cos \Psi_\epsilon \mathbf{v} \quad (4.33b)$$

Aligning F_ϵ towards \mathbf{t}

Recall that \tilde{F}_ϵ is obtained by parallel transporting F_ϵ from \mathbf{t}_ϵ to \mathbf{t} . This operation could be seen as a rotation around $\mathbf{t}_\epsilon \times \mathbf{t}$ of an angle α_ϵ . Where :

$$\mathbf{b} = \mathbf{t}_\epsilon \times \mathbf{t} = \cos \gamma \tilde{\mathbf{u}}_\epsilon + \sin \gamma \tilde{\mathbf{v}}_\epsilon = \cos \gamma \mathbf{u}_\epsilon + \sin \gamma \mathbf{v}_\epsilon \quad (4.34)$$

Expressing F_ϵ on the basis \tilde{F}_ϵ gives for \mathbf{u}_ϵ and \mathbf{v}_ϵ :

$$\mathbf{u}_\epsilon = \sin \gamma \mathbf{b} + \cos \gamma \left(\sin \alpha_\epsilon \tilde{\mathbf{t}} + \cos \alpha_\epsilon (\cos \gamma \tilde{\mathbf{u}}_\epsilon - \sin \gamma \tilde{\mathbf{v}}_\epsilon) \right) \quad (4.35a)$$

$$\mathbf{v}_\epsilon = \cos \gamma \mathbf{b} + \sin \gamma \left(-\sin \alpha_\epsilon \tilde{\mathbf{t}} + \cos \alpha_\epsilon (\sin \gamma \tilde{\mathbf{u}}_\epsilon - \cos \gamma \tilde{\mathbf{v}}_\epsilon) \right) \quad (4.35b)$$

Which can be rearranged in :

$$\mathbf{u}_\epsilon = \cos \gamma \sin \alpha_\epsilon \mathbf{t} + (\cos \alpha_\epsilon \cos^2 \gamma + \cos^2 \gamma) \tilde{\mathbf{u}}_\epsilon + \sin \gamma \cos \gamma (1 - \cos \alpha_\epsilon) \tilde{\mathbf{v}}_\epsilon \quad (4.36a)$$

$$\mathbf{v}_\epsilon = -\sin \gamma \sin \alpha_\epsilon \mathbf{t} + \cos \gamma \sin \gamma (1 - \cos \alpha_\epsilon) \tilde{\mathbf{u}}_\epsilon + (\cos^2 \gamma + \cos \alpha_\epsilon \sin^2 \gamma) \tilde{\mathbf{v}}_\epsilon \quad (4.36b)$$

Variation of Bishop frame with respect to x

Finally, one can express F_ϵ on the basis F as the composition of two rotations :

$$\mathbf{u}_\epsilon = \begin{bmatrix} 1 & 0 & 0 \\ 0 & \cos \Psi_\epsilon & -\sin \Psi_\epsilon \\ 0 & \sin \Psi_\epsilon & \cos \Psi_\epsilon \end{bmatrix} \begin{bmatrix} \cos \gamma \sin \alpha_\epsilon \\ 1 - 2 \cos^2 \gamma \sin^2 \alpha_\epsilon / 2 \\ 2 \sin \gamma \cos \gamma \sin^2 \alpha_\epsilon / 2 \end{bmatrix} = \begin{bmatrix} \alpha_\epsilon \cos \gamma \\ 1 \\ \Psi_\epsilon \end{bmatrix} + o(\lambda) \quad (4.37a)$$

$$\mathbf{v}_\epsilon = \begin{bmatrix} 1 & 0 & 0 \\ 0 & \cos \Psi_\epsilon & -\sin \Psi_\epsilon \\ 0 & \sin \Psi_\epsilon & \cos \Psi_\epsilon \end{bmatrix} \begin{bmatrix} -\sin \gamma \sin \alpha_\epsilon \\ 2 \sin \gamma \cos \gamma \sin^2 \alpha_\epsilon / 2 \\ 1 - 2 \sin \gamma^2 \sin^2 \alpha_\epsilon / 2 \end{bmatrix} = \begin{bmatrix} -\alpha_\epsilon \sin \gamma \\ -\Psi_\epsilon \\ 1 \end{bmatrix} + o(\lambda) \quad (4.37b)$$

Here, the expressions have been developed in first order of λ as far as α_ϵ and Ψ_ϵ it's been proofed in eq [] that those quantities tends two zero when the perturbation of the centerline is infinitesimal.

Finally, one can express the variation of material directors with respect to an infinitesimal variation of rod's centerline :

$$\mathbf{u}_\epsilon = \alpha_\epsilon \cos \gamma \mathbf{t} + \mathbf{u} + \Psi_\epsilon \mathbf{v} + o(\lambda) \quad (4.38a)$$

$$\mathbf{v}_\epsilon = -\alpha_\epsilon \sin \gamma \mathbf{t} + \mathbf{v} - \Psi_\epsilon \mathbf{u} + o(\lambda) \quad (4.38b)$$

Variation of material frame with respect to x

Recalling the expression of the material frame expressed in the reference Bishop frame, it's now easy to deduce the variation of material frame with respect to a variation of the rod's centerline :

$$\mathbf{d}_1[\mathbf{x} + \lambda \mathbf{h}_x] = \cos \theta \mathbf{u}_\epsilon + \sin \theta \mathbf{v}_\epsilon \quad (4.39a)$$

$$\mathbf{d}_2[\mathbf{x} + \lambda \mathbf{h}_x] = -\sin \theta \mathbf{u}_\epsilon + \cos \theta \mathbf{v}_\epsilon \quad (4.39b)$$

Which leads according to the previous equation to :

$$\mathbf{d}_1[\mathbf{x} + \lambda \mathbf{h}_x] = \mathbf{d}_1[\mathbf{x}] + \Psi_\epsilon \mathbf{d}_2[\mathbf{x}] + \alpha_\epsilon \cos(\theta - \gamma) \mathbf{t}[\mathbf{x}] + o(\lambda) \quad (4.40a)$$

$$\mathbf{d}_2[\mathbf{x} + \lambda \mathbf{h}_x] = \mathbf{d}_2[\mathbf{x}] - \Psi_\epsilon \mathbf{d}_1[\mathbf{x}] - \alpha_\epsilon \sin(\theta + \gamma) \mathbf{t}[\mathbf{x}] + o(\lambda) \quad (4.40b)$$

4.8.2 Derivative of the material curvatures vector with respect to x

It's know straightforward from the previous section to express the variation of the material curvatures with respect to a variation $\epsilon = \lambda \mathbf{h}_x$ of \mathbf{x} while θ remains unchanged.

$$(\mathbf{x} + \lambda \mathbf{h}_x)'' \cdot \mathbf{d}_1[\mathbf{x} + \lambda \mathbf{h}_x] = (\mathbf{x}'' + \lambda \mathbf{h}_x'') \cdot (\mathbf{d}_1 + \Psi_\epsilon \mathbf{d}_2 + \alpha_\epsilon \cos(\theta - \gamma) \mathbf{t} + o(\lambda)) \quad (4.41a)$$

$$(\mathbf{x} + \lambda \mathbf{h}_x)'' \cdot \mathbf{d}_2[\mathbf{x} + \lambda \mathbf{h}_x] = (\mathbf{x}'' + \lambda \mathbf{h}_x'') \cdot (\mathbf{d}_2 - \Psi_\epsilon \mathbf{d}_1 - \alpha_\epsilon \sin(\theta + \gamma) \mathbf{t} + o(\lambda)) \quad (4.41b)$$

Thus, recalling that $\mathbf{x}'' \cdot \mathbf{d}_3 = 0$ and that α_ϵ and Ψ_ϵ are first order quantities in λ :

$$(\mathbf{x} + \lambda \mathbf{h}_x)'' \cdot \mathbf{d}_1[\mathbf{x} + \lambda \mathbf{h}_x] = \mathbf{x}'' \cdot \mathbf{d}_1 + \Psi_\epsilon \mathbf{x}'' \cdot \mathbf{d}_2 + \lambda \mathbf{h}_x'' \cdot \mathbf{d}_1 + o(\lambda) \quad (4.42a)$$

$$(\mathbf{x} + \lambda \mathbf{h}_x)'' \cdot \mathbf{d}_2[\mathbf{x} + \lambda \mathbf{h}_x] = \mathbf{x}'' \cdot \mathbf{d}_2 - \Psi_\epsilon \mathbf{x}'' \cdot \mathbf{d}_1 + \lambda \mathbf{h}_x'' \cdot \mathbf{d}_2 + o(\lambda) \quad (4.42b)$$

Which finally leads to :

$$\boldsymbol{\omega}[\mathbf{x} + \lambda \mathbf{h}_x] = \boldsymbol{\omega}[\mathbf{x}] - \Psi_\epsilon \mathbf{J} \boldsymbol{\omega}[\mathbf{x}] + \lambda \begin{bmatrix} -\mathbf{h}_x'' \cdot \mathbf{d}_2 \\ \mathbf{h}_x'' \cdot \mathbf{d}_1 \end{bmatrix} + o(\lambda) \quad (4.43)$$

Reminding the expression of Ψ_ϵ computed in paragraph[], one can express the derivative of the material curvatures vector with respect to \mathbf{x} :

$$\mathbf{D}_x \boldsymbol{\omega}(s) \cdot \mathbf{h}_x = \left(\int_0^L ((\delta_s - \delta_0) \kappa \mathbf{b} - (1 - H_s) \kappa \mathbf{b}') \cdot \mathbf{h}_x dt \right) \mathbf{J} \boldsymbol{\omega} + \begin{bmatrix} -\mathbf{d}_2^T \\ \mathbf{d}_1^T \end{bmatrix} \cdot \mathbf{h}_x'' \quad (4.44)$$

4.8.3 Computation of the forces acting on the centerline

The forces acting on the centerline are given by the functional derivative of the potential elastic energy with respect to x which can be decomposed according to the chaine rule :

$$\begin{aligned} \langle -f(s), \mathbf{h}_x \rangle &= \mathbf{D}_x \mathcal{E}_p(s) \cdot \mathbf{h}_x = \mathbf{D}_x \mathcal{E}_b(s) \cdot \mathbf{h}_x + \mathbf{D}_x \mathcal{E}_t(s) \cdot \mathbf{h}_x \\ &= \mathbf{D}_x \mathcal{E}_b[\boldsymbol{\omega}[\mathbf{x}]](s) \cdot \mathbf{h}_x + \mathbf{D}_x \mathcal{E}_t[\mathbf{x}](s) \cdot \mathbf{h}_x \end{aligned} \quad (4.45)$$

Derivative of the torsion energy with respect to x

Recall that the torsion energy only depends on θ which is independent of x . Thus, \mathcal{E}_t is independent of x :

$$\mathbf{D}_x \mathcal{E}_t[\mathbf{x}](s) \cdot \mathbf{h}_x = \frac{d}{d\lambda} \mathcal{E}_t[\mathbf{x} + \lambda \mathbf{h}_x] \Big|_{\lambda=0} = 0 \quad (4.46)$$

Derivative of the bending energy with respect to x

The derivative of \mathcal{E}_b is obtained with the chain rule :

$$\mathbf{D}_{\omega}\mathcal{E}_b[\boldsymbol{\omega}](s) \cdot \mathbf{h}_{\omega} = \frac{d}{d\lambda} \mathcal{E}_b[\boldsymbol{\omega} + \lambda \mathbf{h}_{\omega}] \Big|_{\lambda=0} = \int_0^L (\boldsymbol{\omega} - \bar{\boldsymbol{\omega}})^T \mathbf{B} \cdot \mathbf{h}_{\omega} dt \quad (4.47)$$

Finally, reminding eq 4.14 :

$$\mathbf{D}_x \mathcal{E}_b[\boldsymbol{\omega}[x]](s) \cdot \mathbf{h}_x = \mathbf{D}_{\omega} \mathcal{E}_b[\boldsymbol{\omega}](s) \cdot (\mathbf{D}_x \boldsymbol{\omega}[x](s) \cdot \mathbf{h}_x) = \mathcal{A} + \mathcal{B} + \mathcal{C} \quad (4.48)$$

Where :

$$\mathcal{A} = \int_0^L (\boldsymbol{\omega} - \bar{\boldsymbol{\omega}})^T \mathbf{B} \begin{bmatrix} -\mathbf{d}_2^T \\ \mathbf{d}_1^T \end{bmatrix} \cdot \mathbf{h}_x'' dt \quad (4.49a)$$

$$\mathcal{B} = \int_{t=0}^L (\boldsymbol{\omega} - \bar{\boldsymbol{\omega}})^T \mathbf{B} \mathbf{J} \boldsymbol{\omega} \left(\int_{u=0}^L (\delta_t - \delta_0) \kappa \mathbf{b} \cdot \mathbf{h}_x du \right) dt \quad (4.49b)$$

$$\mathcal{C} = \int_{t=0}^L -(\boldsymbol{\omega} - \bar{\boldsymbol{\omega}})^T \mathbf{B} \mathbf{J} \boldsymbol{\omega} \left(\int_{u=0}^L (1 - H_t) \kappa \mathbf{b}' \cdot \mathbf{h}_x du \right) dt \quad (4.49c)$$

Calculus of \mathcal{A} :

$$\mathcal{A} = \int_0^L (\boldsymbol{\omega} - \bar{\boldsymbol{\omega}})^T \mathbf{B} \begin{bmatrix} -\mathbf{d}_2^T \\ \mathbf{d}_1^T \end{bmatrix} \cdot \mathbf{h}_x'' dt \quad (4.50)$$

Recalling the bending moment is given by :

$$\mathbf{M} = (\kappa_1 - \bar{\kappa}_1) EI_1 \mathbf{d}_1 + (\kappa_2 - \bar{\kappa}_2) EI_2 \mathbf{d}_2 = M_1 \mathbf{d}_1 + M_2 \mathbf{d}_2 \quad (4.51)$$

One can remark that :

$$(\boldsymbol{\omega} - \bar{\boldsymbol{\omega}})^T \mathbf{B} \begin{bmatrix} -\mathbf{d}_2^T \\ \mathbf{d}_1^T \end{bmatrix} = M_2 \mathbf{d}_1^T - M_1 \mathbf{d}_2^T = -(\mathbf{d}_3 \times \mathbf{M})^T \quad (4.52)$$

Rq : on mixe abusivement 2 formes d'écritures, matricielle et vectorielle, à cause du produit scalaire que l'on écrit tantôt sous sa forme vectorielle et parfois matricielle (à l'aide de la transposée).

Thus, \mathcal{A} could be rewritten in it's vectoriel form :

$$\begin{aligned} \mathcal{A} &= - \int_0^L (\mathbf{d}_3 \times \mathbf{M}) \cdot \mathbf{h}_x'' dt \\ &= - [(\mathbf{d}_3 \times \mathbf{M}) \cdot \mathbf{h}_x']_0^L + \int_0^L (\mathbf{d}_3 \times \mathbf{M}') \cdot \mathbf{h}_x' dt \\ &= - [(\mathbf{d}_3 \times \mathbf{M}) \cdot \mathbf{h}_x']_0^L + \int_0^L ((\mathbf{d}_3 \times \mathbf{M}') \cdot \mathbf{h}_x' + (\mathbf{h}_x' \times \mathbf{d}_3') \cdot \mathbf{M}) dt \end{aligned} \quad (4.53)$$

Recall that from (4.6) that $\mathbf{h}_x' \cdot \mathbf{d}_3 = 0$ and from (4.1) that $\mathbf{d}_3' \cdot \mathbf{d}_3 = 0$. Hence, $\mathbf{h}_x' \times \mathbf{d}_3'$ is

4.8. Energy gradient with respect to x : internal forces

colinear to \mathbf{d}_3 . Or by definition \mathbf{M} is orthogonal to \mathbf{d}_3 . Thus, $(\mathbf{h}'_x \times \mathbf{d}'_3) \cdot \mathbf{M} = 0$. Finally, after a second integration by parts :

$$\begin{aligned}\mathcal{A} &= -[(\mathbf{d}_3 \times \mathbf{M}) \cdot \mathbf{h}'_x]_0^L + \int_0^L (\mathbf{d}_3 \times \mathbf{M}') \cdot \mathbf{h}'_x dt \\ &= [(\mathbf{d}_3 \times \mathbf{M}') \cdot \mathbf{h}''_x - (\mathbf{d}_3 \times \mathbf{M}) \cdot \mathbf{h}'_x]_0^L - \int_0^L (\mathbf{d}_3 \times \mathbf{M}')' \cdot \mathbf{h}_x dt\end{aligned}\tag{4.54}$$

Calculus of \mathcal{B} :

$$\begin{aligned}\mathcal{B} &= \int_{t=0}^L (\boldsymbol{\omega} - \bar{\boldsymbol{\omega}})^T \mathbf{B} \mathbf{J} \boldsymbol{\omega} \left(\int_{u=0}^L (\delta_t - \delta_0) \kappa \mathbf{b} \cdot \mathbf{h}_x du \right) dt \\ &= -(\kappa \mathbf{b} \cdot \mathbf{h}_x)(0) \int_{t=0}^L (\boldsymbol{\omega} - \bar{\boldsymbol{\omega}})^T \mathbf{B} \mathbf{J} \boldsymbol{\omega} dt + \int_{t=0}^L (\boldsymbol{\omega} - \bar{\boldsymbol{\omega}})^T \mathbf{B} \mathbf{J} \boldsymbol{\omega} \kappa \mathbf{b} \cdot \mathbf{h}_x dt\end{aligned}\tag{4.55}$$

Calculus of \mathcal{C} :

$$\begin{aligned}\mathcal{C} &= \int_{t=0}^L -(\boldsymbol{\omega} - \bar{\boldsymbol{\omega}})^T \mathbf{B} \mathbf{J} \boldsymbol{\omega} \left(\int_{u=0}^L (1 - H_t) \kappa \mathbf{b}' \cdot \mathbf{h}_x du \right) dt \\ &= \int_{u=0}^L \int_{t=u}^L -((\boldsymbol{\omega} - \bar{\boldsymbol{\omega}})^T \mathbf{B} \mathbf{J} \boldsymbol{\omega})(t) (\kappa \mathbf{b}' \cdot \mathbf{h}_x)(u) dt du \\ &= \int_{u=0}^L -\left(\int_{t=u}^L (\boldsymbol{\omega} - \bar{\boldsymbol{\omega}})^T \mathbf{B} \mathbf{J} \boldsymbol{\omega} dt \right) (\kappa \mathbf{b}' \cdot \mathbf{h}_x) du\end{aligned}\tag{4.56}$$

By several integration by parts, using Fubini's theorem once and supposing that the terms vanishes at $s = 0$ and $s = L$:

$$\begin{aligned}\mathcal{B} + \mathcal{C} &= \int_{t=0}^L \left((\boldsymbol{\omega} - \bar{\boldsymbol{\omega}})^T \mathbf{B} \mathbf{J} \boldsymbol{\omega} \kappa \mathbf{b} - \left(\int_{u=t}^L (\boldsymbol{\omega} - \bar{\boldsymbol{\omega}})^T \mathbf{B} \mathbf{J} \boldsymbol{\omega} du \right) \kappa \mathbf{b}' \right) \cdot \mathbf{h}_x dt \\ &= \int_{t=0}^L \left(-\left(\int_{u=t}^L (\boldsymbol{\omega} - \bar{\boldsymbol{\omega}})^T \mathbf{B} \mathbf{J} \boldsymbol{\omega} du \right)' \kappa \mathbf{b} - \left(\int_{u=t}^L (\boldsymbol{\omega} - \bar{\boldsymbol{\omega}})^T \mathbf{B} \mathbf{J} \boldsymbol{\omega} du \right) \kappa \mathbf{b}' \right) \cdot \mathbf{h}_x dt \\ &= \int_{t=0}^L \left(-\left(\int_{u=t}^L (\boldsymbol{\omega} - \bar{\boldsymbol{\omega}})^T \mathbf{B} \mathbf{J} \boldsymbol{\omega} du \right) \kappa \mathbf{b} \right)' \cdot \mathbf{h}_x dt\end{aligned}\tag{4.57}$$

Which can be rewritted using the quasi-static hypothesis :

$$\begin{aligned}\mathcal{B} + \mathcal{C} &= \int_{t=0}^L \left(-\left(\int_{u=t}^L (\boldsymbol{\omega} - \bar{\boldsymbol{\omega}})^T \mathbf{B} \mathbf{J} \boldsymbol{\omega} du \right) \kappa \mathbf{b} \right)' \cdot \mathbf{h}_x dt \\ &= \int_{t=0}^L \left(-\left(\int_{u=t}^L \beta(\theta' - \bar{\theta}')(\delta_L - \delta_0) - (\beta(\theta' - \bar{\theta}'))' du \right) \kappa \mathbf{b} \right)' \cdot \mathbf{h}_x dt \\ &= \int_{t=0}^L \left(-\left(\beta(\theta' - \bar{\theta}')(L) - [\beta(\theta' - \bar{\theta}')]_t^L \right) \kappa \mathbf{b} \right)' \cdot \mathbf{h}_x dt \\ &= \int_{t=0}^L -(\beta(\theta' - \bar{\theta}') \kappa \mathbf{b})' \cdot \mathbf{h}_x dt\end{aligned}\tag{4.58}$$

Finally :

$$\mathbf{D}_x \mathcal{E}_b[\boldsymbol{\omega}[\mathbf{x}]](s) \cdot \mathbf{h}_x = \int_0^L \left(-(\mathbf{d}_3 \times \mathbf{M}')' - (\beta(\theta' - \bar{\theta}')\kappa\mathbf{b})' \right) \cdot \mathbf{h}_x dt \quad (4.59)$$

Internal forces

Thus, the internal forces are related to the variation of internal elastic energy as :

$$\langle -\mathbf{f}(s), \mathbf{h}_x \rangle = \mathbf{D}_x \mathcal{E}_p(s) \cdot \mathbf{h}_x = - \int_0^L \left((\mathbf{d}_3 \times \mathbf{M}')' + (\beta(\theta' - \bar{\theta}')\kappa\mathbf{b})' \right) \cdot \mathbf{h}_x dt \quad (4.60)$$

Finally, we can conclude on the expression of the internal forces :

$$\mathbf{f}(s) = (\mathbf{d}_3 \times \mathbf{M}')' + (\beta(\theta' - \bar{\theta}')\kappa\mathbf{b})' \quad (4.61)$$

Remarquer ici que l'expression est purement locale. Elle ne dépend pas du sens de parcours de la poutre, contrairement au raisonnement suivi. Cette différence est notable avec la démarche de B. Audoly. Faire le bilan des bénéfices de l'hypothèse quasi-statique : - expressions rigoureusement vraies à l'équilibre statique - simplification ds le calcul des efforts - rapidité dans le calcul avec des expressions plus simples - il n'est pas forcément intéressant en terme d'algorithmie d'imposer l'hypothèse quasistatique au cours du calcul. Il faudrait faire un bench pour savoir.

On retombe sur les équations de Kirchhoff à un terme manquant pret. Qui exprime la contribution de la variation moment de flexion à cause de la torsion $\tau\mathbf{M}'$. Peut-être que ce terme est finalement d'un ordre supérieur, si l'on suppose une variation lente de la torsion ? Comment comprendre la disparition de ce terme qui semble nécessaire à l'équilibre statique d'un élément de poutre si l'on en croit les équations de Kirchhoff ?

4.9 Conclusion

On retrouve les équations de kirchhoff dynamique où l'on a négligé les forces inertielles de rotation d'un élément de poutre autour de \mathbf{d}_1 et \mathbf{d}_2 pour ne garder que la dynamique de rotation de la section autour de la fibre neutre \mathbf{d}_3 .

The shear force acting on the right side of a section is nothing but $\mathbf{T} = \int \mathbf{f}$:

$$\mathbf{T}(s) = \mathbf{d}_3 \times \mathbf{M}' + Q\kappa\mathbf{b} \quad (4.62)$$

The linear momentum acting on the centerline is given by :

$$m(s) = Q' - \kappa\mathbf{b} \cdot (\mathbf{d}_3 \times \mathbf{M}) \quad (4.63)$$

The main hypothesis are :

- Bernoulli : $\mathbf{d}_i \cdot \mathbf{d}_j = \delta_{ij}$
- Inextensibility : $\|\mathbf{d}'_3\| = 1$
- Quasistatic : at each timestep regarding bending motion $m(s) = 0$

4.10 References

- [AAP10] B. Audoly, M. Amar, and Y. Pomeau. *Elasticity and geometry*. 2010, p. 600.
- [ABW99] S. Adriaenssens, M. Barnes, and C. Williams. “A new analytic and numerical basis for the form-finding and analysis of spline and gridshell structures”. In: *Computing Developments in Civil and Structural Engineering*. Ed. by B. Kumar and B. H. V. Topping. Edinburgh: Civil-Comp Press, 1999, pp. 83–91.
- [Ber+08] M. Bergou, M. Wardetzky, S. Robinson, B. Audoly, and E. Grinspun. “Discrete elastic rods”. In: *ACM SIGGRAPH* (2008), pp. 1–12.
- [Ber+10] M. Bergou, B. Audoly, E. Vouga, M. Wardetzky, and E. Grinspun. “Discrete viscous threads”. In: *ACM Transactions on ...* (2010), pp. 1–10.
- [Ber09] M. Berger. “Topological Quantities: Calculating Winding, Writhing, Linking, and Higher order Invariants”. In: *Lecture Notes in Mathematics* 1973 (2009), pp. 75–97.
- [Bis75] R. Bishop. “There is more than one way to frame a curve”. In: *Mathematical Association of America* (1975).
- [dVri05] R. de Vries. “Evaluating changes of writhe in computer simulations of supercoiled DNA”. In: *The Journal of Chemical Physics* 122.6 (2005).
- [Ful78] F. B. Fuller. “Decomposition of the linking number of a closed ribbon : A problem from molecular biology”. In: 75.8 (1978), pp. 3557–3561.
- [Jun+10] P. Jung, S. Leyendecker, J. Linn, and M. Ortiz. “A discrete mechanics approach to the Cosserat rod theory—Part 1: static equilibria”. eng. In: *International journal for numerical methods in engineering* 85.1 (2010), pp. 31–60.
- [Lew03] W. Lewis. *Tension structures: form and behaviour*. Telford, Thomas, 2003, p. 201.
- [Nab14] S. Nabaei. “Mechanical form-finding of timber fabric structures”. PhD thesis. EPFL, 2014.
- [ST07] J. Spillmann and M. Teschner. “CORDE : Cosserat Rod Elements for the Dynamic Simulation of One-Dimensional Elastic Objects”. In: *Eurographics/ACM SIGGRAPH Symposium on Computer Animation* (2007), pp. 1–10.
- [Vau00] R. Vauquelin. “Writhing Geometry at Finite Temperature : Random Walks and Geometric phases for Stiff Polymers”. In: 1 (2000).

5 Elastic rod : equilibrium approach

5.1 Introduction

Ici on explique que l'approche par les équations d'équilibre est beaucoup plus directe que l'approche énergétique.

5.1.1 Goals and contribution

Dans ce chapitre, après un bref rappel sur le cadre mathématique d'étude des courbes paramétrique de l'espace, on présente les notions de courbures et de torsion géométrique associées au repère de Frenet. On montre ensuite le cas plus général d'un repère mobile quelconque attaché à une courbe gamma. On définit enfin la particularité d'un repère mobile adapté à un courbe, et on présente, en sus du repère de Frenet, une approche différente pour accrocher des repères le long d'une courbe (Bishop / RMF / Zéro-twisting frame)

Ici il faudrait préciser la terminologie des auteurs / équations / hypothèses : Euler-Bernoulli, Navier-Bernoulli, Kirchhoff, Love, Clebsch, Cosserat, Vlassov

5.1.2 Related work

On peu s'instruire dans la publi de Dill [Dil92]. Regarder en particulier le premier chapitre de l'HDR de Neukirch [Neu09]. Regarder également la chronologie des modèles proposée dans la thèse de Theetten [The07]. Pourquoi pas proposer une frise chronologique + un tableau de synthèse des hypothèses.

[Dil92] Neukirch [Neu09] [ABW99] [Hoo06] [LL09] [Spi08] [Ant05]

[Neu09] : p69 - [Dil92] : p16

Dans les tentatives dans notre domaine, citer :

Kirchhoff : [Kir50, Kir76]

Clebsch : [Cle83]

Love : [Lov92]

Timoshenko : [Tim21, Tim22, TG51]

“Note that γ having unit speed corresponds to the rod being inextensible; this is not always assumed in the theory, nor is the material frame necessarily assumed to be orthonormal as it is here” [LS96, p. 607]

“Natural frames and the curve angle representation of rod” [LS96, p. 607]

Départ : [Day65] : already includes a rotational DOF !! [Wak80] [Bar99] : revue intéressante de la DR.

3 pts classique : [ABW99] [DBC06]

2 x 3pts : [BAK13]

6 Dofs : [DKZ14]

4Dofs : [dPel+15] [DZK16]

Dans le champ de l'animation avec élément finis [DLP13] [MPW14]

Pour des cas test : [Ibr95] [Láz+16]

Pour la cinématique, superposition d'un mouvement rigide et d'un warping de la section : [SV91] dans l'extension de [Rei73]

5.1.3 Overview

Résumé du chapitre

1 2 3

“The battle between weight and rigidity constitutes, in itself, the single aesthetic theme of art in architecture : and to bring out this conflict in the most varied and clearest way is its office.” [Ben91b, p. xvii]

The theory of elastic structures is, by definition, the collection of all reasonable models, proposed during almost three centuries, concerned with simplifying

¹For a shearable rod, the condition that d_3 and t coincide is relaxed.

²in the directions of the principal axes of inertia of its cross-section

³The parameter \bar{s} , usually chosen as the arc length parameter for the undeformed rod, is no longer the arc length parameter for the deformed rod, since there are deformations of shear and extension. The current arc length of the deformed rod is a function of \bar{s} , which is often denoted by $s(\bar{s})$.

the solutions of problems involving elastic bodies. The equations describing the motion and equilibrium of a three-dimensional elastic body were formulated in full generality during the first half of the nineteenth century, but their solutions are known only in a few cases. [Vil97, p. xvii]

In a deformed state, the center line has no particular reason to remain straight and, in general, \mathbf{d}_1 and \mathbf{d}_2 will twist along the center line. However, in the case of small strain that we consider, the triad $(\mathbf{d}_1, \mathbf{d}_2, \mathbf{d}_3)$ remains approximately orthonormal, provided it has been chosen orthonormal in the reference configuration. This is known as the Euler-Bernoulli or Navier-Bernoulli kinematical hypothesis, or sometimes the assumption of unshearable rods. [AAP10, p. 68]

Extension to the case of thin-walled sections by [DA15, Vet14] in the case of ribbons. From the Vlasov

For thin beams having a slender cross-section, $h \ll w$, the classical rod theory of Kirchhoff is known to be inapplicable. Such beams are usually modeled using Vlasov's theory for thin-walled beams. Vlasov's models can be justified from 3D elasticity but only in the case of moderate deformations, when the cross-sections bend by a small amount. In the present work, however, we have considered large deformations of thin strips. The strip has been modeled as an inextensible plate, and the geometric constraint of inextensibility has been treated exactly : the cross-sections are allowed to bend by a significant amount. Our model extends the classical strip model of Sadowsky, and reformulate it in a way that fits into the classical theory of rods. [DA14, p.]

5.2 Introduction to the special Cosserat theory of rods

This paragraph gives a very brief overview of the *special Cosserat theory of rods*, as presented in [Ant05], that accounts for bending, torsion, extension and shear behaviors of slender beams.⁴ This theory – which is a *director theory* of rods – was first introduced by [Ant74]. It gives a larger scope to the basements of the present work – which relies on the *Kirchhoff theory of rods* – as the last is a special case of this larger theoretical framework. Thus, what is presented in this paragraph could be considered as a reasonable starting point to extend the present work, for instance to take account for shear or large extension, which might be relevant for some engineering problems or form-finding processes.

It has been largely employed in various fields [SBH95, Ber+10].

5.2.1 Description of the motion

The special Cosserat theory of rods consider dynamics of rods. It relies on a precise geometric description (see fig. 5.1) of rods build upon three vector-valued functions that are time dependent :

- \mathbf{x} , a position vector describing the geometry in space of a specific *fiber* called the rod *axis* or *centerline*. This function describes the rod in its longitudinal dimension. This dimension is of prime importance in the case of slender bodies such as rods as what is intend is to build a reduced theory, namely a 1-dimensional theory. This curve will often be understood as the curve passing through the cross-section centroids along the rod, although this is not mandatory in the theory.
- $\mathbf{d}_1, \mathbf{d}_2$, two unit vector fields describing the lateral spatiality of the rod and called material *directors*. These vectors will often be understood as the principal axis of the cross-section, although this is not mandatory in the theory.

Modeling the geometry of the rod in any configuration is not sufficient to build a mechanical model. Indeed, one must know a *reference* state for the solid as strains measure relative change in geometry and stresses are related to strains through the constitutive relation of the rod material. Thus, the special Cosserat theory of rods consider two configurations :

- The *actual* configuration, that is the configuration of the rod at time t during the motion.
- The *reference* configuration, that is the configuration of the rod in a specific state where its geometry (possibly curved and twisted) is known and its mechanical state (strains, stresses) under possible loads (dead weight, temperature, wind, snow , pre-stress, ...) and possible boundary conditions is known. In practice, this configuration

⁴“[we formulate] a general dynamical theory of rods that can undergo large deformations in space by suffering flexure, torsion, extension, and shear. We call the resulting geometrically exact theory the *special Cosserat theory of rods*.” [Ant05, p. 270]

will often be chosen as a *stress-free* configuration when the beam is not subject to any loads nor restraints of any kind, although this is not mandatory in the theory.

Thus, the equations governing the motion of a *special Cosserat rod* will be based on the description of a fully known reference configuration and the description of the actual or deformed configuration of the rod at time t during its motion (see [fig. 5.1](#)). Usually, what is intended is to predict the motion of a particular rod given its reference configuration, material properties, boundary conditions, and loading. In this thesis, the equations of the motion will be integrated to converge as fast as possible to the quasi-static response of the system, as this work only deals with statics of structures. However, it is still possible to use a more convenient and accurate time integrator to compute the motion, if one wants to study the (true) dynamic of a rod and go beyond the knowledge of its static equilibrium.

Hereafter, when ambiguity is possible, symbols referring to the reference configuration will be marked with an overline while symbols referring to the actual configuration will be marked with a subscript in the variable t . Generally, scalar quantities are marked with the subscript t and vector quantities with an overline in order to avoid double subscripts when one will refer to vector components.

Actual configuration

At time t , the *actual* or *deformed* configuration of the rod $\{\mathbf{x}, \mathbf{d}_1, \mathbf{d}_2\}$ is described by its *centerline* $\gamma_t \in \mathcal{C}^1([0, L] \times \mathbb{R}^3)$, a regular space curve :

$$\begin{aligned} \gamma_t(t, \cdot) : [0, L] &\longrightarrow \mathbb{R}^3 \\ s &\longmapsto \mathbf{x}(t, s) \end{aligned} \tag{5.1}$$

and two perpendicular unit vector fields : ⁵

$$\begin{aligned} (\mathbf{d}_1, \mathbf{d}_2)(t, \cdot) : [0, L] &\longrightarrow \mathbb{R}^3 \times \mathbb{R}^3 \\ s &\longmapsto (\mathbf{d}_1(t, s), \mathbf{d}_2(t, s)) / \mathbf{d}_1(t, s) \cdot \mathbf{d}_2(t, s) = 0 \end{aligned} \tag{5.2}$$

In addition, we define a third unit vector field as :

$$\mathbf{d}_3 = \mathbf{d}_1 \times \mathbf{d}_2 \tag{5.3}$$

Thus, the centerline is framed with the orthonormal moving frame $\{\mathbf{d}_1, \mathbf{d}_2, \mathbf{d}_3\}$. The unit vectors $\mathbf{d}_i(t, s)$ are called *material directors*.

Note that the centerline is parametrized by s chosen to be the arc length parameter of the *reference* configuration. It may not coincide with the arc length parameter of the *actual* configuration denoted by $s_t = \Psi(t, s) = \Psi_t(s)$ as the rod may suffer elongation. L denotes the length of the centerline in the reference configuration. The actual length of γ_t is denoted

⁵Requiring that $\mathbf{d}_1 \perp \mathbf{d}_2$ implies that the description of the motion is convenient only for small in-plane stretching and shearing of the cross-section. This constraint can be relaxed to lead to an even more general theory, called the *2-director Cosserat theory*.

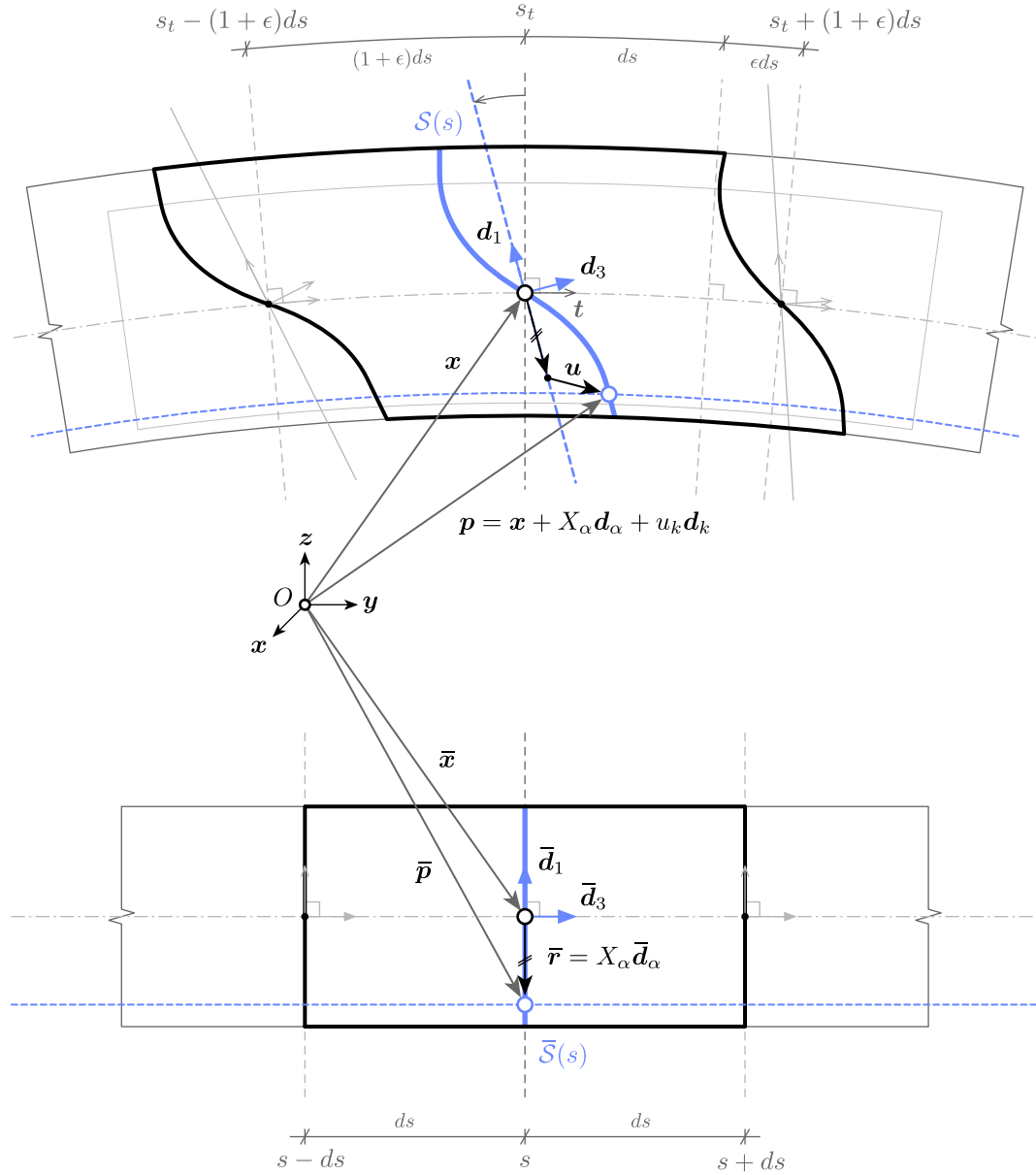


Figure 5.1 – Description of the motion for a Cosserat rod. This is a typical longitudinal section of a rectangular beam deformed from a reference configuration (bottom) to an actual configuration (top) at time t . Cross-sections are defined in the reference configuration to be planar surfaces perpendicular to the beam axis (\bar{S}). A material point $\bar{p} \in \bar{S}(s)$ is located relatively to the cross-section centroid ($\bar{x}(s)$) thanks to its material coordinates (X_1, X_2, s) . During the motion, this material point reaches a new position $p \in S(s)$. The deformed cross-section $S(s)$ is no more planar. The material frame is no more aligned with the beam axis (d_3 and t are not parallel any more). The actual position is measured from the centroid of the deformed cross-section ($x(s)$) plus an in-plane component $(X_\alpha d_\alpha)$ and a deformation vector (u). If the cross-sections deform in a rigid-body manner, then u is null everywhere.

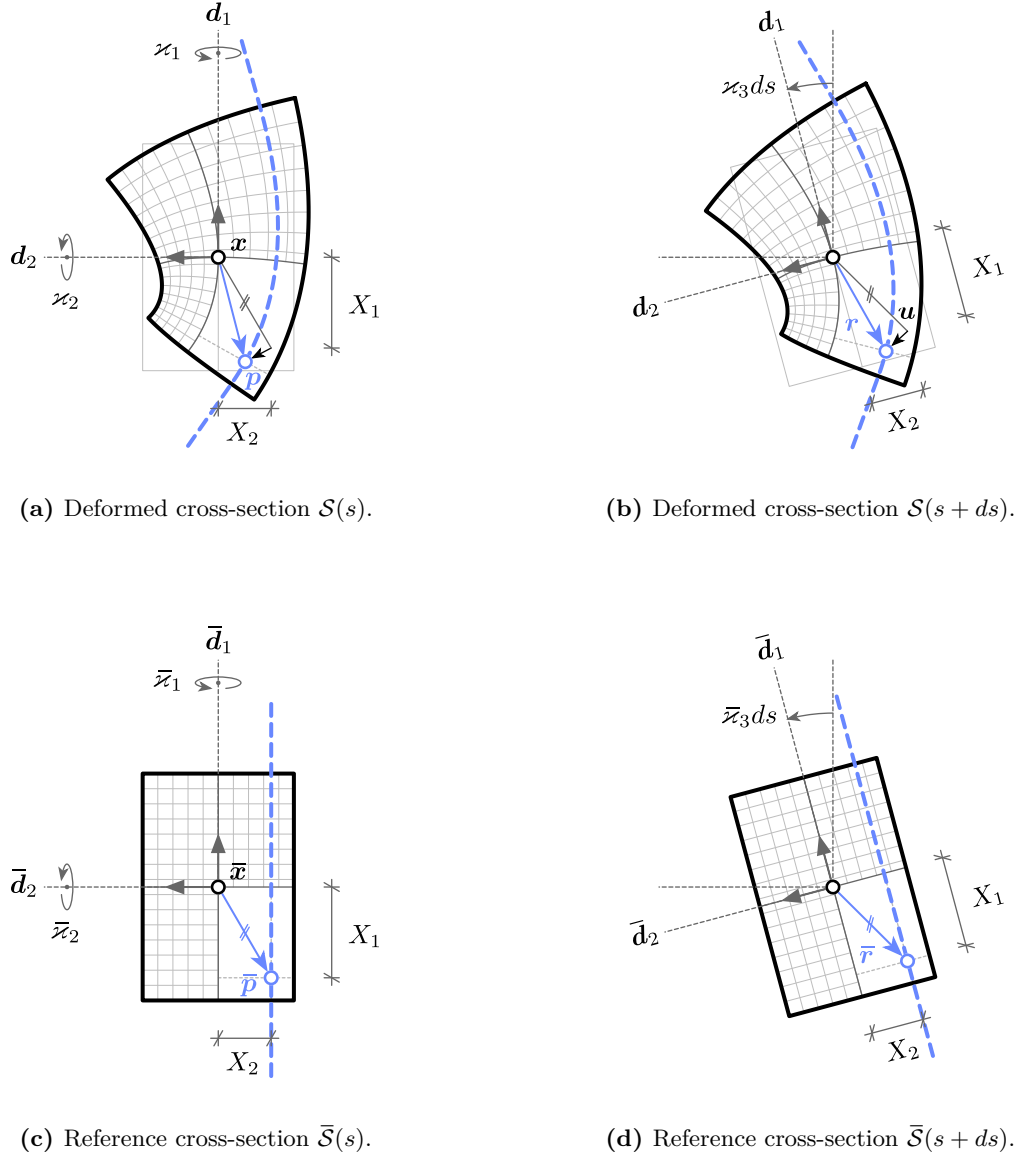


Figure 5.2 – Description of the motion for a Cosserat rod. These are the transverse sections from fig. 5.1 (however note that fig. 5.1 is drawn with $\varkappa_2 < 0$ while $\varkappa_2 > 0$ in fig. 5.2). The section curve is drawn in a dashed blue fashion. Remark how the deformed material point is located through \mathbf{x} and $\mathbf{r} = X_\alpha \mathbf{d}_\alpha + u_k \mathbf{d}_k$. Cross-sections are rotating around \mathbf{d}_3 at speed \varkappa_3 . The beam is subjected to flexion ($\varkappa_1 > 0$, $\varkappa_2 > 0$), torsion ($\varkappa_3 > 0$) and extension ($\epsilon > 0$). Fibers that are compressed – both directly by axial compression or indirectly by flexion – are subjected to transverse expansion due to the Poisson effect (see up-right of figures 5.2a and 5.2b). Reciprocally, fibers in tension – both directly by axial tension or indirectly by flexion – are subjected to transverse contraction (see bottom-left of figures 5.2a and 5.2b).

by L_t so that $s_t \in [0, L_t]$.

Finally, a material point \mathbf{p} of the body is located relatively to the centerline with the help of the local position vector \mathbf{r} such that (see figures 5.2a and 5.2b) :

$$\mathbf{p}(\bar{\mathbf{r}}, t) = \bar{\mathbf{x}}(s, t) + \bar{\mathbf{r}}(\bar{\mathbf{x}}(s, t), \bar{\mathbf{d}}_1(s, t), \bar{\mathbf{d}}_2(s, t), \bar{\mathbf{r}}, t) \quad (5.4)$$

Note that in the above expression a material point is uniquely identified – in a very generic manner – by its local position in the reference configuration ($\bar{\mathbf{r}} = \bar{\mathbf{p}} - \bar{\mathbf{x}}$).

Reference configuration

We now identify a *reference* configuration of the rod $\{\bar{\mathbf{x}}, \bar{\mathbf{d}}_1, \bar{\mathbf{d}}_2\}$ with centerline $\bar{\gamma} \in C^1([0, L] \times \mathbb{R}^3)$, a regular space curve. This time, s is the arc length parameter of $\bar{\gamma}$, which leads to the important relation between $\bar{\mathbf{x}}$ and the unit tangent vector $\bar{\mathbf{t}}$ of $\bar{\gamma}$:

$$\frac{d\bar{\mathbf{x}}}{ds} = \bar{\mathbf{t}} \quad , \quad \|\bar{\mathbf{t}}\| = 1 \quad (5.5)$$

In this configuration, we define a cross-section $\mathcal{S}(s)$ as the set of material points lying in a plane perpendicular to $\bar{\gamma}$ at position $\bar{\mathbf{x}}(s)$. By definition, it is a planar surface in the reference configuration. However, there is no evidence that this surface will remain planar in any other configuration. Moreover, and only for this configuration, it makes sens to choose the centerline as the curve passing through the cross-section centroids.

Finally, we call *material coordinates* of point $\bar{\mathbf{p}} \in \mathcal{S}(s)$ the triple $(X_1, X_2, s = X_3)$ such that (see figures 5.2c and 5.2d) :

$$\bar{\mathbf{p}}(\bar{\mathbf{r}}) = \bar{\mathbf{x}}(s) + \bar{\mathbf{r}}(\bar{\mathbf{x}}(s), \bar{\mathbf{d}}_1(s), \bar{\mathbf{d}}_2(s), X_1, X_2) \quad (5.6a)$$

$$\bar{\mathbf{r}}(X_1, X_2, s) = X_1 \bar{\mathbf{d}}_1(s) + X_2 \bar{\mathbf{d}}_2(s) \quad (5.6b)$$

We also identify a *fiber* as the set of material points that share the same cross-section coordinates (X_1, X_2) all along the rod in the reference configuration.

5.2.2 Time evolution

The evolution in time of the rod is simply given by the velocity of its centerline ($\dot{\mathbf{x}}$) and the angular velocity or *spin vector* ($\boldsymbol{\omega}$) of its material directors :

$$\frac{\partial \mathbf{x}}{\partial t}(s, t) = \dot{\mathbf{x}} \quad (5.7a)$$

$$\frac{\partial \mathbf{d}_k}{\partial t}(s, t) = \dot{\mathbf{d}}_k = \boldsymbol{\omega}(s, t) \times \mathbf{d}_k(s, t) \quad (5.7b)$$

From now on, the derivative with respect to time is denoted with an overdot symbol.

5.2.3 Strains

Strains are described with the help of the strains vectors $\boldsymbol{\eta}$ and $\boldsymbol{\varkappa}$ – respectively the force strains vector and moment strains vector [Rei73] :

$$\frac{\partial \mathbf{x}}{\partial s}(s, t) = \mathbf{x}' = \boldsymbol{\eta}(s, t) \quad (5.8a)$$

$$\frac{\partial \mathbf{d}_k}{\partial s}(s, t) = \mathbf{d}'_k = \boldsymbol{\varkappa}(s, t) \times \mathbf{d}_k(s, t) \quad (5.8b)$$

where the derivative with respect to s is denoted with a prime symbol.⁶ The components of $\boldsymbol{\eta} = \eta_k \mathbf{d}_k$ and $\boldsymbol{\varkappa} = \varkappa_k \mathbf{d}_k$ expressed in the material frame basis $\{\mathbf{d}_1, \mathbf{d}_2, \mathbf{d}_3\}$ can be interpreted as the classical engineering strains that lead to the engineering stresses.^{7,8} In particular $\eta_1 = \mathbf{x}' \cdot (\mathbf{d}_1 \times \mathbf{d}_2)$ characterizes the change in volume of the body while η_2 and η_3 characterize the shear deformations ; \varkappa_3 is the material twist of the rod while \varkappa_1 and \varkappa_2 are the material curvatures of the rod.⁹

Observe the symmetry of eq. (5.7a) and (5.7b) and eq. (5.8a) and (5.8b) regarding the parameters s and t :

- $(\dot{\mathbf{x}}, \boldsymbol{\omega})$ governs the time evolution of the material frame.
- $(\mathbf{x}', \boldsymbol{\varkappa})$ governs the spatial evolution of the material frame along the centerline.

5.2.4 Parametrization of the centerline

Recall that because the centerline of the reference configuration is parametrized by arc length, the unit tangent vector in this configuration is given by :

$$\bar{\mathbf{t}}(s) = \frac{d\bar{\mathbf{x}}}{ds}(\bar{s}) = \bar{\mathbf{x}}'(s) \quad , \quad \|\bar{\mathbf{x}}'\| = 1 \quad (5.9)$$

In the deformed configuration, the centerline is still parametrized by s which is no more an arc length parameter because the centerline has suffered stretch. Thus, the unit tangent vector in this configuration is given by :¹⁰

$$\mathbf{t}(s, t) = \frac{\mathbf{x}'(s, t)}{\|\mathbf{x}'(s, t)\|} \quad , \quad \|\mathbf{x}'\| = \|\boldsymbol{\eta}'\| \neq 1 \quad (5.10)$$

⁶For an extensible rod, the derivative with respect to s and s_t are not equivalent. The prime notation stands only for the derivation with respect to s , the arc length parameter of the rod in the reference configuration.

⁷For a complete interpretation, see [Ant05, p. 285] or [AAP10, ch. 3].

⁸Einstein's notation is employed here. For instance : $\boldsymbol{\eta} = \eta_k \mathbf{d}_k = \eta_1 \mathbf{d}_1 + \eta_2 \mathbf{d}_2 + \eta_3 \mathbf{d}_3$.

⁹Here, the term “material” is necessary as the material curvatures don't coincide with the geometric curvatures, although they are related one to each other. Precisely, the distinction originates in the fact that s is not a unit-speed parametrization of the centerline in the actual configuration.

¹⁰However, because s_t is an arc length parameter of γ_t : $\mathbf{t}(s, t) = \frac{\partial \mathbf{x}}{\partial s_t}(s, t)$.

We introduce ϵ , the extension of the rod which characterizes the local change in length of the rod centerline, defined as :

$$\|\boldsymbol{\eta}'(s, t)\| = \frac{\partial s_t}{\partial s}(s, t) = \Psi'(s, t) = 1 + \epsilon(s, t) \quad (5.11)$$

Inextensibility

The rod is said to be inextensible if $\epsilon = 0$ everywhere and at all time. In this case, s is a valid arc length parameter for the centerline in every configurations. Later, we will restrict to the case of rods subjected to small extension, that is $\epsilon(t, s) \ll 1$.

Reparametrization

Although either s and s_t can be chosen as the third material coordinate to describe a rod, the definition of the material strains are given with respect to s and not s_t . This is a matter of concern as the constitutive relations – classically of the form $M = EI\kappa$, $N = ES\epsilon$, $Q = GJ\tau$ – relies upon material strains. Thus, in these equations, what takes place is a derivation with respect to s and not to s_t , which matters if the rod is not required to be inextensible.

5.2.5 To go further

The reader is invited to refer to [Ant05] to get a deeper understanding of the *Cosserat theory for rods*, in particular to see how the governing equations are derived. Here, only the geometric description of a Cosserat rod has been presented in a very generic but still concise manner. This description will be used in the next sections in the narrower scope of the (first order) *Kirchhoff theory for rods* but could be usefully employed for richer theories.

	reference configuration	actual configuration
arc length	$s = \Psi_t^{-1}(s_t)$	$s_t = \Psi_t(s)$
length	L	L_t
centerline	$\bar{\gamma}$	γ_t
position vector	\bar{x}	x
material frame	$\{\bar{d}_1, \bar{d}_2, \bar{d}_3\}$	$\{d_1, d_2, d_3\}$
material coordinates	(X_1, X_2, s)	(X_1, X_2, s)
force strains	$\bar{\eta}$	η
moment strains	$\bar{\kappa}$	κ
spin vector	$\bar{\omega}$	ω
axial extension	$\bar{\epsilon} = 0$	$\ \eta\ = \Psi'_t(s) = 1 + \epsilon$
arc length derivative	$\frac{\partial}{\partial s} \cdot = (\cdot)'$	$\frac{\partial}{\partial s_t} \cdot = (1 + \epsilon)^{-1}(\cdot)'$
time derivative	$\frac{\partial}{\partial t} \cdot = (\dot{\cdot})$	$\frac{\partial}{\partial t} \cdot = (\dot{\cdot})$

Table 5.1 – Summary of the notations employed throughout this section.

5.3 Kirchhoff theory of rods

The theory for the finite displacement of thin rods has been developed by Kirchhoff, Clebsch and Love.

force and moment strains (Reissner) : \propto S'inspirer de l'intro de Reissner 1973

In this section we follow [Dil92] to introduce *Kirchhoff's theory of rods*, where Dill “examine the classical theory of finite displacements of thin rods as developped by Kirchhoff and Clebesch, and presented by Love”. “The classical elastic rod theory of Kirchhoff (1859), called the kinetic analogue, is is a special case of our rod theory [...]” [Ant05, p. 238]

Dans un même genre, le papier de Reissner (1973) vaut le détour [Rei73]

We assume that material and section properties are slowly varying along the centerline. Note that symbols referring to this configuration will carry an overbar.

référence importante pour la rod [MLG13] , [Vil97, p. 109]. modeling of DNA molecules, pipes or hosing, plant, hair, surgery,

^{11 12 13} A thorough order-of-magnitude analysis is exposed in [Dil92, Col+93] ^{14 15}

Pour la rod extensible : [CH02]

ces équations sont valables à l'ordre 2 en α [Col+93] où :

Kirchhoff's theory is a first order theory regarding the parameter α , valid when α is small. This means that terms of order $O(\alpha^2)$ will be considered negligible :

$$\alpha = \sup_{s \in [0, L]} \{h/L, h\|\boldsymbol{\omega}\|, h\|\bar{\boldsymbol{\omega}}\|, \epsilon\} \quad (5.12)$$

The model is valid for uniform torsion. No restrained warping. For more and warping, see :

¹¹“The principal normal, binormal, and torsion of the axis, viewed as an element of a space curve, have no special significance in the theory of rods. Use of those special directions as base vectors does not simplify the theory and can mislead the reader into attributing significance to them when none exists. In particular, the curvature of the rod should not be confused with the curvature of the space curve which the axis forms.” [Dil92, p. 5]

¹²“Kirchhoff's theory can only apply to that class of problems for three dimensional bodies such that the loads on the sides are relatively small and slowly varying. The dominate mode of deformation must be a global bending and twisting with small axial extension. If there are substantial local variations in curvatures or substantial transverse shears, his theory of bending of rods will not provide a satisfactory first approximation.” [Dil92, p. 18]

¹³“There are no constitutive relations for F_1 or F_2 . They are determined by the balance of momentum as in the elementary linear theory of bending of rods.” [Dil92, p. 15]

¹⁴“We discuss here the dynamical equations of a theory of elastic rods that is due to Kirchhoff and Clebsch. This properly invariant theory is applicable to motions in which the strains relative to an undistorted configuration remain small, although rotations may be large. It is constructed to be a first-order theory, i.e., a theory that is complete to within an error of order two in an appropriate dimensionless measure of thickness, curvature, twist, and extension.” [Col+93, p. 1]

¹⁵“In a first-order theory of thin rods, one can treat the rod as inextensible [...]” [Col+93, p. 1]

The correction for shear in Kirchhoff's theory, introduce by Timoshenko in [Tim21] The *Timoshenko theory of beams* : [Tim45a, Tim45b, Tim45c] Include non uniform torsion

The problem becomes more complicated if cross sections are not free to warp or if the torque varies along the length of the bar. Warping in such cases varies along the bar and torsion is accompanied by tension or compression of longitudinal fibers. The rate of change of the angle of twist along the axis of the bar also varies, and we call this the case of non-uniform torsion. [Tim45b]

Linear theory for non uniform torsion [Vla61] Formula for shear center [Elt84] A geometrically exact Kirchhoff beam model including torsion warping : [MG16]

Pioneer works on non linear dynamics of rods [Wei02] More recent works : [MG16]

For an historical review : [Ben91a] Short review of the history of 1D beam models :[Ant05, p. 243]

See [Rei73] for an extension of Kirchhoff's theory, as mentioned also in [Rei81]

going further with non uniform torsion [Alv14]

In the traditional theory of non-uniform torsion the axial displacement field is expressed as the product of the unit twist angle and the warping function. The first one, variable along the beam axis, is obtained by a global congruence condition; the second one, instead, defined over the cross-section, is determined by solving a Neumann problem associated to the Laplace equation, as well as for the uniform torsion problem. So, as in the classical theory the warping function doesn't punctually satisfy the first indefinite equilibrium equation, the principal aim of this work is to develop a new theory for non-uniform torsion of beams with axial symmetric cross-section, fully restrained on both ends and loaded by a constant torque, that permits to punctually satisfy the previous equation, by means of a trigonometric expansion of the axial displacement and unit twist angle functions. Furthermore, as the classical theory is generally applied with good results to the global and local analysis of ship structures, two beams having the first one an open profile, the second one a closed section, have been analyzed, in order to compare the two theories. [Cam+09]

Hypothesis

- the rod is slender
- cross-section deformations remain small, although rotations may be large
- cross-section shear-center and centroid are at the same location
- material and cross-section properties vary slowly along the rod

5.3.1 Description of the motion

To describe the motion of a Kirchhoff rod, we use the framework presented in §5.2.1 for Cosserat rods.¹⁶ However, we restrict its scope by requiring that transverse shear strains are negligible quantities, which is one of the fundamental assumptions made by Kirchhoff in his theory :

$$\eta_1 \simeq 0 \quad (5.13a)$$

$$\eta_2 \simeq 0 \quad (5.13b)$$

As a consequence, the material frame remains adapted to the centerline. The rod is not supposed to be strictly inextensible. However, as strains are assumed to be small, the axial strain is supposed to be small itself ($\epsilon \ll 1$), which translates to :

$$\eta_3(s, t) = 1 + \epsilon(s, t) \quad (5.14a)$$

$$\mathbf{d}_3(s, t) = \mathbf{t}(s, t) \quad (5.14b)$$

$$\mathbf{x}'(s, t) = (1 + \epsilon)\mathbf{t}(s, t) \quad (5.14c)$$

Stress-free configuration

We now consider a *stress-free* configuration of the rod as the *reference* configuration.¹⁷ The rod is described by its centerline $\bar{\gamma}$ and its material frame $\{\bar{\mathbf{d}}_1, \bar{\mathbf{d}}_2, \bar{\mathbf{d}}_3\}$. Again, a planar cross-section is defined as the set of material points lying in the plane perpendicular to $\bar{\gamma}$ and passing through $\bar{\mathbf{x}}(s)$. The material directors $\bar{\mathbf{d}}_1$ and $\bar{\mathbf{d}}_2$ are now chosen to be aligned with the principal axes of inertia of the cross-section.¹⁸ Thus, $\bar{\mathbf{d}}_3 = \bar{\mathbf{d}}_1 \times \bar{\mathbf{d}}_2$ is normal to the plane of the cross-section and adapted to the centerline ($\bar{\mathbf{d}}_3 = \bar{\mathbf{t}}$). Moreover, the centerline is chosen to be the curve passing through the cross-section centroids and is required to be at least a regular space curve, which means that its tangent is continuously defined.

For a sufficiently slender rod, the position of material point $\bar{\mathbf{p}}$ that belongs to cross-section $\mathcal{S}(s)$ (see figures 5.1, 5.2a and 5.2b) is expressed through its material coordinates (X_1, X_2, s) as :¹⁹

$$\bar{\mathbf{p}}(X_1, X_2, s) = \bar{\mathbf{x}}(s) + \bar{\mathbf{r}}(X_1, X_2, s) \quad (5.15a)$$

$$\bar{\mathbf{r}}(X_1, X_2, s) = X_1 \bar{\mathbf{d}}_1(s) + X_2 \bar{\mathbf{d}}_2(s) \quad (5.15b)$$

Consequently, for each s in the reference configuration, (X_1, X_2) is a cartesian coordinate system for the plane $\mathcal{S}(s)$. In this system the local coordinates of the cross-section centroid

¹⁶We use the notation employed by Antman in his *special Cosserat theory of rods* : “The motion of a special Cosserat rod is defined by three vector-valued functions : $[s_1, s_2] \times \mathbb{R} \ni (s, t) \mapsto \mathbf{r}(s, t), \mathbf{d}_1(s, t), \mathbf{d}_2(s, t) \in \mathbb{E}^3$ ” [Ant05, p. 270]. However, some specific assumptions will be made over the directors in the context of Kirchhoff’s theory.

¹⁷See [AAP10, p. 20] for precisions when such a configuration may not exist.

¹⁸In case of an axisymmetric section, any pair of perpendicular unit vectors lying in the cross-section plane will be valid.

¹⁹The lateral dimension of the rod must be smaller than its radius of curvature. Otherwise, this description would lead to self intersecting cross-sections.

are $(0, 0)$.

Finally, the cross-section is assumed to be bounded and the planar boundary curve is defined by the implicit equation : $f_s(X_1, X_2) = 0$. It is also required that the shear center and the centroid of the cross-section are at the same location, otherwise one would require a more complex kinematic description of the rod.²⁰

Deformed configuration

We now examine the motion of a Krichhoff rod and we call *deformed* configuration its actual configuration at time t . In this configuration the rod undergoes internal stresses under body loads, external loads and constraints.

The deformed configuration of the rod at time t is described by its centerline γ_t , its material frame $\{\mathbf{d}_1, \mathbf{d}_2, \mathbf{d}_3\}$ and a local displacement field \mathbf{u} . The centerline of the rod is deformed into the space curve γ_t with position vector \mathbf{x} :

$$\begin{aligned} \gamma_t : [0, L] &\longrightarrow \mathbb{R}^3 \\ s &\longmapsto \mathbf{x}(s, t) \end{aligned} \tag{5.16}$$

A material point $\bar{\mathbf{p}}$ in the *reference* configuration is transported to position \mathbf{p} in the *actual* configuration so that (see figures 5.1, 5.2c and 5.2d) :

$$\mathbf{p}(X_1, X_2, s, t) = \mathbf{x}(s, t) + \mathbf{r}(X_1, X_2, s, t) \tag{5.17a}$$

$$\mathbf{r}(X_1, X_2, s, t) = X_1 \mathbf{d}_1(s, t) + X_2 \mathbf{d}_2(s, t) + \mathbf{u}(X_1, X_2, s, t) \tag{5.17b}$$

$$\mathbf{u}(X_1, X_2, s, t) = u_k(X_1, X_2, s, t) \mathbf{d}_k(s, t) \tag{5.17c}$$

Although the cross-section $\mathcal{S}(s)$ is a planar surface in the reference configuration, it deforms to a non-planar surface in the actual configuration since $\mathbf{u} \neq \mathbf{0}$.²¹ The components $(u_1, u_2, u_3)^T$ of the local displacement field expressed in the material frame basis are required to be small in Kirchhoff's theory of rods.²² In practice, as explained by [Dil92] this means that the considered motions must satisfy :

$$\frac{u_k}{h} = O(\alpha) \quad , \quad \frac{\partial u_k}{\partial X_1} = O(\alpha) \quad , \quad \frac{\partial u_k}{\partial X_2} = O(\alpha) \quad , \quad \frac{\partial u_k}{\partial s} = O(\alpha^2) \tag{5.18}$$

In this theory, the material frame in the reference configuration deforms in a rigid-body manner so that it remains orthonormal and aligned to the principal axes of the cross-section

²⁰Some details are given in the conclusion.

²¹ $\mathcal{S}(s)$ refers to the same set of material points in any configurations. Sometimes a distinction is made between $\bar{\mathcal{S}}(s)$ and $\mathcal{S}(s)$ to highlight that the planarity of cross-sections is lost during the motion.

²²Note that this hypothesis is the one made by Kirchhoff and does not correspond to the well-known *Euler-Bernoulli* or *Navier-Bernoulli* assumption where the sections remain planar, undeformed and normal to the centerline during the rod deformation. In particular, torsion is responsible for the warping of cross-sections – that is cross-sections don't remain planar during the motion – and leads to a distinct value of the twist modulus. This is clearly stipulated in [Dil92, AAP10] but is often treated with confusion in the literature.

– within an error $O(\alpha^2)$.²³ Remark that this is different than assuming that cross-sections deform in a rigid-body manner, which is known as the *Euler-Bernoulli* hypothesis and is equivalent to the special case $\mathbf{u} = \mathbf{0}$.

5.3.2 Reparametrization

This subsection highlights the role played by the change in length of the rod during its motion. It was found that this aspect is often treated partially or with confusion in the literature, although it is of prime importance to understand correctly the influence of axial stretch in the computation of moment strains. Indeed, for an inextensible rod, the notions of geometric curvature and (flexural) material curvatures are somehow the same notions. But this is not the case for extensible rods as explained in §5.3.3.

The rod is parametrized by s , the arc length parameter of the *reference* configuration, as the constitutive laws will be expressed relatively to this configuration. But recall once again that s is no more the arc length parameter of the *deformed* centerline as the rod may have suffered axial extension.²⁴ Kirchhoff's theory assumes that the material frame remains adapted to the centerline during deformation, or equivalently that transverse shear strains are neglected.²⁵ The extension of the centerline is characterized by ϵ defined such that :

$$\bar{\mathbf{x}}' = \bar{\mathbf{d}}_3 \quad (5.19a)$$

$$\mathbf{x}' = (1 + \epsilon)\mathbf{d}_3 \quad (5.19b)$$

However, one can parametrize the deformed centerline by its own arc length parameter, denoted s_t . Let's call L_t the length of the deformed centerline and Ψ_t the \mathcal{C}^1 diffeomorphism that maps s onto s_t ($s_t = \Psi_t(s) \Leftrightarrow s = \Psi_t^{-1}(s_t)$). Thus, the centerline is equivalently described by :

$$\begin{aligned} \gamma_t : [0, L_t] &\longrightarrow \mathbb{R}^3 \\ s_t &\longmapsto \mathbf{x}(s_t) \end{aligned} \quad (5.20)$$

Because s_t is the arc length parameter of γ_t the following relations hold :

$$\frac{\partial \mathbf{x}}{\partial s_t} = \mathbf{d}_3 \quad (5.21a)$$

$$\frac{\partial s_t}{\partial s} = \eta_3 = 1 + \epsilon \quad (5.21b)$$

Consequently, one can deduce that the derivation with respect to s is proportional to the derivation with respect to s_t by a factor $1 + \epsilon$. This factor has to be taken into account

²³“[...] upon deformation, the principal axes of $\mathcal{S}(s)$ do remain normal to each other and to the rod axis, at least to within the approximations of the present theory, i.e., to within an error $O(\alpha^2)$.” [Col+93, p. 344].

²⁴In Kirchhoff's theory, rods are not supposed to be strictly inextensible but extension has to remain small. Thus, the internal axial force is given by a constitutive law and not considered as a geometric constraint. However, some authors have remarked that it might be convenient and reasonable to solve the equations of motion considering the geometric constraint $\epsilon = 0$. See [AAP10, p. 98] for a detailed discussion of the subject.

²⁵This is also known as the “unsharable” assumption. Indeed, if $\frac{\partial \mathbf{x}}{\partial s} = \eta_k \mathbf{d}_k = (1 + \epsilon) \mathbf{d}_3 \Leftrightarrow \eta_1 = \eta_2 = 0$.

when computing the material curvatures, which are no more equivalents to their geometric counterparts in the deformed configuration. This is detailed in the next section dedicated to the strains vectors.

5.3.3 Strains

This section, introduces the material force and moment strains vectors of a Kirchhoff rod. It shows how they are related – yet distinct if $\epsilon \neq 0$ – to the geometric curvature of the centerline.

Reference configuration

Since the material frame is orthonormal and adapted to the centerline, its evolution along the undeformed centerline is described thanks to the *reference material curvature vector* $\bar{\boldsymbol{\kappa}}$ defined as :

$$\bar{\mathbf{d}}_i' = \bar{\boldsymbol{\kappa}} \times \bar{\mathbf{d}}_i \quad (5.22)$$

In the reference configuration, because s is the centerline's arc length parameter, the strains vector components expressed in the material frame basis take the form : ²⁶

$$\bar{\kappa}_1 = \bar{\mathbf{d}}_3' \cdot \bar{\mathbf{d}}_2 = \bar{k}_1 = \bar{\boldsymbol{\kappa}} \bar{\mathbf{b}} \cdot \bar{\mathbf{d}}_1 \quad (5.23a)$$

$$\bar{\kappa}_2 = \bar{\mathbf{d}}_1' \cdot \bar{\mathbf{d}}_3 = \bar{k}_2 = \bar{\boldsymbol{\kappa}} \bar{\mathbf{b}} \cdot \bar{\mathbf{d}}_2 \quad (5.23b)$$

$$\bar{\kappa}_3 = \bar{\mathbf{d}}_1' \cdot \bar{\mathbf{d}}_2 = \bar{\tau} = \bar{\mathbf{d}}_1' \cdot \bar{\mathbf{d}}_2 \quad (5.23c)$$

where $\bar{\boldsymbol{\kappa}} \bar{\mathbf{b}}$ (see eq. (3.17)) is the curvature binormal vector of $\bar{\gamma}$:

$$\bar{\boldsymbol{\kappa}} \bar{\mathbf{b}} = \bar{\mathbf{t}} \times \frac{\partial \bar{\mathbf{t}}}{\partial s} = \bar{\mathbf{t}} \times \bar{\mathbf{t}}' \quad (5.24)$$

$\bar{\kappa}_1$ and $\bar{\kappa}_2$ are called the reference *material* curvatures. $\bar{\kappa}_3$ is called the reference *material* twist. In this configuration, $\bar{\kappa}_1$ and $\bar{\kappa}_2$ are simply computed as the projection of the curvature binormal vector along $\bar{\mathbf{d}}_1$ and $\bar{\mathbf{d}}_2$.

Note the important distinction between the reference material twist ($\bar{\tau}$) and the torsion of Frenet (τ_f) of the centerline, as defined in §3.5.5.

Deformed configuration

Since the material frame is orthonormal and adapted to the centerline, it's evolution along the *deformed* centerline is described thanks to the *actual strains vector* $\boldsymbol{\kappa}$ defined as :

$$\frac{\partial \mathbf{d}_k}{\partial s} = \mathbf{d}'_k = \boldsymbol{\kappa} \times \mathbf{d}_k \quad (5.25)$$

²⁶Recall the following result for an adapted frame : eq. (3.34).

Note that the strains vector is defined relatively to the arc length s of the *reference* configuration and not the arc length s_t of the *actual* configuration. Thus the strains vector components expressed in the material frame basis are given by :

$$\varkappa_1 = \mathbf{d}'_3 \cdot \mathbf{d}_2 = (1 + \epsilon) k_1 = (1 + \epsilon) \boldsymbol{\kappa} \mathbf{b} \cdot \mathbf{d}_1 \quad (5.26a)$$

$$\varkappa_2 = \mathbf{d}'_1 \cdot \mathbf{d}_3 = (1 + \epsilon) k_2 = (1 + \epsilon) \boldsymbol{\kappa} \mathbf{b} \cdot \mathbf{d}_2 \quad (5.26b)$$

$$\varkappa_3 = \mathbf{d}'_1 \cdot \mathbf{d}_2 = (1 + \epsilon) \tau = (1 + \epsilon) \frac{\partial \mathbf{d}_1}{\partial s_t} \cdot \mathbf{d}_2 \quad (5.26c)$$

where $\boldsymbol{\kappa} \mathbf{b}$ (see eq. (3.17)) is the curvature binormal vector of γ_t given by :

$$\boldsymbol{\kappa} \mathbf{b} = \mathbf{t} \times \frac{\partial \mathbf{t}}{\partial s_t} = (1 + \epsilon) \mathbf{t} \times \mathbf{t}' \quad (5.27)$$

\varkappa_1 and \varkappa_2 are called the *material* curvatures. \varkappa_3 is called the *material* twist. Note this time the dependence of the material strains components $(\varkappa_1, \varkappa_2, \varkappa_3)^T$ regarding the extension of the rod. These are the strains employed in the classical constitutive laws that lead to the determination of the internal axial force ($N = E S \epsilon$), internal bending moments ($M_1 = EI_1(\varkappa_1 - \bar{\varkappa}_1)$, $M_2 = EI_2(\varkappa_2 - \bar{\varkappa}_2)$) and internal twisting moment ($Q = GJ((\varkappa_3 - \bar{\varkappa}_3))$).

Often in the literature the flexural material curvatures are computed as the projection of the curvature binormal vector onto the first two material axes. Here it is demonstrated that this is not exact as it omits the contribution of the rod extension, although it could be a reasonable approximation when $\epsilon \ll 1$.

5.3.4 Balance of momentum

Let \mathcal{P} be the first *Piola-Kirchhoff* stress tensor. \mathcal{P} expresses how contact forces are acting in a *deformed* body, referring to its (known) *reference* configuration. Let $d\mathbf{S} = n dS$ be an elementary oriented surface of the rod in the *reference* configuration, of centroid $\mathbf{p}(X_1, X_2, s, t) \in \mathcal{S}(s)$.²⁷ The contact forces exerted on $d\mathbf{S}$ are given by :

$$d\mathbf{F}(X_1, X_2, s, t) = \boldsymbol{\sigma}_n(X_1, X_2, s, t) dS \quad (5.28a)$$

$$\boldsymbol{\sigma}_n(X_1, X_2, s, t) = \mathcal{P}(X_1, X_2, s, t) \cdot \mathbf{n} \quad (5.28b)$$

The *Piola stress vector* ($\boldsymbol{\sigma}_n$) introduced in eq. (5.28b) expresses the contact forces exerted on the body per unit area of the *reference* configuration.²⁸

The generic laws for the balance of linear and angular momentums are obtained by summation over the reference configuration, where \mathbf{b} are the body forces per unit volume

²⁷ dS is the area and \mathbf{n} is the unit normal of the elementary oriented surface $d\mathbf{S}$.

²⁸ For a detailed introduction to the Piola-Kirchhoff stress tensor, refer to [AAP10, p. 52].

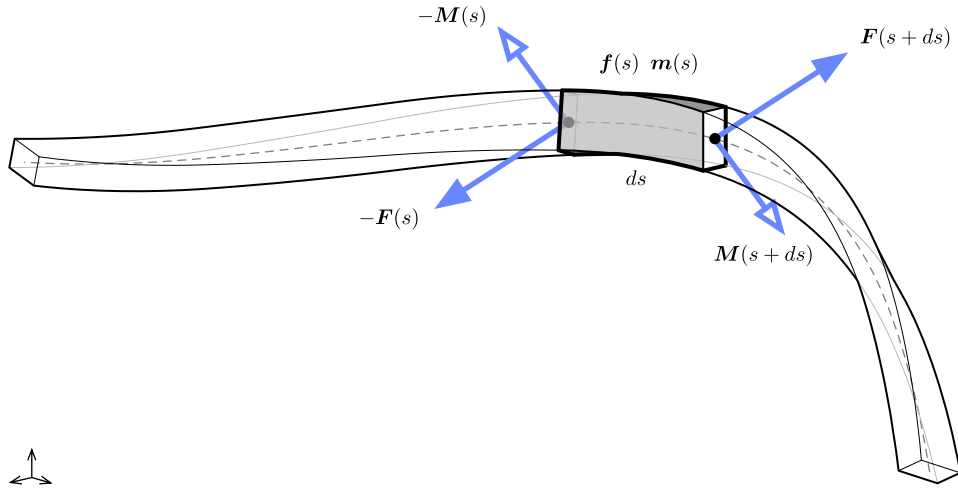


Figure 5.3 – Internal forces (\mathbf{F}) and moments (\mathbf{M}) acting on an infinitesimal beam slice of length ds . The beam is also subject to distributed external forces (\mathbf{f}) and moments (\mathbf{m}).

By convention, internal forces and moments are forces and moments applied by the right part to the left part of the beam.

of the *reference* configuration :

$$\iiint_{\mathcal{V}} \rho \ddot{\mathbf{p}} \, dV = \iint_{\partial \mathcal{V}} \boldsymbol{\sigma}_n \, dS + \iiint_{\mathcal{V}} \rho \mathbf{b} \, dV \quad (5.29a)$$

$$\iiint_{\mathcal{V}} \rho (\mathbf{p} \times \ddot{\mathbf{p}}) \, dV = \iint_{\partial \mathcal{V}} \mathbf{p} \times \boldsymbol{\sigma}_n \, dS + \iiint_{\mathcal{V}} \rho (\mathbf{p} \times \mathbf{b}) \, dV \quad (5.29b)$$

Here, and subsequently, \mathcal{V} denotes the volume of a slice of the rod in the *reference* configuration, encompassed between two cross-sections ($\mathcal{S}_1 = \mathcal{S}(s_1)$, $\mathcal{S}_2 = \mathcal{S}(s_2)$, $s_1 < s_2$). We also denote \mathcal{L}_{12} the lateral surface of the rod in the *reference* configuration so that the exterior surface of the volume is : $\partial \mathcal{V} = \mathcal{S}_1 \cup \mathcal{L}_{12} \cup \mathcal{S}_2$.

The cross-section $\mathcal{S}(s)$ splits the rod in two parts. Hereafter, the upstream part of the rod over $[s, L]$ will be called the “right part”. Reciprocally, the downstream part of the rod over $[0, s]$ will be called the “left part”.

Internal forces and moments

At the cross-section $\mathcal{S}(s)$, the contact forces applied by the right part onto the left part of the rod yield the following resultant force \mathbf{F} and resultant moment \mathbf{M} about the centroid point $\mathbf{x}(s, t)$:

$$\mathbf{F}(s, t) = \iint_{\mathcal{S}(s)} \boldsymbol{\sigma}_n(X_1, X_2, s, t) \, dX_1 dX_2 \quad (5.30a)$$

$$\mathbf{M}(s, t) = \iint_{\mathcal{S}(s)} \mathbf{r}(X_1, X_2, s, t) \times \boldsymbol{\sigma}_n(X_1, X_2, s, t) \, dX_1 dX_2 \quad (5.30b)$$

\mathbf{F} and \mathbf{M} are commonly known as the *internal forces* and the *internal moments* of the rod.

External forces and moments

We assume that the resultant of the contact forces on \mathcal{L}_{12} and the body forces on \mathcal{V} reduce to the following forms :

$$\iint_{\mathcal{L}_{12}} \boldsymbol{\sigma}_n \, dS + \iiint_{\mathcal{V}} \rho \mathbf{b} \, dV = \int_{s_1}^{s_2} \mathbf{f}_s + (1 + \epsilon) \mathbf{f}_{st} \, ds \quad (5.31a)$$

$$\begin{aligned} \iint_{\mathcal{L}_{12}} \mathbf{p} \times \boldsymbol{\sigma}_n \, dS + \iiint_{\mathcal{V}} \rho (\mathbf{p} \times \mathbf{b}) \, dV &= \int_{s_1}^{s_2} \mathbf{m}_s + (1 + \epsilon) \mathbf{m}_{st} \\ &\quad + \mathbf{x} \times (\mathbf{f}_s + (1 + \epsilon) \mathbf{f}_{st}) \, ds \end{aligned} \quad (5.31b)$$

where \mathbf{f}_s (resp. \mathbf{f}_{st}) is the distributed resultant force per unit length of the reference (resp. deformed) configuration ; and \mathbf{m}_s (resp. \mathbf{m}_{st}) is the distributed resultant moment per unit length of the reference (resp. deformed) configuration. For instance, these distributed forces and moments include external and body loads such as weight, snow, wind, ... ²⁹

Note that Kirchhoff's theory require that the stress components on the sides of the rod are small [Dil92, p. 11] – that is $\boldsymbol{\sigma}_n \cdot \mathbf{n} = O(\alpha^2)$ over \mathcal{L}_{12} . Thus, the first two terms in the above expression will be neglected :

$$\iint_{\mathcal{L}_{12}} \boldsymbol{\sigma}_n \, dS \simeq 0 \quad (5.32a)$$

$$\iint_{\mathcal{L}_{12}} \mathbf{p} \times \boldsymbol{\sigma}_n \, dS \simeq 0 \quad (5.32b)$$

Although the continuous model does not account formally for punctual loads,³⁰ they will be introduced seamlessly in the discrete model as the dynamical equations for the motion of the rod will translate into rigid body equations for the discrete segments composing the rod.

Inertial forces

The inertial forces for a volume of the rod encompassed between cross-sections \mathcal{S}_1 and \mathcal{S}_2 are obtained by summation as :

$$\iiint_{\mathcal{V}} \rho \ddot{\mathbf{p}} \, dV = \iiint_{\mathcal{V}_t} \rho_t \ddot{\mathbf{p}} \, dV_t \quad (5.33a)$$

$$\iiint_{\mathcal{V}} \rho (\mathbf{p} \times \dot{\mathbf{p}}) \, dV = \iiint_{\mathcal{V}_t} \rho_t (\mathbf{p} \times \dot{\mathbf{p}}) \, dV_t \quad (5.33b)$$

²⁹ At this stage, although this is uncommon in the literature, it has been found convenient to mark the distinction between loads referring to the reference configuration and loads referring to the actual configuration. Indeed, various distributed loads depend on the actual length of an element such as pressure and wind loads. On the other hand, some loads are independent of the extension of the rod, such as its weight.

³⁰This is possible but would require more math. However, local effects of such loads would not be properly modeled in the theory of Kirchhoff (Saint-Venant's Principle).

Here, ρ (resp. ρ_t) is the mass density of the rod in the reference (resp. deformed) configuration. Expressions are given in both coordinate systems.³¹

In the context of Kirchhoff's approximation, the local deformations of the cross-sections can be neglected in the computation of the inertial forces [Dil92, p. 16]. This yields :

$$\mathbf{p} \simeq \mathbf{x} + X_1 \mathbf{d}_1 + X_2 \mathbf{d}_2 \quad (5.34a)$$

$$\dot{\mathbf{p}} = \dot{\mathbf{x}} + \boldsymbol{\omega} \times (X_1 \mathbf{d}_1 + X_2 \mathbf{d}_2) \quad (5.34b)$$

$$\ddot{\mathbf{p}} = \ddot{\mathbf{x}} + \dot{\boldsymbol{\omega}} \times (X_1 \mathbf{d}_1 + X_2 \mathbf{d}_2) + \boldsymbol{\omega} \times (\boldsymbol{\omega} \times (X_1 \mathbf{d}_1 + X_2 \mathbf{d}_2)) \quad (5.34c)$$

Since X_1 and X_2 are the coordinates with respect to the centroid (\mathbf{x}) and the principal axes of the cross-section ($\mathbf{d}_1, \mathbf{d}_2$), the cross-section area (S) and principal moments of inertia (I_1, I_2) are given by :^{32,33}

$$0 = \iint_{\mathcal{S}(s)} (X_1 X_2) dX_1 dX_2 \quad (5.35a)$$

$$S = \iint_{\mathcal{S}(s)} dX_1 dX_2 \quad (5.35b)$$

$$I_1 = \iint_{\mathcal{S}(s)} X_2^2 dX_1 dX_2 \quad (5.35c)$$

$$I_2 = \iint_{\mathcal{S}(s)} X_1^2 dX_1 dX_2 \quad (5.35d)$$

More over, for a given cross-section the definition of the centroid yields :

$$\mathbf{0} = \iint_{\mathcal{S}(s)} (X_1 \mathbf{d}_1 + X_2 \mathbf{d}_2) dX_1 dX_2 \quad (5.36a)$$

$$0 = \iint_{\mathcal{S}(s)} X_1 dX_1 dX_2 \quad (5.36b)$$

$$0 = \iint_{\mathcal{S}(s)} X_2 dX_1 dX_2 \quad (5.36c)$$

For a thin slice of the rod ($\delta\mathcal{V}$) between cross-sections $\mathcal{S}(s)$ and $\mathcal{S}(s+ds)$, eq. (5.33a)

³¹In [Dil92] the change in volume and the conservation of mass is expressed through the determinants of the metric tensors of the reference and deformed configurations. Recall that this determinant is the square of the volume of the elementary cell defined by $\frac{\partial \mathbf{p}}{\partial s}, \frac{\partial \mathbf{p}}{\partial X_1}, \frac{\partial \mathbf{p}}{\partial X_2}$ in the reference configuration, which is convected to the elementary cell defined by $\frac{\partial \mathbf{p}}{\partial s}, \frac{\partial \mathbf{p}}{\partial X_1}, \frac{\partial \mathbf{p}}{\partial X_2}$ in the deformed configuration.

³²This is exact in the reference configuration but only approximately true in the deformed configuration as the theory consider only small deformations of cross-sections.

³³eq. (5.36a) is nothing but the definition of the centroid position. eq. (5.35a) holds because the tensor of inertia of the cross-section is diagonal in the basis $\{\mathbf{d}_1, \mathbf{d}_2, \mathbf{d}_3\}$ and thus $I_{12} = I_{21} = 0$.

and (5.33b) yield respectively : ³⁴

$$\iiint_{\delta V} \rho \ddot{\mathbf{p}} \, dV = (\rho S \ddot{\mathbf{x}}) ds \quad (5.37a)$$

$$\iiint_{\delta V} \rho (\mathbf{p} \times \ddot{\mathbf{p}}) \, dV = \left(\rho S \ddot{\mathbf{x}} + \rho \iint_{\mathcal{S}(s)} \mathbf{r} \times \ddot{\mathbf{r}} \, dX_1 dX_2 \right) ds \quad (5.37b)$$

Finally, remark that :

$$\mathbf{r} \times \ddot{\mathbf{r}} = (X_1)^2 \mathbf{d}_1 \times \ddot{\mathbf{d}}_1 + (X_2)^2 \mathbf{d}_2 \times \ddot{\mathbf{d}}_2 + X_1 X_2 (\mathbf{d}_1 \times \ddot{\mathbf{d}}_2 + \mathbf{d}_2 \times \ddot{\mathbf{d}}_1) \quad (5.38)$$

Thus, reminding eq. (5.35) and (5.36), one can conclude that the inertial forces reduce to :

$$\iiint_{\delta V} \rho \ddot{\mathbf{x}} \, dV = (\rho S \ddot{\mathbf{x}}) ds \quad (5.39a)$$

$$\iiint_{\delta V} \rho (\mathbf{p} \times \ddot{\mathbf{p}}) \, dV = (\rho S \ddot{\mathbf{x}} + \rho I_1 \mathbf{d}_1 \times \ddot{\mathbf{d}}_1 + \rho I_2 \mathbf{d}_2 \times \ddot{\mathbf{d}}_2) ds \quad (5.39b)$$

Balance of linear momentum

For a thin slice of the rod (δV) between cross-sections $\mathcal{S}(s)$ and $\mathcal{S}(s+ds)$, using eq. (5.30a) and (5.31a), the balance of linear momentum referring to the *reference configuration* expressed in eq. (5.29a) yields :

$$\begin{aligned} \iiint_{\delta V} \rho \ddot{\mathbf{p}} \, dV &= \iint_{\partial V} \boldsymbol{\sigma}_n \, dS + \iiint_{\delta V} \rho \mathbf{b} \, dV \\ &= \iint_{\mathcal{S}(s)} \boldsymbol{\sigma}_n \, dS + \iint_{\mathcal{S}(s+ds)} \boldsymbol{\sigma}_n \, dS + \left(\iint_{\delta \mathcal{L}} \boldsymbol{\sigma}_n \, dS + \iiint_{\delta V} \rho \mathbf{b} \, dV \right) \\ &= -\mathbf{F}(s) + \mathbf{F}(s+ds) + \left(\mathbf{f}_s(s) + (1+\epsilon) \mathbf{f}_{st}(s) \right) ds \\ &= \left(\frac{\partial \mathbf{F}}{\partial s} + \mathbf{f}_s + (1+\epsilon) \mathbf{f}_{st} \right) (s) ds \end{aligned} \quad (5.40)$$

Thus, using eq. (5.39a), the equation for the balance of linear momentum reduce to either equations :

$$\frac{\partial \mathbf{F}}{\partial s} + \mathbf{f}_s + (1+\epsilon) \mathbf{f}_{st} = \rho S \ddot{\mathbf{x}} \quad (5.41a)$$

$$(1+\epsilon) \frac{\partial \mathbf{F}}{\partial s_t} + \mathbf{f}_s + (1+\epsilon) \mathbf{f}_{st} = \rho S \ddot{\mathbf{x}} \quad (5.41b)$$

³⁴Indeed, since $\iint_{\mathcal{S}(s)} \mathbf{r} \, dX_1 dX_2 = \mathbf{0}$ from eq. (5.36a) we have $\iint_{\mathcal{S}(s)} \ddot{\mathbf{r}} \, dX_1 dX_2 = \iint_{\mathcal{S}(s)} \dot{\boldsymbol{\omega}} \times \mathbf{r} + \boldsymbol{\omega} \times (\boldsymbol{\omega} \times \mathbf{r}) \, dX_1 dX_2 = \mathbf{0}$ and $\iint_{\mathcal{S}(s)} \mathbf{r} \times \ddot{\mathbf{x}} \, dX_1 dX_2 = \mathbf{0}$ as $\boldsymbol{\omega}$ and \mathbf{x} are independent of X_1 and X_2 .

Balance of angular momentum

Similarly, for a thin slice of the rod ($\delta\mathcal{V}$) between cross-sections $\mathcal{S}(s)$ and $\mathcal{S}(s+ds)$, using eq. (5.30a) and (5.30b) yields :

$$\begin{aligned} \iint_{\mathcal{S}(s) \cup \mathcal{S}(s+ds)} \mathbf{p} \times \boldsymbol{\sigma}_n \, dS &= \iint_{\mathcal{S}(s) \cup \mathcal{S}(s+ds)} (\mathbf{x} + \mathbf{r}) \times \boldsymbol{\sigma}_n \, dS \\ &= -(\mathbf{x} \times \mathbf{F})(s) + (\mathbf{x} \times \mathbf{F})(s+ds) - \mathbf{M}(s) + \mathbf{M}(s+ds) \\ &= \frac{\partial}{\partial s} (\mathbf{M} + \mathbf{x} \times \mathbf{F})(s) \, ds \end{aligned} \quad (5.42)$$

Using eq. (5.31b) the balance of linear momentum referring to the *reference configuration* expressed in eq. (5.29b) yields :

$$\iiint_{\delta\mathcal{V}} \rho(\mathbf{p} \times \ddot{\mathbf{p}}) \, dV = \iint_{\partial\delta\mathcal{V}} \mathbf{p} \times \boldsymbol{\sigma}_n \, dS + \iiint_{\delta\mathcal{V}} \rho(\mathbf{p} \times \mathbf{b}) \, dV \quad (5.43)$$

$$= \frac{\partial}{\partial s} (\mathbf{M} + \mathbf{x} \times \mathbf{F})(s) \, ds + \mathbf{m}_s + (1 + \epsilon) \mathbf{m}_{s_t} \quad (5.44)$$

$$+ \mathbf{x} \times (\mathbf{f}_s + (1 + \epsilon) \mathbf{f}_{s_t}) \, ds \quad (5.45)$$

Finally, combining eq. (5.43) with eq. (5.39b) and (5.41a), the equation for the balance of angular momentum reduce to either equations : ³⁵

$$\frac{\partial \mathbf{M}}{\partial s} + \frac{\partial \mathbf{x}}{\partial s} \times \mathbf{F} + \mathbf{m}_s + (1 + \epsilon) \mathbf{m}_{s_t} = \rho I_1 \mathbf{d}_1 \times \ddot{\mathbf{d}}_1 + \rho I_2 \mathbf{d}_2 \times \ddot{\mathbf{d}}_2 \quad (5.46a)$$

$$(1 + \epsilon) \left(\frac{\partial \mathbf{M}}{\partial s_t} + \frac{\partial \mathbf{x}}{\partial s_t} \times \mathbf{F} + (1 + \epsilon)^{-1} \mathbf{m}_s + \mathbf{m}_{s_t} \right) = \rho I_1 \mathbf{d}_1 \times \ddot{\mathbf{d}}_1 + \rho I_2 \mathbf{d}_2 \times \ddot{\mathbf{d}}_2 \quad (5.46b)$$

³⁵Note the simplification of the term $\rho S \ddot{\mathbf{x}}$. Alternatively, the balance equations could be written for the slice considered as a rigid body. In the barycentric frame of the slice : $\frac{d}{dt}(dI_G) = \mathbf{M}(s+ds) - \mathbf{M}(s) + \mathbf{m}(s)ds + (\frac{1}{2}ds\mathbf{x}') \times \mathbf{F}(s+ds) + (-\frac{1}{2}ds\mathbf{x}') \times -\mathbf{F}(s) = (\frac{\partial \mathbf{M}}{\partial s}(s) + \mathbf{m}(s) + \mathbf{x}' \times \mathbf{F}(s)) \, ds$ with $dI_G \simeq \rho ds(I_1 \mathbf{d}_1 + I_2 \mathbf{d}_2 + (I_1 + I_2) \mathbf{d}_3)$.

5.3.5 Equations of motion

With some scaling arguments [Dil92] shows that terms in ω_1 and ω_2 should be negligible in the inertial forces of the rod given in eq. (5.39b), which yields to :^{36,37}

$$\rho I_1(\dot{\omega}_1 + \omega_2\omega_3) \simeq 0 \quad (5.47a)$$

$$\rho I_2(\dot{\omega}_2 - \omega_1\omega_3) \simeq 0 \quad (5.47b)$$

$$\rho(I_1 + I_2)\dot{\omega}_3 + \rho(I_2 - I_1)\omega_1\omega_2 \simeq \rho(I_1 + I_2)\dot{\omega}_3 \quad (5.47c)$$

For our application – a beam model for quasi-static analysis of gridshell structures – this approximation is clearly sufficient as what matters is the quasi-static response of the structural system and there is no need for a too accurate modeling of the transient phase. More over, the quasi-static response will be determined through a fictitious dynamic process appropriately damped to speed up the convergence to the steady state, and so there is no reason that the transient phase has any real physical meaning. This means that its is enough to keep only the twisting dynamic of the rod around its centerline.

Thus, the final dynamical equations for the motion of the rod to be retained are :

$$\frac{\partial \mathbf{F}}{\partial s} + \mathbf{f}_s + (1 + \epsilon)\mathbf{f}_{st} = \rho S \ddot{\mathbf{x}} \quad (5.48a)$$

$$\frac{\partial \mathbf{M}}{\partial s} + \frac{\partial \mathbf{x}}{\partial s} \times \mathbf{F} + \mathbf{m}_s + (1 + \epsilon)\mathbf{m}_{st} \simeq \rho(I_1 + I_2)\dot{\omega}_3 \mathbf{d}_3 \quad (5.48b)$$

5.3.6 Hookean elasticity

From now on we consider that the rod material is isotropic and linear elastic.³⁸ This is the framework of the so called *Hookean Elasticity*. This assumption allows the determination of the local displacement field (\mathbf{u}), the strain tensor ($\boldsymbol{\epsilon}$), the stress tensor ($\boldsymbol{\sigma}$) and the constitutive equations that link the axial force (\mathbf{F}_3), the bending moments ($\mathbf{M}_1, \mathbf{M}_2$) and the twisting moment (\mathbf{M}_3) to the strains ($\epsilon, \boldsymbol{\varkappa}, \bar{\boldsymbol{\varkappa}}$).

Such a material is characterized by a linear relation between the strain and stress tensors that takes the form :³⁹

$$\boldsymbol{\sigma} = 2\mu\boldsymbol{\epsilon} + \lambda Tr(\boldsymbol{\epsilon})\boldsymbol{\mathcal{I}} \quad (5.49)$$

where λ and μ are known as the elastic coefficients of Lamé. These coefficients are related

³⁶“It follows that \varkappa_1 and \varkappa_2 can be neglected in the kinetic energy [...]. However, \varkappa_3 , which provides the angular momentum about the axis of the rod, must be retained, This assumption of Kirchhoff is consistent with the technical theory of beams where rotary inertia is known to provide corrections to the natural frequencies of vibration of $O(\alpha^2)$ if the length measure is the half-wave length” [Dil92, p. 17].

³⁷This assumption is made in numerous publications but often with ambiguous or no justifications, as of instance : “neglecting inertial momentum due to the vanishing cross-section lead to the following dynamic equations for a Kirchhoff rod” [CB13].

³⁸This is true at first order for small strains anyway.

³⁹Using Einstein notation this expression yields : $\sigma_{ij} = \lambda\epsilon_{kk}\delta_{ij} + 2\mu\epsilon_{ij}$.

to the elastic (E) and shear (G) modulus and to the Poisson ratio (ν) :

$$\mu = \frac{E}{2(1 + \nu)} = G \quad (5.50\text{a})$$

$$\lambda = \frac{2\mu\nu}{1 - 2\nu} \quad (5.50\text{b})$$

A worthwhile presentation of the theory of elasticity in the specific context of elastic rods can be found in [AAP10].

5.3.7 Deformation of cross-sections

In this paragraph, we simply recall the canonical form of the local displacement field (\mathbf{u}) for the cross-section $\mathcal{S}(s)$ in the context of Kirchhoff's approximation : ⁴⁰

$$u_1 = -\nu\epsilon X_1 - \nu(\varkappa_1 - \bar{\varkappa}_1)X_1X_2 + \frac{1}{2}\nu(\varkappa_2 - \bar{\varkappa}_2)(X_1^2 - X_2^2) \quad (5.51\text{a})$$

$$u_2 = -\nu\epsilon X_2 + \nu(\varkappa_2 - \bar{\varkappa}_2)X_1X_2 + \frac{1}{2}\nu(\varkappa_1 - \bar{\varkappa}_1)(X_1^2 - X_2^2) \quad (5.51\text{b})$$

$$u_3 = (\varkappa_3 - \bar{\varkappa}_3)\varphi_s(X_1, X_2) \quad (5.51\text{c})$$

where φ_s is the warping function (in torsion) of $\mathcal{S}(s)$, determined by the following differential equation and the boundary condition over the contour of the cross-section : ⁴¹

$$0 = \frac{\partial^2 \varphi_s}{\partial X_1^2} + \frac{\partial^2 \varphi_s}{\partial X_2^2}, \quad \forall (X_1, X_2) \in \mathcal{S}(s) \quad (5.52\text{a})$$

$$0 = \frac{\partial f_s}{\partial X_1} \left(\frac{\partial \varphi_s}{\partial X_1} - X_2 \right) + \frac{\partial f_s}{\partial X_2} \left(\frac{\partial \varphi_s}{\partial X_2} + X_1 \right), \quad f_s(X_1, X_2) = 0 \quad (5.52\text{b})$$

These equations have known analytical solutions for classical shapes such as circles, ellipses, squares or rectangles. For other shapes, when it is not easy to find analytical solutions, the membrane analogy introduced by Prandtl [Pra03] can be employed.⁴²

⁴⁰Remark that the local displacement field results from the superposition of the three displacement fields obtained for pure and uniform extension, flexion and twist. For a detailed analysis of pure and uniform flexion and twist of rods; refer to [AAP10, ch. 3].

⁴¹ $\mathbf{n} = (\partial f_s / \partial X_1, \partial f_s / \partial X_2)^T$ is the unit normal vector to the boundary curve of $\mathcal{S}(s)$ defined implicitly by the equation $f_s(X_1, X_2) = 0$.

⁴²Recent advances [Koo14] in the formfinding of soap films with the force density method might be of practical use to evaluate the warping function.

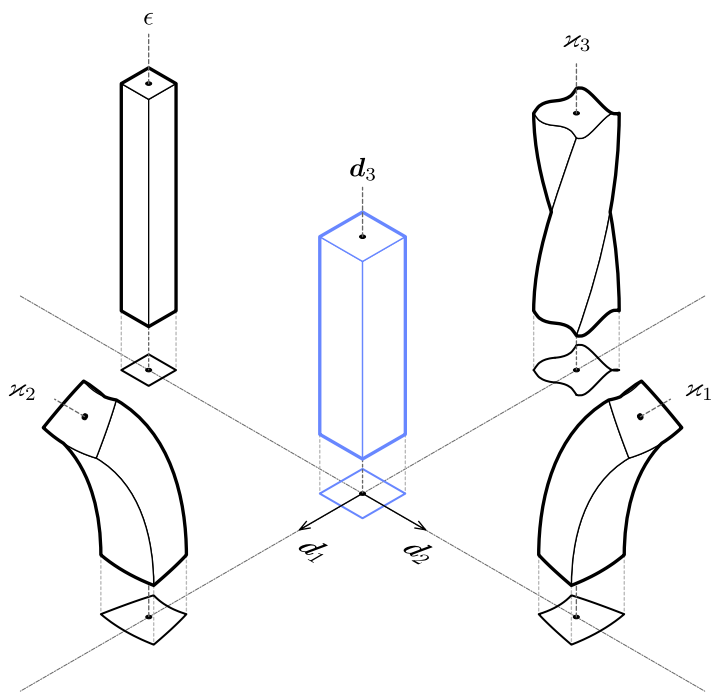


Figure 5.4 – Typical deformation modes of cross-sections in Kirchhoff's theory. Flexion around \mathbf{d}_1 (resp. \mathbf{d}_2) is measured through the material curvature κ_1 (resp. κ_2) ; torsion around \mathbf{d}_3 is measured through the material twist κ_3 ; and ϵ measures the axial extension. Remark that cross-sections are subjected to both in-plane deformations (κ_1 , κ_2 , ϵ) and out-of-plane deformations (κ_3).

5.3.8 Strain tensor

In this paragraph, we simply recall the canonical form of the strain tensor ($\boldsymbol{\epsilon}$) for the cross-section $S(s)$ in the context of Kirchhoff's approximation :

$$\epsilon_{33} = \epsilon + (\kappa_1 - \bar{\kappa}_1)X_2 - (\kappa_2 - \bar{\kappa}_2)X_1 \quad (5.53a)$$

$$\epsilon_{11} = \epsilon_{22} = -\nu\epsilon_{33} \quad (5.53b)$$

$$\epsilon_{12} = 0 \quad (5.53c)$$

$$\epsilon_{31} = \frac{1}{2}(\kappa_3 - \bar{\kappa}_3) \left(\frac{\partial \varphi_s}{\partial X_1} - X_2 \right) \quad (5.53d)$$

$$\epsilon_{32} = \frac{1}{2}(\kappa_3 - \bar{\kappa}_3) \left(\frac{\partial \varphi_s}{\partial X_2} + X_1 \right) \quad (5.53e)$$

5.3.9 Stress tensor

In this paragraph, we simply recall the canonical form of the strain tensor ($\boldsymbol{\epsilon}$) for the cross-section $S(s)$ in the context of Kirchhoff's approximation :

$$\sigma_{33} = E\epsilon_{33} \quad (5.54a)$$

$$\sigma_{11} = \sigma_{22} = \sigma_{12} = 0 \quad (5.54b)$$

$$\sigma_{31} = 2G\epsilon_{31} \quad (5.54c)$$

$$\sigma_{32} = 2G\epsilon_{32} \quad (5.54d)$$

Thus, the Piola stress vector defined in [eq. \(5.28b\)](#) becomes :

$$\boldsymbol{\sigma}_n = \sigma_{31}\mathbf{d}_1 + \sigma_{32}\mathbf{d}_2 + \sigma_{33}\mathbf{d}_3 \quad (5.55)$$

5.3.10 Constitutive equations for internal forces and moments

In Kirchhoff's theory, constitutive equations for internal forces and moments should not be considered as assumptions. Indeed, as shown hereafter, they are somehow consequences of the assumptions made on the motion – that is the rod remains close to a motion where cross-sections remain planar, undistorted and perpendicular to the centerline – and on the material – the Hookean elasticity – of the rod.

From [eq. \(5.30a\)](#), [\(5.53a\)](#), [\(5.54a\)](#) and [\(5.55\)](#) we deduce the constitutive equation for the

axial component of the internal forces : ⁴³

$$\begin{aligned}
 F_3 &= \iint_{\mathcal{S}(s)} \boldsymbol{\sigma}_n(X_1, X_2, s, t) \cdot \mathbf{d}_3 \, dX_1 dX_2 \\
 &= ES\epsilon - (\varkappa_2 - \bar{\varkappa}_2) \iint_{\mathcal{S}(s)} X_1 \, dX_1 dX_2 + (\varkappa_1 - \bar{\varkappa}_1) \iint_{\mathcal{S}(s)} X_2 \, dX_1 dX_2 \quad (5.56) \\
 &= ES\epsilon
 \end{aligned}$$

From eq. (5.30b), (5.53d), (5.53e), (5.54c), (5.54d) and (5.55) we deduce the constitutive equation for the axial component of the internal moments :

$$\begin{aligned}
 M_3 &= \iint_{\mathcal{S}(s)} (\mathbf{r} \times \boldsymbol{\sigma}_n(X_1, X_2, s, t)) \cdot \mathbf{d}_3 \, dX_1 dX_2 \\
 &= \iint_{\mathcal{S}(s)} -X_2 \sigma_{31} + X_1 \sigma_{32} \, dX_1 dX_2 \quad (5.57) \\
 &= G(\varkappa_3 - \bar{\varkappa}_3) \iint_{\mathcal{S}(s)} X_1 \left(\frac{\partial \varphi_s}{\partial X_2} + X_1 \right) - X_2 \left(\frac{\partial \varphi_s}{\partial X_1} - X_2 \right) \, dX_1 dX_2
 \end{aligned}$$

From eq. (5.30b), (5.53a), (5.54a) and (5.55) we deduce the constitutive equation for the first component of the internal moments :

$$\begin{aligned}
 M_1 &= \iint_{\mathcal{S}(s)} (\mathbf{r} \times \boldsymbol{\sigma}_n(X_1, X_2, s, t)) \cdot \mathbf{d}_1 \, dX_1 dX_2 \\
 &= \iint_{\mathcal{S}(s)} X_2 \sigma_{33} \, dX_1 dX_2 \quad (5.58) \\
 &= E(\varkappa_1 - \bar{\varkappa}_1) \iint_{\mathcal{S}(s)} X_2^2 \, dX_1 dX_2
 \end{aligned}$$

From eq. (5.30b), (5.53a), (5.54a) and (5.55) we deduce the constitutive equation for the second component of the internal moments :

$$\begin{aligned}
 M_2 &= \iint_{\mathcal{S}(s)} (\mathbf{r} \times \boldsymbol{\sigma}_n(X_1, X_2, s, t)) \cdot \mathbf{d}_2 \, dX_1 dX_2 \\
 &= \iint_{\mathcal{S}(s)} -X_1 \sigma_{33} \, dX_1 dX_2 \quad (5.59) \\
 &= E(\varkappa_2 - \bar{\varkappa}_2) \iint_{\mathcal{S}(s)} X_1^2 \, dX_1 dX_2
 \end{aligned}$$

⁴³Also recall from eq. (5.36) that $\iint_{\mathcal{S}(s)} X_1 \, dX_1 dX_2 = 0$ and $\iint_{\mathcal{S}(s)} X_2 \, dX_1 dX_2 = 0$.

5.3.11 Summary of the theory

Let's summarize the assumptions and results of Kirchhoff's theory of rods on which our discret beam model will be based on.

In the reference configuration the rod is described by its reference strains :

$$\bar{d}'_i = \bar{\varkappa} \times \bar{d}_i \quad (5.60)$$

In the actual configuration the rod is described by its strains and spin vector :

$$x' = (1 + \epsilon)t \quad (5.61a)$$

$$d'_i = \varkappa \times d_i \quad (5.61b)$$

$$\dot{d}_i = \omega \times d_i \quad (5.61c)$$

The rod is subjected to internal forces and moments :

$$\mathbf{F} = F_1 \mathbf{d}_1 + F_2 \mathbf{d}_2 + F_3 \mathbf{d}_3 \quad (5.62a)$$

$$\mathbf{M} = M_1 \mathbf{d}_1 + M_2 \mathbf{d}_2 + M_3 \mathbf{d}_3 \quad (5.62b)$$

The rod is subjected to external and body loads described as distributed forces and moments acting on the centerline – either given per unit length of the reference configuration (\mathbf{f}_s , \mathbf{m}_s) or per unit length of the actual configuration (\mathbf{f}_{st} , \mathbf{m}_{st}) – and given in the condensed form :

$$\mathbf{f} = \mathbf{f}_s + (1 + \epsilon) \mathbf{f}_{st} = f_1 \mathbf{d}_1 + f_2 \mathbf{d}_2 + f_3 \mathbf{d}_3 \quad (5.63a)$$

$$\mathbf{m} = \mathbf{m}_s + (1 + \epsilon) \mathbf{m}_{st} = m_1 \mathbf{d}_1 + m_2 \mathbf{d}_2 + m_3 \mathbf{d}_3 \quad (5.63b)$$

The internal axial force, the internal bending moments and the internal twisting moment are computed with the following constitutive equations :

$$F_3 = ES\epsilon \quad (5.64a)$$

$$M_1 = EI_1(\varkappa_1 - \bar{\varkappa}_1) \quad (5.64b)$$

$$M_2 = EI_2(\varkappa_2 - \bar{\varkappa}_2) \quad (5.64c)$$

$$M_3 = GJ(\varkappa_3 - \bar{\varkappa}_3) \quad (5.64d)$$

where S , I_1 , I_2 , J are respectively the area, the second moments of inertia and the torsional stiffness of the cross-section :

$$S = \iint_{\mathcal{S}(s)} dX_1 dX_2 \quad (5.65a)$$

$$I_1 = \iint_{\mathcal{S}(s)} X_2^2 dX_1 dX_2 \quad (5.65b)$$

$$I_2 = \iint_{\mathcal{S}(s)} X_1^2 dX_1 dX_2 \quad (5.65c)$$

$$J = \iint_{\mathcal{S}(s)} X_1 \left(\frac{\partial \varphi_s}{\partial X_2} + X_1 \right) - X_2 \left(\frac{\partial \varphi_s}{\partial X_1} - X_2 \right) dX_1 dX_2 \quad (5.65d)$$

and φ_s is the warping function of the cross-section that satisfies the differential system :

$$0 = \frac{\partial^2 \varphi_s}{\partial X_1^2} + \frac{\partial^2 \varphi_s}{\partial X_2^2}, \quad \forall (X_1, X_2) \in \mathcal{S}(s) \quad (5.66a)$$

$$0 = \frac{\partial f_s}{\partial X_1} \left(\frac{\partial \varphi_s}{\partial X_1} - X_2 \right) + \frac{\partial f_s}{\partial X_2} \left(\frac{\partial \varphi_s}{\partial X_2} + X_1 \right), \quad f_s(X_1, X_2) = 0 \quad (5.66b)$$

The dynamical equations for the motion of the rod are :

$$\frac{\partial \mathbf{F}}{\partial s} + \mathbf{f} = \rho S \ddot{\mathbf{x}} \quad (5.67a)$$

$$\frac{\partial \mathbf{M}}{\partial s} + \frac{\partial \mathbf{x}}{\partial s} \times \mathbf{F} + \mathbf{m} = \rho I_1 \mathbf{d}_1 \times \ddot{\mathbf{d}}_1 + \rho I_2 \mathbf{d}_2 \times \ddot{\mathbf{d}}_2 \quad (5.67b)$$

Neglecting the rotational dynamics around \mathbf{d}_1 and \mathbf{d}_2 the components of the above equations are written :

$$F'_1 + \varkappa_2 F_3 - \varkappa_3 F_2 + f_1 = \rho S \ddot{x}_1 \quad (5.68a)$$

$$F'_2 + \varkappa_3 F_1 - \varkappa_1 F_3 + f_2 = \rho S \ddot{x}_2 \quad (5.68b)$$

$$F'_3 + \varkappa_1 F_2 - \varkappa_2 F_1 + f_3 = \rho S \ddot{x}_3 \quad (5.68c)$$

$$M'_1 + \varkappa_2 M_3 - \varkappa_3 M_2 - (1 + \epsilon) F_2 + m_1 \simeq 0 \quad (5.68d)$$

$$M'_2 + \varkappa_3 M_1 - \varkappa_1 M_3 + (1 + \epsilon) F_1 + m_2 \simeq 0 \quad (5.68e)$$

$$M'_3 + \varkappa_1 M_2 - \varkappa_2 M_1 + m_3 \simeq \rho(I_1 + I_2)\dot{\omega}_3 \quad (5.68f)$$

The local displacements of the cross-sections are given by :

$$u_1 = -\nu \epsilon X_1 - \nu(\varkappa_1 - \bar{\varkappa}_1) X_1 X_2 + \frac{1}{2}\nu(\varkappa_2 - \bar{\varkappa}_2)(X_1^2 - X_2^2) \quad (5.69a)$$

$$u_2 = -\nu \epsilon X_2 + \nu(\varkappa_2 - \bar{\varkappa}_2) X_1 X_2 + \frac{1}{2}\nu(\varkappa_1 - \bar{\varkappa}_1)(X_1^2 - X_2^2) \quad (5.69b)$$

$$u_3 = (\varkappa_3 - \bar{\varkappa}_3)\varphi_s(X_1, X_2) \quad (5.69c)$$

The non-zero components of the strain tensor are given by :

$$\epsilon_{33} = \epsilon + (\varkappa_1 - \bar{\varkappa}_1) X_2 - (\varkappa_2 - \bar{\varkappa}_2) X_1 \quad (5.70a)$$

$$\epsilon_{31} = \frac{1}{2}(\varkappa_3 - \bar{\varkappa}_3) \left(\frac{\partial \varphi_s}{\partial X_1} - X_2 \right) \quad (5.70b)$$

$$\epsilon_{32} = \frac{1}{2}(\varkappa_3 - \bar{\varkappa}_3) \left(\frac{\partial \varphi_s}{\partial X_2} + X_1 \right) \quad (5.70c)$$

$$\epsilon_{11} = \epsilon_{22} = -\nu \epsilon_{33} \quad (5.70d)$$

The non-zero components of the stress tensor are given by :

$$\sigma_{33} = E \epsilon_{33} \quad (5.71a)$$

$$\sigma_{31} = 2G \epsilon_{31} \quad (5.71b)$$

$$\sigma_{32} = 2G \epsilon_{32} \quad (5.71c)$$

5.3.12 Comments

- The internal shear forces are reacting parameters and are given by the balance equations. Transverse shear deformations and stresses are not given by the present theory.
- There is a noticeable symmetry in the equations between the roles played by F_1 , F_2 and M_1 , M_2 and by the roles played by F_2 and M_3 .
- Warping is supposed to happen freely.
- Going further with torsion : donner des citations
- Going further with shear and extension : [Rei73]

5.4 Geometric interpretation of Kirchhoff's equations

The previous equations for the motion of the rod (see eq. (5.68a) to (5.68f)) have been established expressing the fundamental principles of balance of linear and angular momentums. An alternative approach, leading to the same results, consists in differentiating the elastic energy of a given configuration of the rod – assumed to be stationary – with respect to the degrees of freedom of the mechanical system (principle of virtual work).⁴⁴ However, the approach through equilibrium seems easier to understand as it is (almost) just a matter of balance between forces and moments on infinitesimal slices of the rods (see fig. 5.5). This is of obvious pedagogical interest as it allows to understand how the geometry of the rod influence the distribution of the elastic energy between extension, flexion and torsion. To emphasize this, we provide the proper drawings (see figures 5.6 to 5.8) and computations for the contribution of internal forces and moments to the balance of linear and angular momentums. This is what we call the “geometric interpretation” of Kirchhoff's equations.

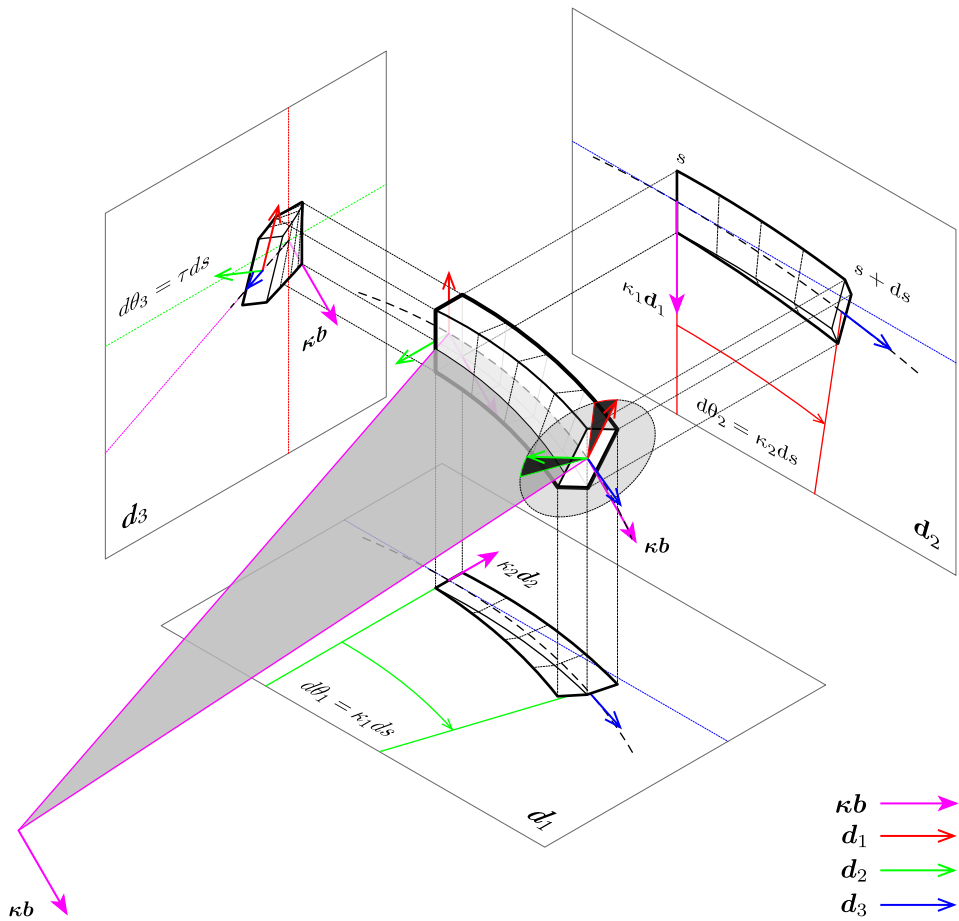
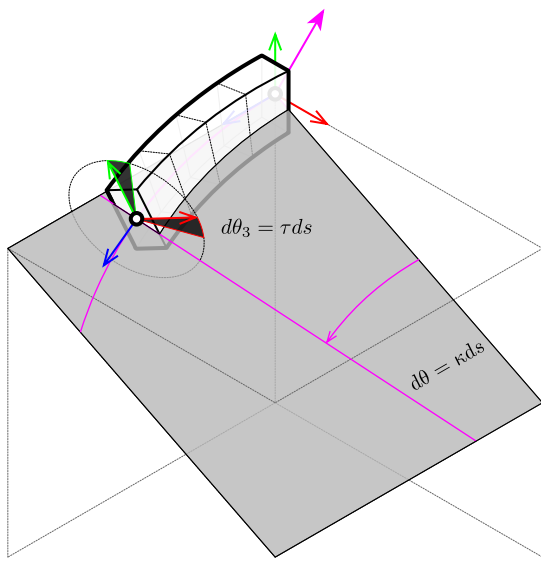
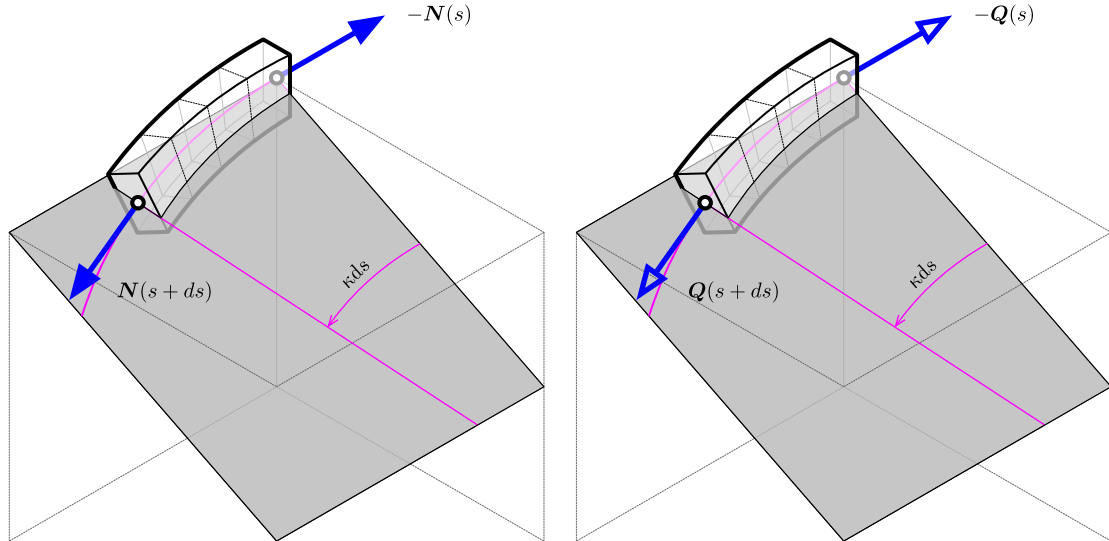


Figure 5.5 – Flexion and torsion of an elementary slice of a Kirchhoff rod of length ds . Projections of the deformations are given in the material planes defined by d_1 , d_2 , d_3 .

⁴⁴This is the approach employed in the theory presented in chapter 4 and is also the one developed in [AAP10] for strictly inextensible rods. It was yet employed in 1973 by Reissner in [Rei73].



(a) Infinitesimal deformation.



(b) Contributions of the internal forces.

(c) Contributions of the internal moments.

Figure 5.6 – Influence of the curvature (κ) in the deflection of internal forces and moments along the centerline.

Contributions to the balance of forces

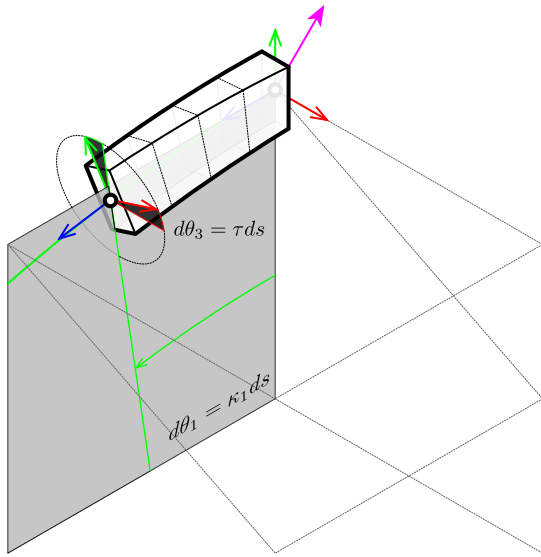
$\mathbf{N}(s + ds)$ is deflected from $\mathbf{d}_3(s)$ by the rotation of angle κds around $\boldsymbol{\kappa b}$ (fig. 5.6b). Thus, its contribution to the balance of forces onto $\mathbf{d}_3(s)$ is :

$$N(s + ds) \cos(\kappa ds) - N(s) = N'(s)ds + o(ds)$$

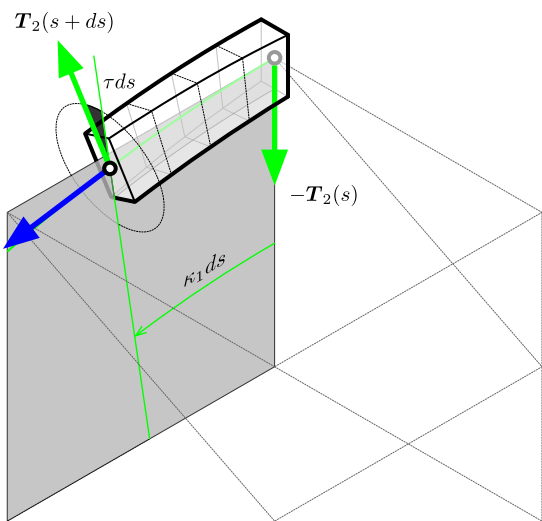
Contributions to the balance of moments

$\mathbf{Q}(s + ds)$ is deflected from $\mathbf{d}_3(s)$ by the rotation of angle κds around $\boldsymbol{\kappa b}$ (fig. 5.6c). Thus, its contribution to the balance of moments onto $\mathbf{d}_3(s)$ is :

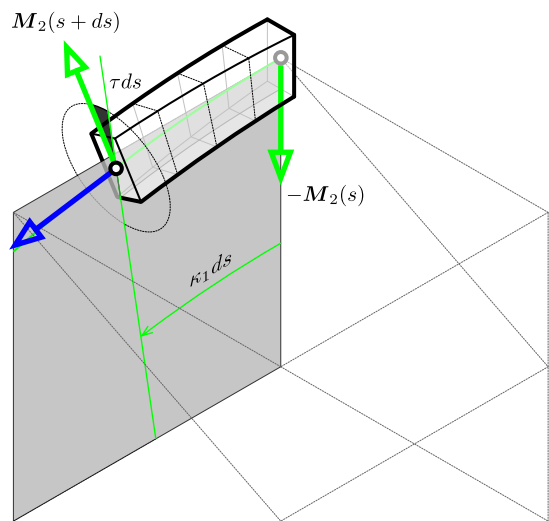
$$Q(s + ds) \cos(\kappa ds) - Q(s) = Q'(s)ds + o(ds)$$



(a) Infinitesimal deformation.



(b) Contributions of the internal forces.



(c) Contributions of the internal moments.

Figure 5.7 – Influence of the first material curvature (κ_1) in the deflection of internal forces and moments along the centerline.

Contributions to the balance of forces

$\mathbf{T}_2(s + ds)$ is deflected from $\mathbf{d}_2(s)$ by the combined rotations of angle τds around \mathbf{d}_3 and $\kappa_2 ds$ around \mathbf{d}_2 (fig. 5.7b). Thus, its contribution to the balance of forces onto $\mathbf{d}_1(s)$ is :

$$-\mathbf{T}_2(s + ds) \sin(\tau ds) \cos(\kappa_2 ds) = -\tau \mathbf{T}_2(s) ds + o(ds)$$

$\mathbf{T}_2(s + ds)$ is deflected from $\mathbf{d}_2(s)$ by the combined rotations of angle τds around \mathbf{d}_3 and $\kappa_1 ds$ around \mathbf{d}_1 (fig. 5.7b). Thus, its contribution to the balance of forces onto $\mathbf{d}_2(s)$ is :

$$-\mathbf{T}_2(s) + \mathbf{T}_2(s + ds) \cos(\tau ds) \cos(\kappa_1 ds) = \mathbf{T}'_2(s) ds + o(ds)$$

$\mathbf{T}_2(s + ds)$ is deflected from $\mathbf{d}_2(s)$ by the combined rotations of angle τds around \mathbf{d}_3 and $\kappa_1 ds$ around \mathbf{d}_1 (fig. 5.7b). Thus, its contribution to the balance of forces onto $\mathbf{d}_3(s)$ is :

$$\mathbf{T}_2(s + ds) \cos(\tau ds) \sin(\kappa_1 ds) = \kappa_1 \mathbf{T}_2(s) ds + o(ds)$$

$\mathbf{N}(s + ds)$ is deflected from $\mathbf{d}_3(s)$ by the combined rotations of angle $\kappa_2 ds$ around \mathbf{d}_2 and $\kappa_1 ds$ around \mathbf{d}_1 (fig. 5.7b). Thus, its contribution to the balance of forces onto $\mathbf{d}_2(s)$ is :

$$-\mathbf{N}(s + ds) \cos(\kappa_2 ds) \sin(\kappa_1 ds) = -\kappa_1 \mathbf{N}(s) ds + o(ds)$$

Contributions to the balance of moments

$\mathbf{T}_2(s + ds)$ is deflected from the plane normal to $\mathbf{d}_1(s)$ by a rotation of angle τds around \mathbf{d}_3 (fig. 5.7b). It produces a moment around \mathbf{d}_1 with the lever arm $b = \cos(\kappa_2 ds)ds$. Thus, its contribution to the balance of moments onto $\mathbf{d}_1(s)$ is :

$$-\mathbf{T}_2(s + ds) \cos(\tau ds)(\cos(\kappa_2 ds)ds) = -\mathbf{T}_2(s) ds + o(ds)$$

$\mathbf{M}_2(s + ds)$ is deflected from $\mathbf{d}_2(s)$ by the combined rotations of angle τds around \mathbf{d}_3 and $\kappa_2 ds$ around \mathbf{d}_2 (fig. 5.7c). Thus, its contribution to the balance of moments onto $\mathbf{d}_1(s)$ is :

$$-\mathbf{M}_2(s + ds) \sin(\tau ds) \cos(\kappa_2 ds) = -\tau \mathbf{M}_2(s) ds + o(ds)$$

$\mathbf{M}_2(s + ds)$ is deflected from $\mathbf{d}_2(s)$ by the combined rotations of angle τds around \mathbf{d}_3 and $\kappa_1 ds$ around \mathbf{d}_1 (fig. 5.7c). Thus, its contribution to the balance of moments onto $\mathbf{d}_2(s)$ is :

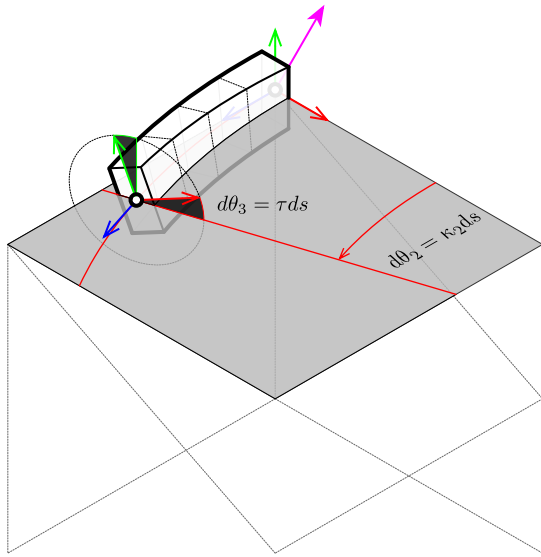
$$-\mathbf{M}_2(s) + \mathbf{M}_2(s + ds) \cos(\tau ds) \cos(\kappa_1 ds) = \mathbf{M}'_2(s) ds + o(ds)$$

$\mathbf{M}_2(s + ds)$ is deflected from $\mathbf{d}_2(s)$ by the combined rotations of angle τds around \mathbf{d}_3 and $\kappa_1 ds$ around \mathbf{d}_1 (fig. 5.7c). Thus, its contribution to the balance of moments onto $\mathbf{d}_3(s)$ is :

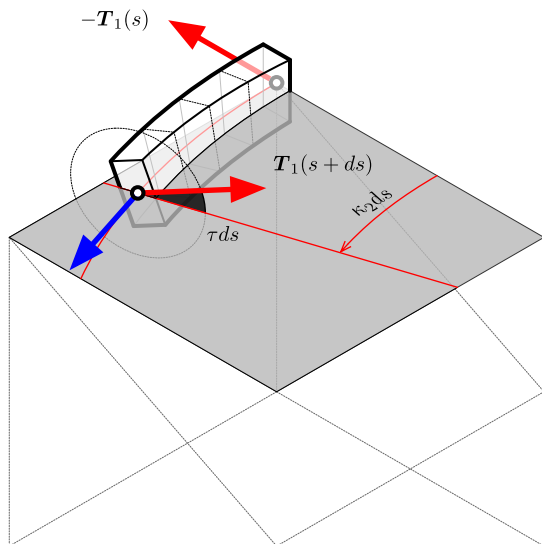
$$\mathbf{M}_2(s + ds) \cos(\tau ds) \sin(\kappa_1 ds) = \kappa_1 \mathbf{M}_2(s) ds + o(ds)$$

$\mathbf{Q}(s + ds)$ is deflected from $\mathbf{d}_3(s)$ by the combined rotations of angle $\kappa_2 ds$ around \mathbf{d}_2 and $\kappa_1 ds$ around \mathbf{d}_1 (fig. 5.7c). Thus, its contribution to the balance of moments onto $\mathbf{d}_2(s)$ is :

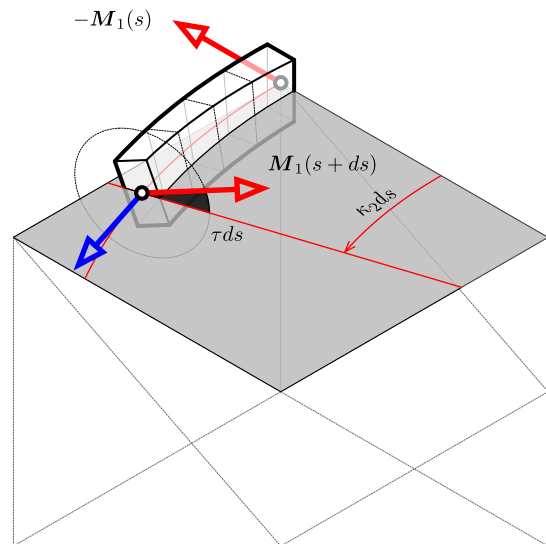
$$-\mathbf{Q}(s + ds) \cos(\kappa_2 ds) \sin(\kappa_1 ds) = -\kappa_1 \mathbf{Q}(s) ds + o(ds)$$



(a) Infinitesimal deformation.



(b) Contributions of the internal forces.



(c) Contributions of the internal moments.

Figure 5.8 – Influence of the second material curvature (κ_2) in the deflection of internal forces and moments along the centerline.

Contributions to the balance of forces

$\mathbf{T}_1(s + ds)$ is deflected from $\mathbf{d}_1(s)$ by the combined rotations of angle τds around \mathbf{d}_3 and $\kappa_2 ds$ around \mathbf{d}_2 (fig. 5.8b). Thus, its contribution to the balance of forces onto $\mathbf{d}_1(s)$ is :

$$-T_1(s) + T_1(s + ds) \cos(\tau ds) \cos(\kappa_2 ds) = T'_1(s)ds + o(ds)$$

$\mathbf{T}_1(s + ds)$ is deflected from $\mathbf{d}_1(s)$ by the combined rotations of angle τds around \mathbf{d}_3 and $\kappa_1 ds$ around \mathbf{d}_1 (fig. 5.8b). Thus, its contribution to the balance of forces onto $\mathbf{d}_2(s)$ is :

$$T_1(s + ds) \sin(\tau ds) \cos(\kappa_1 ds) = \tau T_1(s)ds + o(ds)$$

$\mathbf{T}_1(s + ds)$ is deflected from $\mathbf{d}_1(s)$ by the combined rotations of angle τds around \mathbf{d}_3 and $\kappa_2 ds$ around \mathbf{d}_2 (fig. 5.8b). Thus, its contribution to the balance of forces onto $\mathbf{d}_3(s)$ is :

$$-T_1(s + ds) \cos(\tau ds) \sin(\kappa_2 ds) = -\kappa_2 T_1(s)ds + o(ds)$$

$\mathbf{N}(s + ds)$ is deflected from $\mathbf{d}_3(s)$ by the combined rotations of angle $\kappa_1 ds$ around \mathbf{d}_1 and $\kappa_2 ds$ around \mathbf{d}_2 (fig. 5.8b). Thus, its contribution to the balance of forces onto $\mathbf{d}_1(s)$ is :

$$N(s + ds) \cos(\kappa_1 ds) \sin(\kappa_2 ds) = \kappa_2 N(s)ds + o(ds)$$

Contributions to the balance of moments

$\mathbf{T}_1(s + ds)$ is deflected from the plane normal to $\mathbf{d}_2(s)$ by the angle τds around \mathbf{d}_3 along ds (fig. 5.8b). It produces a moment around \mathbf{d}_2 with the lever arm $b = \cos(\kappa_1 ds)ds$. Thus, its contribution to the balance of moments onto $\mathbf{d}_2(s)$ is :

$$T_1(s + ds) \cos(\tau ds)(\cos(\kappa_1 ds)ds) = T_1(s)ds + o(ds)$$

$\mathbf{M}_1(s + ds)$ is deflected from $\mathbf{d}_1(s)$ by the combined rotations of angle τds around \mathbf{d}_3 and $\kappa_2 ds$ around \mathbf{d}_2 (fig. 5.8c). Thus, its contribution to the balance of moments onto $\mathbf{d}_1(s)$ is :

$$-M_1(s) + M_1(s + ds) \cos(\tau ds) \cos(\kappa_2 ds) = M'_1(s)ds + o(ds)$$

$\mathbf{M}_1(s + ds)$ is deflected from $\mathbf{d}_1(s)$ by the combined rotations of angle τds around \mathbf{d}_3 and $\kappa_2 ds$ around \mathbf{d}_2 (fig. 5.8c). Thus, its contribution to the balance of moments onto $\mathbf{d}_2(s)$ is :

$$M_1(s + ds) \sin(\tau ds) \cos(\kappa_2 ds) = \tau M_1(s)ds + o(ds)$$

$\mathbf{M}_1(s + ds)$ is deflected from $\mathbf{d}_1(s)$ by the combined rotations of angle τds around \mathbf{d}_3 and $\kappa_2 ds$ around \mathbf{d}_2 (fig. 5.8c). Thus, its contribution to the balance of moments onto $\mathbf{d}_3(s)$ is :

$$-M_1(s + ds) \cos(\tau ds) \sin(\kappa_2 ds) = -\kappa_2 M_1(s)ds + o(ds)$$

$\mathbf{Q}(s + ds)$ is deflected from $\mathbf{d}_3(s)$ by the combined rotations of angle $\kappa_1 ds$ around \mathbf{d}_1 and $\kappa_2 ds$ around \mathbf{d}_2 (fig. 5.8c). Thus, its contribution to the balance of moments onto $\mathbf{d}_1(s)$ is :

$$Q(s + ds) \cos(\kappa_1 ds) \sin(\kappa_2 ds) = \kappa_2 Q(s)ds + o(ds)$$

5.5 Conclusion

Remind that the beam is subject to a distributed external force \mathbf{f}_{ext} and a distributed external moment \mathbf{m}_{ext} .

We neglect rotational inertial effects on \mathbf{d}_1 et \mathbf{d}_2 in (??) and (??) which leads to the following shear force :

$$\mathbf{F}^\perp(s) = \mathbf{d}_3 \times (\mathbf{M}' + \boldsymbol{\kappa} \times \mathbf{M} + \mathbf{m}_{ext}) \quad (5.72)$$

$$\mathbf{F}^\parallel(s) = N\mathbf{d}_3 \quad (5.73)$$

We may neglect as well the last term ($\tau\mathbf{M}$) and get back to the shear force obtained by the variational approach. The total internal force acting on the beam is hence given by :

$$\mathbf{F}(s) = \mathbf{N}(s) + \mathbf{T}(s) \quad (5.74)$$

Sections are subject to the following rotational moment around the centerline :

$$\boldsymbol{\Gamma}(s) = Q' + \mathbf{d}_3 \cdot (\kappa\mathbf{b} \times \mathbf{M} + \mathbf{m}_{ext}) \quad (5.75)$$

5.6 References

- [AAP10] B. Audoly, M. Amar, and Y. Pomeau. *Elasticity and geometry*. 2010, p. 600.
- [ABW99] S. Adriaenssens, M. Barnes, and C. Williams. “A new analytic and numerical basis for the form-finding and analysis of spline and gridshell structures”. In: *Computing Developments in Civil and Structural Engineering*. Ed. by B. Kumar and B. H. V. Topping. Edinburgh: Civil-Comp Press, 1999, pp. 83–91.
- [Alv14] J. M. Alves. “Dynamic analysis of bridge girders subjected to moving loads : Numerical and analytical beam models considering warping effects”. PhD thesis. Tecnico Lisboa, 2014, p. 129.
- [Ant05] S. Antman. *Nonlinear problems of elasticity*. Applied mathematical sciences. New York: Springer, 2005, p. 838.
- [Ant74] S. Antman. “Kirchhoff’s problem for nonlinearly elastic rods”. In: *Quarterly of Applied Mathematics* XXXIV.3 (1974), pp. 221–240.
- [BAK13] M. Barnes, S. Adriaenssens, and M. Krupka. “A novel torsion/bending element for dynamic relaxation modeling”. In: *Computers & Structures* 119 (Apr. 2013), pp. 60–67.
- [Bar99] M. Barnes. “Form finding and analysis of tension structures by dynamic relaxation”. In: *International Journal of Space Structures* 14.2 (1999), pp. 89–104.
- [Ben91a] E. Benvenuto. *An introduction to the history of structural mechanics : statics and resistance of solids*. New York: Springer Verlag, 1991, pp. XXI, 306.
- [Ben91b] E. Benvenuto. *An introduction to the history of structural mechanics : vaulted structures and elastic systems*. New York: Springer Verlag, 1991, pp. XXI, 255.
- [Ber+10] M. Bergou, B. Audoly, E. Vouga, M. Wardetzky, and E. Grinspun. “Discrete viscous threads”. In: *ACM Transactions on ...* (2010), pp. 1–10.
- [Cam+09] A. Campanile, M. Mandarino, V. Piscopo, and A. Pranzitelli. “On the exact solution of non-uniform torsion for beams with asymmetric cross-section”. In: *World Academy of Science, Engineering and Technology* 31 (2009), pp. 36–45.
- [CB13] R. Casati and F. Bertails-descoubes. “Super space clothoids”. In: *SIGGRAPH*. 2013.
- [CH02] J. Cisternas and P. Holmes. “Buckling of extensible thermoelastic rods”. In: *Mathematical and Computer Modelling* 36.3 (2002), pp. 233–243.
- [Cle83] A. Clebsch. *Théorie de l’élasticité des corps solides*. Paris: Dunod, 1883, p. 900.
- [Col+93] B. Coleman, E. H. Dill, M. Lembo, L. Zheng, and I. Tobias. “On the dynamics of rods in the theory of Kirchhoff and Clebsch”. In: *Archive for Rational Mechanics and Analysis* 121.4 (1993), pp. 339–359.

- [DA14] M. A. Dias and B. Audoly. “A non-linear rod model for folded elastic strips”. In: *Journal of the Mechanics and Physics of Solids* 62.1 (2014), pp. 57–80. arXiv: [1306.5035](https://arxiv.org/abs/1306.5035).
- [DA15] M. A. Dias and B. Audoly. ““Wunderlich, meet kirchhoff” : a general and unified description of elastic ribbons and thin rods”. In: *Journal of Elasticity* 119.1 (2015), pp. 49–66. arXiv: [arXiv:1403.2094v2](https://arxiv.org/abs/1403.2094v2).
- [Day65] A. Day. “An Introduction to dynamic relaxation”. In: *The Engineer* (1965).
- [DBC06] C. Douthe, O. Baverel, and J.-F. Caron. “Formfinding of a grid shell in composite materials”. In: *Journal of the IASS* 47 (2006), pp. 53–62.
- [Dil92] E. H. Dill. “Kirchhoff’s theory of rods”. In: *Archive for History of Exact Sciences* (1992), p. 23.
- [DKZ14] B. D’Amico, A. Kermani, and H. Zhang. “Form finding and structural analysis of actively bent timber grid shells”. In: *Engineering Structures* 81 (2014), pp. 195–207.
- [DLP13] Y. Duan, D. Li, and P. F. Pai. “Geometrically exact physics-based modeling and computer animation of highly flexible 1D mechanical systems”. In: *Graphical Models* 75.2 (2013), pp. 56–68.
- [dPel+15] L. du Peloux, F. Tayeb, B. Lefevre, O. Baverel, and J.-F. Caron. “Formulation of a 4-DoF torsion / bending element for the formfinding of elastic gridshells”. In: *Proceedings of the International Association for Shell and Spatial Structures*. August. Amsterdam, 2015, pp. 1–14.
- [DZK16] B. D’Amico, H. Zhang, and A. Kermani. “A finite-difference formulation of elastic rod for the design of actively bent structures”. In: *Engineering Structures* 117 (2016), pp. 518–527.
- [Elt84] E. Elter. “Two formulii of the shear center”. In: *Periodica Polytechnica Mechanical Engineering* 28.2-3 (1984), pp. 179–193.
- [Hoo06] P. C. J. Hoogenboom. “7 Vlasov torsion theory”. In: October (2006), pp. 1–12.
- [Ibr95] A. Ibrahimbegović. “On finite element implementation of geometrically nonlinear Reissner’s beam theory: three-dimensional curved beam elements”. In: *Computer Methods in Applied Mechanics and Engineering* 122.1-2 (1995), pp. 11–26.
- [Kir50] G. Kirchhoff. *Über das gleichgewicht und die bewegung einer elastischen scheibe*. Berlin, 1850, p. 38.
- [Kir76] G. Kirchhoff. *Vorlesungen über mathematische, physik, mechanik*. Ed. by B. G. Teubner. Leipzig, 1876, p. 483.
- [Koo14] K. Koohestani. “Nonlinear force density method for the form-finding of minimal surface membrane structures”. In: *Communications in Nonlinear Science and Numerical Simulation* 19.6 (2014), pp. 2071–2087.

- [Láz+16] C. Lázaro, S. Monleón, J. Bessini, and J. Casanova. “A review on geometrically exact models for very flexible rods”. In: *Proceedings of the IASS Annual Symposium 2016* (2016), pp. 1–10.
- [LL09] H. Lang and J. Linn. “Lagrangian field theory in space-time for geometrically exact Cosserat rods”. In: 150 (2009), p. 21.
- [Lov92] A. Love. *A treatise on the mathematical theory of elasticity*. First. Cambridge University Press, 1892.
- [LS96] J. Langer and D. Singer. “Lagrangian Aspects of the Kirchhoff elastic rod”. In: *Society for Industrial and Applied Mathematics Review* 38.4 (1996), pp. 605–618.
- [MG16] D. Manta and R. Gonçalves. “A geometrically exact Kirchhoff beam model including torsion warping”. In: *Computers and Structures* 177 (2016), pp. 192–203.
- [MLG13] D. Moulton, T. Lessinnes, and A. Goriely. “Morphoelastic rods. Part I : A single growing elastic rod”. In: *Journal of the Mechanics and Physics of Solids* 61.2 (2013), pp. 398–427.
- [MPW14] C. Meier, A. Popp, and W. A. Wall. “An objective 3D large deformation finite element formulation for geometrically exact curved Kirchhoff rods”. In: *Computer Methods in Applied Mechanics and Engineering* 278.August (2014), pp. 445–478.
- [Neu09] S. Neukirch. “Enroulement, contact et vibrations de tiges élastiques”. PhD thesis. 2009, p. 97.
- [Pra03] L. Prandtl. “Zur torsion von prismatischen stäben”. In: *Physikalische Zeitschrift* 4 (1903), pp. 758–770.
- [Rei73] E. Reissner. “On one-dimensional large-displacement finite-strain beam theory.” In: *Studies in Applied Mathematics* 52.2 (1973), pp. 87–95.
- [Rei81] E. Reissner. “On the effect of shear center location on the values of axial and lateral cantilever buckling loads for singly symmetric cross-section beams”. In: *Journal of Applied Mathematics and Physics* 32.1 (1981), pp. 182–188.
- [SBH95] Y. Shi, A. E. Borovik, and J. E. Hearst. “Elastic rod model incorporating shear and extension, generalized nonlinear Schrödinger equations, and novel closed-form solutions for supercoiled DNA”. In: *The Journal of Chemical Physics* 103.8 (1995), pp. 3166–3183.
- [Spi08] J. Spillmann. “CORDE : Cosserat rod elements for the animation of interacting elastic rods”. PhD thesis. 2008.
- [SV91] J. C. Simo and L. Vu-Quoc. “A Geometrically-exact rod model incorporating shear and torsion-warping deformation”. In: *International Journal of Solids and Structures* 27.3 (1991), pp. 371–393.
- [TG51] S. Timoshenko and J. N. Goodier. *Theory of elasticity*. Second. New York: McGraw-Hill, 1951, p. 506.

- [The07] A. Theetten. “Splines dynamiques géométriquement exactes : simulation haute performance et interaction”. PhD thesis. Université des Sciences et Technologies de Lille, 2007.
- [Tim21] S. Timoshenko. “On the correction for shear of the differential equation for transverse vibrations of prismatic bars”. In: *Philosophical Magazine Series 6* 41.245 (1921), pp. 744–746.
- [Tim22] S. Timoshenko. “On the transverse vibrations of bars of uniform cross-section”. In: *Philosophical Magazine Series 6* 43.253 (1922), pp. 125–131.
- [Tim45a] S. Timoshenko. “Theory of bending, torsion and buckling of thin-walled members of open cross section : Part I.” In: *Journal of The Franklin Institute* 239.3 (1945), pp. 201–219.
- [Tim45b] S. Timoshenko. “Theory of bending, torsion and buckling of thin-walled members of open cross section : Part II.” In: *Journal of The Franklin Institute* 249.4 (1945), pp. 249–268.
- [Tim45c] S. Timoshenko. “Theory of bending, torsion and buckling of thin-walled members of open cross section : Part III.” In: *Journal of The Franklin Institute* 239.5 (1945), pp. 343–336.
- [Vet14] Y. Vetyukov. *Nonlinear mechanics of thin-walled structures : asymptotics, direct approach and numerical analysis*. 1st ed. 2014, pp. X, 272.
- [Vil97] P. Villaggio. *Mathematical models for elastic structures*. Cambridge University Press, 1997.
- [Vla61] V. Z. Vlasov. *Thin-walled elastic beams*. Second. National Technical Information Service, 1961.
- [Wak80] D. Wakefield. “Dynamic relaxation analysis of pretensioned networks supported by compression arches”. PhD thesis. City University London, 1980, p. 281.
- [Wei02] H. Weiss. “Dynamics of geometrically nonlinear rods : Mechanical models and equations of motion”. In: *Nonlinear Dynamics* 30 (2002), pp. 357–381.

6 Numerical Model

6.1 Introduction

Penser à expliquer le dualisme edge / vertex. En pratique, on a envie de contrôler le model par les noeuds et les propriétés sur les bords. Ce que peu de models savent faire. C'est aussi mieux pour les conditions de bords. C'est le vrai avantage de ce modèle.

Expliquer l'interpolation des efforts. Il y a un choix à faire dans la DR. Soit on écrit l'équilibre sur le noeud (de dimension null). Soit on écrit l'équilibre sur une tranche de dimension $l_i + li + 1/2$. Mais si l'on veut maintenir la précision des conditions de passage, la DR fonctionne avec des noeuds et pas des tranches, le mieux est d'opter pour un équilibre du noeud. La DR va minimiser les résidus aux noeuds et donc on aura les bonnes conditions de passage sous Fext et Mext. J'ai montré que la convergence était plus rapide et précise. On a pas de décalage dans les diagrammes des efforts (si il y en a, ce sont uniquement les défauts de convergence, le résidu , n'étant pas strictement nul au noeud à la fin de la DR).

6.1.1 Main hypothesis

On néglige les forces d'inertie liées à la rotation de l'élément (devant quoi ?? traitement quasi-statique par rapport à la rotation). Cette hypothèse est faite explicitement chez Florence Bertail :

Cette hypothèse est faite mais passée sous silence chez Douthé, Adriaenssen, D'Amico lorsqu'ils déduisent l'effort tranchant du moment de flexion.

Principe :

- les équations constitutives permettent le calcul de M_1, M_2, Q à partir de la géométrie $\{x, \theta\}$.

- La seconde loi de kirchhoff projetée sur les axes matériels 1 et 2 de la section me donnent accès aux efforts tranchants T_1 et T_2 .
- La seconde loi de kirchhoff projetée sur les axes matériel 3 (tangente à la centerline) de la section me donnent l'hypothèse quasi-statique de Audoly.

6.1.2 Discret beam model

Let's introduce the discrete biarc model to describe the configuration of a beam. It is composed of a discrete curve called *centerline* (Γ) and a discrete adapted frame called *material frame* as its axes are chosen to be the principal axes of the beam cross-section (fig. 6.1a). The centerline itself is organized in n_s consecutive adjacent segments which are three-vertices and two-edges elements with uniform material and section properties.

Beams can either be closed or open. The corresponding number of vertices, edges and segments are reported in fig. 6.1b.

Centerline

The discrete centerline is a polygonal space curve (fig. 6.1a) defined as an ordered sequence of $n + 1$ pairwise disjoint *vertices* : $\Gamma = (\mathbf{x}_0, \mathbf{x}_1, \dots, \mathbf{x}_n) \in \mathbb{R}^{3(n+1)}$. Consecutive pairs of vertices define n straight segments $(\mathbf{e}_0, \mathbf{e}_1, \dots, \mathbf{e}_{n-1})$ called *edges* and pointing from one vertex to the next one :

$$\mathbf{e}_i = \mathbf{x}_{i+1} - \mathbf{x}_i \quad (6.1a)$$

$$l_i = \|\mathbf{e}_i\| \quad (6.1b)$$

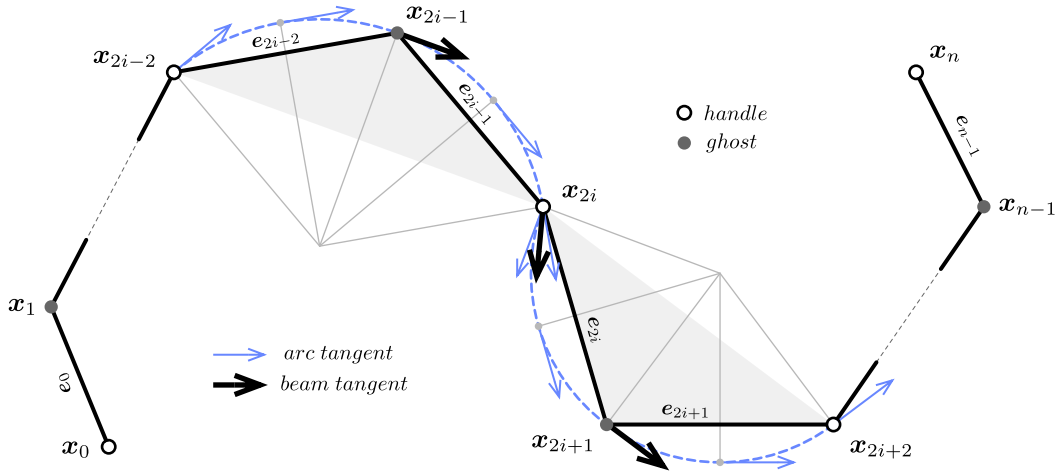
$$\mathbf{u}_i = \mathbf{e}_i / l_i = \mathbf{d}_{3,i+1/2} \quad (6.1c)$$

The length of the i th edge is denoted l_i and its normalized direction vector is denoted \mathbf{u}_i . The arc length of the i th vertex is denoted s_i and is given by :

$$\begin{cases} s_0 = 0 & i = 0 \\ s_i = \sum_{k=0}^{i-1} l_k & i \in \llbracket 1, n-1 \rrbracket \\ s_n = L & i = n \end{cases} \quad (6.2)$$

Thus, the centerline is parametrized by arc length and $\Gamma(s_i) = \mathbf{x}_i$. Additionally, we define the vertex-based mean length at vertex \mathbf{x}_i :

$$\begin{cases} \bar{l}_0 = \frac{1}{2}l_0 & i = 0 \\ \bar{l}_i = \frac{1}{2}(l_{i-1} + l_i) & i \in \llbracket 1, n-1 \rrbracket \\ \bar{l}_n = \frac{1}{2}l_{n-1} & i = n \end{cases} \quad (6.3)$$



(a) Centerline of the discrete biarc model.

Item	Symbol	Centerline	
		Open	Closed
segments	n_s	n_s	n_s
edges	n_e	$2n_s$	$2n_s$
vertices	n	$2n_s + 1$	$2n_s$
ghosts	n_g	n_s	n_s
handles	n_h	$n_s + 1$	n_s

(b) Number of segments, edges and vertices whether the centerline is closed or open.

Figure 6.1 – Biarc model for a discrete beam. The centerline is divided into curved segments (grey solid hatch). Each segment is defined as a three-noded element with uniform material and section properties. It has two end vertices (white) called *handle* as they are used to interact with the model, for instance to apply loads or restraints. It has one mid vertex (grey) called *ghost* as it is used only to enrich the segment kinematics and is not accessible to the end user.

Segments

The discrete centerline is divided into n_s curved segments. Each segment is a three-noded element – see [fig. 6.1a](#) where the area covered by a segment is represented as a grey solid hatch. The i th segment is composed of three vertices ($\mathbf{x}_{2i}, \mathbf{x}_{2i+1}, \mathbf{x}_{2i+2}$) spanning two edges ($\mathbf{e}_{2i}, \mathbf{e}_{2i+1}$). The (i-1)th segment and the i th segment share the same vertex \mathbf{x}_{2i} at arc length s_{2i} .

Each segment has two end vertices called *handle* ($\mathbf{x}_{2i}, \mathbf{x}_{2i+2}$) and one mid vertex called *ghost* (\mathbf{x}_{2i+1}) as this one is not accessible to the end user in order to interact with the model (link, restrain, loading, ...). Ghost vertices are used only for internal purpose to give a higher richness in the kinematic description of a segment than a two-noded segment would.

Finally, we define the *chord length* of the i th segment as the distance between \mathbf{x}_{2i} and \mathbf{x}_{2i+2} :

$$L_i = \|\mathbf{e}_{2i} + \mathbf{e}_{2i+1}\| \quad , \quad i \in \llbracket 0, n_s - 1 \rrbracket \quad (6.4)$$

Material and section properties

In addition, the model assumes that a segment has uniform section (S, I_1, I_2, J)¹ and material (E, G)² properties over its length $s \in]s_{2i}, s_{2i+2}[$. For the sake of simplicity, we introduce for further calculations the *material stiffness matrix* (\mathbf{B}_i) attached to each segment. It has the following form in the material frame basis :

$$\mathbf{B}_i = \begin{bmatrix} EI_1 & 0 & 0 \\ 0 & EI_2 & 0 \\ 0 & 0 & GJ \end{bmatrix}_i \quad , \quad i \in \llbracket 0, n_s - 1 \rrbracket \quad (6.5)$$

where EI_1 and EI_2 are the bending stiffnesses and GJ is the torsional stiffness. The axial stiffness of the i th segment is denoted by :

$$ES_i \quad , \quad i \in \llbracket 0, n_s - 1 \rrbracket \quad (6.6)$$

Distributed loads

The model assumes that each segment can be loaded with some distributed forces ($\mathbf{f}^{ext} = f_k \mathbf{d}_k$) and moments ($\mathbf{m}^{ext} = m_k \mathbf{d}_k$). These forces and moments are required to be uniform over each segment but can vary from one segment to another. They can represent body loads such as self weight or thermal loads or external loads such as wind, snow, pressure, ...

¹ S is the cross-section area ; I_1, I_2 and J are the principal moments of inertia of the cross-section.

² E is the elastic modulus and G is the shear modulus for the considered material

Concentrated loads

Additional External concentrated forces (\mathbf{F}^{ext}) and moments (\mathbf{M}^{ext}) are applied to the segment's end vertices (\mathbf{x}_{2i} , \mathbf{x}_{2i+2}). Note that the model does not allow to load ghost vertices, and this is precisely why they are called “ghost”.

Internal forces and moments

Under deformations the discrete rod is subject to internal forces and moments. Their components in the material frame basis are named as follow :

- The shear force : $\mathbf{F}^\perp = F_1 \mathbf{d}_1 + F_2 \mathbf{d}_2$
- The axial force : $\mathbf{N} = N \mathbf{d}_3$
- The bending moment : $\mathbf{M} = M_1 \mathbf{d}_1 + M_2 \mathbf{d}_2$
- The twisting moment : $\mathbf{Q} = Q \mathbf{d}_3$

6.1.3 Modeling discontinuities

The model assumes that cross-section and material properties as well as distributed loads are uniform over each segment. Referring to the structure of the equations of motion, and because the centerline is required to be a regular curve in the stress-free configuration, strains, stresses, displacements, internal forces and internal moments must be piecewise continuous functions of the arc length parameter, continuous over each segment $]s_{2i}, s_{2i+2}[$. Discontinuities of these functions might occur at handle vertices (\mathbf{x}_{2i}), for instance if there is a jump in material or cross-section properties or if concentrated loads are applied at handle vertices. Moreover, the centerline curve itself will stay \mathcal{C}^1 during the motion, as it is chosen to be \mathcal{C}^1 in the reference configuration.^{3,4}

Here and subsequently, for such a function, the left and right limits at handle vertices (s_{2i}) will be denoted with superscripts f_{2i}^- and f_{2i}^+ . Possibly, the function is continuous so that the left and right limits agree ($f_{2i}^- = f_{2i}^+$).

6.1.4 Matrix notation

Here and subsequently, matrix notation will often be used to provide compact expressions for the equations, where the components of vector-valued functions are given in the material

³This preclude the modeling of beams with kinks as the tangent vector would not be continuously defined at those points. In such a case, the beam should be modeled in two separate parts linked together in a rigid manner.

⁴The centerline is not \mathcal{C}^2 as discontinuities in curvature may occur. For instance, if no punctual loads are applied, the bending moment is continuous over the rod. As the bending moment is linked to the curvature through the constitutive equation $M = EI\nu$, a discontinuity in I will lead to a discontinuity in ν . Conversely, a discontinuity in ν will lead to a discontinuity in I .

frame basis. This notation will be mixed with the vector notation employed more generally throughout this document. Usually, if there is no comment in the manuscript, the meaning should be obvious and with no ambiguity to the reader.

For instance, all this expressions for the curvature binormal vector and the material curvatures vector will be considered equivalent and could be mixed together in the same equation :

$$\boldsymbol{\kappa} \mathbf{b} = \kappa_1 \mathbf{d}_1 + \kappa_2 \mathbf{d}_2 = [\kappa_1 \quad \kappa_2 \quad 0]^T \quad (6.7a)$$

$$\boldsymbol{\kappa} = \kappa_1 \mathbf{d}_1 + \kappa_2 \mathbf{d}_2 + \kappa_3 \mathbf{d}_3 = [\kappa_1 \quad \kappa_2 \quad \kappa_3]^T = (1 + \epsilon) [\kappa_1 \quad \kappa_2 \quad \tau]^T \quad (6.7b)$$

The force strains vector is given by :

$$\boldsymbol{\eta} = (1 + \epsilon) \mathbf{d}_3 = [0 \quad 0 \quad 1 + \epsilon]^T \quad (6.8)$$

Internal forces are composed of a shear force and an axial force given by :

$$\mathbf{F} = F_1 \mathbf{d}_1 + F_2 \mathbf{d}_2 + N \mathbf{d}_3 = [F_1 \quad F_2 \quad N]^T \quad (6.9a)$$

$$\mathbf{F}^\perp = F_1 \mathbf{d}_1 + F_2 \mathbf{d}_2 = [F_1 \quad F_2 \quad 0]^T \quad (6.9b)$$

$$\mathbf{F}^{\parallel} = \mathbf{N} = N \mathbf{d}_3 = [0 \quad 0 \quad N]^T \quad (6.9c)$$

Internal moments are composed of a bending moment and a twisting moment given by :

$$\mathbf{M} = M_1 \mathbf{d}_1 + M_2 \mathbf{d}_2 + Q \mathbf{d}_3 = [M_1 \quad M_2 \quad Q]^T \quad (6.10a)$$

$$\mathbf{M}^\perp = M_1 \mathbf{d}_1 + M_2 \mathbf{d}_2 = [M_1 \quad M_2 \quad 0]^T \quad (6.10b)$$

$$\mathbf{M}^{\parallel} = \mathbf{Q} = Q \mathbf{d}_3 = [0 \quad 0 \quad Q]^T \quad (6.10c)$$

With the help of the matrix notation, the constitutive equations eq. (5.64b) to (5.64d) together write in a single equation :

$$\mathbf{M} = \mathbf{B}(\boldsymbol{\kappa} - \bar{\boldsymbol{\kappa}}) = EI_1(\kappa_1 - \bar{\kappa}_1)\mathbf{d}_1 + EI_2(\kappa_2 - \bar{\kappa}_2)\mathbf{d}_2 + GJ(\kappa_3 - \bar{\kappa}_3)\mathbf{d}_3 \quad (6.11)$$

6.1.5 Discret extension and axial force

We assume the axial force (\mathbf{N}) to vary linearly over $[\mathbf{x}_{2i}, \mathbf{x}_{2i+2}]$ regarding the arc length parameter. The variation occurs if the segment is subject to a uniform distributed load f_3 over the segment. Consequently, the axial strain $(1 + \epsilon)$ is also required to vary linearly. The value of the axial extension at mid span of each edge are given by :

$$\epsilon_{i+1/2} = l_i / \bar{l}_i - 1 \quad , \quad i \in \llbracket 0, n_e - 1 \rrbracket \quad (6.12)$$

Consequently, the axial force at mid span of each edge is computed directly with the constitutive equation eq. (5.64a) as :

$$\mathbf{N}_{2i+1/2} = N_{2i+1/2} \mathbf{u}_{2i} \quad \text{where} \quad N_{2i+1/2} = E S_i \epsilon_{2i+1/2} \quad (6.13a)$$

$$\mathbf{N}_{2i+3/2} = N_{2i+3/2} \mathbf{u}_{2i+1} \quad \text{where} \quad N_{2i+3/2} = E S_i \epsilon_{2i+3/2} \quad (6.13b)$$

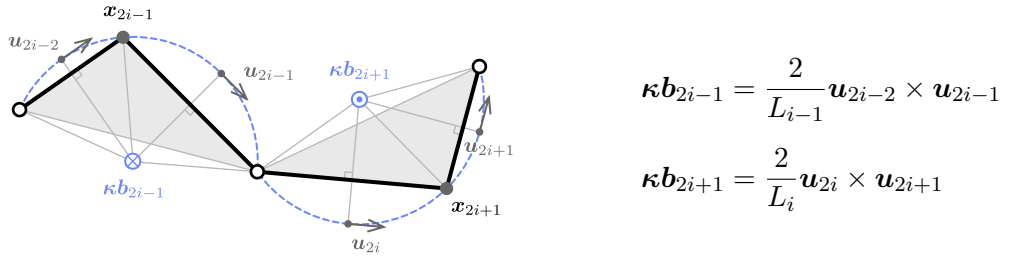
Remark the sign convention : as expected, when edge \mathbf{e}_i suffers a positive extension ($\epsilon_{i+1/2} > 0$), vertex \mathbf{x}_{i+1} “attracts” vertex \mathbf{x}_i to it as $\mathbf{d}_{3,i+1/2} = \mathbf{u}_i$ is pointing from \mathbf{x}_i towards \mathbf{x}_{i+1} . Remark also that $\epsilon_{i+1/2} = 0 \Leftrightarrow l_i = \bar{l}_i$ when the rod is not stretched.

6.1.6 Discret curvature and bending moment

We assume that the internal bending moment and curvature are quadratic functions of the arc length parameter over $[\mathbf{x}_{2i}, \mathbf{x}_{2i+2}]$. Although they must be continuous over this interval, they might be discontinuous at handle vertices and be subjected to jump discontinuities in direction and magnitude.

Geometric curvature at ghost vertices

For a given geometry of the centerline, the curvature binormal vector at ghost vertex \mathbf{x}_{2i-1} (resp. \mathbf{x}_{2i+1}) is computed considering the circumscribed osculating circle passing through the vertices $(\mathbf{x}_{2i-2}, \mathbf{x}_{2i-1}, \mathbf{x}_{2i})$ of the $(i-1)$ th segment – resp. through the vertices $(\mathbf{x}_{2i}, \mathbf{x}_{2i+1}, \mathbf{x}_{2i+2})$ of the i th segment.

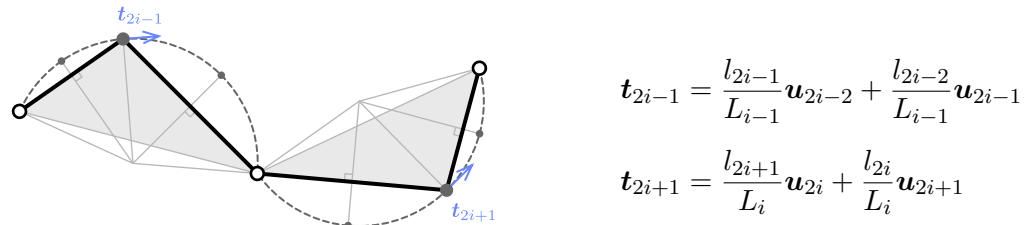


$$\kappa \mathbf{b}_{2i-1} = \frac{2}{L_{i-1}} \mathbf{u}_{2i-2} \times \mathbf{u}_{2i-1}$$

$$\kappa \mathbf{b}_{2i+1} = \frac{2}{L_i} \mathbf{u}_{2i} \times \mathbf{u}_{2i+1}$$

Unit tangent vector at ghost vertices

This definition of the curvature leads to a natural definition of the unit tangent vector at ghost vertex \mathbf{x}_{2i-1} (resp. \mathbf{x}_{2i+1}), as the unit vector tangent to the osculating circle of the $(i-1)$ th segment (resp. i th segment) at that point.

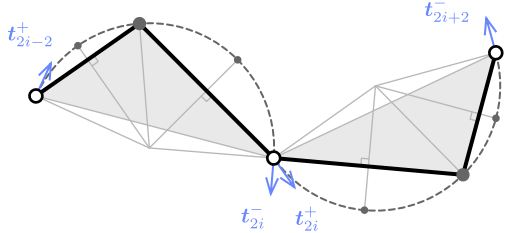


$$\mathbf{t}_{2i-1} = \frac{l_{2i-1}}{L_{i-1}} \mathbf{u}_{2i-2} + \frac{l_{2i-2}}{L_{i-1}} \mathbf{u}_{2i-1}$$

$$\mathbf{t}_{2i+1} = \frac{l_{2i+1}}{L_i} \mathbf{u}_{2i} + \frac{l_{2i}}{L_i} \mathbf{u}_{2i+1}$$

Left/right unit tangent vector at handle vertices

Equivalently, the definition of the osculating circles of the $(i - 1)$ th and i th segments leads to a natural definition of the left (\mathbf{t}_{2i}^-) and right (\mathbf{t}_{2i}^+) unit tangent vectors at handle vertex \mathbf{x}_{2i} , for segments of uniform curvature. When both segments have the same curvature, left and right vectors agree.

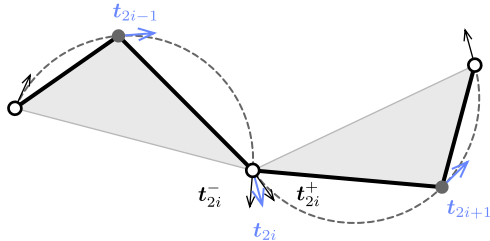


$$\mathbf{t}_{2i}^- = 2(\mathbf{t}_{2i-1} \cdot \mathbf{u}_{2i-1})\mathbf{u}_{2i-1} - \mathbf{t}_{2i-1}$$

$$\mathbf{t}_{2i}^+ = 2(\mathbf{t}_{2i+1} \cdot \mathbf{u}_{2i})\mathbf{u}_{2i} - \mathbf{t}_{2i+1}$$

Unit tangent vector at handle vertices

The unit tangent vector \mathbf{t}_{2i} – that is the beam section normal – at handle vertex \mathbf{x}_{2i} is chosen to be the mean of the left and right unit tangent vectors at that vertex.⁵



$$\mathbf{t}_{2i} = \frac{\mathbf{t}_{2i}^- + \mathbf{t}_{2i}^+}{\|\mathbf{t}_{2i}^- + \mathbf{t}_{2i}^+\|}$$

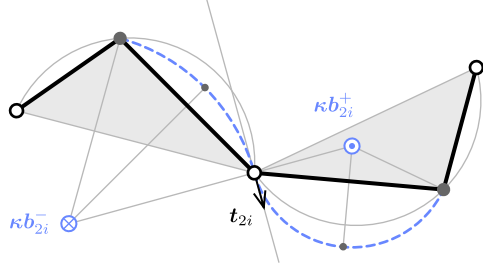
This way, the determination of the tangent vectors – or equivalently the section normals – in the static equilibrium configuration will be done in the flow of the dynamic relaxation process, without the need of introducing any additional degrees of freedom (for instance the usual Euler angles). The position of the vertices rules the orientation of the section normals.

Left/right bending moment at handle vertices

Given the unit tangent vector \mathbf{t}_{2i} , one can define the left (κ_{2i}^-) and right (κ_{2i}^+) curvature at handle vertex \mathbf{x}_{2i} . The left curvature is initially evaluated from the left osculating circle, defined as the circle passing through \mathbf{x}_{2i-1} and \mathbf{x}_{2i} and tangent to \mathbf{t}_{2i} at \mathbf{x}_{2i} . The right curvature is initially evaluated from the right osculating circle, defined as the circle passing

⁵Consequently, this model assumes that the field of tangents along the centerline is continuous and is thus unable to model cases where the centerline is not at least C^1 . In such case the beam must be considered as two parts glued together.

through \mathbf{x}_{2i} and \mathbf{x}_{2i+1} and tangent to \mathbf{t}_{2i} at \mathbf{x}_{2i} .^{6,7}



$$\begin{aligned}\kappa b_{2i}^- &= \frac{2}{l_{2i-1}} \mathbf{u}_{2i-1} \times \mathbf{t}_{2i} \\ \kappa b_{2i}^+ &= \frac{2}{l_{2i}} \mathbf{t}_{2i} \times \mathbf{u}_{2i}\end{aligned}$$

However, this values need to be adjusted so that the static condition for rotational equilibrium is satisfied at all time ($\mathbf{M}^{ext} + \mathbf{M}^+ - \mathbf{M}^- = 0$). Then, this condition will be satisfied in particular at the end of the solving process. To achieve this goal, we first compute a realistic mean value (\mathbf{M}_{2i}) for the internal bending moment as :

$$\mathbf{M}_{2i}^\perp = \frac{1}{2} \mathbf{B}_{i-1} (\kappa b_{2i}^- - \bar{\kappa} b_{2i}^-) + \frac{1}{2} \mathbf{B}_i (\kappa b_{2i}^+ - \bar{\kappa} b_{2i}^+) \quad (6.14)$$

To enforce the jump discontinuity in bending moment ($\mathbf{M}^{ext} = \mathbf{M}^- - \mathbf{M}^+$) across the handle vertex, we define the left and right bending moments at \mathbf{x}_{2i} as :

$$\mathbf{M}_{2i}^{\perp-} = \mathbf{M}_{2i} + \frac{1}{2} \mathbf{M}_{2i}^{ext} \quad (6.15a)$$

$$\mathbf{M}_{2i}^{\perp+} = \mathbf{M}_{2i} - \frac{1}{2} \mathbf{M}_{2i}^{ext} \quad (6.15b)$$

Note that in the case where no external concentrated bending moment is applied to the handle vertex, the internal bending moment is continuous across the vertex.

Left/right curvature at handle vertices

Finally, the left and right curvature at handle vertex \mathbf{x}_{2i} are computed back with the constitutive law :

$$\kappa b_{2i}^- = \mathbf{B}_{i-1}^{-1} \mathbf{M}_{2i}^{\perp-} + \bar{\kappa} b_{2i}^- \quad (6.16a)$$

$$\kappa b_{2i}^+ = \mathbf{B}_i^{-1} \mathbf{M}_{2i}^{\perp+} + \bar{\kappa} b_{2i}^+ \quad (6.16b)$$

⁶Remark that the centerline is now approximated with a biarc in the vicinity of \mathbf{x}_{2i} . This is the reason why this model is called the “biarc model”.

⁷This model offers the ability to represent discontinuities in curvature – thus in bending moment – at handle vertices as the left and right curvatures does not necessarily agree. This is quite different from the classical 3-dof element [Bar99, ABW99, DBC06] which assumes that the curvature – thus the bending moment – is C^0 and can be evaluated at every vertices from the circumscribed osculating circle.

Bending moment at ghost vertices

The internal bending moment at ghost vertices is simply given by the constitutive law as :

$$M_{2i-1}^\perp = B_{i-1}(\kappa b_{2i-1} - \bar{\kappa} \bar{b}_{2i-1}) \quad (6.17a)$$

$$M_{2i+1}^\perp = B_i(\kappa b_{2i+1} - \bar{\kappa} \bar{b}_{2i+1}) \quad (6.17b)$$

6.1.7 Discret rate of twist and twisting moment

We assume the twisting moment and the rate of twist to vary linearly over $\mathbf{x}_{2i}, \mathbf{x}_{2i+2}$. Thus, the material twist of the rod at mid edge is given by :

$$\tau_{i+1/2} = \frac{\Delta\theta_i}{l_i} \quad (6.18a)$$

$$\varkappa_{3,i+1/2} = \frac{\Delta\theta_i}{\bar{l}_i} \quad (6.18b)$$

To compute $\Delta\theta_i = \theta_{i+1} - \theta_i$ imagine that the rod si framed with a Bishop frame $\{\mathbf{u}, \mathbf{v}, \mathbf{t}\}$. Because the material frame $\{\mathbf{d}_1, \mathbf{d}_2, \mathbf{d}_3\}$ is also adapted to the rod centerline, it can be transformed into the Bishop frame with a single rotation of angle $\theta(s)$ around $\mathbf{d}_3(s) = \mathbf{t}(s)$. Because the Bishop frame does not twist around \mathbf{d}_3 , the rate of change of angle θ along the curve directly leads to the computation of the rate of twist as exposed in eq. (6.18b).

In the discrete case, although it is possible to frame the whole curve with a Bishop frame to achieve the computation of the rate of twist, it is more convenient to measure $\Delta\theta_i$ step by step using the existing material frames at vertices \mathbf{x}_i and \mathbf{x}_{i+1} . This is done in a to step process :

1. Parallel transport the material frame $\{\mathbf{d}_{1,i}, \mathbf{d}_{2,i}, \mathbf{d}_{3,i}\}$ at vertex \mathbf{x}_i onto vertex \mathbf{x}_{i+1} . We call $\{\mathbf{d}_{1,i}^{\parallel}, \mathbf{d}_{2,i}^{\parallel}, \mathbf{d}_{3,i}^{\parallel}\}$ the resulting framed positioned at \mathbf{x}_{i+1} such that $\mathbf{d}_{3,i}^{\parallel} = \mathbf{d}_{3,i+1}$.
2. Measure $\Delta\theta_i = \angle(\mathbf{d}_{1,i}^{\parallel}, \mathbf{d}_{1,i+1}) = \angle(\mathbf{d}_{2,i}^{\parallel}, \mathbf{d}_{2,i+1})$ as the oriented angle needed to align $\mathbf{d}_{1,i}^{\parallel}$ with $\mathbf{d}_{1,i+1}$ (or $\mathbf{d}_{2,i}^{\parallel}$ with $\mathbf{d}_{2,i+1}$) by a rotation of angle $\Delta\theta_i$ around $\mathbf{d}_{3,i+1} = \mathbf{t}_{i+1}$.

Consequently, the twisting moment at mid span of each edge is computed directly with the appropriate constitutive equation :

$$Q_{2i+1/2} = Q_{2i+1/2} \mathbf{u}_{2i} \quad , \quad Q_{2i+1/2} = G J_i (\varkappa_{3,2i+1/2} - \bar{\varkappa}_{3,2i+1/2}) \quad (6.19a)$$

$$Q_{2i+3/2} = Q_{2i+3/2} \mathbf{u}_{2i+1} \quad , \quad Q_{2i+3/2} = G J_i (\varkappa_{3,2i+3/2} - \bar{\varkappa}_{3,2i+3/2}) \quad (6.19b)$$

Remark the sign convention : as expected, when edge \mathbf{e}_i suffers a positive twist ($\varkappa_{3,i+1/2} > 0$), frame $\{\mathbf{d}_{1,i+1}, \mathbf{d}_{2,i+1}, \mathbf{d}_{3,i+1}\}$ makes frame $\{\mathbf{d}_{1,i}, \mathbf{d}_{2,i}, \mathbf{d}_{3,i}\}$ to rotate positively around \mathbf{u}_i as $Q_{i+1/2} > 0$.

6.1.8 Discret shear force

Recall that in Kirchhoff's theory the shear force is a reacting parameter, computed from the equilibrium equations and not from a constitutive law. Firstly, remark that the shear force can be factorized under the following expression :

$$\mathbf{F}^\perp = F_1 \mathbf{d}_1 + F_2 \mathbf{d}_2 = -\mathbf{d}_3 \times (\mathbf{d}_3 \times \mathbf{F}) \quad (6.20)$$

Then, combining eq. (5.68d) and (5.68e) – where the inertial terms are neglected – with eq. (6.20) leads to the following vectoriel form of the shear force :

$$\mathbf{F}^\perp = (1 + \epsilon)^{-1} \mathbf{d}_3 \times \left(\frac{\partial \mathbf{M}}{\partial s} + \mathbf{m} \right) = \mathbf{d}_3 \times \left(\frac{\partial \mathbf{M}}{\partial s_t} + \frac{\mathbf{m}}{1 + \epsilon} \right) \quad (6.21)$$

In the discrete case, the shear force is evaluated at mid span of each edge by :

$$\mathbf{F}_{2i+1/2}^\perp = \mathbf{u}_{2i} \times \left(\frac{\mathbf{M}_{2i+1} - \mathbf{M}_{2i}^+}{l_{2i}} + \frac{\bar{l}_{2i}}{l_{2i}} \mathbf{m}_i \right) \quad (6.22a)$$

$$\mathbf{F}_{2i+3/2}^\perp = \mathbf{u}_{2i+1} \times \left(\frac{\mathbf{M}_{2i+2}^- - \mathbf{M}_{2i+1}}{l_{2i+1}} + \frac{\bar{l}_{2i+1}}{l_{2i+1}} \mathbf{m}_i \right) \quad (6.22b)$$

Remark that the derivative of the internal moments at mid edge is evaluated by the finite difference of the moment between the two closest vertices. This is in accordance with the quadratic interpolation method of a vector-valued function given in appendix B.

Expressed in the form of eq. (6.22a) and (6.22b), the discrete shear force has the interesting property to remain strictly orthogonal to $\mathbf{d}_{3,i+1/2} = \mathbf{u}_i$. While this is true in the continuous world, this property can easily be lost in the discrete case where mean values and derivatives are evaluated through finite summations or finite differences.

Matrix notation

Because there is a derivation with respect to s in eq. (6.22a) and (6.22b), one must be very careful when writing these equations in matrix notation. Indeed, their counterparts will translate differently whether the symbols will be decomposed in the *global* frame basis or in the *material* frame basis.

If the symbols are decomposed in the *global* frame basis the translation is straightforward as the derivative of a vector is the vector of the derived components :

$$\mathbf{M} = \begin{bmatrix} M_x \\ M_y \\ M_z \end{bmatrix}, \quad \mathbf{M}' = \begin{bmatrix} M_x \\ M_y \\ M_z \end{bmatrix}' = \begin{bmatrix} M'_x \\ M'_y \\ M'_z \end{bmatrix} \quad (6.23)$$

Thus, in the discrete case, the evaluation of the derivative of the moment at mid-edge is

achieved thanks to the finite difference formula :

$$\mathbf{M}'_{2i+1/2} \simeq \frac{1}{l_{2i}} \left([\mathbf{M}_x \quad \mathbf{M}_y \quad \mathbf{M}_z]_{2i+1}^T - [\mathbf{M}_x \quad \mathbf{M}_y \quad \mathbf{M}_z]_{2i}^T \right) \quad (6.24)$$

However, if the symbols are given in the *material* frame basis, the derivation must take into account the spatial velocity $\boldsymbol{\varkappa}$ of the material frame :

$$\mathbf{M} = \begin{bmatrix} M_1 \\ M_2 \\ Q \end{bmatrix}, \quad \mathbf{M}' = \begin{bmatrix} M_1 \\ M_2 \\ Q \end{bmatrix}' = \begin{bmatrix} M'_1 \\ M'_2 \\ Q' \end{bmatrix} + \begin{bmatrix} \varkappa_1 \\ \varkappa_2 \\ \varkappa_3 \end{bmatrix} \times \begin{bmatrix} M_1 \\ M_2 \\ Q \end{bmatrix} \quad (6.25)$$

Thus, in the discrete case, the evaluation of the derivative of the moment at mid-edge is still achieved thanks to the finite difference formula, but takes a very different matrix form :

$$\begin{aligned} \mathbf{M}'_{2i+1/2} &\simeq \frac{1}{l_{2i}} \left([\mathbf{M}_1 \quad \mathbf{M}_2 \quad Q]_{2i+1}^T - [\mathbf{M}_1 \quad \mathbf{M}_2 \quad Q]_{2i}^T \right) \\ &+ \frac{1}{2} \left([\varkappa_1 \quad \varkappa_2 \quad \varkappa_3]_{2i}^T + [\varkappa_1 \quad \varkappa_2 \quad \varkappa_3]_{2i+1}^T \right) \\ &\times \frac{1}{2} \left([\mathbf{M}_1 \quad \mathbf{M}_2 \quad Q]_{2i}^T + [\mathbf{M}_1 \quad \mathbf{M}_2 \quad Q]_{2i+1}^T \right) \end{aligned} \quad (6.26)$$

Although this paragraph could seem superfluous to the reader, this point is a matter of concern when implementing the model into an algorithm. Indeed, the developer always has the choice between two natural data structures where vectors are represented by a triplet either in the global frame basis or in the material frame basis (see eq. (6.5)). Even more, he can decide to mix the two for practical reasons, for instance if it leads to less arithmetic computations. In particular, the stiffness matrix has a nice diagonal shape when written in the material frame basis. Thus it seems desirable to do the computation of the bending moment in this basis. On the contrary, we've just seen that it seems easier to compute the shear force in the global frame basis.

6.1.9 Interpolation

6.2 Conclusion

Remind that the beam is subject to a distributed external force \mathbf{f}_{ext} and a distributed external moment \mathbf{m}_{ext} .

We neglect rotational inertial effects on \mathbf{d}_1 et \mathbf{d}_2 in (??) and (??) which leads to the following shear force :

$$\mathbf{F}^\perp(s) = \mathbf{d}_3 \times (\mathbf{M}' + \boldsymbol{\varkappa} \times \mathbf{M} + \mathbf{m}_{ext}) \quad (6.27)$$

$$\mathbf{F}^\parallel(s) = N\mathbf{d}_3 \quad (6.28)$$

We may neglect as well the last term ($\tau \mathbf{M}$) and get back to the shear force obtained by the variational approach. The total internal force acting on the beam is hence given by :

$$\mathbf{F}(s) = \mathbf{N}(s) + \mathbf{T}(s) \quad (6.29)$$

Sections are subject to the following rotational moment around the centerline :

$$\boldsymbol{\Gamma}(s) = Q' + \mathbf{d}_3 \cdot (\kappa \mathbf{b} \times \mathbf{M} + \mathbf{m}_{ext}) \quad (6.30)$$

6.3 References

- [ABW99] S. Adriaenssens, M. Barnes, and C. Williams. “A new analytic and numerical basis for the form-finding and analysis of spline and gridshell structures”. In: *Computing Developments in Civil and Structural Engineering*. Ed. by B. Kumar and B. H. V. Topping. Edinburgh: Civil-Comp Press, 1999, pp. 83–91.
- [Bar99] M. Barnes. “Form finding and analysis of tension structures by dynamic relaxation”. In: *International Journal of Space Structures* 14.2 (1999), pp. 89–104.
- [DBC06] C. Douthe, O. Baverel, and J.-F. Caron. “Formfinding of a grid shell in composite materials”. In: *Journal of the IASS* 47 (2006), pp. 53–62.

Appendix Part III

A Calculus of variations

A.1 Introduction

In this appendix we drawback essential mathematical concepts for the calculus of variations. Recall how the notion of energy, gradients are extended to function spaces.

[AMR02]

A.2 Spaces

A.2.1 Normed space

A *normed space* $V(\mathbb{K})$ is a vector space V over the scalar field \mathbb{K} with a norm $\|\cdot\|$.

A *norm* is a map $\|\cdot\| : V \times V \mapsto \mathbb{K}$ which satisfies :

$$\forall x \in V, \quad \|x\| = 0_{\mathbb{K}} \Rightarrow x = 0_V \quad (\text{A.1a})$$

$$\forall x \in V, \forall \lambda \in \mathbb{K}, \quad \|\lambda x\| = |\lambda| \|x\| \quad (\text{A.1b})$$

$$\forall (x, y) \in V^2, \quad \|x + y\| \leq \|x\| + \|y\| \quad (\text{A.1c})$$

A.2.2 Inner product space

A *inner product space* or *pre-hilbert space* $E(\mathbb{K})$ is a vector space E over the scalar field \mathbb{K} with an inner product.

An *inner product* is a map $\langle ; \rangle : E \times E \mapsto \mathbb{K}$ which is bilinear, symmetric and positive-

Appendix A. Calculus of variations

definite :

$$\forall(x, y, z) \in E^3, \forall(\lambda, \mu) \in \mathbb{K}^2, \quad \begin{aligned} \langle \lambda x + \mu y ; z \rangle &= \lambda \langle x ; z \rangle + \mu \langle y ; z \rangle \\ \langle x ; \lambda y + \mu z \rangle &= \lambda \langle x ; y \rangle + \mu \langle x ; z \rangle \end{aligned} \quad (\text{A.2a})$$

$$\forall(x, y) \in E^2, \quad \langle x ; y \rangle = \langle y ; x \rangle \quad (\text{A.2b})$$

$$\forall x \in E, \quad \langle x ; x \rangle \geqslant 0_{\mathbb{K}} \quad (\text{A.2c})$$

$$\forall x \in E, \quad \langle x ; x \rangle = 0_{\mathbb{K}} \Rightarrow x = 0_E \quad (\text{A.2d})$$

Moreover, an inner product naturally induces a norm on E defined by :

$$\forall x \in E, \quad \|x\| = \sqrt{\langle x ; x \rangle} \quad (\text{A.3})$$

Thus, an inner product vector space is also naturally a normed vector space.

A.2.3 Euclidean space

An *Euclidean space* $\mathcal{E}(\mathbb{R})$ is a finite-dimensional real vector space with an inner product. Thus, distances and angles between vectors could be defined and measured regarding to the norm associated with the chosen inner product.

An Euclidean space is nothing but a finite-dimensional real pre-hilbert space.

A.2.4 Banach space

A *Banach space* $\mathcal{B}(\mathbb{K})$ is a complete normed vector space, which means that it is a normed vector space in which every Cauchy sequence of \mathcal{B} converges in \mathcal{B} for the given norm.

Thus, a Banach space is a vector space with a metric that allows the computation of vector length and distance between vectors and is complete in the sense that a Cauchy sequence of vectors always converges to a well defined limit in that space.

A.2.5 Hilbert space

A *Hilbert space* is an inner product vector space $\mathcal{H}(\mathbb{K})$ such that the natural norm induced by the inner product turns \mathcal{H} into a complete metric space (i.e. every Cauchy sequence of \mathcal{H} converges in \mathcal{H}).

The Hilbert space concept is a generalization of the Euclidean space concept. In physics it's common to encounter Hilbert spaces as infinite-dimensional function spaces.

Hilbert spaces are Banach spaces, but the converse does not hold generally.

For example, $\mathcal{L}^2([a, b])$ is an infinite-dimensional Hilbert space with the canonical inner product $\langle f ; g \rangle = \int_a^b fg$.

Note that \mathcal{L}^2 is the only Hilbert space among the \mathcal{L}^p spaces.

A.3 Derivative

The well known notion of function derivative in $\mathbb{R}^{\mathbb{R}}$ can be extended to maps between Banach spaces. This is useful in physics when formulating problems as variational problems, usually in terms of energy minimization. Indeed, energy is generally defined over a functional vector space and not simply over the real line.

In this case, the research of minimal values of a potential energy rests on the calculus of variations of the energy function compared to variations to other functions defining the problem (geometry, materials, boundary conditions, ...).

Mathematical concepts extended well-known notions of derivative, jacobian and hessian in Euclidean spaces (typically \mathbb{R}^2 or \mathbb{R}^3) for Banach functional spaces.

A.3.1 Fréchet derivative

Differentiability

Let \mathcal{B}_V and \mathcal{B}_W be two Banach spaces and $U \subset \mathcal{B}_V$ an open subset of \mathcal{B}_V . Let $f : u \mapsto f(u)$ be a function of $U^{\mathcal{B}_W}$. f is said to be *Fréchet differentiable* at $u_0 \in U$ if there exists a continuous linear operator $\mathbf{D}f(u_0) \in \mathcal{L}(\mathcal{B}_V, \mathcal{B}_W)$ such that :

$$\lim_{h \rightarrow 0} \frac{f(u_0 + h) - f(u_0) - \mathbf{D}f(u_0) \cdot h}{\|h\|} = 0 \quad (\text{A.4a})$$

Or, equivalently :

$$f(u_0 + h) = f(u_0) + \mathbf{D}f(u_0) \cdot h + o(h) \quad , \quad \lim_{h \rightarrow 0} \frac{o(h)}{\|h\|} = 0 \quad (\text{A.4b})$$

In the literature, it is common to find the following notations : $df = \mathbf{D}f(u_0) \cdot h = \mathbf{D}f_{u_0}(h) = \mathbf{D}f(u_0, h)$ for the differential of f , which means nothing but $\mathbf{D}f(u_0)$ is linear regarding h . The dot denotes the evaluation of $\mathbf{D}f(u_0)$ at h . This notation can be ambiguous as far as the linearity of $\mathbf{D}f(u_0)$ in h is denoted as a product which is not explicitly defined.

Derivative

If f is Fréchet differentiable at $u_0 \in U$, the continuous linear operator $\mathbf{D}f(u_0) \in \mathcal{L}(\mathcal{B}_V, \mathcal{B}_W)$ is called the *Fréchet derivative* of f at u_0 and is also denoted :

$$f'(u_0) = \mathbf{D}f(u_0) \quad (\text{A.5})$$

Appendix A. Calculus of variations

f is said to be \mathcal{C}^1 in the sens of Fréchet if f is Fréchet differentiable for all $u \in U$ and the function $\mathbf{D}f : u \mapsto f'(u)$ of $U^{\mathcal{L}(\mathcal{B}_V, \mathcal{B}_W)}$ is continuous.

Differential or total derivative

$df = \mathbf{D}f(u_0) \cdot h$ is sometimes called the *differential* or *total derivative* of f and represents the change in the function f for a perturbation h from u_0 .

Higer derivatives

Because the differential of f is a linear map from \mathcal{B}_V to $\mathcal{L}(\mathcal{B}_V, \mathcal{B}_W)$ it is possible to look for the differentiability of $\mathbf{D}f$. If it exists, it is denoted \mathbf{D}^2f and maps \mathcal{B}_V to $\mathcal{L}(\mathcal{B}_V, \mathcal{L}(\mathcal{B}_V, \mathcal{B}_W))$.

A.3.2 Gâteaux derivative

Directional derivative

Let \mathcal{B}_V and \mathcal{B}_W be two Banach spaces and $U \subset \mathcal{B}_V$ an open subset of \mathcal{B}_V . Let $f : u \mapsto f(u)$ be a function of $U^{\mathcal{B}_W}$. f is said to have a *derivative in the direction* $h \in \mathcal{B}_V$ at $u_0 \in U$ if :

$$\frac{d}{d\lambda} f(u_0 + \lambda h) \Big|_{\lambda=0} = \lim_{\lambda \rightarrow 0} \frac{f(u_0 + \lambda h) - f(u_0)}{\lambda} \quad (\text{A.6})$$

exists. This element of \mathcal{B}_W is called the *directional derivative* of f in the direction h at u_0 .

Differentiability

Let \mathcal{B}_V and \mathcal{B}_W be two Banach spaces and $U \subset \mathcal{B}_V$ an open subset of \mathcal{B}_V . Let $f : u \mapsto f(u)$ be a function of $U^{\mathcal{B}_W}$. f is said to be *Gâteaux differentiable* at $u_0 \in U$ if there exists a continious linear operator $\mathbf{D}f(u_0) \in \mathcal{L}(\mathcal{B}_V, \mathcal{B}_W)$ such that :

$$\forall h \in \mathcal{U}, \quad \lim_{\lambda \rightarrow 0} \frac{f(u_0 + \lambda h) - f(u_0)}{\lambda} = \frac{d}{d\lambda} f(u_0 + \lambda h) \Big|_{\lambda=0} = \mathbf{D}f(u_0) \cdot h \quad (\text{A.7a})$$

Or, equivalently :

$$\forall h \in \mathcal{U}, \quad f(u + \lambda h) = f(u) + \lambda \mathbf{D}f(u_0) \cdot h + o(\lambda) \quad , \quad \lim_{\lambda \rightarrow 0} \frac{o(\lambda)}{\lambda} = 0 \quad (\text{A.7b})$$

In other words, it means that all the directional derivatives of f exist at u_0 .

Derivative

If f is Gâteaux differentiable at $u_0 \in U$, the continuous linear operator $\mathbf{D}f(u_0) \in \mathcal{L}(\mathcal{B}_V, \mathcal{B}_W)$ is called the *Gâteaux derivative* of f at u_0 and is also denoted :

$$f'(u_0) = \mathbf{D}f(u_0) \quad (\text{A.8})$$

f is said to be \mathcal{C}^1 in the sens of Gâteaux if f is Gâteaux differentiable for all $u \in U$ and the function $\mathbf{D}f : u \mapsto f'(u)$ of $U^{\mathcal{L}(\mathcal{B}_V, \mathcal{B}_W)}$ is continuous.

The Gâteaux derivative is a weaker form of derivative than the Fréchet derivative. If f is Fréchet differentiable, then it is also Gâteaux differentiable and its Fréchet and Gâteaux derivatives agree, but the converse does not hold generally.

A.3.3 Useful properties

Let $\mathcal{B}_V, \mathcal{B}_W$ and \mathcal{B}_Z be three Banach spaces. Let $f, g : \mathcal{B}_V \rightarrow \mathcal{B}_W$ and $h : \mathcal{B}_W \rightarrow \mathcal{B}_Z$ be three Gâteaux differentiable functions. Then, the following useful properties holds :

$$\mathbf{D}(f + g)(u) = \mathbf{D}f(u) + \mathbf{D}g(u) \quad (\text{A.9})$$

$$\mathbf{D}(f \circ h)(u) = \mathbf{D}h(f(u)) \circ \mathbf{D}f(u) = \mathbf{D}h(f(u)) \cdot \mathbf{D}f(u) \quad (\text{A.10})$$

Recall that the composition of $\mathbf{D}h(f(u))$ with $\mathbf{D}f(u)$ means “ $\mathbf{D}h(f(u))$ applied to $\mathbf{D}f(u)$ ” and is also denoted by \cdot as explained previously.

A.3.4 Partial derivative

Following [AMR02] the main results on partial derivatives of two-variables functions are presented here. They are generalizable to n-variables functions.

Definition

Let $\mathcal{B}_{V_1}, \mathcal{B}_{V_2}$ and \mathcal{B}_W be three Banach spaces and $U \subset \mathcal{B}_{V_1} \oplus \mathcal{B}_{V_2}$ an open subset of $\mathcal{B}_{V_1} \oplus \mathcal{B}_{V_2}$. Let $f : u \mapsto f(u)$ be a function of $U^{\mathcal{B}_W}$. Let $u_0 = (u_{01}, u_{02}) \in U$. If the derivatives of the following functions exist :

$$\begin{aligned} f_1 : \mathcal{B}_{V_1} &\longrightarrow \mathcal{B}_W \\ u_1 &\mapsto f(u_1, u_{02}) \end{aligned} \quad , \quad \begin{aligned} f_2 : \mathcal{B}_{V_2} &\longrightarrow \mathcal{B}_W \\ u_2 &\mapsto f(u_{01}, u_2) \end{aligned} \quad (\text{A.11})$$

they are called *partial derivatives* of f at u_0 and are denoted $\mathbf{D}_1 f(u_0) \in \mathcal{L}(\mathcal{B}_{V_1}, \mathcal{B}_W)$ and $\mathbf{D}_2 f(u_0) \in \mathcal{L}(\mathcal{B}_{V_2}, \mathcal{B}_W)$.

Differentiability

Let \mathcal{B}_{V_1} , \mathcal{B}_{V_2} and \mathcal{B}_W be three Banach spaces and $U \subset \mathcal{B}_{V_1} \oplus \mathcal{B}_{V_2}$ an open subset of $\mathcal{B}_{V_1} \oplus \mathcal{B}_{V_2}$. Let $f : u \mapsto f(u)$ be a function of $U^{\mathcal{B}_W}$. If f is differentiable, then the partial derivatives exist and satisfy for all $h = (h_1, h_2) \in \mathcal{B}_{V_1} \oplus \mathcal{B}_{V_2}$:

$$\mathbf{D}_1 f(u) \cdot h_1 = \mathbf{D}f(u) \cdot (h_1, 0) \quad (\text{A.12})$$

$$\mathbf{D}_2 f(u) \cdot h_2 = \mathbf{D}f(u) \cdot (0, h_2) \quad (\text{A.13})$$

$$\mathbf{D}f(u) \cdot (h_1, h_2) = \mathbf{D}_1 f(u) \cdot h_1 + \mathbf{D}_2 f(u) \cdot h_2 \quad (\text{A.14})$$

A.4 Gradient vector

Let \mathcal{H} be a Hilbert space with the inner product denoted $\langle \cdot, \cdot \rangle$. Let $U \subset \mathcal{H}$ an open subset of \mathcal{H} . Let $F : u \mapsto F(u)$ be a scalar function of $U^{\mathbb{R}}$. The *gradient* of F is the map $\text{grad } F : x \mapsto (\text{grad } F)(x)$ of $U^{\mathcal{H}}$ such that :

$$\forall h \in \mathcal{H}, \quad \langle (\text{grad } F)(x), h \rangle = \mathbf{D}F(x) \cdot h \quad (\text{A.15})$$

Note that the gradient vector depends on the chosen inner product. For $\mathcal{H} = \mathbb{R}^n$ with the canonical inner product, one can recall the usual definition of the gradient vector and the corresponding linear approximation of F :

$$\mathbf{F}_{x+h} = \mathbf{F}_x + (\text{grad } F)_x^T H + o(H) \quad , \quad \text{grad } F_x = \begin{bmatrix} \frac{\partial F}{\partial x_1} \\ \vdots \\ \frac{\partial F}{\partial x_n} \end{bmatrix} \in \mathbb{R}^n \quad (\text{A.16})$$

Recall that the canonical inner product on \mathbb{R}^n is such that $\langle x, y \rangle = X^T Y$ in a column vector representation. In this case it is common to denote $\text{grad } F = \nabla F$.

For function spaces the usual definition of the gradient can be extended. For instance if F is a scalar function on \mathcal{L}^2 , the gradient of F is the unique function (if it exists) from \mathcal{L}^2 which satisfies :

$$\forall h \in \mathcal{L}^2, \quad \mathbf{D}F(x) \cdot h = \langle (\text{grad } F)(x), h \rangle = \int (\text{grad } F) h \quad (\text{A.17})$$

In this case it is common to denote $\text{grad } F = \frac{\delta F}{\delta x}$. The gradient is also known as the *functional derivative*. The existence and unicity of $\text{grad } F$ is ensured by the *Riesz representation theorem*.

A.5 Jacobian matrix

Let f be a differentiable function from \mathbb{R}^n to \mathbb{R}^m . The *differential* or *total derivative* of such a fonction is a linear application from \mathbb{R}^n to \mathbb{R}^m which could be represented with the

following matrix called the *jacobian matrix* :

$$\mathbf{D}f(x) = \mathbf{J}_x = \frac{df}{dx} = \begin{bmatrix} \frac{\partial f}{\partial x_1} & \cdots & \frac{\partial f}{\partial x_n} \end{bmatrix} = \begin{bmatrix} \frac{\partial f_1}{\partial x_1} & \cdots & \frac{\partial f_1}{\partial x_n} \\ \vdots & \ddots & \vdots \\ \frac{\partial f_m}{\partial x_1} & \cdots & \frac{\partial f_m}{\partial x_n} \end{bmatrix} \in \mathcal{M}_{m,n}(\mathbb{R}) \quad (\text{A.18})$$

Thus, with the matrix notation, the Taylor expansion takes the following form :

$$\mathbf{F}_{x+h} = \mathbf{F}_x + \mathbf{J}_x H + o(H) \quad (\text{A.19})$$

In the cas $m = 1$, the jacobian matrix of the functional F is nothing but the gradient vector transpose itself :

$$\mathbf{D}F(x) = \mathbf{J}_x = \frac{dF}{dx} = \begin{bmatrix} \frac{\partial F}{\partial x_1} & \cdots & \frac{\partial F}{\partial x_n} \end{bmatrix} = \nabla F^T \quad (\text{A.20})$$

A.6 Hessian

Let F be a differentiable scalar function from \mathbb{R}^n to \mathbb{R} . The second order differential of such a fonction is a linear application from \mathbb{R}^n to \mathbb{R}^n which could be represented with the following matrix called the *hessian matrix* :

$$\mathbf{D}^2F(x) = \mathbf{H}_x = \frac{d^2F}{dx}(x) = \begin{bmatrix} \frac{\partial F_1^2}{\partial x_1^2} & \frac{\partial F_1^2}{\partial x_1 \partial x_2} & \cdots & \frac{\partial F_1^2}{\partial x_1 \partial x_n} \\ \frac{\partial F_1^2}{\partial x_2 \partial x_1} & \frac{\partial F_1^2}{\partial x_2^2} & \cdots & \frac{\partial F_1^2}{\partial x_2 \partial x_n} \\ \vdots & \ddots & \ddots & \vdots \\ \frac{\partial F_p^2}{\partial x_n \partial x_1} & \frac{\partial F_p^2}{\partial x_n \partial x_2} & \cdots & \frac{\partial F_p^2}{\partial x_n^2} \end{bmatrix} \in \mathcal{M}_{n,n}(\mathbb{R}) \quad (\text{A.21})$$

Thus, with the matrix notation, the Taylor expansion takes the following form :

$$\mathbf{F}_{x+h} = \mathbf{F}_x + \mathbf{J}_x H + \frac{1}{2}H^T \mathbf{H}_x H + o(H) \quad (\text{A.22})$$

A.7 Functional

A *functional* is a map from a vector space $E(\mathbb{K})$ into its underlying scalar field \mathbb{K} . Here $\mathcal{E}_p[\mathbf{x}, \theta]$ is a functional depending over \mathbf{x} and θ .

A.8 References

- [AMR02] R. Abraham, J. E. Marsden, and T. Ratiu. *Manifolds, Tensor Analysis, and Applications (Ralph Abraham, Jerrold E. Marsden and Tudor Ratiu)*. 2002, p. 617.

B Parabolic interpolation

B.1 Introduction

In this appendix, we give the required formulas to conduct a parabolic interpolation of a scalar or vector-valued function over an interval.

We look for a polynomial interpolation of order 2 of a continuous scalar or vector-valued function $\mathbf{V}: t \mapsto \mathbf{V}(t)$ over the interval $[t_0, t_2]$; supposing that the value of the function is known for three distinct parameters $t_0 < t_1 < t_2$:

$$\mathbf{V}(t_0) = \mathbf{V}_0 \tag{B.1a}$$

$$\mathbf{V}(t_1) = \mathbf{V}_1 \tag{B.1b}$$

$$\mathbf{V}(t_2) = \mathbf{V}_2 \tag{B.1c}$$

This interpolation method is employed several times in this thesis, for instance to evaluate the position of a kinetic energy peak during the dynamic relaxation process. It is also employed for evaluating the bending moment and the curvature of a discrete rod at mid-edge, knowing its values at vertices.

Note that this interpolation method is valid if the basis in which \mathbf{V} is decomposed does not depend on the parameter t . Otherwise, the classical transportation term should be considered ($\boldsymbol{\omega} \times \mathbf{V}$).

B.2 Lagrange interpolating polynomial

The Lagrange interpolation of order two is given by the following polynomial :

$$\mathbf{V}(t) = \mathbf{V}_0 \frac{(t - t_1)(t - t_2)}{(t_0 - t_1)(t_0 - t_2)} + \mathbf{V}_1 \frac{(t - t_0)(t - t_2)}{(t_1 - t_0)(t_1 - t_2)} + \mathbf{V}_2 \frac{(t - t_0)(t - t_1)}{(t_2 - t_0)(t_2 - t_1)} \tag{B.2}$$

B.3 Reparametrization

Lets introduce the distances l_0 and l_1 in the parametric space :

$$l_0 = t_1 - t_0 \quad (\text{B.3a})$$

$$l_1 = t_2 - t_1 \quad (\text{B.3b})$$

Lets introduce the change of variable $u = t - t_1$. The polynomial in [eq. \(B.2\)](#) can be rewritten in the form :

$$\mathbf{V}(u) = \mathbf{V}_0 \frac{u(u - l_1)}{l_0(l_0 + l_1)} - \mathbf{V}_1 \frac{(u + l_0)(u - l_1)}{l_0 l_1} + \mathbf{V}_2 \frac{u(u + l_0)}{l_1(l_0 + l_1)} \quad (\text{B.4})$$

where :

$$u_0 = -l_0 \quad (\text{B.5a})$$

$$u_1 = 0 \quad (\text{B.5b})$$

$$u_2 = l_1 \quad (\text{B.5c})$$

The derivative of this polynomial is also required to determine the extremum value of \mathbf{V} . Differentiating [eq. \(B.4\)](#) gives :

$$\mathbf{V}'(u) = \mathbf{V}_0 \frac{2u - l_1}{l_0(l_0 + l_1)} - \mathbf{V}_1 \frac{2u + (l_0 - l_1)}{l_0 l_1} + \mathbf{V}_2 \frac{2u + l_0}{l_1(l_0 + l_1)} \quad (\text{B.6})$$

This expression can be factorized to give the more compact form :

$$\mathbf{V}'(u) = \left(\frac{\mathbf{V}_1 - \mathbf{V}_0}{l_0} \right) \frac{l_1 - 2u}{l_0 + l_1} + \left(\frac{\mathbf{V}_2 - \mathbf{V}_1}{l_1} \right) \frac{l_0 + 2u}{l_0 + l_1} \quad (\text{B.7})$$

B.4 Characteristic values

Using [eq. \(B.4\)](#) the interpolated values of \mathbf{V} at mid distance between t_0 and t_1 ($u = -l_0/2$), and at mid distance between t_1 and t_2 ($u = +l_1/2$) are given by :

$$\mathbf{V}_{01} = \mathbf{V}_0 \frac{l_0 + 2l_1}{4(l_0 + l_1)} + \mathbf{V}_1 \frac{l_0 + 2l_1}{4l_1} - \mathbf{V}_2 \frac{l_0^2}{4l_1(l_0 + l_1)} \quad (\text{B.8a})$$

$$\mathbf{V}_{12} = -\mathbf{V}_0 \frac{l_1^2}{4l_0(l_0 + l_1)} + \mathbf{V}_1 \frac{2l_0 + l_1}{4l_0} + \mathbf{V}_2 \frac{2l_0 + l_1}{4(l_0 + l_1)} \quad (\text{B.8b})$$

Using [eq. \(B.7\)](#) the interpolated values of \mathbf{V}' at mid distance between t_0 and t_1 ($u = -l_0/2$), and at mid distance between t_1 and t_2 ($u = +l_1/2$) are given by :

$$\mathbf{V}'_{01} = \frac{\mathbf{V}_1 - \mathbf{V}_0}{l_0} \quad (\text{B.9a})$$

$$\mathbf{V}'_{12} = \frac{\mathbf{V}_2 - \mathbf{V}_1}{l_1} \quad (\text{B.9b})$$

Remark that this is an interesting result as at these parameters the evaluation of \mathbf{V}' boils down to a finite difference scheme.

Using eq. (B.7) and introducing $\alpha = \frac{l_0}{l_0 + l_1}$ the interpolated values of \mathbf{V}' at t_0 , t_1 and t_2 are given by :

$$\mathbf{V}'_0 = (1 + \alpha)\mathbf{V}'_{01} - \alpha\mathbf{V}'_{12} \quad (\text{B.10a})$$

$$\mathbf{V}'_1 = (1 - \alpha)\mathbf{V}'_{01} + \alpha\mathbf{V}'_{12} \quad (\text{B.10b})$$

$$\mathbf{V}'_2 = (\alpha - 1)\mathbf{V}'_{01} + (2 - \alpha)\mathbf{V}'_{12} \quad (\text{B.10c})$$

Lets rewrite eq. (B.8a) and (B.8b) with the help of α :

$$\mathbf{V}_{01} = \frac{1}{4} \left((2 - \alpha)\mathbf{V}_0 + \frac{2 - \alpha}{1 - \alpha}\mathbf{V}_1 - \frac{\alpha^2}{1 - \alpha}\mathbf{V}_2 \right) \quad (\text{B.11a})$$

$$\mathbf{V}_{01} = \frac{1}{4} \left(-\frac{(1 - \alpha)^2}{\alpha}\mathbf{V}_0 + \frac{1 + \alpha}{\alpha}\mathbf{V}_1 + (1 + \alpha)\mathbf{V}_2 \right) \quad (\text{B.11b})$$

B.5 Extremum value

The extremum value of the parabola is obtained for $\mathbf{V}'(u^*) = 0$. It's a minimum if $\mathbf{V}'_{12} > \mathbf{V}'_{01}$ and it's a maximum if $\mathbf{V}'_{12} < \mathbf{V}'_{01}$:

$$u^* = \frac{l_1\mathbf{V}'_{01} + l_0\mathbf{V}'_{12}}{2(\mathbf{V}'_{01} - \mathbf{V}'_{12})} \quad (\text{B.12})$$

Remark that if $\mathbf{V}'_{12} = \mathbf{V}'_{01}$ it does not make sens to compute u^* as in this case the parabola degenerates into a line. The value of the function at this parameter is given by :

$$\mathbf{V}(u^*) = \mathbf{V}_1 + \frac{(l_1\mathbf{V}'_{01} + l_0\mathbf{V}'_{12})^2}{4(l_0 + l_1)(\mathbf{V}'_{01} - \mathbf{V}'_{12})} \quad (\text{B.13})$$

The parabola in eq. (B.4) now writes :

$$\mathbf{V}(u) = -\frac{\mathbf{V}'_{01} - \mathbf{V}'_{12}}{l_0 + l_1}(u - u^*)^2 + \mathbf{V}(u^*) \quad (\text{B.14})$$

The extremum is located in $[t_0, t_2]$ if the sign of \mathbf{V}' changes on this interval. This condition is satisfied whenever $\mathbf{V}'_{01} \cdot \mathbf{V}'_{12} < 0$.

Finally, in the special case of a uniform discretization where $l_0 = l_1 = l$, eq. (B.12) and (B.13) become :

$$u^* = \frac{l}{2} \left(\frac{\mathbf{V}_0 - \mathbf{V}_2}{\mathbf{V}_0 - 2\mathbf{V}_1 + \mathbf{V}_2} \right) \quad (\text{B.15a})$$

$$\mathbf{V}(u^*) = \mathbf{V}_1 - \frac{u^*}{4l}(\mathbf{V}_2 - \mathbf{V}_0) \quad (\text{B.15b})$$

Bibliography

- [AAP10] B. Audoly, M. Amar, and Y. Pomeau. *Elasticity and geometry*. 2010, p. 600.
- [AB01] S. Adriaenssens and M. Barnes. “Tensegrity spline beam and grid shell structures”. In: *Engineering Structures* 23.1 (2001), pp. 29–36.
- [ABW99] S. Adriaenssens, M. Barnes, and C. Williams. “A new analytic and numerical basis for the form-finding and analysis of spline and gridshell structures”. In: *Computing Developments in Civil and Structural Engineering*. Ed. by B. Kumar and B. H. V. Topping. Edinburgh: Civil-Comp Press, 1999, pp. 83–91.
- [Add13] B. Addis. “‘Toys that save millions’ - A history of using physical models in structural design”. In: *The Structural Engineer* 91.4 (2013), pp. 12–27.
- [Adr00] S. Adriaenssens. “Stressed spline structures”. PhD thesis. University of Bath, 2000.
- [Alv14] J. M. Alves. “Dynamic analysis of bridge girders subjected to moving loads : Numerical and analytical beam models considering warping effects”. PhD thesis. Tecnico Lisboa, 2014, p. 129.
- [AMR02] R. Abraham, J. E. Marsden, and T. Ratiu. *Manifolds, Tensor Analysis, and Applications (Ralph Abraham, Jerrold E. Marsden and Tudor Ratiu)*. 2002, p. 617.
- [Ant05] S. Antman. *Nonlinear problems of elasticity*. Applied mathematical sciences. New York: Springer, 2005, p. 838.
- [Ant74] S. Antman. “Kirchhoff’s problem for nonlinearly elastic rods”. In: *Quarterly of Applied Mathematics* XXXIV.3 (1974), pp. 221–240.
- [BAK13] M. Barnes, S. Adriaenssens, and M. Krupka. “A novel torsion/bending element for dynamic relaxation modeling”. In: *Computers & Structures* 119 (Apr. 2013), pp. 60–67.
- [Ban06] L. C. Bank. *Composites for construction : structural design with FRP materials*. 2006, p. 560.
- [Bar99] M. Barnes. “Form finding and analysis of tension structures by dynamic relaxation”. In: *International Journal of Space Structures* 14.2 (1999), pp. 89–104.

Bibliography

- [Bav+12] O. Baverel, J.-F. Caron, F. Tayeb, and L. du Peloux. “Gridshells in composite materials : construction of a 300 m² forum for the solidays’ festival in Paris”. In: *Structural Engineering International* 22.3 (2012), pp. 408–414.
- [BBC09] L. Bouhana, O. Baverel, and J.-F. Caron. “Mapping two-way continuous elastic grid on an imposed surface : application to grid shells”. In: *IASS 2009*. Valencia, Spain, 2009, pp. 989–998.
- [BBC14] L. Bouhana, O. Baverel, and J. F. Caron. “Optimization of gridshell bar orientation using a simplified genetic approach”. In: *Structural and Multidisciplinary Optimization* 50.5 (2014), pp. 839–848.
- [BDH98] R. Burton, M. Dickson, and R. Harris. “The use of roundwood thinnings in buildings : a case study”. In: *Building Research & Information* 26.2 (1998), pp. 76–93.
- [Bdo02] Bdonline.co.uk. *The other gridshell*. 2002.
- [Ben91a] E. Benvenuto. *An introduction to the history of structural mechanics : statics and resistance of solids*. New York: Springer Verlag, 1991, pp. XXI, 306.
- [Ben91b] E. Benvenuto. *An introduction to the history of structural mechanics : vaulted structures and elastic systems*. New York: Springer Verlag, 1991, pp. XXI, 255.
- [Ber+08] M. Bergou, M. Wardetzky, S. Robinson, B. Audoly, and E. Grinspun. “Discrete elastic rods”. In: *ACM SIGGRAPH* (2008), pp. 1–12.
- [Ber+10] M. Bergou, B. Audoly, E. Vouga, M. Wardetzky, and E. Grinspun. “Discrete viscous threads”. In: *ACM Transactions on ...* (2010), pp. 1–10.
- [Ber09] M. Berger. “Topological Quantities: Calculating Winding, Writhing, Linking, and Higher order Invariants”. In: *Lecture Notes in Mathematics* 1973 (2009), pp. 75–97.
- [Ber28] J. Bernoulli. *Johannis Bernoulli... Opera omnia, tam antea sparsim edita, quam hactenus inedita*. IV. sumptibus Marci-Michaelis Bousquet, 1728, p. 584.
- [BHS74] B. Burkhardt, J. Hennicke, and E. Schauer, eds. *IL10 Grid Shells*. Institut für leichte Flächentragwerke (IL). Stuttgart, 1974.
- [Bis75] R. Bishop. “There is more than one way to frame a curve”. In: *Mathematical Association of America* (1975).
- [Blo90] J. Bloomenthal. “Calculation of reference frames along a space curve”. In: *Graphics Gems*. Ed. by A. S. Glassner. Vol. 1. San Diego, CA, USA: Academic Press Professional, Inc., 1990, pp. 567–571.
- [Bob15] A. Bobenko. *Discrete differential geometry*. Second. 2015, p. 144.
- [Bou10] L. Bouhana. “Optimisation structurelle des gridshells”. PhD thesis. Université Paris-Est, 2010, p. 154.
- [Bur+78] B. Burkhardt, M. Chaitos, J. Langner, W. Langner, and G. Lubberger, eds. *IL13 Multihalle Mannheim*. Institut für leichte Flächentragwerke (IL). Stuttgart, 1978.

- [Cam+09] A. Campanile, M. Mandarino, V. Piscopo, and A. Pranzitelli. “On the exact solution of non-uniform torsion for beams with asymmetric cross-section”. In: *World Academy of Science, Engineering and Technology* 31 (2009), pp. 36–45.
- [Car+14] D. Carroll, E. Hankins, E. Kose, and I. Sterling. “A survey of the differential geometry of discrete curves”. In: *The Mathematical Intelligencer* 36.4 (2014), pp. 28–35. arXiv: [arXiv:1311.5862v1](https://arxiv.org/abs/1311.5862v1).
- [CB13] R. Casati and F. Bertails-descoubes. “Super space clothoids”. In: *SIGGRAPH*. 2013.
- [CC16] M. Collins and T. Cosgrove. “A Review of the State of the Art of Timber Gridshell Design and Construction”. In: *Civil Engineering Research in Ireland*. 2016.
- [CH02] J. Cisternas and P. Holmes. “Buckling of extensible thermoelastic rods”. In: *Mathematical and Computer Modelling* 36.3 (2002), pp. 233–243.
- [Cla03] J. L. Clarke. *Eurocomp design code and handbook : structural design of polymer composites*. 2003, p. 672.
- [Cle83] A. Clebsch. *Théorie de l'élasticité des corps solides*. Paris: Dunod, 1883, p. 900.
- [Col+93] B. Coleman, E. H. Dill, M. Lembo, L. Zheng, and I. Tobias. “On the dynamics of rods in the theory of Kirchhoff and Clebsch”. In: *Archive for Rational Mechanics and Analysis* 121.4 (1993), pp. 339–359.
- [Coo13] J. L. Coolidge. *A history of geometrical methods*. Ed. by C. Corporation. Dover Books on Mathematics. Dover Publications, 2013, p. 480.
- [CT17] J. Chilton and G. Tang. *Timber Gridshells: Architecture, structure and craft*. Routledge, 2017.
- [Cuv+17] P. Cuvilliers, C. Douthe, L. du Peloux, and R. Le Roy. “Hybrid structural skin : prototype of an elastic gridshell braced by a fibre-reinforced concrete envelope”. In: *Journal of The International Association for Shell and Spatial Structures* (2017), pp. 1–12.
- [DA14] M. A. Dias and B. Audoly. “A non-linear rod model for folded elastic strips”. In: *Journal of the Mechanics and Physics of Solids* 62.1 (2014), pp. 57–80. arXiv: [1306.5035](https://arxiv.org/abs/1306.5035).
- [DA15] M. A. Dias and B. Audoly. ““Wunderlich, meet kirchhoff” : a general and unified description of elastic ribbons and thin rods”. In: *Journal of Elasticity* 119.1 (2015), pp. 49–66. arXiv: [arXiv:1403.2094v2](https://arxiv.org/abs/1403.2094v2).
- [DAm+15a] B. D’Amico, A. Kermani, H. Zhang, A. Pugnale, S. Colabella, and S. Pone. “Timber gridshells: Numerical simulation, design and construction of a full scale structure”. In: *Structures* 3.May 2016 (2015), pp. 227–235.
- [DAm+15b] B. D’Amico, A. Kermani, H. Zhang, P. Sheperd, and C. Williams. “Optimisation of cross-section of actively bent grid shells with strength and geometric compatibility constraints”. In: *Computers & Structures* 154 (2015), pp. 163–176.

Bibliography

- [Day65] A. Day. “An Introduction to dynamic relaxation”. In: *The Engineer* (1965).
- [DBC06] C. Douthe, O. Baverel, and J.-F. Caron. “Formfinding of a grid shell in composite materials”. In: *Journal of the IASS* 47 (2006), pp. 53–62.
- [DCB10] C. Douthe, J.-F. Caron, and O. Baverel. “Gridshell structures in glass fibre reinforced polymers”. In: *Construction and Building Materials* 24.9 (2010), pp. 1580–1589.
- [Del07] J. Delcourt. “Analyse et géométrie : les courbes gauches de Clairaut à Serret”. PhD thesis. Université de Paris VI, 2007, p. 302.
- [Del11] J. Delcourt. “Analyse et géométrie, histoire des courbes gauches de Clairaut à Darboux”. In: *Archive for History of Exact Sciences* 65.3 (2011), pp. 229–293.
- [Dil92] E. H. Dill. “Kirchhoff’s theory of rods”. In: *Archive for History of Exact Sciences* (1992), p. 23.
- [DKZ14] B. D’Amico, A. Kermani, and H. Zhang. “Form finding and structural analysis of actively bent timber grid shells”. In: *Engineering Structures* 81 (2014), pp. 195–207.
- [DLP13] Y. Duan, D. Li, and P. F. Pai. “Geometrically exact physics-based modeling and computer animation of highly flexible 1D mechanical systems”. In: *Graphical Models* 75.2 (2013), pp. 56–68.
- [Dou+16] C. Douthe, R. Mesnil, H. Orts, and O. Baverel. “New shapes for elastic gridshells covered by planar facets”. In: *Proceedings of the IASS Annual Symposium*. Tokyo, Japan, 2016, pp. 1–9.
- [Dou07] C. Douthe. “Etude de structures élancées précontraintes en matériaux composites : application à la conception des gridshells”. PhD thesis. Université Paris Est, 2007, p. 274.
- [dPel+11] L. du Peloux, O. Baverel, J.-F. Caron, and F. Tayeb. “From shape to shell : a design tool to materialize freeform shapes using gridshell structures”. In: *Design Modelling Symposium*. Berlin, Deutschland, 2011.
- [dPel+15] L. du Peloux, F. Tayeb, B. Lefevre, O. Baverel, and J.-F. Caron. “Formulation of a 4-DoF torsion / bending element for the formfinding of elastic gridshells”. In: *Proceedings of the International Association for Shell and Spatial Structures*. August. Amsterdam, 2015, pp. 1–14.
- [dPel+16] L. du Peloux, F. Tayeb, O. Baverel, and J.-F. Caron. “Construction of a large composite gridshell structure: a lightweight structure made with pultruded glass fibre reinforced polymer tubes”. In: *Structural Engineering International* 26.2 (2016), pp. 160–167.
- [dVri05] R. de Vries. “Evaluating changes of writhe in computer simulations of supercoiled DNA”. In: *The Journal of Chemical Physics* 122.6 (2005).
- [DZK16] B. D’Amico, H. Zhang, and A. Kermani. “A finite-difference formulation of elastic rod for the design of actively bent structures”. In: *Engineering Structures* 117 (2016), pp. 518–527.

- [Elt84] E. Elter. “Two formulæ of the shear center”. In: *Periodica Polytechnica Mechanical Engineering* 28.2-3 (1984), pp. 179–193.
- [Eul75] L. Euler. “Continens analysin, pro incuruatione fili in fingulis punctis inuenienda”. In: *Novi Commentarii academiae scientiarum Petropolitanae* 19 (1775), pp. 340–370.
- [Far+14] R. T. Farouki, C. Giannelli, M. L. Sampoli, and A. Sestini. “Rotation-minimizing osculating frames”. In: *Computer Aided Geometric Design* 31.1 (2014), pp. 27–42.
- [Fib03] Fiberline Composites A/S. *Fiberline design manual*. May. 2003, pp. 1–326.
- [FKB16] J. G. Fernandes, P. H. Kirkegaard, and J. M. Branco. “Tectonic Design of Elastic Timber Gridshells”. In: *World Conference on Timber Engineering*. Vienna, Austria, 2016.
- [FN15] G. Filz and D. Naicu. “2 Landscapes – interaction of 2 gridshells based on a modified Stewart - Gough - principle”. In: *Proceedings of the IASS Working Groups 12 + 18*. Tokyo, Japan, 2015.
- [Fou03] Fourthdoor.org. *Growing and making Flimwell’s chestnut gridshell*. 2003.
- [Fre52] F. Frenet. “Sur les courbes à double courbure”. In: *Journal de Mathématiques Pures et Appliquées* 17 (1852), pp. 437–447.
- [Ful78] F. B. Fuller. “Decomposition of the linking number of a closed ribbon : A problem from molecular biology”. In: 75.8 (1978), pp. 3557–3561.
- [GAS06] A. Gray, E. Abbena, and S. Salamon. *Modern differential geometry of curves and surfaces with Mathematica*. Ed. by E. A. Salamon and Simon. Third. CRC Press, 2006, p. 1016.
- [Gug89] H. Guggenheimer. “Computing frames along a trajectory”. In: *Computer Aided Geometric Design* 6.1 (1989), pp. 77–78.
- [Had+16] J. Haddal Mork, S. Dyvik Hillersøy, B. Manum, A. Rønnquit, and N. Labonne. “Introducing the Segment Lath - a Simplified Modular Timber Gridshell Built in Trondheim Norway”. In: *World Conference on Timber Engineering*. 3. Vienna, Austria, 2016.
- [Har+03] R. Harris, J. Romer, O. Kelly, and S. Johnson. “Design and construction of the Downland Gridshell”. eng. In: *Building research and information* 31.6 (2003), pp. 427–454.
- [HHR08] R. Harris, S. Haskins, and J. Roynon. “The Savill Garden gridshell : Design and construction”. In: *The Structural Engineer* 86.17 (2008), pp. 27–34.
- [HK02] R. Harris and O. Kelly. “The structural engineering of the Downland gridshell”. In: *Space Structures* 5 1.April 2002 (2002), pp. 161–172.
- [HL75] E. Happold and I. Liddell. “Timber lattice roof for the Mannheim Bundesgartenschau”. In: *The structural engineer* 53.3 (1975), pp. 99–135.
- [HM95] A. J. Hanson and H. Ma. *Parallel Transport Approach to Curve Framing*. Tech. rep. 1995.

Bibliography

- [Hof08] T. Hoffmann. “Discrete Differential Geometry of Curves and Surfaces”. In: 18 (2008).
- [Hoo06] P. C. J. Hoogenboom. “7 Vlasov torsion theory”. In: October (2006), pp. 1–12.
- [Ibr95] A. Ibrahimbegović. “On finite element implementation of geometrically nonlinear Reissner’s beam theory: three-dimensional curved beam elements”. In: *Computer Methods in Applied Mechanics and Engineering* 122.1-2 (1995), pp. 11–26.
- [JBD13] T.-J. Jensen, O. Baverel, and C. Douthe. “Morphological and mechanical investigation of interconnected elastic gridshells”. In: *International Journal of Space Structures* 28.3-4 (2013), pp. 175–186.
- [Jun+10] P. Jung, S. Leyendecker, J. Linn, and M. Ortiz. “A discrete mechanics approach to the Cosserat rod theory—Part 1: static equilibria”. eng. In: *International journal for numerical methods in engineering* 85.1 (2010), pp. 31–60.
- [Kim16] L. Kim-Lan Vaulot. “Form-Finding of Elastic Gridshells”. PhD thesis. Massachusetts Institute of Technology, 2016.
- [Kir50] G. Kirchhoff. *Über das gleichgewicht und die bewegung einer elastischen scheibe*. Berlin, 1850, p. 38.
- [Kir76] G. Kirchhoff. *Vorlesungen über mathematische, physik, mechanik*. Ed. by B. G. Teubner. Leipzig, 1876, p. 483.
- [Klo86] F. Klok. “Two moving coordinate frames for sweeping along a 3D trajectory”. In: *Computer Aided Geometric Design* 3.3 (1986), pp. 217–229.
- [Koo14] K. Koohestani. “Nonlinear force density method for the form-finding of minimal surface membrane structures”. In: *Communications in Nonlinear Science and Numerical Simulation* 19.6 (2014), pp. 2071–2087.
- [Kot12] N. Kotelnikova-Weiler. “Optimisation mécanique et énergétique d’enveloppes en matériaux composites pour les bâtiments”. PhD thesis. Université Paris-Est, 2012, p. 310.
- [Lab+16] N. Labonnote, J. H. Mork, S. H. Dyvik, A. Rønnquist, and B. Manum. “Experimental and Numerical Study of the Structural Performance of a Timber Gridshell”. In: *World Conference on Timber Engineering*. 2. Vienna, Austria, 2016, pp. 3–10.
- [Laf15] E. Lafuente Hernández. “Design and Optimisation of Elastic Gridshells”. PhD thesis. Universität der Künste Berlin, 2015.
- [Láz+16] C. Lázaro, S. Monleón, J. Bessini, and J. Casanova. “A review on geometrically exact models for very flexible rods”. In: *Proceedings of the IASS Annual Symposium 2016* (2016), pp. 1–10.
- [LDB15] B. Lefevre, C. Douthe, and O. Baverel. “Buckling of elastic gridshells”. In: *Journal of the IASS* September (2015).

- [Lew03] W. Lewis. *Tension structures: form and behaviour*. Telford, Thomas, 2003, p. 201.
- [LG14] E. Lafuente Hernández and C. Gengnagel. “A new hybrid: Elastic gridshells braced by membranes”. In: *WIT Transactions on the Built Environment* 136 (2014), pp. 157–170.
- [Lid15] I. Liddell. “Frei Otto and the development of gridshells”. In: *Case Studies in Structural Engineering* 4 (2015), pp. 39–49.
- [LL09] H. Lang and J. Linn. “Lagrangian field theory in space-time for geometrically exact Cosserat rods”. In: 150 (2009), p. 21.
- [Lov92] A. Love. *A treatise on the mathematical theory of elasticity*. First. Cambridge University Press, 1892.
- [Low02] O. Lowenstein. “Lothian Gridshell”. In: *Building for a Future Winter* (2002), p. 29.
- [Low04] O. Lowenstein. “Gridshells in England. Ideas from the U.K. make stunning use of small timber”. In: *Wood Design & Building* (2004).
- [LP15] A. Liuti and A. Pugnale. “Erection of post-formed gridshells by means of inflatable membrane technology membrane technology”. In: *International Conference of the Architectural Science Association*. 2015, pp. 678–687.
- [LPD16] Liuti, A. Pugnale, and B. D’Amico. “Building timber gridshells with air : Numerical simulations and technique challenges”. In: *Structures and Architecture* (2016).
- [LS96] J. Langer and D. Singer. “Lagrangian Aspects of the Kirchhoff elastic rod”. In: *Society for Industrial and Applied Mathematics Review* 38.4 (1996), pp. 605–618.
- [Mal12] S. R. Malek. “The effect of geometry and topology on the mechanics of grid shells”. PhD thesis. MIT, 2012.
- [Men13] T. Menninger. *Frenet curves and successor curves : generic parametrizations of the helix and slant helix*. Tech. rep. 2013, pp. 1–15. arXiv: [1302.3175](https://arxiv.org/abs/1302.3175).
- [Mes+17] R. Mesnil, C. Douthe, O. Baverel, and B. Léger. “Linear buckling of quadrangular and kagome gridshells: A comparative assessment”. In: *Engineering Structures* 132 (2017), pp. 337–348.
- [MG16] D. Manta and R. Gonçalves. “A geometrically exact Kirchhoff beam model including torsion warping”. In: *Computers and Structures* 177 (2016), pp. 192–203.
- [MKS16] A. Menges, O. D. Krieg, and T. Schwinn. *Advancing Wood Architecture. A computational approach*. Routledge, July 2016, p. 256.
- [MLG13] D. Moulton, T. Lessinnes, and A. Goriely. “Morphoelastic rods. Part I : A single growing elastic rod”. In: *Journal of the Mechanics and Physics of Solids* 61.2 (2013), pp. 398–427.

Bibliography

- [MM17] Y. Masson and L. Monasse. “Existence of global Chebyshev nets on surfaces of absolute Gaussian curvature less than 2π ”. In: *Journal of Geometry* 108.1 (2017), pp. 25–32.
- [MOB06] M. McQuaid, F. Otto, and S. Ban. “Building the Japan pavilion”. In: *Shigeru Ban*. Phaidon Press, 2006, pp. 8–11.
- [MOD15] R. Mesnil, J. Ochsendorf, and C. Douthe. “Stability of Elastic Grid Shells”. In: *International Journal of Space Structures* 30.1 (2015), pp. 27–36.
- [Mon09] G. Monge. *Application de l’analyse à la géométrie*. 1809, p. 475.
- [MPW14] C. Meier, A. Popp, and W. A. Wall. “An objective 3D large deformation finite element formulation for geometrically exact curved Kirchhoff rods”. In: *Computer Methods in Applied Mechanics and Engineering* 278.August (2014), pp. 445–478.
- [Nab14] S. Nabaei. “Mechanical form-finding of timber fabric structures”. PhD thesis. EPFL, 2014.
- [Neu09] S. Neukirch. “Enroulement, contact et vibrations de tiges élastiques”. PhD thesis. 2009, p. 97.
- [NLG13] P. Nicholas, E. Lafuente Hernández, and C. Gengnagel. “The Faraday Pavilion : activating bending in the design and analysis of an elastic gridshell”. In: *Proceedings of the Symposium on Simulation for Architecture & Urban Design*. April. San Diego, CA, USA, 2013, Article No. 21.
- [PFL95] T. Poston, S. Fang, and W. Lawton. “Computing and approximating sweeping surfaces based on rotation minimizing frames”. In: *Proceedings of the 4th International Conference on CAD/CG*. 1995, pp. 1–8.
- [Pit26] H. Pitot. “Quadrature de la moitié d’une courbe des arcs appelée la compagne de la cycloïde”. In: *Mémoires de l’Académie Royale des Sciences (1724)* (1726), pp. 107–113.
- [Pon+16] S. Pone, G. Mirra, E. Pignatelli, D. Lancia, and S. Colabella. “Specialised algorithms for different project stages in a post-formed timber gridshell design”. In: *Structures and Architecture* September (2016), pp. 259–266.
- [Pou15] E. Poulsen. “Structural design and analysis of elastically bent gridshells”. PhD thesis. Chalmers University of Technology, Gothenburg Sweden, 2015.
- [Pra03] L. Prandtl. “Zur torsion von prismatischen stäben”. In: *Physikalische Zeitschrift* 4 (1903), pp. 758–770.
- [QG14] G. Quinn and C. Gengnagel. “A review of elastic grid shells, their erection methods and the potential use of pneumatic formwork”. In: *WIT Transactions on the Built Environment* 136 (2014), pp. 129–144.
- [Rei73] E. Reissner. “On one-dimensional large-displacement finite-strain beam theory.” In: *Studies in Applied Mathematics* 52.2 (1973), pp. 87–95.
- [Rei81] E. Reissner. “On the effect of shear center location on the values of axial and lateral cantilever buckling loads for singly symmetric cross-section beams”. In: *Journal of Applied Mathematics and Physics* 32.1 (1981), pp. 182–188.

- [Rom13] P. Romon. *Introduction à la géométrie différentielle discrète*. Références sciences. Ellipses, 2013, p. 216.
- [SBH95] Y. Shi, A. E. Borovik, and J. E. Hearst. “Elastic rod model incorporating shear and extension, generalized nonlinear Schrödinger equations, and novel closed-form solutions for supercoiled DNA”. In: *The Journal of Chemical Physics* 103.8 (1995), pp. 3166–3183.
- [Sit] Site Sécurité. *Règlement ERP type CTS (big tops & tents)*.
- [Spi08] J. Spillmann. “CORDE : Cosserat rod elements for the animation of interacting elastic rods”. PhD thesis. 2008.
- [ST07] J. Spillmann and M. Teschner. “CORDE : Cosserat Rod Elements for the Dynamic Simulation of One-Dimensional Elastic Objects”. In: *Eurographics/ACM SIGGRAPH Symposium on Computer Animation* (2007), pp. 1–10.
- [SV91] J. C. Simo and L. Vu-Quoc. “A Geometrically-exact rod model incorporating shear and torsion-warping deformation”. In: *International Journal of Solids and Structures* 27.3 (1991), pp. 371–393.
- [Tay+13] F. Tayeb, J.-F. Caron, O. Baverel, and L. du Peloux. “Stability and robustness of a 300m² composite gridshell structure”. In: *Construction & Building Materials* (2013).
- [Tay15] F. Tayeb. “Simulation numérique du comportement mécanique non linéaire de gridshells composés de poutres élancées en matériaux composites et de sections quelconques”. PhD thesis. 2015.
- [TG51] S. Timoshenko and J. N. Goodier. *Theory of elasticity*. Second. New York: McGraw-Hill, 1951, p. 506.
- [The07] A. Theetten. “Splines dynamiques géométriquement exactes : simulation haute performance et interaction”. PhD thesis. Université des Sciences et Technologies de Lille, 2007.
- [Tim21] S. Timoshenko. “On the correction for shear of the differential equation for transverse vibrations of prismatic bars”. In: *Philosophical Magazine Series 6* 41.245 (1921), pp. 744–746.
- [Tim22] S. Timoshenko. “On the transverse vibrations of bars of uniform cross-section”. In: *Philosophical Magazine Series 6* 43.253 (1922), pp. 125–131.
- [Tim45a] S. Timoshenko. “Theory of bending, torsion and buckling of thin-walled members of open cross section : Part I.” In: *Journal of The Franklin Institute* 239.3 (1945), pp. 201–219.
- [Tim45b] S. Timoshenko. “Theory of bending, torsion and buckling of thin-walled members of open cross section : Part II.” In: *Journal of The Franklin Institute* 249.4 (1945), pp. 249–268.
- [Tim45c] S. Timoshenko. “Theory of bending, torsion and buckling of thin-walled members of open cross section : Part III.” In: *Journal of The Franklin Institute* 239.5 (1945), pp. 343–336.

Bibliography

- [Tra06] Trada. “The Savill Building. A visitor centre with a timber gridshell roof Gridshell structures”. In: *TRADA* (2006), pp. 1–7.
- [Vau00] R. Vauquelin. “Writhing Geometry at Finite Temperature : Random Walks and Geometric phases for Stiff Polymers”. In: 1 (2000).
- [Vet14] Y. Vetyukov. *Nonlinear mechanics of thin-walled structures : asymptotics, direct approach and numerical analysis*. 1st ed. 2014, pp. X, 272.
- [Vil97] P. Villaggio. *Mathematical models for elastic structures*. Cambridge University Press, 1997.
- [Vla61] V. Z. Vlasov. *Thin-walled elastic beams*. Second. National Technical Information Service, 1961.
- [Vou14] E. Vouga. “Plane Curves”. In: *Lectures in discrete differential geometry*. 2014. Chap. 1, pp. 1–11.
- [Wak80] D. Wakefield. “Dynamic relaxation analysis of pretensioned networks supported by compression arches”. PhD thesis. City University London, 1980, p. 281.
- [Wan+08] W. Wang, B. Jüttler, D. Zheng, and Y. Liu. “Computation of rotation minimizing frames”. In: *ACM Transactions on Graphics* 27.1 (2008), pp. 1–18.
- [Wei02] H. Weiss. “Dynamics of geometrically nonlinear rods : Mechanical models and equations of motion”. In: *Nonlinear Dynamics* 30 (2002), pp. 357–381.